Scour Prediction Around Jacket Wind Turbine Foundations under current-only conditions

David Garagorri Linares

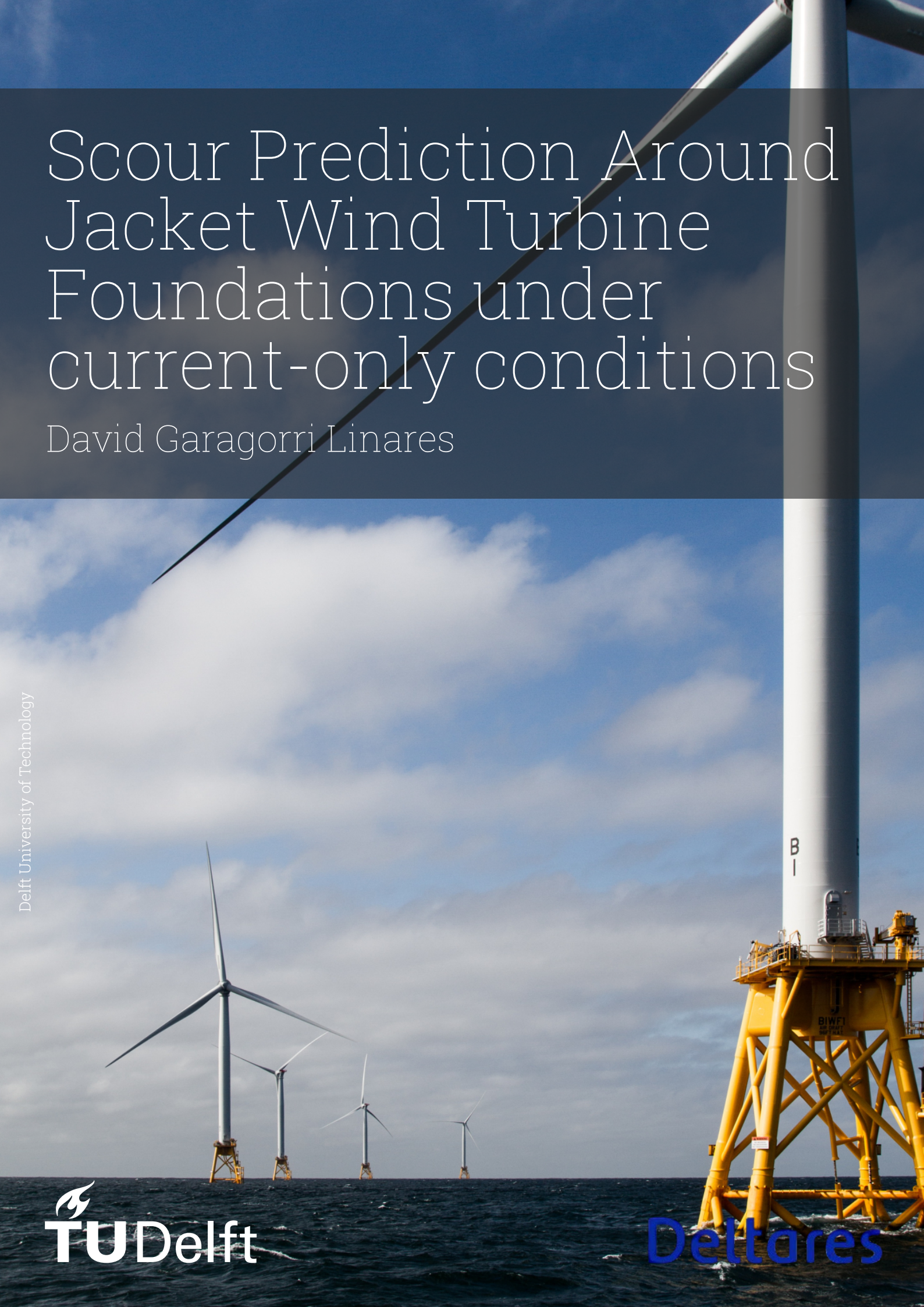

Delft University of Technology

TU Delft

Deltares

Scour Prediction Around Jacket Wind Turbine Foundations under current-only conditions

by

David Garagorri Linares

in partial fulfillment of the requirements for the degree of

Master of Science

in Civil Engineering

at the Delft University of Technology,

to be defended publicly on Friday August 29th, 2025

Student number:	5918928	
Project duration:	February, 2025 – July, 2025	
Thesis committee:	Dr. ir. Robert Jan Labeur,	TU Delft, Main Supervisor
	Dr. ir. Bas Hofland,	TU Delft, Chair
	PhD. Yorick Broekema,	Deltares
	PhD. Lynyrd De Wit	Deltares
	PhD. Mario Welzel	Leibniz Universität Hannover

TU Delft

Deltares

Preface

This master's thesis is the result of a collaboration between TU Delft and Deltares, bridging the gap between academic research and industry needs. Through this partnership, I conclude my Master of Science in Civil Engineering, specializing in Hydraulic Engineering. This project converges my passion for hydraulic and numerical modeling with the culmination of my MSc program, which challenged me many times and made this process really enjoyable.

I would like to express my sincere gratitude to my thesis committee, whose guidance made this work possible. To Robert Jan Labeur, for his orientation on the broader research vision and for his support through all the steps of this project. To Bas Hofland, for his guidance in applying physical concepts and for his critical perspective, which strengthened the analysis of the results. To Yorick Broekema, for his continuous and valuable feedback during my time at Deltares, ranging from the smallest details to the general overview of the project, and for introducing me to this topic. To Lynyrd de Wit, for the numerous sessions dedicated to the model and for his enthusiasm in discussing the results. To Mario Welzel, for sharing the data from his experiment and for the insightful comments that helped interpreting the results in a correct manner.

I am also very grateful to Deltares for hosting this project and providing the resources needed to carry it out, as well as to all the colleagues there, to whom I am thankful.

On a personal note, I would like to thank my parents and my brother for their unwavering love and support from afar, and my friends Evi, Danai, Julie, Fede, Auke, Conor, Katia, Greg, and Juan for their support throughout these months.

David Garagorri Linares
Delft, August 2025

Abstract

This thesis investigates local and global scour processes around four-legged jacket (4LJ) foundations for offshore wind turbines under current-only conditions using the 3D CFD Large Eddy Simulation (LES) model TUDflow3D. Jacket foundations, while increasingly deployed in deeper offshore environments, remain less studied than monopiles on local scour and scale effects and introduce new scour patterns like global scour. The research addresses this gap by evaluating the predictive performance of TUDflow3D against laboratory experiments, extending simulations to field scale, and assessing the applicability of monopile-based empirical scour relations to jacket configurations.

Laboratory-scale numerical simulations replicate the experimental study of Welzel et al. (2023) for both clear-water and live-bed regimes, validating the model for a 4LJ foundation. Model performance is assessed through morphodynamic comparison and time-averaged observation of the hydrodynamics, supplemented by a sensitivity analysis on numerical parameters: morphological acceleration factor, relaxation factors, and grid resolution.

The validated model is then scaled to field conditions using a mobility similarity approach, enabling investigation of scale effects on scour magnitude, spatial extent, and equilibrium timescales.

After the scaling up, both models are analyzed in order to enhance the knowledge that is known until now from 4LJ foundations. For local scour, the spatial extent of scour was determined by adapting a formulation for monopiles and quantified throughout the entire scour evolution, revealing a consistent footprint over time. Scaling to field conditions demonstrated that the upstream–downstream scour pattern persists, but with reduced magnitudes in local scour depth due to scale effects, observed by the reduction of time-averaged bed shear stresses around the legs. This reduction in magnitude was approximately 30%–35% when compared in terms of dimensionless scour for both regimes and for both upstream and downstream piles. Timescale analysis showed that scour equilibrium occurs later at locations farther from the piles. When scaling, it was also found that scour on clear-water regimes require months while live-bed regimes is in the order of agnitude of days to reach local scour equilibrium.

For global scour, live-bed conditions produced a footprint extending up to twice the jacket footprint radius with rapid initial development, while clear-water conditions yielded slower, more confined scour. The order of magnitude for the global scour is variable depending on the location, but it reached values around 0.9 - 1 D on the center of the jacket and downstream of it

Finally, empirical monopile scour formulas were evaluated, showing that they still provide reasonable order-of-magnitude estimates for upstream piles and capturing scale effects, as well it was proved that the scaling up from laboratory scale to field scale developed for monopiles can be useful also for 4LJ foundations.

The study demonstrates that CFD LES modeling is a robust and flexible tool for detailed, process-based scour prediction around complex foundation geometries. Beyond validation, its ability to simulate field-scale morphodynamics and provide high-resolution temporal and spatial data makes it a valuable complement to laboratory testing, supporting both scientific understanding and engineering design of offshore wind infrastructure.

David Garagorri Linares
Delft, August 2025

Contents

1

Introduction

1.1. Research Context

In recent decades, global efforts to mitigate climate change have increasingly focused on reducing CO_2 emissions, with the transformation of the energy grid identified as one of the most important mitigation targets The transition to a low-carbon energy system lies at the core of policy frameworks such as the 2030 European Climate and Energy Framework, which sets targets for emission reductions, renewable energy deployment, and improvements in energy efficiency. Within this context, offshore wind energy has emerged as a promising solution to help achieve decarbonization objectives (Díaz & Soares, 2020).

The number of offshore wind turbines, their individual capacities, and the total installed power generation have increased in recent years. Among the critical components of these systems is the foundation, which can represent up to 30% of the total installation cost in water depths of 20–40 meters (Oh et al., 2018). This underscores the need for optimized foundation design and a thorough understanding of the physical processes that may compromise structural integrity, such as seabed erosion around the structure.

Scour refers to this mentioned erosion of sediment around hydraulic structures, resulting from flow disturbances induced by the presence of these structures. For offshore wind turbines, it is a critical design consideration, as it directly affects the stability and long-term performance of the foundation. Experimental studies have demonstrated that the shape and depth of scour holes significantly influence structural fatigue and overall stability (Cao et al., 2024; Li et al., 2020). In large-scale structures such as offshore wind turbines, unmitigated scour can lead to a reduction in operational lifetime—up to 24% for critical scour depths—impacting both the foundation and the turbine system as a whole.

An essential component of offshore wind turbines (OWTs) operation is the transmission of generated energy to onshore facilities or offshore substations, which is done by sub sea cables placed under the sea bed. Any exposure or damage to these cables can compromise system reliability. Understanding the development of scour and the timescales for bed stabilization is therefore important to prevent cable exposure or failure (Deltares, 2020). A well-known case highlighting this issue is the Barrow Offshore Wind Farm, where post-installation inspections revealed that scour had left export cables exposed, necessitating costly offshore repairs (Department for Business, Enterprise and Regulatory Reform, 2008).

Key parameters in cable design include the predicted maximum scour depth, the footprint of the scour hole, the time required to reach equilibrium conditions and persistent bedforms in the shape of sand waves. Since cable installation can even precede full scour development due to project timelines, reliable prediction of these parameters is essential (Deltares, 2020).

Figure 1.1 illustrates a standard cross-section of a monopile foundation with cable protection. The cable is buried beyond the expected scour extent and depth.

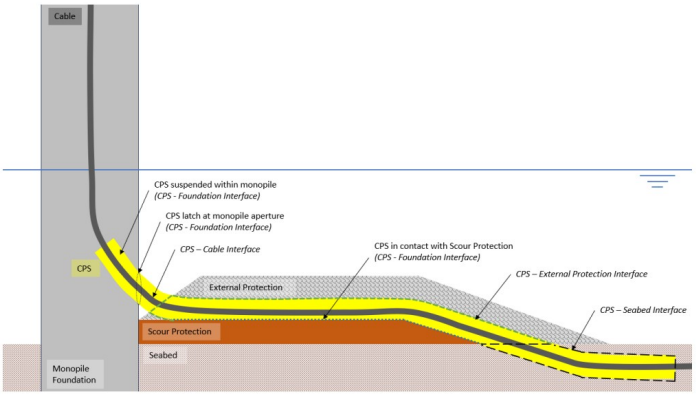

Figure 1.1: Typical cable burial and protection layout for monopile foundations (The Carbon Trust, 2021).

Offshore wind turbines (OWTs) foundations come in various forms, with monopiles, gravity-based structures, and jacket foundations being the most commonly used. In water depths of approximately 20–40 meters, monopiles and jackets are the most used options, with jacket foundations often preferred due to a better structural performance (John Smith, 2021). In recent years, the shift toward deeper offshore sites—driven by the need for greater installed capacity and more consistent wind resources—has further increased the adoption of jacket foundations, a trend that is expected to continue (John Smith, 2021).

Jacket foundations are leg-based support structures that provide enhanced structural performance in deeper waters compared to monopiles. Among the various configurations, four-legged jackets are the most widely used, owing to their efficient load distribution and well-established application (Park et al., 2023). An example of the significance of this foundation type is the Quattropod—a four-legged jacket—which has been adopted as the standard configuration in offshore wind design tools (Damiani et al., 2016), while project data from South Korea identifies the four-legged jacket (4LJ) as the most commonly implemented system in regions with water depths around 30 meters (Tran et al., 2022).

In jacket-supported wind farms, cables often pass within the footprint of the jacket structure and connect multiple turbines or substations, with cables going out even in each leg of the structure. This creates routing challenges where the magnitude, time evolution and spatial extent of scour must be accounted for. Figure 1.2 provides a plan view of cable layout at Scroby Sands Offshore Wind Farm, showing the concatenation of cables in wind farms and how bathymetric changes can affect cable alignment.

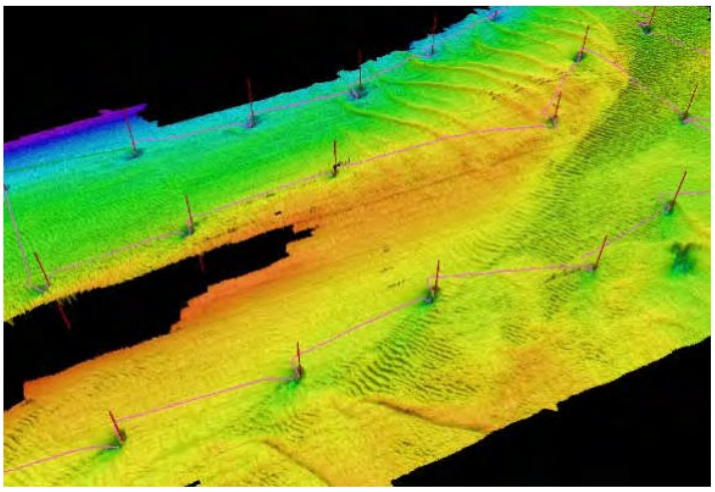

Figure 1.2: Plan view showing subsea cable layout and scour features at Scroby Sands Offshore Wind Farm (Sharples, 2011).

These risks are addressed in industry guidance documents such as the Cable Protection Systems

(CPS) Best Practice Guidelines (The Carbon Trust, 2021), Deltares recommendations on cable burial and protection (Deltares, 2020), and reports such as the BSEE review on offshore cable burial standards and sand wave interactions (Sharples, 2011) focusing mainly on monopiles, which is the most common foundation.

For designing these structures and account for the seabed response around hydraulic structures, physical scale-model experiments in laboratory settings have traditionally been the standard and final approach. These experiments provide accurate and reliable representations of real-world conditions, and numerous studies have demonstrated their effectiveness in capturing scour depth and patterns under a range of hydrodynamic scenarios (Sumer & Fredsøe, 2002). However, physical experiments are often expensive, time-consuming, and difficult to adapt to multiple design variations.

In recent years, numerical models have emerged as a cost-effective and detailed alternative for simulating morphodynamic processes like scour. Computational Fluid Dynamics (CFD), particularly three-dimensional approaches, have proven capable of capturing the complex flow structures and sediment transport dynamics around offshore structures (Roulund et al., 2005) with flexible and detailed outputs. As will be discussed in Chapter 2, previous studies have demonstrated the ability of 3D CFD to replicate laboratory results for scour around monopile foundations with high accuracy. These advancements underscore the potential of numerical modeling to complement physical experiments.

1.2. Predicting Scour through numerical modeling as an opportunity

Scour has long been recognized as a challenging process to predict, prompting extensive research to develop reliable methods. The first empirical relations were made for bridge piers exposed to river loads, and then for the marine environment early laboratory experiments led to empirical relationships (B. M. Sumer & Fredsøe, 1998), while field measurements from existing structures resulted in similar expressions (Bayram & Larson, 2000).

Compared to monopiles and pile groups, jacket foundations have received significantly less attention in scour-related studies. Consequently, their design often relies on approaches developed for monopiles, such as treating each leg as an isolated cylinder. While some aspects of local scour, which is the scour around a monopile, can be extrapolated from monopile research, the interaction between multiple legs in a jacket introduces distinct flow complexities that alter scour development. Moreover, jackets are subject to global scour—a lowering of the entire seabed beneath the structure—which is non existent for monopiles and has only been partially explored for pile groups. The flow patterns generated by the open-frame structure, combined with variability in jacket geometry and spacing, reduce the reliability of simplified design methods and highlight the need for more tailored investigations into their behavior.

As research progressed, numerical models emerged as a viable alternative, validated against experimental tests. These models have gained widespread adoption in the research community due to their accuracy and detailed outputs on scour predictions (Zhou et al., 2013). 3D CFD modeling has been applied to predict hydrodynamic and morphodynamic interactions, particularly for geometries such as bridge foundations and off-shore monopiles foundations, where it has shown strong agreement with laboratory experiments (Khosronejad et al., 2011; Lai et al., 2022; Zhou et al., 2013). These simulations provide a more flexible and comprehensive approach than empirical relationships, allowing for the evaluation of a wide range of conditions, geometries, and design scenarios. They also offer more detailed output than a laboratory experiment, making them a valuable and efficient tool for accurately predicting scour processes and at the same time enabling in-depth post-processing analysis.

Although these models offer considerable advantages, their application comes with challenges. These include the need for thorough validation against experimental data, a deep understanding of the underlying physical processes to correctly interpret the results, and significant computational costs—particularly for large domains or high-resolution, long-term morphodynamic simulations.

Recent research by de Wit et al. (2023) demonstrated promising results using the 3D CFD LES model TUDflow3D to simulate scour around an OHVS jacket foundation with clustered piles, showing good agreement with experimental data for local scour. To build on these findings, it is essential to assess the performance and limitations of the model for a different jacket configuration, 4LJ for Offshore wind

turbines (OWTs), and to extend the analysis to include global scour behavior.

Another topic that remains under investigation is the influence of scale effects on morphodynamic timescales and scour magnitudes when comparing laboratory-scale models to field-scale conditions. While several studies have explored these effects for monopiles at different laboratory scales Ettema et al. (2006), numerical modeling offers the advantage of directly addressing scaling challenges by simulating realistic field conditions. Notably, Broekema and de Wit (2025) proposed a framework to account for these effects in monopiles, and in this study, that approach is further evaluated and applied to jacket foundations.

Despite the growing deployment of jacket foundations, specially 4LJ, in offshore wind energy, some gaps remain in understanding their morphodynamic interaction with the seabed. Most existing design approaches and industry guidelines are based on monopile foundations, which do not account for the flow patterns and global scour behavior unique to jackets. While local scour has been studied experimentally, global scour beneath the entire structure remains underexplored. Numerical modeling—particularly 3D CFD and LES approaches—offers a promising alternative to studying in detail the scour behavior, yet its application to this day to jacket foundations is still limited. Additionally, scale effects between laboratory and field conditions remain a challenge, with limited frameworks available for translating findings across scales. These gaps highlight the need for targeted numerical investigations on jacket scour dynamics, global scour development, and scaling methodologies to improve design reliability and reduce offshore infrastructure risks.

1.3. Research Questions and Objectives

1.3.1. Research Objectives

To address the research opportunities mentioned on the previous section the main objective of this research is presented:

To further explore and develop the predictive capabilities of scour behavior under current-only conditions around a 4-legged jacket foundations through CFD LES modeling

This research aims to address knowledge gaps in scour prediction around jacket foundations by applying and evaluating the performance of the 3D CFD LES model TUDflow3D under current-only conditions.

The focus is on a widely adopted 4LJ OWTs configuration, for which laboratory-scale data are available for validation (Welzel et al., 2023) of the numerical model, covering both local and global scour development. Leveraging the flexibility of numerical modeling, the study also explores the influence of field-scale conditions on scour evolution by scaling up laboratory simulations. This enables a detailed assessment of scale effects on scour magnitude and morphodynamic timescales, which are critical for real application.

When validated and scaled to field conditions, the numerical model results provide a detailed view of local and global scour patterns, offering insights into critical erosion zones and the timescales of scour development. These findings inform design considerations such as foundation embedment, burial depth, and cable protection strategies.

Ultimately, this study seeks to enhance predictive capabilities for scour around jacket foundations and evaluate the applicability and limitations of empirical relationships originally developed for monopiles when applied to jacket geometries.

1.3.2. Research Questions

Translating the research objectives outlined before, the research questions are proposed:

How can CFD LES be applied to represent the morphodynamic response of the seabed around a four-legged jacket foundation for offshore wind turbines under current-only conditions?

- How accurately can TUDflow3D predict the morphodynamic evolution of the seabed around a 4LJ foundation?

- What insights can be gained into local and global scour development under a 4LJ configuration using CFD LES?
- How do field-scale conditions influence the hydrodynamic and morphodynamic behavior around jacket foundations?
- How well do existing empirical scour relations for monopiles perform when applied to jacket foundations, and what are the limitations affecting their use in practice?

1.4. Methodology

To address the objectives of this research and answer the key questions outlined in the previous section, the methodology is outlined in this section.

In order to build on the existing knowledge of monopiles and 4LJ, a literature review is presented in Chapter 2 which serves as the base for all the other chapters.

Based on this knowledge, the next step then involves evaluating the performance of the numerical model (TUDflow3D) by comparing its results with the laboratory experiments conducted by Welzel et al. (2023). This comparison helps identify the model's strengths and limitations in replicating the morphodynamic behavior observed at laboratory scale. This is described in Chapter 4.

Building on this understanding, a field-scale model is implemented to investigate scaling effects on Chapter 5. This model allows the understanding of scaling effects for scour implication on field conditions, offering insight into the validity and applicability of scaling laws.

After completing the model simulations, a detailed analysis and interpretation of the results is performed on Chapter 6. This step leverages the capabilities of numerical modeling to investigate scour magnitude, spatial extent, and temporal evolution across different regimes and scales.

Finally, the discussion of the limitation of the results is addressed in Chapter 7, followed by Chapter 8 which shows the conclusions, summarizing the main outcomes and linking them back to the research objectives and guiding questions.

2

Literature review

This chapter provides a comprehensive review of the state of the art in scour behavior around offshore foundations, with a focus on monopiles and jacket structures. It synthesizes knowledge from experimental studies, empirical relations, numerical simulations, and field observations, forming the theoretical and practical basis for the present research. The chapter is structured around key concepts that underpin the modeling and understanding of scour processes, with particular attention to the transition from monopile to jacket foundation research, highlighting the identified knowledge gap.

To establish this foundation, the chapter first introduces the governing physical mechanisms of scour, beginning with sediment mobilization and bed response. It then examines scour behavior around monopiles and pile groups, which serve as a comparative framework. Although the geometrical configurations differ, the extensive literature on monopiles provides valuable insights into flow–structure–sediment interactions.

Subsequently, the chapter reviews the current state of knowledge regarding scour around jacket foundations. It introduces the case study by Welzel et al. (2023) used in this research that will be used for the model assessment. This includes findings from laboratory experiments, numerical simulations under both current-only and wave–current conditions, and real-scale field data. Finally, the chapter introduces the CFD model used in this research—TUDflow3D—detailing its features for application in simulating local and global scour under turbulent flow conditions.

2.1. Scour mechanisms around pile foundations

Scour behavior can be defined as the response of the seabed level to the disturbance of flow conditions due to the presence of hydraulic structures. This process is governed by a range of physical parameters and also depends on the type of structure that originates this response. While this thesis focuses on jacket foundations, much of the foundational knowledge on scour stems from studies on structures such as monopiles and piers. Therefore, this section introduces the key mechanisms and scaling principles that underpin scour development, bridging the gap between well-established insights and the behavior observed around jacket structures. It begins by defining sediment mobility conditions, then addresses scaling challenges, explores the scour processes around single and grouped piles, and finally discusses temporal scour development and the distinction between local and global scour.

2.1.1. Initiation of Motion and Bed Response

An essential first step in understanding scour is to determine the conditions under which sediment becomes mobile or the bed begins to respond dynamically to the flow. This evaluation begins with the concept of bed shear stress, defined as the tangential force per unit area exerted by the flowing fluid on the bed surface.

A widely used formulation to estimate bed shear stress is:

$$\tau_b = \rho C_f U^2 \tag{2.1}$$

where:

- τ_b is the bed shear stress [Pa],
- ρ is the fluid density [kg/m³],
- C_f is a dimensionless friction coefficient,
- U is the near-bed flow velocity [m/s].

This equation demonstrates that the bed shear stress scales with the square of the flow velocity for hydraulic rough beds, underscoring the dominant role of velocity in the forces that are exerted on the bed.

However, bed shear stress alone is not sufficient to determine whether sediment will actually move. The characteristics of the bed material also play a critical role. To evaluate whether the flow conditions are capable of initiating sediment motion, the Shields number (θ) is introduced. Originally proposed by Shields (1936), the Shields number is a dimensionless parameter that represents the ratio between the bed shear stress and the submerged weight of sediment particles:

$$\theta = \frac{\tau_b}{(\rho_s - \rho) g D_{50}} \tag{2.2}$$

where:

- τ_b is the bed shear stress,
- ρ_s is the sediment density [kg/m³],
- ρ is the fluid density [kg/m³],
- g is the gravitational acceleration [m/s²],
- D_{50} is the median sediment grain diameter [m].

The Shields number provides a useful threshold-based framework to assess sediment initiation. When θ exceeds a critical value (θ_c), sediment particles begin to move, leading to bed deformation and scour, assuming uniform flow.

When the Shields number exceeds a certain threshold, known as the critical Shields number (θ_{cr}), sediment motion initiates and the bed becomes active. However, this does not imply a binary behavior in which transport is entirely absent below the threshold and fully developed above it; rather, sediment mobility increases gradually as θ surpasses θ_{cr}.

The critical Shields number depends on both grain size and flow conditions, particularly the sediment Reynolds number. An empirical formulation proposed by Soulsby (1997) is commonly used to estimate this threshold and is used in this project for the computation of this critical value. The complete set of formulas for estimating the critical shields number and sediment Reynolds numbers used in this project is provided in Appendix A.

Based on the Shields number and its relation to the critical threshold, the concept of bed regime is introduced. The bed regime characterizes the sediment transport condition on the bed in the absence of any structure. Two primary regimes are identified:

- **Clear-water regime**: occurs when $\theta < \theta_{cr}$. In this regime, the bed remains largely inactive and sediment transport is minimal. Scour development is driven solely by local flow acceleration near the structure.
- **Live-bed regime**: occurs when $\theta \geq \theta_{cr}$. The bed is already mobilized by the flow, and sediment is actively transported. In this case, the presence of a structure interacts with an already mobile bed, often accelerating the rate and magnitude of scour development.

These regimes lead to different scour behaviors, in terms of time scale and magnitude, which will be extensively discussed in this research proposal.

2.1.2. Flow Behavior and relation to scour around monopiles and pile groups

Scour analysis begins with an understanding of the flow behavior around a single pile. Several vortex structures develop in the vicinity of the pile.

Under steady current conditions, various flow characteristics contribute to scour development. A horseshoe vortex forms at the base of the structure, wrapping around its upstream face. The size and strength of this vortex are influenced by the boundary layer thickness -which refers to the boundary layer from the bed where the velocity transitions from being strongly influenced by bed friction to free stream velocity- and the Reynolds number (Qu et al., 2024), as well as the blockage ratio caused by the structure.

Specifically, a smaller ratio of boundary layer thickness to pile diameter results in a more compact vortex, while the vortex length increases with Reynolds number (Sumer & Fredsøe, 2002). On the lee side of the structure, a wake vortex develops, extending downstream and transporting sediment away from the pile. Flow contraction around the sides of the pile leads to acceleration, while a down-flow just upstream further enhances local scour. The displaced sediment is typically deposited downstream of the structure (Satari et al., 2024). These flow mechanisms are illustrated in Figure 2.1.

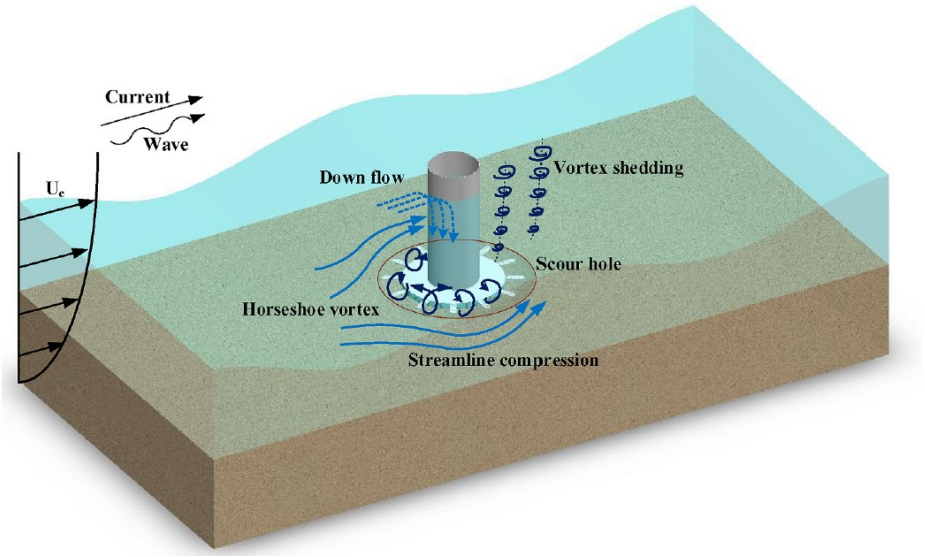

Figure 2.1: Flow mechanisms important for scour development around a pile. Adapted from Qu et al. (2024)

Scour is also influenced by the bed shear stress behavior. A common approach involves comparing the averaged bed shear stresses in time with and without the structure under otherwise identical flow conditions, quantifying the amplification of it. This is done because the peak areas for this amplification can be related to critical areas of scour (Satari et al., 2024). Early work by Sumer and Fredsøe (2002) suggested that the amplification of the bed shear stresses typically ranges from 4 to 5 on monopiles, with localized peaks up to 10. More recent studies, however, indicate that amplification factors can reach values around 3 to 4 for monopiles and for jackets the amplification seems to be higher, with amplifications around 7 to 8, for the same hydrodynamic conditions (Qu et al., 2024; Satari et al., 2024).

Several variables play a crucial role in scour development, including the pile diameter, bed grain size, current velocity, and Shields number. This was observed by Ettema et al. (2006) through the following parametrization:

$$\frac{S_{\text{eq}}}{D} = \varphi_1 \left(\frac{U_0}{U_c}, \frac{U_0^2}{gD}, \frac{\rho U_0 D}{\mu}, \frac{D}{D_{50}}, \frac{D}{y_0} \right) \tag{2.3}$$

This parametrization will serve later to understand how different processes affect scour and the scaling effects. For example, according to Melville (2008), when the ratio of pile diameter to median grain

size (D/D_{50}) in lab conditions, reaches approximately 50, a threshold is observed where the maximum scour depth is attained. Beyond this point, scour depth decreases for both larger and smaller values of D/D_{50}, which can be useful for scaling comparisons from lab to field.

On the other hand, pile groups have additional flow patterns that relate to the interaction pile to pile. In such configurations, the spacing between piles plays a critical role in determining the nature of flow interactions. Literature on pile groups suggests that for staggered arrangements, spacing in both the streamwise and transverse directions significantly influences whether vortices interact or remain independent (Sumner, 2010). For a spacing ratio G/D, where G is the center-to-center distance between piles and D is the pile diameter, it has been observed that when $G/D > 3$, the lee-wake vortices tend to remain uncoupled (Sumer & Fredsøe, 2002). This spacing criterion applies primarily to the wake region. In contrast, the formation of a horseshoe vortex at the downstream pile only occurs when $G/D > 3$, whereas the upstream pile's horseshoe vortex may still be influenced by the overall flow obstruction. Furthermore, as noted by Satari et al. (2024), the ratio between pile diameters also affects vortex shedding behavior, further complicating the hydrodynamics in pile group configurations.

Regarding scour in pile groups, fewer studies exist compared to single piles. However, scour behavior can generally be categorized into two configurations:

- **Side-by-side arrangement**: In this case, piles are aligned transverse to the flow direction. Scour is more pronounced compared to a single pile when $G/D < 1$ but gradually converges to the single-pile scour depth as G/D approaches 6.0 according to (Sumer & Fredsøe, 2002) and according to(Kim et al., 2014) these behavior happens when the ratio approaches 3.75-5.0 . Although interference effects may persist beyond this value, they become negligible.
- **Tandem arrangement**: In this configuration, piles are aligned in the streamwise direction. Maximum scour occurs when $G/D = 2$, followed by a gradual decrease, reaching the single-pile scour depth at $G/D = 10 - 15$ or higher. For the upstream pile, scour follows this trend, while for the downstream pile, scour remains consistently lower than in the single-pile case, reaching its peak at $G/D = 5$ (Sumer & Fredsøe, 2002). According to most recent studies (Kim et al., 2014) these relations are maintained, and studied with more detail.

2.1.3. Local and Global Scour

For monopiles, scour is limited to the immediate surroundings of the pile, as it is the only location where the structure directly influences the bed. In contrast, for pile groups, an additional type of scour—referred to as global scour—has been identified. This form of scour occurs across the area enclosed by the group. Jacket foundations exhibit a similar behavior to pile groups, and global scour has also been observed in such configurations.

Local scour can be defined as the area of influence of erosion occurring around an individual pile, which is typically more critical in terms of magnitude. It is primarily caused by the horseshoe vortex and the contraction of streamlines. There have been already efforts by different research studies to try to determine the length of the footprint of local scour.Bolle et al. (2010) defines the footprint of local scour at 0.5 D, and then the extension of it with the tangent of the angle representative of the sediment on question, while Welzel et al. (2023) defines it as 1.5 D, as the overall footprint.

Various approaches have been proposed to estimate the local scour depth around monopiles, typically expressed in non-dimensional form as the ratio S_{eq}/D, where S_{eq} is the equilibrium scour depth and D is the pile diameter. This normalization allows for consistent comparison across different scales and conditions. The equilibrium scour depth represents the maximum depth of scour reached over time, beyond which no significant further development occurs, indicating a dynamic balance between sediment transport and flow forces.

Sumer and Fredsøe (2002) reviewed a wide range of literature values for this ratio under live-bed conditions and reported typical values ranging from 1.0 to 2.5. The average within this range is approximately 1.3, with a standard deviation of 0.7. For design applications, it is common practice to adopt a conservative approach by using one or two standard deviations above the mean, resulting in design values of 2.0 or 2.7.

From an analytical approach, scour around a pile can be determined with different hydrodynamic and

physical conditions according to (Sheppard, 2003) who developed equations for piers that can be useful to compare. These formulas relate water depth, pile diameter, bed material grain size, critical flow velocity, and live-bed peak scour velocity. They account for the prevailing bed conditions indirectly at the time of scour estimation. The complete set of formulas is provided in Appendix A.

It is important to note that these formulas were developed to provide an envelope of scour values—that is, they account for the maximum expected scour depth. Also, when applied to a jacket structure, they would yield the same envelope for all piles within the configuration, regardless of the flow interaction between piles.

On the other hand, global scour for a group of piles occurs in the areas shared between piles. It is driven by changes in velocity in the gaps between the piles and the interaction of vortices generated by the piles. This global scour can also be described as a lowering of the bed level within the group of piles.

In practical terms, global scour increases as the number of piles in the configuration grows. For example, (Sumer & Fredsøe, 2002) examines a square arrangement with an $N \times N$ configuration, where N is the number of piles per side and the G/D ratio is 4. The study found that global scour increases from 0 to nearly 1.5 times the pile diameter for $N = 5$, after which it stabilizes. Regarding localized scour, the study compares it to the scour around a single pile. As N increases, localized scour also rises, reaching up to twice the scour of a single pile for $N = 5$, beyond which it ceases to grow further. In the case of N being 2 -which can be compared to a 4LJ because of the same number of piles- the scour magnitude expected will be around 0.4 S/D for live bed conditions.

2.1.4. Temporal Evolution of Scour

Another important aspect of scour analysis is not only the final equilibrium depth but also the rate at which scour develops over time.

Melville (2008) observed that the time-dependent scour development around monopiles follows an asymptotic trend, gradually approaching an equilibrium state. A commonly used expression to describe this behavior is the hyperbolic formulation applied by Welzel et al. (2023), which defines the scour depth $S(t)$ at time t as a function of the equilibrium scour depth S_{eq}:

$$S(t) = S_{\mathrm{eq}} \left(1 - \frac{1}{1 + \beta t}\right) \tag{2.4}$$

Here, β is a time-scale parameter that controls the rate of scour development. This offers an effective approximation for local scour, particularly during the early stages when the increase in depth is most pronounced.

Recently it has been observed that the scour process evolves in distinct phases or exhibits changes in the rate of development over time, as observed in experimental and numerical studies compiled by Silva-Muñoz and Broekema (2025). The shape of the curve shows more a double hyperbolic behavior that captures this multi-stage behavior more effectively than a single asymptotic curve.

However, one of the main challenges in applying a double hyperbolic relation lies in selecting appropriate parameter values for calibration. When working with experimental or numerical data, the choice of initial estimates plays a critical role in ensuring convergence and producing physically meaningful results. This challenge becomes even more pronounced when you need more parameters, as the increased number of variables introduces a larger space for potential error and greater sensitivity to initial guesses, which can lead to poor or non-unique fits. Therefore in this project the time evolution of scour is done with 2.4.

Another way to understand the scour timescale response is by identifying the physical variables that influence its development. The framework proposed by Silva-Muñoz and Broekema (2025), in which the characteristic scour timescale T_c is linked to key flow and sediment parameters, provides a useful basis for analyzing scour under different hydraulic conditions:

$$T_c \propto g \left(\frac{S_{\text{eq}}^2}{U^3} \right) \tag{2.5}$$

From this formulation, it becomes clear that the flow velocity U exerts a dominant influence on the scour timescale due to its cubic relationship. All other factors being equal, a higher velocity results in a significantly faster scour development. As a result, under identical sediment and structural conditions, scour in the live-bed regime is expected to progress more rapidly than in the clear-water regime.

An additional insight from the formulation is that, for piles subject to the same hydrodynamic conditions and operating within the same bed regime, those with a greater equilibrium scour depth will require more time to reach that equilibrium. In other words, a larger ultimate scour depth implies a longer timescale for the scour process to stabilize.

2.1.5. Scaling from lab to field conditions

Scour is influenced by different parameters, as explained before. The consistency of the values or magnitudes of these parameters when comparing lab to field-scale cases cannot always be achieved Ettema et al. (2006). Then, scaling scour processes from laboratory-scale experiments or numerical simulations to real-world field conditions presents a major challenge for hydrodynamic and morphodynamic processes. Traditional scaling methods rely on matching dimensionless parameters, most notably the Froude number and the Reynolds number. However, each has inherent limitations when applied to sediment transport and scour modeling.

The Froude number governs the relationship between inertial and gravitational forces and is particularly relevant when free-surface effects, such as wave action or open-channel flow, are dominant. In contrast, the Reynolds number describes the ratio between inertial and viscous forces and is critical in determining whether the flow is laminar or turbulent.

In physical model studies, it is complicated to simultaneously satisfy both Froude and Reynolds similarity due to scale effects—particularly because viscosity and gravity do not scale proportionally. As a result, laboratory models often prioritize Froude similarity to correctly simulate free-surface flow, while accepting that Reynolds similarity cannot be maintained. This leads to reduced turbulence intensity at smaller scales, which in turn affects sediment entrainment and scour development.

As highlighted by Veldhuizen et al. (2023), this scaling mismatch is especially problematic when modeling scour, as sediment transport is highly sensitive to near-bed turbulence. They emphasize that relying solely on hydrodynamic scaling parameters like the Froude number is insufficient to replicate the true sediment response observed at field scale.

To address this, a mobility-based scaling is mentioned by Veldhuizen et al. (2023) by preserving the ratio between the Shields number and its critical value. This concept, known as mobility similarity, focuses directly on the sediment transport regime rather than on matching all aspects of the hydrodynamics. By ensuring that both the laboratory and field cases operate under the same sediment mobility conditions, the scour behavior can be reproduced reliably, even if the turbulence characteristics or flow depths differ. The relative Shields number or mobility ratio, defined as:

$$\left(\frac{\theta}{\theta_{cr}} \right)_{\text{Field}} = \left(\frac{\theta}{\theta_{cr}} \right)_{\text{Lab}}, \tag{2.6}$$

This shift in focus—from reproducing fluid dynamics to matching sediment response—offers a more practical and physically grounded strategy for bridging the gap between lab and field. It enables a better representation of scour patterns which are often distorted by traditional scaling methods. Veldhuizen et al. (2023) highlights that matching the Shields number alone is insufficient unless the corresponding scour development timescale is also considered. This is then the method selected for this research to scale from lab to field conditions.

However, scaling time is not a straightforward process. There are still different effects by choosing this method on the physical processes when compared the lab to field conditions. The main two aspects

observed in this research project are the scour magnitude and the temporal evolution of scour, therefore effects on both are addressed in this section.

Scour magnitude is influenced by several parameters that are not always properly scaled. For instance, Ettema et al. (2006) found that pile diameter significantly affects scour depth when other variables are held constant. Specifically, larger pile diameters tend to result in shallower equilibrium scour depths, an effect that might be important for mobility-similarity scaling. In the present study, while the grain size and bed mobility conditions are maintained between scales, the pile diameter increases in the field-scale model. As a result, a reduction in scour magnitude is expected.

Additionally, Ettema et al. (2006) reported that the maximum vorticity in the wake of a smaller cylinder was approximately twice that observed behind a larger cylinder under identical flow conditions. This indicates that smaller cylinders induce stronger wake vortices, which in turn are more effective at entraining sediment. These vortices can promote sediment mobilization by lifting particles upward through spiral upwelling in the wake region.

Consequently, laboratory-scale models may overestimate scour intensity due to the disproportionately enhanced sediment transport driven by stronger vortices, particularly in the wake region.

The temporal evolution of scour, as shown in Equation (2.5), is influenced by factors such as flow velocity, equilibrium scour depth and also the dimension of the structure, which do not scale linearly. In response to this, a dimensionally consistent approach to time scaling is needed.

To this end, Broekema and de Wit (2025) proposes an empirical scaling relation for $S_{\mathrm{eq,field}}$, based on laboratory-scale results for monopiles, as shown in Equation 2.7. These relations are for local scour development. As previously discussed, one of the dominant scaling effects on scour depth around piles arises from the ratio between pile diameter and sediment grain size. This effect already mentioned by Ettema et al. (2006) is captured in the formulation by Sheppard (2003) through the function $f_2(D_p/D_{50})$, which is incorporated into the factor n_s. The factor n_s quantifies the influence of grain-to-structure scaling, while the geometric scaling itself—such as differences in pile diameter between lab and field—is represented by the factor n. Additionally, when dealing with live-bed conditions, a correction factor ω_s is introduced to account for the increased sediment transport activity associated with such flow regimes.

$$S_{\mathrm{eq,field}} = \omega_s \, n_s n \, S_{\mathrm{eq,lab}}. \tag{2.7}$$

Once the field-scale equilibrium scour depth $S_{\mathrm{eq,field}}$ is obtained, it can be used in the time scale relation (Equation (2.5)) to yield the expression for the characteristic scour time at field scale:

$$T_{c,\mathrm{field}} = \frac{n_s^2 n^2 S_{\mathrm{eq,lab}}^2}{n_d^3 U_{\mathrm{lab}}^3} = \frac{n_s^2 n^2}{n_d^3} T_{c,\mathrm{lab}}. \tag{2.8}$$

For the live-bed regime, additional correction factors are necessary to account for the increased sediment mobility as well on the timescale scaling. The details of the formulations and correction factors are shown in in Appendix A.

These analytical formulations offer a practical framework for extrapolating laboratory-scale scour timescales to field conditions for monopile foundations. However, their application to 4LJ has not yet been explored.

The literature reviewed in this section serves as a starting point understanding the flow dynamics and scour behavior around monopiles both in lab and field conditions, to then build up what can be expected for 4LJ foundations.

2.2. Case study: Lab experience with a 4-legged jacket under different regimes.

In this research project, a laboratory case study for a 4LJ on clear water and live bed regime is used for model assessment and validation. The case is based on the experimental work of Welzel et al. (2023), which investigates scour development around a jacket structure under steady current conditions.

This section presents a detailed description of the experimental setup and results, providing the necessary foundation for later comparison with the model outcomes.

2.2.1. Experimental Setup

The experiment was conducted in the 3D wave and current basin at the Ludwig-Franzius-Institute, Leibniz Universität Hannover, Germany. The experimental setup involved measuring current-induced flow velocities and scour development around the jacket structure using various acoustic sensors.

The measurement of velocities was made to identify the velocity profile and to calculate the velocity near the bed. To monitor scour development around the structure, eight small echo sounders (Ultrasonic Ranging System - URS) were installed at various positions near the piles. These devices, mounted 25 cm above the seabed, recorded scour depth with a 1 mm vertical resolution. The positioning of the sounders was based on expected areas of maximum bed shear stress amplification, particularly at approximately $45°$ to the flow direction. It can be observed the position of this sensors on Figure 2.2. Additional sensors were placed between the upstream and downstream piles to provide further insights into global scour progression. Calibration tests ensured measurement accuracy, though large amounts of suspended sediment occasionally interfered with the acoustic signals.

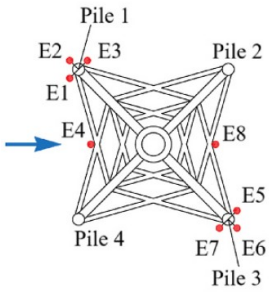

Figure 2.2: Schematic plan view of the positioned echo sounders

The jacket model used in this study is a scaled representation of an offshore foundation, with its dimensions illustrated in Fig. 2.3. The total height of the structure is 158.89 cm, with a base width of 59.56 cm from the end of one pile to the other and a top width of 20.53 cm. The pile diameter is 4 cm, and the braces have a diameter of 2.22 cm.

The domain of the test is shown in Fig. 2.4, where the length on the current side for the bed is 8 m, with 6.6 m as the width of the bed. The inlet velocity (U_0) is applied at the left boundary, while the outlet is positioned at the right side. It can also be observed the location of the ADVs and also a sediment trap located on the downstream side of the bed.

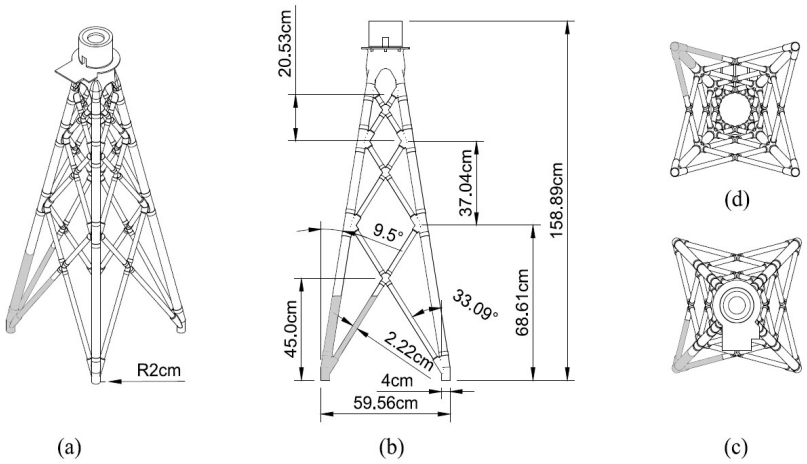

Figure 2.3: Schematic view of the jacket model with dimensions and angles. (a) Isometric view, (b) side view, (c) top view and (d) bottom view.

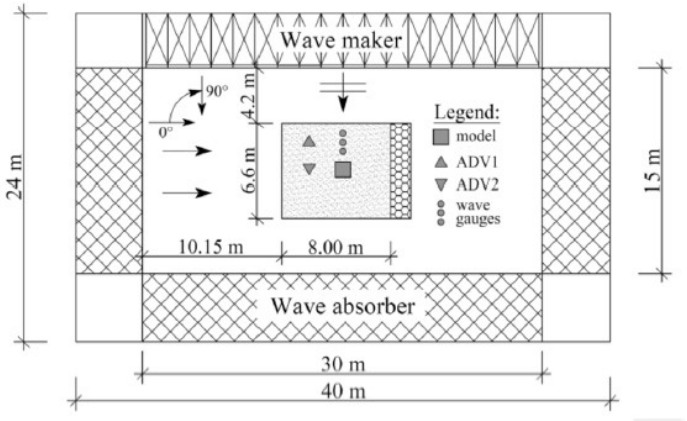

Figure 2.4: Setup of the basin for the test.

As explained before this experiment took into account two bed regimes, clear water and live bed. The general conditions for the experiment are defined in Table 2.1 as the experimental parameters, and the specific variables for each experiment on different bed conditions are defined on Table 2.2. For further detail on the experimental setup refer to Welzel et al. (2023) and Welzel et al. (2019).

Parameter	Value	Unit
Scale to real conditions	1:45	-
Diameter of pile	0.04	m
Water depth	0.66	m
D50	0.19	mm
Density of sand	2.65	g/cm^3

Table 2.1: Experimental parameters.

2.2.2. Results of the case study

The morphological data obtained from the laboratory experiments can be categorized into two main types. The first type consists of 3D bed scans taken at specific time intervals during the experiment—namely, after 15 minutes, 90 minutes, and 420 minutes. These scans, which are also presented in

Case	Parameter	Value	Unit
Clear water regime	Depth-averaged current velocity	0.24	m/s
	Current velocity 10 cm above bed	0.225	m/s
	Shields number	0.033	-
	Mobility criterion	0.67	-
	Flow velocity ratio	0.76	-
	Test duration	420	min
Live bed regime	Depth-averaged current velocity	0.42	m/s
	Current velocity 10 cm above bed	0.388	m/s
	Shields number	0.084	-
	Mobility criterion	1.7	-
	Flow velocity ratio	1.31	-
	Test duration	420	min

Table 2.2: Hydrodynamic parameters for clear water and live bed regimes.

the result figures, provide high spatial resolution over the entire domain but are limited in temporal resolution. All these results can be observed on Figure 2.5.

The second type of data is collected using echo sounders, which provide much more frequent time-series measurements, but only at localized points within the domain. Although this method lacks the spatial coverage of the 3D scans, it offers a much finer temporal resolution. The vertical accuracy of this measurements was calibrated around 1-2 mm.

This combination of data sources allows for a comprehensive analysis by covering both spatial and temporal dimensions of the morphological evolution.

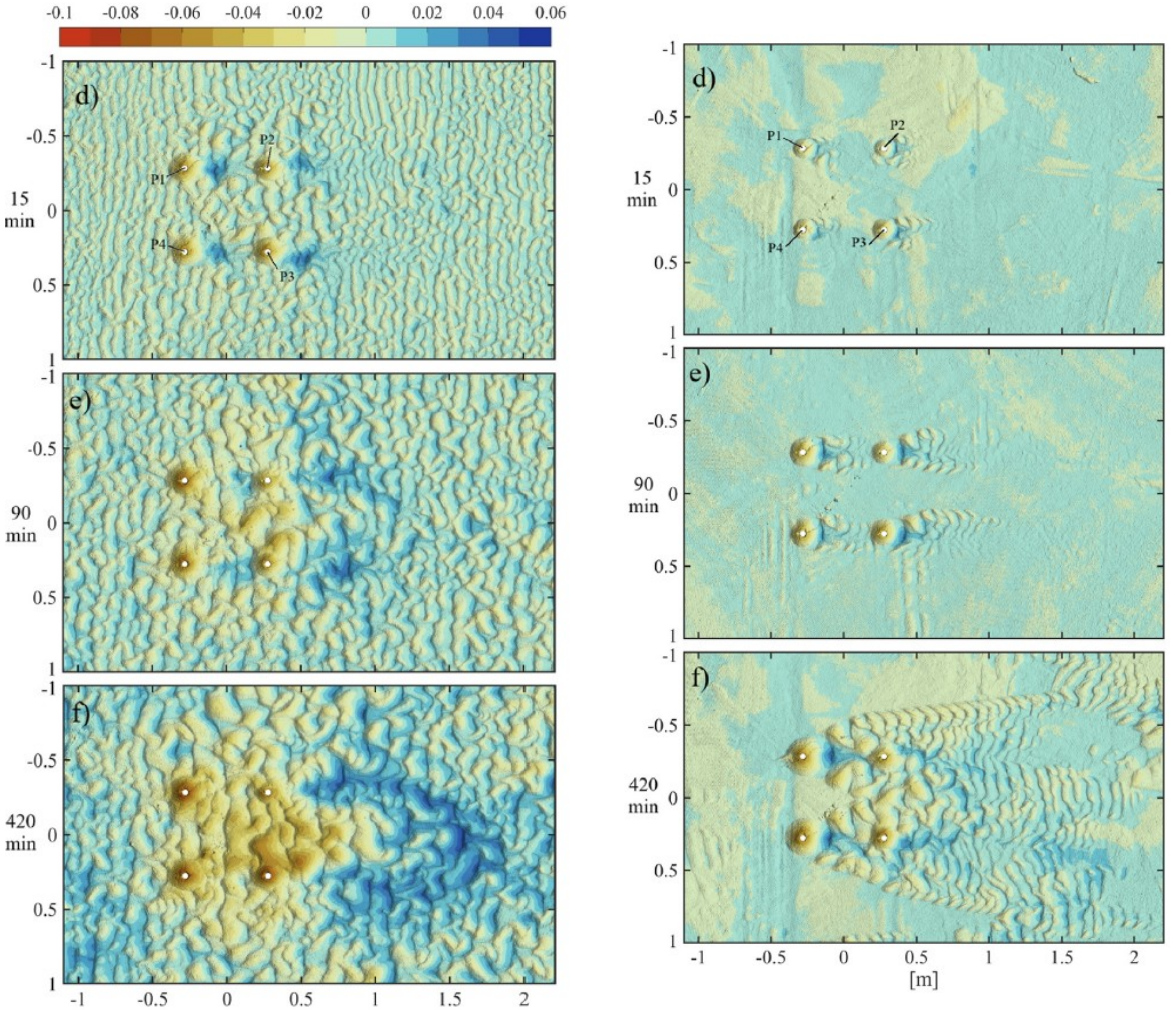

(a) Results for the live bed regime - Welzel, 2023

(b) Results for the clear water regime - Welzel, 2023

Figure 2.5: Comparison of results for live bed and clear water regimes.

The results indicated that local scour depths around the front piles reached approximately 1.5 S/D and 1.7 S/D for the clear water and live bed regime respectively, while the rear piles experienced scour depths of about 1 S/D and 1.4 S/D respectively, showing that for upstream piles, when compared to downstream piles, and for live bed regime, when compared to clear water, the scour magnitude is higher. The extent of the local scour around the piles was observed to be around 1.5 D.

The pile gap ratio was around $12G/D$. Regarding global scour, depths ranged from $0.2S/D$ to $0.6S/D$, with higher erosion occurring on the downstream side, only for live bed conditions.

A comparison of dimensionless time scales revealed a slower scour rate at the jacket structure compared to a monopile for the local scour around the piles. Also that live bed regime had a higher scour rate than clear water. According to the dimensionless timescale calculation, live bed regime reached equilibrium while clear water did not, probably based on the smaller rate observed.

2.3. State of the Art of jacket foundations scour and flow behavior

This section provides a review of existing literature on experimental studies and CFD simulations related to jacket foundations as well as real cases from wind-farms in the north sea, serving as a foundation for this research and complementing what is observed on the case study.

2.3.1. Four-Legged Jacket Foundations - Laboratory scale

Two main studies have conducted experimental investigations for jacket foundations (Chen et al., 2023; Welzel et al., 2019), while two others have focused on numerical modeling (Ahmad et al., 2020; Satari et al., 2024). The case study explained on the previous section already includes the first one.

The other study by Chen et al. (2023) focused exclusively on current-induced scour, investigating various flow angles under clear-water conditions just below the critical Shields number. The pile gap ratio was approximately $G/D = 6$. The results showed that scour depth increased with both flow velocity and water depth. As the foundation angle varied, the shielding effect of the front pile on the rear pile weakened, exposing the back pile directly to the incoming flow. Additionally, reducing the longitudinal distance between the front piles intensified jet flow effects. In terms of magnitude, the maximum scour depth reached approximately $1.5S/D$ on the front piles, comparable to the values reported by Welzel et al. (2023), despite the closer pile spacing. A significant difference was observed between the front and back piles, with the back pile experiencing considerably lower scour depths, around $0.5S/D$, highlighting the importance of the gap in between piles as a matter of the influence it has on the scour magnitude.

On the numerical side, one of the studies is directly related to the previously mentioned experimental research. Satari et al. (2024) developed a hydrodynamic model of the geometry used in Welzel et al. (2023) to validate the hydrodynamic model and gain a deeper understanding of the flow dynamics around jacket structures. The results were compared to existing knowledge of pile groups. It was observed that there was influence on the flow patterns between piles for pile spacing between $9G/D$ and $20G/D$, despite the relatively large gap ratios, larger than what was observed for groups of piles.

Regarding flow patterns, it was observed the presence of strong down flow at the inner lateral sides of the main piles, indicating regions of intensified vortex activity and scour development. Moreover, the study emphasized how structural components beyond the main piles influence vertical flow dynamics. The amplification of horizontal velocities reached a magnitude of 1.5 when compared to the inflow velocities around the piles, with a decrease on intensity on the downstream piles.

The bed shear stresses observed in jacket foundations were higher than those in monopile cases and exhibited asymmetry, unlike the more uniform distribution seen around a monopile. The amplification of bed shear stresses reached around 7 to 8, with higher magnitudes on the upstream piles.

The second numerical study by Ahmad et al. (2020) incorporated wave-induced scour and included a single simulation under current-only conditions, with a critical Shields parameter of 0.05. The scour depths observed for this jacket foundation ranged between $0.85S/D$ and $1.35S/D$, consistent with values reported for similar structures. The study considered a gap ratio of $G/D = 10$, which aligns with typical values for jacket foundations. The numerical results showed an average scour depth of approximately $0.8S/D$ under combined wave and current conditions, while under current-only conditions, the scour depth was slightly lower at $0.7S/D$. These values suggest a potential underestimation of scour development in jacket foundations. However, the study reaffirmed the trend that rear piles experience reduced scour, with depths around $0.5S/D$.

An interesting contrast emerged when comparing this study to Satari et al. (2024). In the numerical model by Ahmad et al. (2020), there was no apparent interaction between the disturbed flow from the upstream pile and the downstream pile. This differs from the findings of Satari et al. (2024), where flow interactions were observed even at a larger G/D ratio, suggesting differences between models.

2.3.2. Four-Legged Jacket Foundations – Field Scale Observations

While laboratory experiments provide valuable insights into scour development, real-scale field measurements are a final confirmation for validating these results and eliminating potential scaling effects. Therefore, it is crucial to analyze full-scale observations and compare them.

In this state-of-the-art review, three different studies on jacket foundations in the North Sea are considered, each conducted under similar physical conditions.

First, (Rudolph et al., 2004) presented results from a site five years after installation. The conditions at the site included a current velocity of 1 m/s, a median grain size $D_{50} = 0.2$ mm, and a pile diameter $D = 1.2$ m. The leg spacing varied between 16 and 20 meters, leading to a G/D ratio of approximately

16, which is larger than in many other jacket structures. The water depth at the site was around 24 meters, corresponding to a Shields number of approximately 0.2, indicating live-bed scour conditions. The results showed scour depths reaching up to three times the pile diameter ($S/D \approx 3$), significantly higher than expected. This value may be attributed to the connection between the pin piles and the jacket structure, effectively increasing the equivalent foundation diameter, making it 2 times the pin diameter. The geometry locally then differs in the foundation with the case of this research study. It was also observed global scour around the jacket, with a footprint of round 2 to 2.5 times the jacket extension, giving an idea that the extension of global scour goes beyond the jacket.

Another case study by (Bolle et al., 2012) investigated jacket foundations on the fields as a four legged case, with a water depth of 25 meters and a current velocity of 0.6 m/s. The typical scour conditions were reached within just one month. Although the seabed consisted of a sandbank, the grain size was not specified, preventing an exact Shields number calculation. However, given the similarities to other cases, live-bed conditions are a reasonable assumption. The scour depth ranged from $S/D \approx 0.65$ before jacket installation to $S/D \approx 0.85 - 1.35$ after installation, which aligns with expected values.

Harris and Whitehouse (2021) examined scour around jacket foundations in the North Sea with a pile diameter of 1.5 m, a water depth of 25 meters, and a median grain size of $D_{50} = 0.16$ mm. The site experienced a depth-averaged current velocity of 1 m/s, leading to a Shields number of approximately 0.3, again indicating live-bed conditions. This reinforces the notion that live-bed scour is the dominant regime under real-scale offshore conditions. The results showed S/D values ranging from 1.1 to 1.3, in agreement with previous studies.

In addition, significant global scour was observed, along with clear interactions between piles at a G/D ratio of 13—exceeding the independence threshold typically suggested in the literature. The presence of secondary elements such as buried cables and tubes was found to intensify scour in their vicinity, emphasizing the importance of accounting for such structures in scour assessments.

In summary, real-scale field measurements confirm the relevance of laboratory results while also highlighting key differences. One important distinction is that laboratory studies typically do not account for wave-induced backfilling when they only take into account current velocities, which can partially refill the scour hole over time and reduce its final depth. As a result, lab experiments tend to capture the worst-case scenario, yielding slightly higher scour depths compared to field conditions. Despite this, the magnitudes of scour depths observed in both contexts remain comparable—often within the same range of S/D—suggesting that the underlying processes are well-represented in scaled models. Additionally, the current velocities recorded in the field (typically between 0.6 and 1.0 m/s) are similar to those used in laboratory setups, supporting the applicability of the lab-derived results. However, when interpreting maximum scour values from experimental studies, it is important to consider that field conditions may be moderated by additional mechanisms such as sediment backfilling and wave action, which can make the scour phenomenon more dynamic, having also a longer timescale in terms of equilibrium to reach.

2.4. Governing equations and turbulence modeling

This research aims to use a CFD LES model to replicate scour development around jacket foundations and enhance the understanding of the underlying physical processes. Accurately modeling such complex flow conditions requires solving the fundamental equations governing fluid motion and turbulence. This section presents the governing equations and key concepts necessary to simulate these flows, including the conservation of mass and momentum, as well as the selected turbulence modeling approach. Additionally, the computational model employed in this study is introduced, along with a description of its capabilities and numerical implementation.

2.4.1. Conservation of mass and Navier Stokes

In this research project, we aim to represent the hydrodynamics of flow around our structure. To achieve this, the governing equations that describe the fluid motion are presented. The conservation of mass and momentum, with the Navier Stokes equations that represent momentum are formulated in three

dimensions, as all spatial axes are considered in this study..

$$\frac{\partial \rho}{\partial t} + \frac{\partial (\rho u)}{\partial x} + \frac{\partial (\rho v)}{\partial y} + \frac{\partial (\rho w)}{\partial z} = 0 \tag{2.9}$$

$$\begin{aligned}
\rho \left(\frac{\partial u}{\partial t} + u\frac{\partial u}{\partial x} + v\frac{\partial u}{\partial y} + w\frac{\partial u}{\partial z} \right) &= -\frac{\partial p}{\partial x} + \mu \left(\frac{\partial^2 u}{\partial x^2} + \frac{\partial^2 u}{\partial y^2} + \frac{\partial^2 u}{\partial z^2} \right) \\
\rho \left(\frac{\partial v}{\partial t} + u\frac{\partial v}{\partial x} + v\frac{\partial v}{\partial y} + w\frac{\partial v}{\partial z} \right) &= -\frac{\partial p}{\partial y} + \mu \left(\frac{\partial^2 v}{\partial x^2} + \frac{\partial^2 v}{\partial y^2} + \frac{\partial^2 v}{\partial z^2} \right) \\
\rho \left(\frac{\partial w}{\partial t} + u\frac{\partial w}{\partial x} + v\frac{\partial w}{\partial y} + w\frac{\partial w}{\partial z} \right) &= -\rho g - \frac{\partial p}{\partial z} + \mu \left(\frac{\partial^2 w}{\partial x^2} + \frac{\partial^2 w}{\partial y^2} + \frac{\partial^2 w}{\partial z^2} \right)
\end{aligned} \tag{2.10}$$

where ρ is the fluid density, u, v, w are the velocity components in the x-, y-, and z-directions, respectively, p is the pressure, and μ is the dynamic viscosity. The viscosity term, multiplied by the velocity gradient, represents the gradient of the shear stress tensor.

In this case density is not considered constant, where it is defined depending on the concentration of sediment fractions. This is done to solve more accurately close to the bed. The concentration is solved by the classical transport equation from advection and diffusion as seen in 2.11

$$\frac{\partial C}{\partial t} + \nabla \cdot (\mathbf{u}C) = \nabla \cdot (\Gamma \nabla C), \tag{2.11}$$

with the diffusion coefficient $\Gamma = \frac{\nu}{Sc}$, a Schmidt number ($Sc = 1.0$ is used), and ν is the kinematic viscosity. Using these concentrations, the mixture density can be obtained by:

$$\rho = \rho_a + (\rho_s - \rho_a)C, \tag{2.12}$$

with ρ as the mixture density, ρ_a as the ambient density, and ρ_s as the sediment density.

2.4.2. LES as an eddy resolving technique

This is one of the most important concepts that needs to be understood in this research, and it revolves around equation 2.10 in the term related to the shear stresses. This term differentiates how turbulence is solved. There are three different turbulent closures used for this term:

- Direct Numerical Simulation **(DNS)**: All turbulence is solved directly in the model.
- Large Eddy Simulation **(LES)**: As the name suggests, the larger energy turbulent scales are resolved, while smaller turbulent scales are modeled with a sub-grid scale model.
- Reynolds-Averaged Navier-Stokes **(RANS)**: All turbulence is modeled using a turbulence model, employing the Boussinesq approximation and Reynolds averaging on velocity.

In the following image, an overview of these three closure types is presented:

Reynolds number (Re) is a key parameter used to quantify the turbulence level of a flow. When performing DNS with highly turbulent flows ($Re > 10^4$), the Reynolds number inversely correlates with mesh size. This means that as turbulence intensity increases, a finer grid is required to accurately capture the turbulent eddies (Cimarelli et al., 2018).

Grid resolution is also linked to the size of turbulent eddies. To properly resolve an eddy in a CFD mesh, at least four grid cells are required (Mansouri et al., 2022). Consequently, grid size becomes a crucial parameter. In DNS, grid sizes are generally very small, especially for highly turbulent cases, since all turbulent kinetic energy scales must be resolved, including smaller eddies that will represent small mesh sizes. This makes DNS computationally expensive.

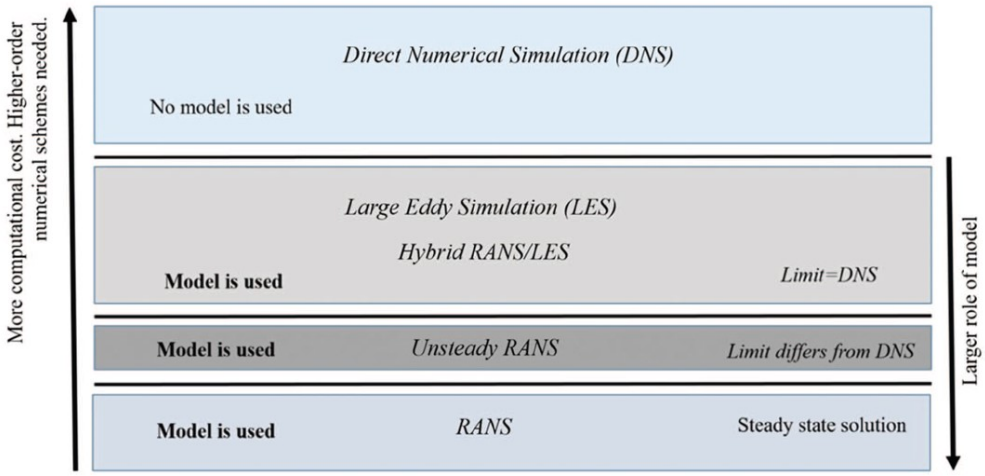

Figure 2.6: Comparison of DNS, LES, and RANS turbulence closures.(Lai et al., 2022)

Large Eddy Simulation (LES) provides a hybrid approach, where the larger, energy-containing eddies are resolved, while the smaller eddies are modeled using a sub-grid scale model. As previously mentioned, the effectiveness of LES depends on grid size. According to (Pope, 2000), at least 80% of the total turbulent kinetic energy must be resolved for a simulation to be classified as LES.

In RANS, unsteady turbulent time filtered eddies are not directly resolved but instead modeled through turbulence closures. This leads to time a filtered representation of the turbulent flow, which may not accurately capture the full complexity of the flow field in highly turbulent scenarios. In contrast, LES offers a more detailed approach by explicitly resolving the larger turbulent structures while modeling only the smaller scales (spatially filtered). This makes LES a suitable compromise for capturing complex turbulent phenomena with greater fidelity than RANS, without incurring the prohibitive computational cost of DNS.

Summary

This chapter has examined the fundamental processes governing scour around offshore structures and provided a focused analysis on how these manifest in the context of jacket foundations. While much of the theoretical foundation stems from research on monopiles, the literature clearly highlights the added complexity introduced by pile group interactions and structural geometry in jackets. Observations from laboratory and field studies confirm the prevalence of both local and global scour, with live-bed conditions often dominating in real-scale environments. The reviewed scaling strategies and scour time evolution models offer valuable tools, although their extension to jacket foundations—particularly four-legged configurations—remains limited. This body of knowledge sets the foundation for the present research by guiding model selection, parameter scaling, and the interpretation of scour behavior under field-relevant hydraulic conditions.

3

Methodology

This chapter outlines the methodological framework adopted to evaluate scour processes around offshore jacket foundations using the CFD model TUDflow3D. The overall methodological workflow followed in this study is illustrated in Figure 3.1. It begins with the general model setup, where the mesh configuration, domain size, and global numerical parameters are defined.

The approach follows a structured progression, beginning with the numerical model description followed by the setup, where the numerical configuration—covering mesh generation, domain definition, and parameter settings—is established as a general template for all simulations.

From this foundation, the methodology branches into two parallel components: laboratory-scale model assessment and field-scale numerical modeling.

The model assessment phase evaluates performance by comparing numerical results with experimental data from laboratory tests conducted by Welzel et al. (2023). This section details the laboratory-scale model configuration, the comparison methodology, and the rationale for performing a sensitivity analysis on key numerical parameters, including the morphological acceleration factor, relaxation factors, numerical domain and grid size. This will be done on Chapter 4

Following validation, the methodology advances to field-scale simulations using a mobility-based scaling approach. This involves adjusting flow velocities and domain dimensions to preserve sediment mobility similarity between scales. The scaling procedures applied are described in this section, and the results are shown on Chapter 5.

The final methodological step involves a detailed analysis phase, leveraging the model's flexibility to investigate practical aspects of scour behavior beyond validation and scaling, focusing on results with direct engineering relevance. The results for this will be presented in Chapter 6.

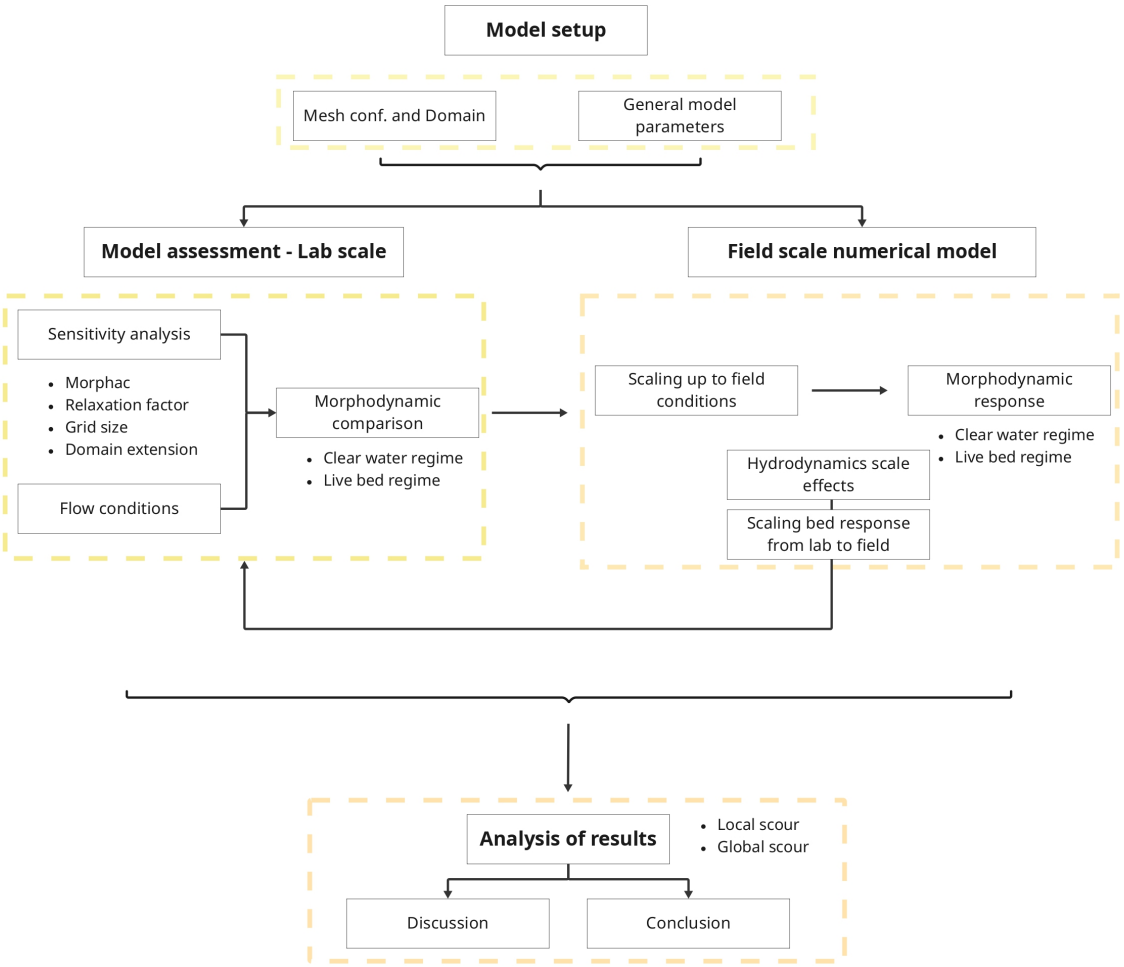

Figure 3.1: Methodology flow chart

3.1. CFD LES Model Description

This section outlines the selection and justification for using the model TUDflow3D. Three-dimensional CFD models are commonly employed to investigate localized fluid–structure interactions due to their capacity to accurately capture turbulent flow behavior. The choice of TUDflow3D is supported by previous research demonstrating the effectiveness of LES in predicting scour around monopiles and jacket structures. de Wit et al. (2023) validated this modeling approach for local scour prediction for an OHVS Horselle jacket. Additionally, Lai et al. (2022) emphasizes that LES provides improved accuracy over other models for simulating flow around complex structures with turbulent flow behavior, reinforcing its potential as a valuable tool for future studies.

Given these advantages, TUDflow3D is employed in this study. Regarding the discretization of the governing equations (see 2.4), the time integration of the advective, viscous, pressure, and force terms is performed using a third-order Adams-Bashforth scheme. Momentum advection is modeled with a stable artificial viscosity scheme (de Wit & van Rhee, 2013), which effectively damps numerical wiggles while preserving physical scales. This feature ensures that the artificial viscosity scheme does not replace the function of a sub-grid scale model. The HY6 convection scheme is used in combination with the Adams–Bashforth method for time discretization.

For turbulence modeling, the WALE-LES sub-grid scale model (Nicoud & Ducros, 1999) is utilized with a constant $C_s = 0.325$. As mentioned earlier, most of the TKE is resolved, while the unresolved smaller eddies are accounted for by the sub-grid scale model. A key advantage of the WALE model is that

it produces zero viscosity for pure shear flow and near solid walls, eliminating the need for damping functions to force turbulent viscosity to zero at walls, in comparison to Smagorisnky sub-grid scale model. This is particularly beneficial when using immersed boundaries with irregular shapes, as in this study.

The model simulates both suspended and bedload transport, and has a morphodynamic update every timestep to simulate the erosion. The erosion flux or sediment pick-up is based on (van Rijn, 1984), while bedload transport follows the bedload formula from (van Rijn, 2007), and the suspended transport is with the advective-diffusion equations in three dimensions for sediment transport. The total bed-update results from the combination of spatial gradients in bedload transport and suspension load contributions.

The sediment bed shear stress is determined depending on the sediment transport relation used for. For the flow and bedload relations is used the flow velocity from the first computational cell above the bed, which lies within $0.5\Delta z$ to $1.5\Delta z$ from the bed, while for the suspended load is used the maximum of the first two cells, to have a better approximation of the vertical velocity for the pickup. The velocity component parallel to the local bed slope is used for the computation of the bed shear stresses to calculate bed load, while sediment pickup acts perpendicular to it.

Obstacles and the sediment bed within the computational grid are treated using an immersed boundary method (IBM), which forces the flow velocity inside bed or obstacle cells to zero. The bed level can vary continuously between $-0.5\Delta z$ and $+0.5\Delta z$ around the topmost computational bed cell. If the bed level falls below $-0.5\Delta z$, the topmost bed cell is lowered by one layer. Conversely, if it exceeds $+0.5\Delta z$, the topmost bed cell is raised by one layer. This approach ensures sediment mass conservation and allows a gradual transition between erosion and deposition states without abrupt changes.

An avalanche routine is included to prevent unrealistically steep bed slopes. If the slope between neighboring cells exceeds the user-defined avalanche slope, sediment is redistributed from higher to lower elevations as an instantaneous bedload adjustment to maintain the threshold slope.

For a more detailed discussion on the model, discretization of physical phenomena, and underlying assumptions, please refer to (de Wit, 2015; de Wit et al., 2023).

3.2. Model Setup

In this section the model setup is explained, which involves the definition of the mesh, domain and obstacle, as well as the numerical settings chosen for the simulation and the physical relations used for it, that are called model parameters. This is done as a general model setup, that is used both for lab scale and field scale models. The specific numerical parameters that are part of the different scaling and regimes will be addressed in their own sections.

3.2.1. Mesh and Obstacle Definition

In order to be able to define the conditions of the simulation, one of the first decisions to be made is the domain size. The domain should guarantee physical enough space for the flow to behave as it would be in open waters, avoiding blockage issued and boundary effects. Following the approach used by de Wit et al. (2023), the domain is scaled relative to the footprint of the jacket, for practical purposes.

As a frame of reference, the x-axis is aligned with the current direction, the y-axis is perpendicular to it in the horizontal plane, and the z-axis represents the vertical direction (depth). The current flows from left to right along the x-direction.

In the present model, the inflow turbulence is generated using the Synthetic Eddy Method (SEM), which superimposes velocity fluctuations onto an imposed logarithmic velocity profile at the boundary, representing realistic flow conditions. As recommended by Jarrin et al. (2008), the SEM requires an adaptation length of approximately five to ten water depths from the inflow boundary to allow the turbulence to reach equilibrium. This development is necessary to achieve realistic turbulent velocity profiles and to accurately represent hydrodynamic turbulence.

To prevent issues, de Wit (2015) advises extending the domain upstream—aligned with the main flow direction—and disabling morphological updates over the first five water depths. This approach allows

the flow to develop correctly. From the fourth water depth onward, the morphological updating should be gradually activated until full updates are applied, ensuring a smooth transition and preventing spurious dune formation near the inflow boundary.

In this case it was adopted a larger domain upstream the domain following the inclusion of five water depths for the flow to develop correctly, resulting in 12 times the footprint in the x-direction (current direction) and 4 times the footprint in the y-direction (perpendicular direction). This differs from the domain used by de Wit et al. (2023), where is used 6 times the jacket footprint as the domain on the current direction. It is important to note that the jacket structure is positioned at the center of the axis, on the 0,0,0 position, resulting in both negative and positive coordinates along the x- and y-axes.

The geometry for the jacket comes from Welzel et al. (2023), lended through an stl. file that can be inserted on the domain already defined as observed on Figure 3.2. It can also be observed that the piles go through the sand bed as expected and continue until the end of the domain in z. This was added as an extra geometry feature to ensure continuity throughout the simulation, in the fluid-structure interaction.

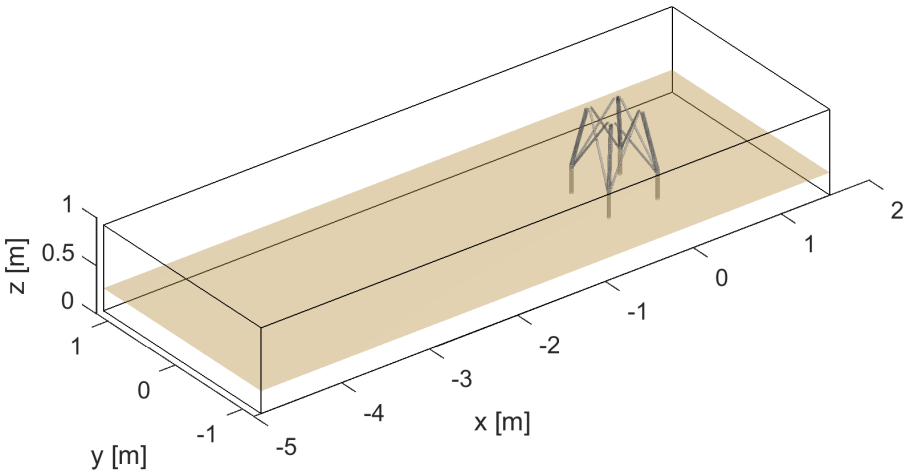

Figure 3.2: Jacket foundation in the domain with the sand bed - Lab scale

Once the domain is defined, the distribution of the grid size also needs to be defined. The grid size acts as a filter to delimit what eddies are solved or not, or a filter on how much TKE is solved and therefore how much is modeled. As done before, on (de Wit, 2015; de Wit & van Rhee, 2013) and as a rule of thumb is estimated that for this model and this specific conditions, at least you require around 10 cells per structure to be able to achieve the required threshold. This can help us to determine the grid size depending on our geometry.

The mesh is defined by the number of cells in each direction, the grid spacing, and a growth factor. The grid configuration features a refined region at the center of the domain in both the x- and y-directions, where the jacket will be located. As shown in Figure 3.3, the minimum cell size is applied around the piles and the perimeter of the jacket footprint, while a coarser resolution is used within the jacket's center. This is done for optimizing the number of cells used for computation.

The minimum grid size is set as D/10 as done by de Wit et al. (2023) where D is the pile diameters in contact with the sand bed. Although the jacket includes structural elements with smaller diameters, like the tilted braces, these are assumed to have less impact in flow dynamics, allowing a coarser mesh resolution. Therefore, they are not considered in the mesh refinement to avoid excessive computational cost, which would result from requiring finer resolution across all three dimensions.

For the outer region—beyond the footprint of the jacket a grid size of 3 times the minimum grid size is adopted on the upstream side of the flow and on the y direction. This choice is consistent with the mesh size selected in the z-direction, which is also D/10, to ensure a symmetric and structured mesh in

the central region. A refinement ratio of 3 between dimensions is maintained, following good practices for 3D simulation meshing to ensure stability.

For the vertical direction (Z), the minimum cell height is used uniformly, as variable resolution in this direction is not possible due to the software setup.

With these conditions, the mesh is generated, as shown in Figure 3.3, comprising 53.5 million cells. Figure 3.3 illustrates the distribution of grid sizes along the different axes.

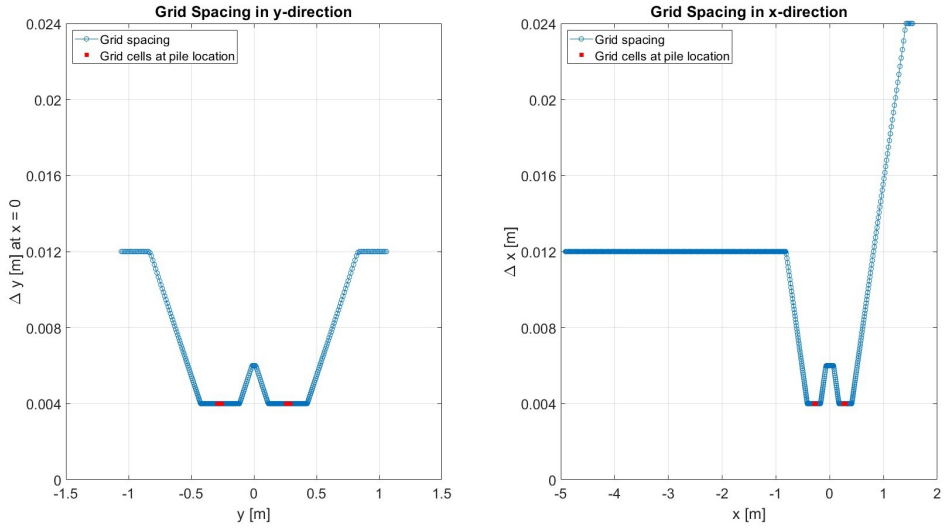

Figure 3.3: 2D mesh distribution along the x- and y-axes for the numerical model - Laboratory scale

3.2.2. Model parameters

With the mesh and geometry defined, additional numerical and physical model parameters must be specified. These parameters are summarized in Table 3.1 for clarity and detailed in this section.

Once the grid size is set, as defined in the previous section, the computation of the timestep needs to be limited. The CFL criterion can be used for this purpose,and a CFL number of 0.5 is adopted throughout the domain. Although the Adams–Bashforth time integration scheme is stable up to a CFL number of 0.67 (Deriaz & Haldenwang, 2020), a conservative value is preferred to ensure numerical stability.

Due to the high number of cells, the use of a morphological acceleration factor (Morphac) is proposed. This is a multiplier applied to the bed level change per hydrodynamic time step in order to simulate longer-term morphological development (Ranasinghe et al., 2011). The selection of the value will be discussed and specified for each numerical model in the regarding section.

For clarity in this report, morphological time refers to the evolution of bed levels under the influence of the morphological acceleration factor (Morphac). Computation time denotes the actual runtime required to execute the simulation, while simulated time corresponds to the hydrodynamic time duration defined as input in the model.

A spin-up time is incorporated to allow the flow field to reach a quasi-steady state before sediment transport calculations begin. In this context, the spin-up period refers to the initial phase during which no bed updates occur, not taken into account on the morphological time. Its minimum duration is assumed as the time required for a fluid particle to traverse the domain more than two times along the x-axis, based on the depth-averaged inlet velocity.

Boundary conditions are defined as follows: a prescribed inflow is imposed at the left boundary, using velocity values derived from the experimental cases presented in Welzel et al. (2023). At the right boundary, an outflow condition with zero pressure is applied. Free-slip boundary conditions are used at the top and side boundaries.

At the bed, an erodible surface is defined with morphological updating enabled, with both erosion and deposition, combined with a partial slip boundary condition. In TUDflow3D, a wall model is employed to compute the bed shear stress based on the near-bed flow velocity. This approach avoids the need for near-wall mesh refinement, which would otherwise be required to resolve the velocity gradient near the bed. By relying on wall functions, the simulation becomes significantly more efficient and stable—an important advantage in morphodynamic modeling. The generalized wall function model by Shih et al. (1995) is used in this case. This model accounts for both pressure gradients and near-wall velocities in the estimation of bed shear stress. For further details on its formulation and implementation, refer to Shih et al. (1995).

The Nikuradse roughness length k_n is set to 2.5 times the median sediment grain size D_{50}, which is consistent across all cases. The threshold concentration for initiating bed update is set to 0.6, in accordance with the formulation described in Section 3.1. The settling velocity is estimated using the formulation for intermediate grain sizes proposed by van Rijn (1984), yielding a value of approximately $0.0195\ \mathrm{m/s}$.

The model can include relaxation factor for the near bed velocities and pressure gradient terms. In this case, a relaxation factor for the terms involving the bed load is chosen based on previous experiences de Wit et al. (2023) where it was found that this factor allows a better prediction of local scour. This relaxation factor acts to avoid big gradients on the computation of the near bed velocities, and it multiplying this factor to the new values in comparison to the previous ones. The one selected both for near bed velocities and pressure gradients is 0.001. On the following equation the computation of the relaxed value on time can be observed, where i serves as an index for the timesteps.

$$\text{relaxed value}_{i+1} = \text{relaxation factor} \cdot \text{new value}_{i+1} + (1 - \text{relaxation factor}) \cdot \text{relaxed value}_i \quad (3.1)$$

The von Kármán constant is set to 0.41, while the avalanche slope is defined as 1:1.6 (V:H) to ensure physically realistic bed slope transitions. The roughness coefficient k_n for both sand pickup and bed load transport remains fixed at 2.5 D_{50}. Erosion scaling parameters are initialized to 1.0, as the focus of the validation is on assessing sensitivity to numerical parameters rather than empirical calibration.

Table 3.1: Summary of model parameters for all simulations

Parameter	Value
CFL number	0.5
Time discretization method	Adams-Bashforth
Convection scheme	HY6
Sub grid scale model	WALE-LES
Depth average velocity at the boundary in x	Case-dependent (Welzel et al. (2023))
Depth average velocity at the boundary in y and z	No velocity (0 m/s)
Nikuradse roughness k_n	$2.5 \times D_{50}$
Settling velocity	0.0195 m/s
Pick up formula	Van Rijn, 1984
Bed load formula	Van Rijn, 2007
Bed threshold concentration	0.6
Von Kármán constant	0.41
Avalanche slope	1:1.6 (V:H)
Calibration factors for erosion	Initially set to 1

3.3. Model Assessment - Laboratory scale numerical model

In this section is explained the methodology to evaluate the performance of the model by comparing its results with the laboratory experiments reported by Welzel et al. (2023). It is specified the specific parameters for the setup of the laboratory scale numerical model. It also includes the methodology for the observation of flow dynamics and for the sensitivity analysis. The results of this methodology will be presented in Chapter 4.

3.3.1. Model Parameters – Lab Scale

For the lab scale numerical model, the total morphological simulation time was set to 7 hours, consistent with the experimental duration reported by Welzel et al. (2023). A morphological acceleration factor (Morphac) of 100 was applied, reducing the total simulated hydrodynamic time to approximately 272 seconds while preserving the desired morphological response. As shown by de Wit et al. (2023), this acceleration factor does not significantly affect local scour development, thus supporting its use in this study. Further justification is provided in the sensitivity analysis (see Section 3.3.4).

Following the methodology described in the previous section, the spin-up time was determined based on the time required for a fluid particle to traverse the domain more than twice along the x-axis, using the depth-averaged inlet velocity. This resulted in a spin-up duration of approximately 26 seconds for the clear-water regime and 16 seconds for the live-bed regime. A conservative value of 30 seconds was adopted for both regimes in all simulations.

Given the presence of different flow regimes and distinct morphodynamic phenomena of interest, specific numerical setups were selected to accurately represent each case.

The configuration summarized in Table 3.2 was adopted for simulating local scour. This included a bed load relaxation factor of 0.001, a minimum grid size of $D/10$, and a domain extending 12 times the pile diameter in the x-direction and 4 times in the y-direction. For the live-bed regime, where global scour is expected to be more dominant, there was no relaxation factor on bed load, as this better captures the magnitude and temporal development of global scour. The rationale behind these parameter choices is further discussed and evaluated in the sensitivity analysis (see Section 3.3.4).

Table 3.2: Final setup – Lab scale

Regime	Morphac	Relaxation factor		Grid size	Domain extension
		Bed load	Susp. load		
Clear water regime	100	0.001	1	D/10	12x vs 4y
Live bed regime – Local scour	100	0.001	1	D/10	12x vs 4y
Live bed regime – Global scour	100	1	1	D/10	12x vs 4y

3.3.2. Morphodynamic comparison

The assessment is conducted through the morphodynamic response of the numerical model. The assessment will be divided into local scour and global scour, as it will be structure for the whole report, and inside each the different regimes will be analyzed.

For local scour, to facilitate a clearer comparison of the results, an error assessment methodology is introduced as part of the assessment process, which will be used in the sensitivity analysis and in the comparison of the morphodynamics results. It focuses on evaluating local scour at the locations of the echo sounders in the lab shown in Figure 2.2.

The primary metrics used for this comparison include the root mean square error (RMSE), expressed both as a percentage (RMSE%) of the maximum scour per pile to provide a relative measure, and in millimeters for an absolute perspective. The RMSE is computed between the lab data and the results of a model configuration. Additionally, the temporal evolution of scour is qualitatively assessed to complement the quantitative indicators. The RMSE percentage is defined as:

$$\text{RMSE\%} = \frac{\text{RMSE}}{\text{Max.scour at each location}} \times 100$$

To complement the analysis, the average scour depth around the pile is calculated at the three available time steps from the 3D bed scans, for both the numerical model and the laboratory measurements. This provides a spatially integrated assessment of scour evolution and enables direct comparison between the two datasets.

For the global scour assessment, two complementary approaches are adopted. First, a qualitative comparison is conducted using plan-view plots at the same three time steps, allowing visual evaluation of overall bed evolution and identification of key scour patterns in the model relative to the laboratory results. This is supplemented by echo-sounder data and the quantification of average scour depths of different areas around the jacket on the three timesteps available of the 3D scans, which supports a time series comparison and spatial comparisons at specific areas. Together, these allow for a more quantitative assessment of scour behavior at the time steps where 3D spatial bed information is available.

3.3.3. Observation of flow conditions

Understanding the flow behavior around the structure is crucial for evaluating the scour response in a morphodynamic model, given the strong relationship between flow amplification, bed shear stresses, and the resulting scour patterns (Satari et al., 2024). To investigate this, both velocity amplification and bed shear stress amplification are analyzed around the piles and across the entire structure, as it has been done before for these type of structures (Satari et al., 2024). Velocity fields are examined through horizontal slices at different elevations to assess the influence of the piles along the vertical extent of the flow, while bed shear stresses are evaluated on the bottom layer of the computational domain, representing the interface with the sediment bed.

TUDflow3D enables the storage of hydrodynamic variables such as velocity and bed shear stress during the spin-up phase of the simulation—when the bed is still fixed and not yet subject to morphological updating. This allows the model to effectively act as a purely hydrodynamic simulation during this period. For the laboratory-scale conditions, flow variables are stored between 20 and 30 seconds, and time-averaged values are computed over this interval.

This 10-second averaging interval is justified by Taylor's frozen turbulence hypothesis (Taylor, 1938), which assumes that turbulent structures are advected past a point with negligible change over time. Given the characteristic flow velocities used in the simulations—approximately 0.24 m/s for the clear-water regime and 0.42 m/s for the live-bed regime—and a turbulence macro-scale approximated by the jacket pile diameter, one can expect between 60 and 105 large eddy structures to pass during this 10-second window, which is statistically sufficient to provide meaningful time-averaged flow fields for interpreting hydrodynamic patterns.

Analyzing the flow field during this initial phase provides valuable insights into the expected bed response, particularly regarding regions of intensified shear that may trigger scour development, as well as the magnitude of this amplification both in velocities and bed shear stresses. Moreover, this approach facilitates comparisons with field-scale conditions by isolating hydrodynamic influences from morphodynamic feedback.

3.3.4. Sensitivity analysis

To evaluate the accuracy of the model in predicting scour development and to understand the influence of numerical parameters a sensitivity analysis is carried out. Different model configurations are tested and compared with experimental results. This analysis assesses how numerical choices affect model performance related to scour evolution.

For consistency, all simulations in the sensitivity analysis follow the same comparison methodology as used in the morphodynamic comparison section. The scour evolution is evaluated quantitatively using echo-sounder data and qualitatively through plan-view comparisons of global scour patterns. The analysis focuses on the influence of four key parameters: relaxation factors, Morphac, grid size, and model domain.

Although previous studies have shown that TUDflow3D is relatively not sensitive to morphac values below 400, it is important to verify this behavior in the present context, particularly for both local and global scour. This is especially relevant given that the morphac parameter significantly improves computational efficiency. Without its application, simulations could take several weeks or even months to complete, potentially limiting the model's feasibility for practical use. Therefore, confirming that Morphac does not significantly alter morphodynamic results is essential. Based on the sensitivity results, a value of 100 was selected for all other scenarios, representing a suitable compromise between sim-

ulation speed and accuracy.

The relaxation factor is included due to its key role in ensuring numerical stability and convergence in sediment transport computations. While it has been successfully applied in previous scour modeling studies, particularly for local scour around jacket foundations (de Wit et al., 2023), its effect on simulations involving the J4L configuration—especially in relation to global scour—has not yet been assessed. For the control setup in this sensitivity analysis, the same values used by de Wit et al. (2023) are adopted: 0.001 for bed load and 1 for suspended load.

The grid size is evaluated for two main reasons. First, it influences the resolution of the flow field and the scour patterns around structural elements. Second, grid refinement improves the geometric representation of the structure, which is expected to enhance the accuracy of scour predictions. However, finer grids significantly increase simulation time and computational demand, raising the question of feasibility for large-scale or long-duration morphodynamic models.

In this study, the minimum grid size, which serves as a reference on the mesh size dimensions, is defined based on the pile diameter. Two configurations are considered: a base case with a minimum grid size of D/10, and a finer mesh with D/13. A coarser grid was not tested, as it did not adequately represent the obstacle, making it unsuitable for producing accurate results.

The need for the extension of the domain upstream is also examined, both from a physical and computational perspective. A larger domain allows for the proper development of turbulence as stated before, which is essential for accurately capturing velocity fields around the structure. However, it also increases the total number of computational cells, thereby affecting simulation runtime. In this study, a domain of 12 times the jacket footprint on the current direction, compared to the 6 times used by (de Wit et al., 2023), results in nearly a 50% reduction in computation time. This highlights an important trade-off between physical accuracy and computational efficiency, particularly for long-duration morphodynamic simulations. For practical purposes, the control domain selected for the other sensitivity analysis was the 6x vs 4y, for a more efficient runtime, while also studying the effects and necesity of the extension of the domain upstream.

In summary, the simulations conducted for this section are presented in Table 3.3. These were performed under both clear-water and live-bed conditions to evaluate the model's sensitivity across regimes where experimental data is available for comparison.

Table 3.3: Sensitivity analysis simulations parameters

Model name	Morphac	Relaxation factor		Min. Grid size	Domain
		Bed load	Susp. load		
M10	**10**	0.001	1	D/10	6x vs 4y
M50	**50**	0.001	1	D/10	6x vs 4y
M100	**100**	0.001	1	D/10	6x vs 4y
M200	**200**	0.001	1	D/10	6x vs 4y
RFA	100	**0.001**	**1**	D/10	6x vs 4y
RFB	100	**0.001**	**0.001**	D/10	6x vs 4y
RFC	100	**1**	**1**	D/10	6x vs 4y
D/10	100	0.001	1	**D/10**	6x vs 4y
D/13	100	0.001	1	**D/13**	6x vs 4y
Smaller domain	100	0.001	1	D/10	**6x vs 4y**
Ext. Domain	100	0.001	1	D/10	**12x vs 4y**

[1] **Bold** values indicate the parameters being varied in each sensitivity scenario.

3.4. Scaling to field conditions

Following the model assessment and the evaluation of its performance, the next step is to leverage the validated setup to simulate scour under field-scale conditions. According to Welzel et al. (2023), the original laboratory experiments were conducted at a 1:45 scale. Then, this scaling number is used as reference to define the geometry and boundary conditions for the field-scale simulations under both flow regimes. The results of this methodology will be presented on Chapter 5.

3.4.1. Scaling methodology

For a dimensionally consistent scaling law that enables the comparison of laboratory and field conditions, mobility similarity is proposed as the scaling for this project. This criterion ensures that the ratio between the Shields parameter and the critical Shields parameter is preserved when transitioning from lab to field scale. Within this approach, sediment properties such as the median grain size D_{50} and relative density s are assumed constant. As a result, scale effects are primarily introduced through the equilibrium scour depth S_{eq}, the flow velocity U, and the geometry of the structure — typically characterized by the pile diameter in laboratory and field conditions. These parameters are adjusted to maintain a consistent mobility number $\theta/\theta_{\mathrm{cr}}$, as described in Equation (2.5).

The domain configuration also needs to be scaled. As in the laboratory-scale numerical models, the jacket footprint is used as a reference unit to define the domain extension. Specifically, the domain extends four times the jacket footprint in the y-axis, and either six or twelve times in the x-axis, depending on the case.

Table 3.4 summarizes the key geometric and sediment properties used in both scales. Most notably, the pile diameter increases from 0.04m in the laboratory to approximately 1.8 m at field scale, and the water depth scales up to nearly 30 m—values that align with typical offshore jacket foundation conditions. Sediment characteristics, such as grain size and density, are kept constant between scales.

Table 3.4: Geometric and sediment parameters for lab and field scale

Lab scale			Real scale		
Parameter	**Value**	**Unit**	**Parameter**	**Value**	**Unit**
Scale to real conditions	1:45	-	Scale number	1:1	-
Diameter of pile	0.04	m	Diameter of pile	1.8	m
Water depth	0.66	m	Water depth	29.7	m
D50	0.19	mm	D50	0.19	mm
Density of sand	2.65	g/cm^3	Density of sand	2.65	g/cm^3

From a hydrodynamic perspective, adjustments are made to the imposed flow velocities to maintain the same mobility criterion at full scale. Specifically, the boundary current velocity is increased by approximately 40%, resulting in a target depth-averaged velocity of 0.59m/s for the live-bed regime and 0.34m/s for the clear-water regime.

Table 3.5: Hydraulic and mobility parameters under different flow regimes for both lab and field scale numerical models

Lab scale			Field scale		
Parameter	**Value**	**Unit**	**Parameter**	**Value**	**Unit**
Live Bed Regime					
Depth averaged current velocity	0.42	m/s	Depth averaged current velocity	0.59	m/s
Critical velocity	0.29	m/s	Critical velocity	0.41	m/s
Critical Shields number	0.049	–	Critical Shields number	0.049	–
Shields number	0.089	–	Shields number	0.090	–
Reynolds	16,680	–	Reynolds	17,523,000	–
Mobility criterion	1.8	–	Mobility criterion	1.8	–
Clear Water Regime					
Depth averaged current velocity	0.24	m/s	Depth averaged current velocity	0.34	m/s
Critical velocity	0.29	m/s	Critical velocity	0.41	m/s
Critical Shields number	0.049	–	Critical Shields number	0.049	–
Shields number	0.030	–	Shields number	0.030	–
Reynolds	158,400	–	Reynolds	10,098,000	–
Mobility criterion	0.6	–	Mobility criterion	0.6	–

A time scaling approach was not applied in this study due to the current lack of a validated framework for translating scour development times from laboratory to field conditions for jacket foundations. Recent work by Silva-Muñoz and Broekema (2025) proposes a correlation between hydrodynamic and morphodynamic parameters and dimensionless scour times for monopiles. Based on this, it was anticipated that the response time for the clear-water regime would be significantly longer than for live-bed conditions.

3.4.2. Model parameters - Field scale

To determine a suitable timeframe for the field-scale numerical model, an alternative approach was adopted to balance model detail with computational feasibility. Due to runtime constraints, the total simulation duration was limited based on practical considerations. For most cases, a maximum of 12 physical days was used. This corresponded to a morphodynamic simulation time of 30 days for the clear-water regime and 12 days for the live-bed regime.

This difference arises primarily from two factors: (1) the live-bed regime required a longer upstream domain extension to prevent numerical instabilities, and (2) the higher flow velocities characteristic of this regime resulted in smaller time steps due to the fixed CFL condition. These considerations are summarized in Table 3.6.

Table 3.6: Summary of computational time implications and morphological time across regimes on field conditions

Variable	**Clear-water regime**		**Live-bed regime**	
	Characteristic	**Computational time implication**	**Characteristic**	**Computational time implication**
Domain	12x vs 4y domain	–	6x vs 4y domain	++ (100% increase)
Velocities	Lower velocities	–	Higher velocities	+ (20% increase)
Morphological time	**30 days**		**12 days**	

It can be observed that, for the same computational time, the clear-water regime allows for a longer morphological response. This is advantageous, as the scour response under clear-water conditions is generally slower compared to that in the live-bed regime.

The increase in domain size and flow velocity at field scale directly impacts the required spin-up time. As described in the laboratory-scale numerical model, a minimum threshold is defined based on the time it takes for a fluid particle to traverse the domain more than twice along the x-axis, using the depth-averaged inlet velocity.

The remaining model parameters—such as the Morphac factor, relaxation factors, and grid size—were kept consistent with the laboratory-scale setup. Only the relaxation factor for bed load transport was actively applied, while the suspended load relaxation factor remained at its default value. The adopted configuration for the field-scale simulations is shown in Table 3.7.

Table 3.7: Final setup for field-scale simulations

Regime	Morphac	Relaxation factor		Grid size	Domain extension
		Bed load	Suspended load		
Clear-water regime	100	0.001	1	D/10	12x vs 4y
Live-bed regime	100	0.001	1	D/10	6x vs 4y

3.4.3. Results of the field scale simulation

The discussion then moves on to the topic of applying a methodology to scale up the lab results for the 4LJ, comparing the field-scale results to expectations from the literature and evaluating the applicability of the scaling methodology developed for monopiles by Broekema and de Wit (2025).

It is also observed the hydrodynamic response on the numerical model, in the same way of section 3.3.3. This allows for the assessment of how hydrodynamic processes scale and enables interpretation of the resulting morphodynamics for both flow regimes.

3.5. Analysis of model results

The final stage of this research focuses on the post-processing, analysis, and interpretation of the numerical simulation results obtained from both the laboratory-scale and field-scale models. This will be done on Chapter 6.

This chapter leverages the flexibility and high spatial and temporal resolution of the numerical model to investigate the evolution of scour magnitudes and timescales. The analysis includes a detailed examination of local scour footprints and their associated equilibrium times, as well as an evaluation of global scour magnitudes across various spatial regions. Including this comparison here aligns with the broader scope of the results and provides a more comprehensive understanding of model performance.

The applicability of the results is further explored by comparing scour magnitudes against the empirical relation proposed by Sheppard and Miller Jr. (2006), as well as the field observations for local scour and overall knowledge of global scour.

Finally, the relevance of both local and global scour findings is discussed in a broader context, with attention given to the limitations of the current study and the interpretation of the results on the discussion chapter.

The final chapters of the thesis presents the discussion, where the limitations are addressed and the main conclusions of the research, directly addressing the stated objectives and research questions.

4

Numerical model assessment - Laboratory scale

This chapter presents a detailed comparison between the numerical model results and experimental data to evaluate the model's ability to simulate both local and global scour processes around a 4LJ foundation. The evaluation is conducted under two sediment transport regimes: clear-water and live-bed conditions. The objective is to assess how accurately the model captures the spatial distribution and temporal evolution of scour, as observed in laboratory experiments by Welzel et al. (2023).

The chapter is organized as follows. It begins with an assessment of local scour development, based on both point measurements from echo sounders and spatially averaged scour depths around each pile. Comparisons are made for upstream and downstream piles in both regimes, with particular focus on the agreement between the numerical and experimental time series and scour magnitude. Next, global scour is analyzed using data from selected monitoring locations and average bed level changes across defined zones within and around the jacket footprint. This spatially integrated approach provides a more comprehensive view of large-scale morphological changes.

In addition to scour predictions, the chapter examines flow behavior near the jacket structure by analyzing velocities and bed shear stress distributions. These hydrodynamic features are key to understanding sediment transport mechanisms and validating the model's ability to replicate flow-induced scour. Finally, a sensitivity analysis is presented, focusing on the effects of key numerical parameters on model outcomes. These insights support the evaluation of the model's robustness and at the same time the effect of these parameters on the model results.

4.1. Morphodynamics comparison with lab experiment

In this section, the comparison between the numerical results and the experimental data for both local and global scour is presented. The numerical model setup used for this comparison is described in Section 3.3.1. Results are evaluated against laboratory experiments conducted by Welzel et al. (2023) under both clear-water and live-bed conditions.

Although the model has previously been calibrated for local scour around a different jacket foundation (de Wit et al., 2023), its performance in predicting global scour and its robustness across different flow regimes needs to be studied. This evaluation addresses these aspects.

Local scour is assessed using data from echo-sounders E1–E3 and E5–E7, positioned near the upstream and downstream piles (Figure 4.1 b–c). In addition to point measurements, spatial scour patterns are evaluated by computing the average scour depth within a concentric ring of thickness D/2 around each pile, allowing comparison with 3D laser scan measurements from the physical model.

To evaluate the model's ability to reproduce global scour, measurements from echo-sounders E4 and E8 are compared (Figure 4.1a). Furthermore, the spatial distribution of global scour is assessed by

comparing the average bed level within predefined rectangular areas, extracted from both the numerical results and the experimental 3D scans shown on Figure 4.1a.

These combined analyses provide a comprehensive assessment of the model's capability to reproduce both the magnitude and temporal evolution of local and global scour processes.

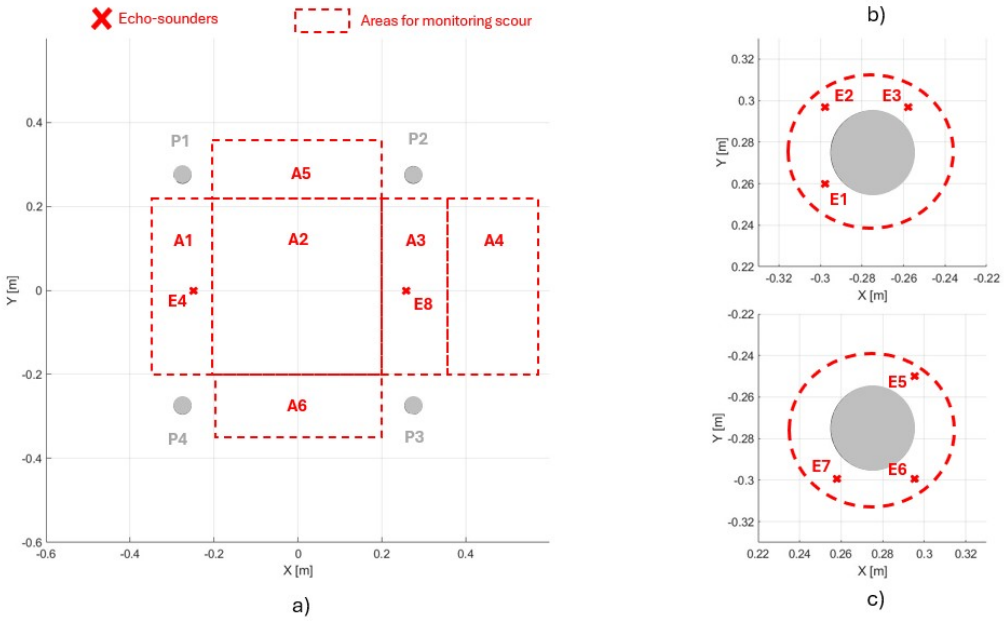

Figure 4.1: (a) Overview of monitoring areas for global scour and positions of echo-sounders E4 and E8. (b) Zoom on pile P1, showing the local positioning of echo-sounders E1–E3 and the corresponding scour evaluation zone. (c) Zoom on pile P4, showing the local positioning of echo-sounders E5–E7 and the corresponding scour evaluation zone.

4.1.1. Local scour

For the upstream pile (P1), the scour depth predictions from echo sounders E2 and E3 closely match the measured values, while E1 slightly overestimates scour depth. The time evolution of scour depth follows a nearly exponential trend for all three probes, consistent with laboratory observations. E1 displays a steeper increase in scour depth during the initial phase, but eventually converges with E2 and E3 toward the end of the simulation. As noted by Welzel et al. (2023), local scour around the upstream piles did not reach equilibrium during the clear-water regime. This behavior is accurately reproduced by the numerical model, where a continued positive growth trend is observed in the upstream echo-sounder measurements toward the end of the simulation.

In contrast, the downstream pile (P4) shows more dynamic scour development and a lower magnitude of scour, as observed in the lab. While some oscillatory behavior is present in the laboratory data, the model tends to amplify these variations, probably due to the existence of considerable sand dunes passing over the piles on the downstream area.

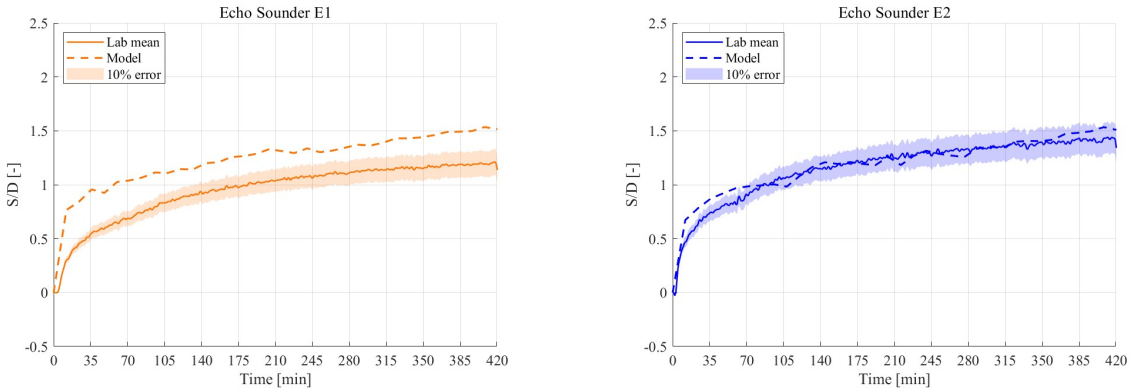

(a) E1 - Clear Water **(b)** E2 - Clear Water

Figure 4.2: Scour depth time series under clear-water conditions for experiments E1 and E2

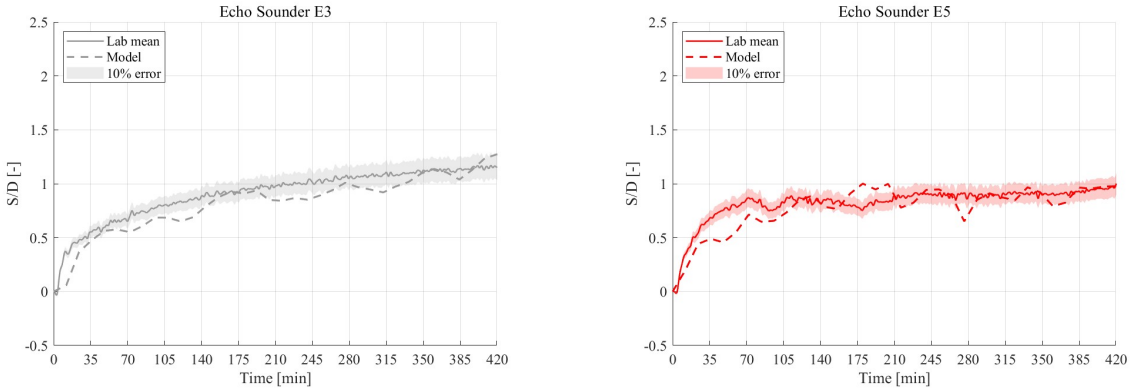

(a) E3 - Clear Water **(b)** E5 - Clear Water

Figure 4.3: Scour depth time series under clear-water conditions for experiments E3 and E5

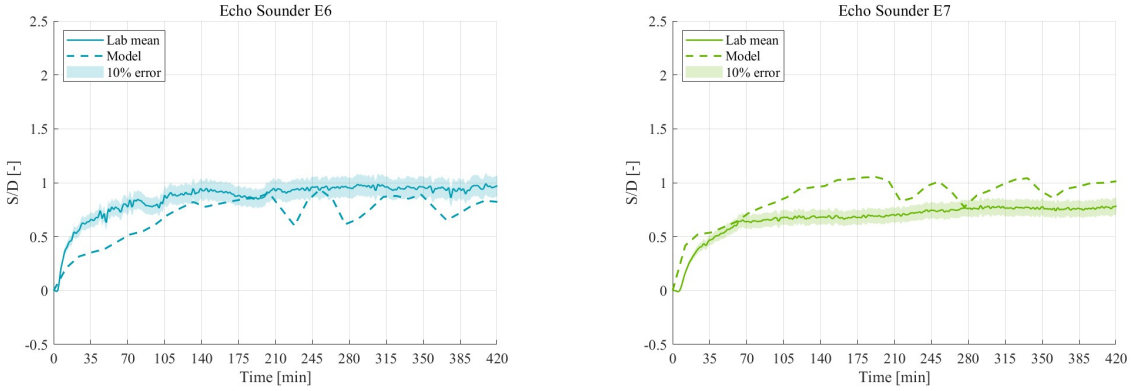

(a) E6 - Clear Water **(b)** E7 - Clear Water

Figure 4.4: Scour depth time series under clear-water conditions for experiments E6 and E7

To complement the qualitative assessment, the RMSE is computed between model predictions and experimental data. Results are summarized in Table 4.1, confirming that upstream probes generally show higher accuracy—with errors around 10%—while downstream probes exhibit larger deviations, round 20%. Overall the absolute error is around order of magnitude of 4 mm upstream and 8 mm downstream.

Table 4.1: RMSE analysis of scour depth predictions under clear-water conditions.

Echo Sounder	RMSE (mm)	RMSE (%)
E1	12	24%
E2	3	5%
E3	4	9%
E5	5	12%
E6	8	19%
E7	9	28%

A complementary spatial analysis of local scour was performed by averaging scour depth values within a ring-shaped zone surrounding each pile. This ring was defined with a thickness of $D/2$, and values were spatially averaged over this region. Table 4.2 presents the resulting averaged scour depths for both upstream and downstream piles. When compared to laboratory measurements, the numerical model shows an error range of 5–15%, demonstrating good agreement not only at discrete points but also in terms of the overall spatial scour behavior.

The numerical model reliably captures key features of the local scour process, including greater scour depths around the upstream piles and in front of the piles, and the inward tilting of the scour footprint to the center of the 4LJ. Furthermore, the close agreement in slope profiles radiating from the maximum scour depth—observed in both the numerical and experimental cross-sections—demonstrates the model's ability to accurately replicate the spatial progression of scour away from the pile. This reinforces the model's effectiveness in reproducing the broader patterns of local scour observed in the laboratory. These cross sections can be observed in Appendix B.

Table 4.2: Clear-Water Regime – Spatial analysis of local scour

Simulation Time	Upstream piles (S/D)			Downstream piles (S/D)		
	Lab Data	Simulation	Error	Lab Data	Simulation	Error
15 min	-0.39	-0.34	15%	-0.42	-0.36	14%
90 min	-0.76	-0.79	5%	-0.71	-0.83	16%
420 min	-1.11	-1.05	5%	-0.94	-0.89	5%

For the live-bed regime, the numerical results also show overall good agreement with experimental measurements of local scour evolution. As expected under live-bed conditions, the scour development is more dynamic, following the asymptotic behavior expected but with small oscillations, with a steeper initial rate of erosion indicating a faster approach to equilibrium. This behavior aligns well with the known physical response of sediment transport in live-bed conditions.

Results in E1 slightly over predicts the final scour depth, while E2 and E3 converge closely with the measured values. A similar pattern is observed for the downstream piles, where the model generally reproduces the scour evolution well. In E7, the final scour depth is slightly overestimated. Despite this, the model successfully replicates the key trends observed in the laboratory, confirming its reliability under live-bed conditions.

The initial steepness in the scour evolution curves reflects the pile-specific response and provides a valuable indicator for analyzing scour timescales. The agreement between model and experiment in this early phase suggests that the model captures not only the final scour depths but also the dynamic process leading to them.

The scour depth time series for all experiments under live-bed conditions are shown in Figures 4.5, 4.6, and 4.7.

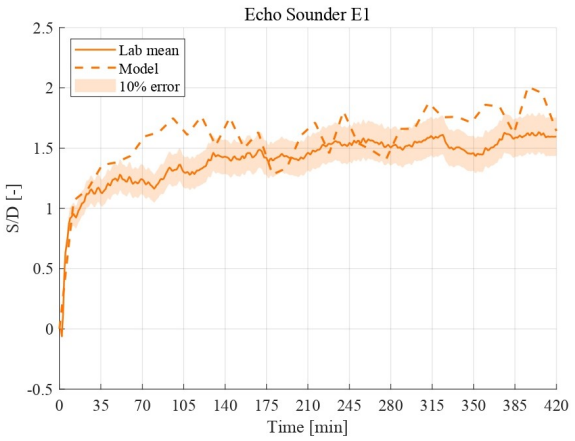

(a) E1 - Live Bed

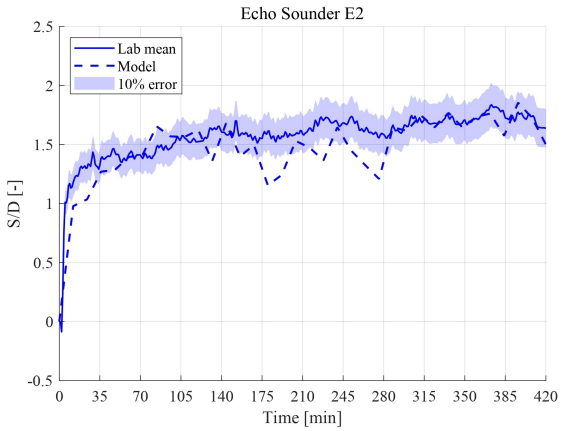

(b) E2 - Live Bed

Figure 4.5: Scour depth time series under live-bed conditions for experiments E1 and E2

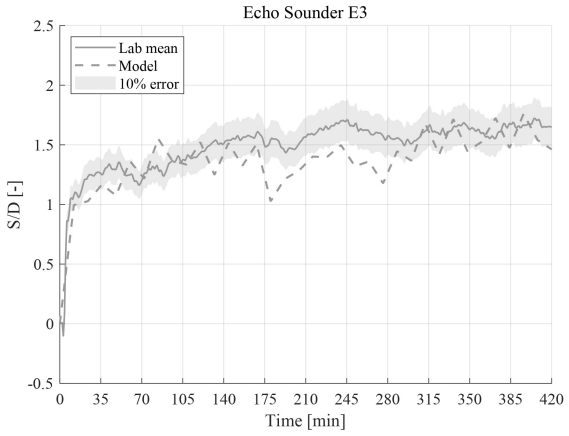

(a) E3 - Live Bed

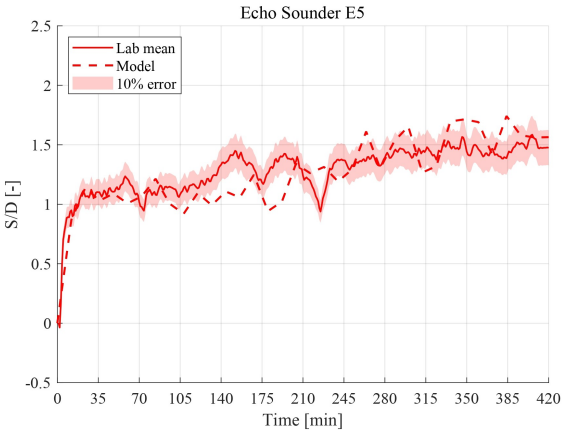

(b) E5 - Live Bed

Figure 4.6: Scour depth time series under live-bed conditions for experiments E3 and E5

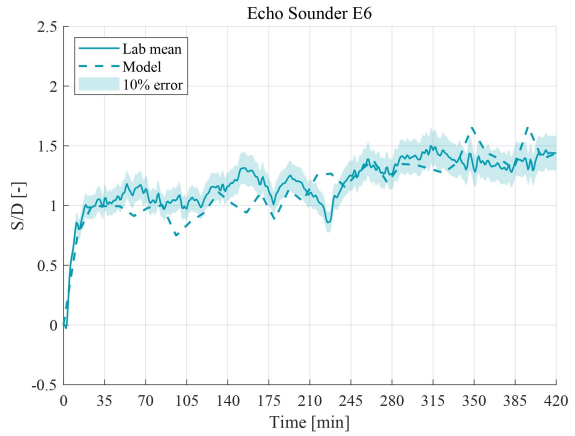

(a) E6 - Live Bed

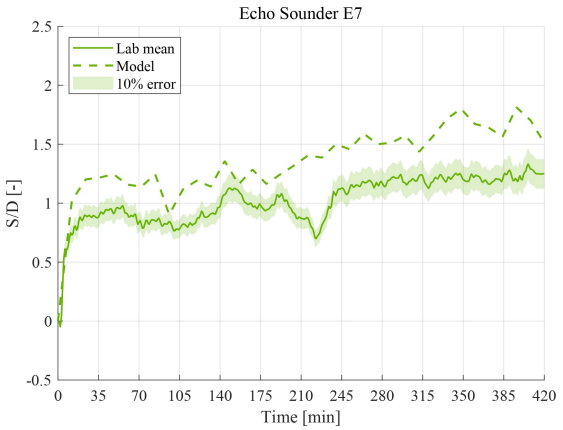

(b) E7 - Live Bed

Figure 4.7: Scour depth time series under live-bed conditions for experiments E6 and E7

Quantitative assessment through RMSE reveals good overall accuracy in the live-bed simulations. Most probes show errors from 5% to a maximum of 28% representing an absolute error value of around 7mm in average(Table 4.3).

Table 4.3: RMSE analysis of scour depth predictions under live-bed conditions.

Echo Sounder	RMSE (mm)	RMSE (%)
E1	9	14%
E2	7	9%
E3	8	10%
E5	7	10%
E6	6	9%
E7	14	27%

Table 4.4 presents the spatial scour analysis under live-bed conditions. This is the same analysis done in the clear water regime of average scour around the pile with half a diameter span area. Upstream values show excellent agreement, with errors as low as 1–4%. Downstream results are also satisfactory, except at 90 minutes, where the error rises to 52%. This is attributed to a local overprediction that does not persist at later times. At the final timestep, both upstream and downstream values exhibit minimal error (0–1%), demonstrating the model's reliability in capturing the equilibrium scour state spatially.

Similar to the clear-water case, the live-bed regime also exhibits the key spatial characteristics of local scour. The numerical model successfully reproduces greater scour depths at the upstream piles, preferential erosion in front of the piles, and the inward tilting of the scour footprint toward the center of the four-legged jacket structure. In addition, the agreement in slope profiles extending from the point of maximum scour—validated against experimental cross-sections—further supports the model's capability to capture the morphological evolution under more dynamic, sediment-transport-active conditions. These consistent patterns across regimes confirm the model's robustness in simulating local scour behavior for different sediment transport scenarios.

Table 4.4: Live-Bed Regime – Spatial analysis of local scour (non-dimensionalized by $D = 0.04$ m)

Simulation Time	**Upstream** (S/D)			**Downstream** (S/D)		
	Lab Data	Simulation	Error	Lab Data	Simulation	Error
15 min	-0.92	-0.89	4%	-0.92	-0.92	1%
90 min	-1.18	-1.14	3%	-0.97	-1.36	52%
420 min	-1.49	-1.48	1%	-1.50	-1.50	0%

In summary, the numerical model demonstrates strong performance in capturing the spatial and temporal development of local scour for both clear-water and live-bed regimes. It accurately reproduces the characteristic features of scour behavior around jacket foundations. The results not only match well with point-based experimental measurements but also show consistent agreement in spatially averaged scour depths and same extent of local scour footprint observed on the cross sections comparison (see Appendix B), confirming the robustness of the model across different flow and sediment transport conditions.

Quantitative validation using RMSE and spatial averaging shows that prediction errors remain within acceptable limits, with an average absolute error of approximately 7 mm and a range between 3 and 14 mm. Errors are generally lower for upstream piles, while slightly higher values are observed downstream. This does not necessarily indicate reduced model accuracy; rather, the increased error in downstream regions reflects the more dynamic scour behavior, including temporal oscillations, which naturally lead to higher variability and thus higher error values. These error levels are consistent with those reported by de Wit et al. (2023), who applied the same numerical model to a different jacket geometry and found comparable errors of around 8 mm. This consistency highlights the robustness of

the present model in capturing realistic scour behavior and reinforces its reliability for predicting local scour in offshore engineering applications.

4.1.2. Global scour

To evaluate global scour development, measurements at locations E4 and E8 were analyzed to estimate the bed level on the inner side of the jacket structure. However, these isolated measurements sometimes can not adequately represent global scour, given that this is a more spatially distributed phenomenon. Inside the jacket, the scour environment is highly dynamic, making it difficult for a single point measurement to reflect the general lowering of the bed. For this reason, a more spatially-integrated comparison is required. In order to asses the behavior it is compared the plan view of the 3D scans from the lab with the model to compare the overall behavior of bed, to then uantify it comparing specific areas of the jacket on different timesteps.

In the clear-water regime, no bed lowering is observed upstream at location E4 for the laboratory measurements, while the numerical model shows a small increase in scour depth (Figure 4.8a). At the downstream position E8, laboratory results indicate a scour depth reaching approximately $0.5D$ by the end of the simulation (Figure 4.8b). In contrast, the numerical model predicts a slightly lower absolute scour depth, in the range of $0.3D$ to $0.4D$. While the numerical model exhibits a more dynamic response, this variability is considered acceptable given the natural fluctuations in bed morphology under clear-water conditions, as observed in both the laboratory and numerical results.

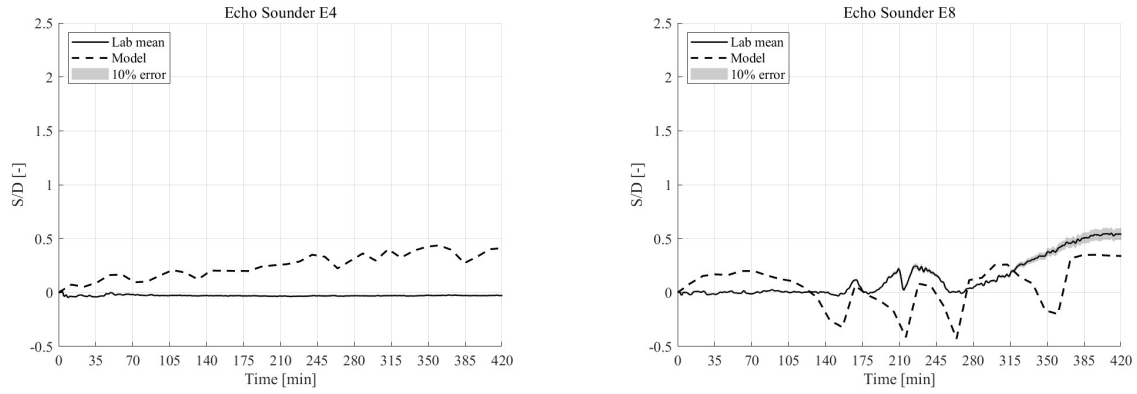

(a) E4 - Clear Water

(b) E8 - Clear Water

Figure 4.8: Scour depth time series under clear-water conditions for echo sounders E4 and E8

From the plan view, it can be observed that the scour magnitudes—both local and global—are of the same order of magnitude for the laboratory and the numerical model results. This is shown in Figure 4.9, which presents a plan view after 7 hours of morphological time. A deposition zone is also visible downstream in both datasets, although the patterns differ slightly. Upstream of the jacket, the numerical model does not show any dune formation or scour/deposition features, as expected for the clear-water regime—consistent with the lab observations. Another similarity is the scour footprint around the piles, which appears consistent in both spatial extent and depth between the lab and the model.

However, some differences are observed in the bedform patterns. The numerical model reproduces distinct ripples or dune-like features, particularly evident after 90 minutes. In contrast, the laboratory results exhibit a smoother scour pattern shaped by the pile geometry, where the eroded region migrates downstream at an angle of approximately 30 degrees from the pile center. These contrasting patterns highlight the model's tendency to generate larger and more defined dunes, whereas the lab data reflect a more diffuse scour pattern influenced by turbulence and structural interference.

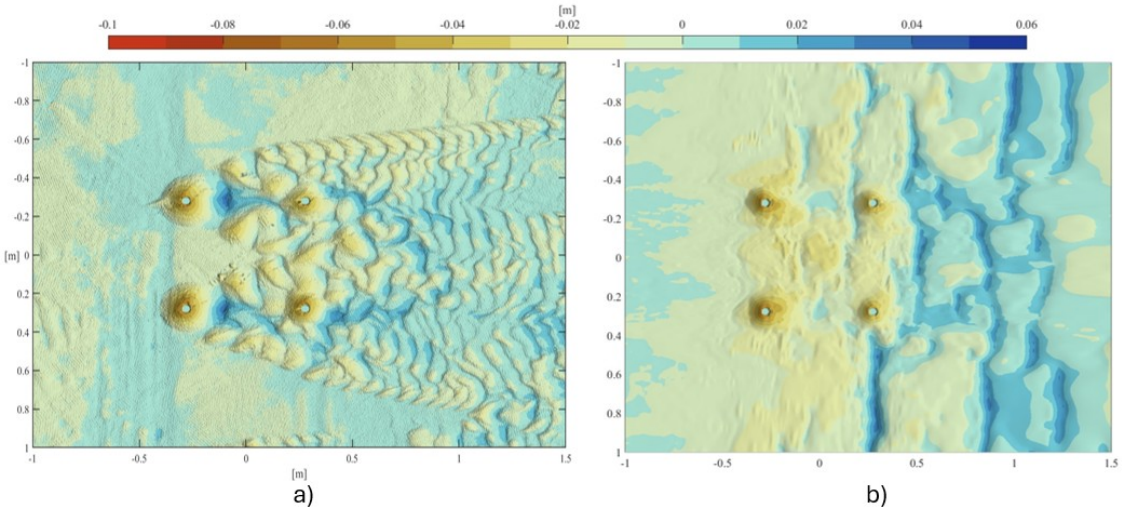

Figure 4.9: Comparison of bed levelat 420 minutes for clear water regime - a) Lab 3D scan - b) TUDflow3D Model results

For a more quantitative assessment, the average bed level within predefined monitoring areas is compared between the laboratory 3D scans and the numerical model, as illustrated in Figure 4.1. The results of this comparison are summarized in Table 4.5.

At 90 minutes, no significant scour is observed in the laboratory measurements; in fact, slight deposition occurs in Areas 5 and 6. The numerical model captures this general trend, except in Area 1, where it predicts a small scour depth of approximately S/D=0.2, indicating a slight overestimation in the upstream region. This was already observed on echosounder 4, with a higher order of magnitude.

By 420 minutes, clear scour patterns are present in both the laboratory and numerical results. Areas 1, 2, and, to a lesser extent, Area 3 exhibit the most pronounced scour, suggesting the development of global scour around the structure. In the laboratory data, scour depths in these regions reach approximately S/D=0.2, while the numerical model predicts higher values around S/D=0.3, particularly overestimating in Area 1 and in the lateral zones (Areas 5 and 6).

Overall, while the model correctly identifies the zones of maximum scour concentration—mainly Areas 1 to 3—it tends to overpredict the magnitude of scour, especially in upstream and side regions. Also the time response of the bed lowering is after 90 minutes, something that can be observed both in the numerical model and on the lab experiment results.

Table 4.5: Comparison of normalized scour depth S/D between numerical model and laboratory data

Time	Area 1	Area 2	Area 3	Area 4	Area 5	Area 6
90 min (Model)	0.25	0.00	0.10	0.00	-0.10	-0.10
90 min (Lab)	0.00	0.00	0.00	0.00	-0.10	-0.10
420 min (Model)	0.40	0.35	0.30	-0.05	0.20	0.15
420 min (Lab)	0.15	0.25	0.25	0.05	-0.05	-0.05

In the live bed regime, the numerical model exhibits an oscillatory scour development from the beginning of the simulation, consistent with the behavior observed in the laboratory experiments (see Figures 4.10a and 4.10b), which is the behavior of global scour when observed on an isolated point. This can also be associated to the oscillating behavior observed on the echo sounders around the piles (E1 to E3 and E5 to E8) for the live bed regime, therefore accounting for the effect of global scour on local scour.

In terms of magnitude, the model shows good agreement with the experimental data, particularly for the downstream echo-sounder. For the upstream sensor, the numerical scour depth oscillates around 0.5 S/D, which closely matches the laboratory value of approximately 0.4 S/D. For the downstream location, the model predicts a scour depth that converges to about 0.8–0.9 S/D, whereas the lab results span between 0.4 and 0.7 S/D with a higher amplitude of values in the oscillation.

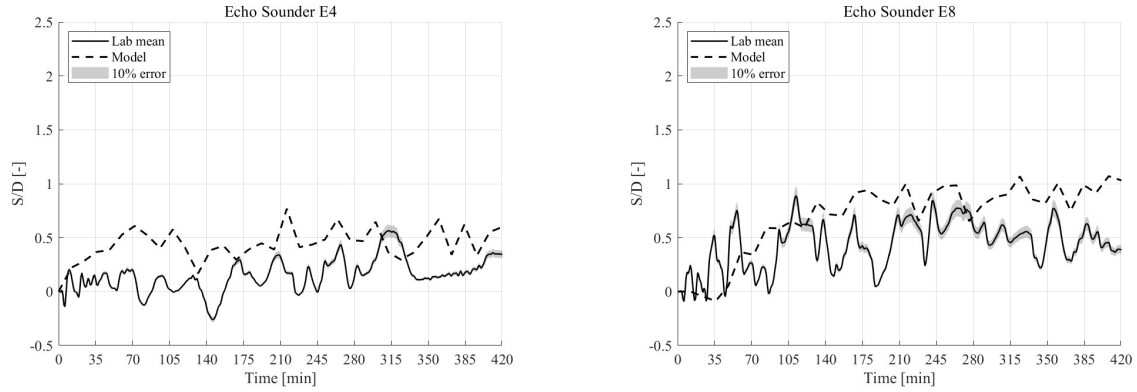

(a) E4 - Live Bed

(b) E8 - Live Bed

Figure 4.10: Scour depth time series under live-bed conditions for experiments E4 and E8

The plan-view representation of bed level evolution provides a valuable overview of the scour footprint around the jacket structure on Figure 4.11 present a comparison between the laboratory measurements and the numerical model results after 7 hours of morphological time.

The global scour pattern is well represented by the numerical model results, with scour observed both within the jacket footprint and downstream of the structure. The scour features inside and beyond the jacket resemble those from the laboratory experiment, indicating that the global scour induced by flow disturbance around the jacket structure peaks near the center and downstream. The scour extends beyond the footprint of the jacket and is accompanied by a deposition zone further downstream.

These results demonstrate the improved performance of the current model setup. However, local scour depths are somewhat underestimated compared to the experimental data, which aligns with the decision to apply a different configuration for capturing local and global scour processes.

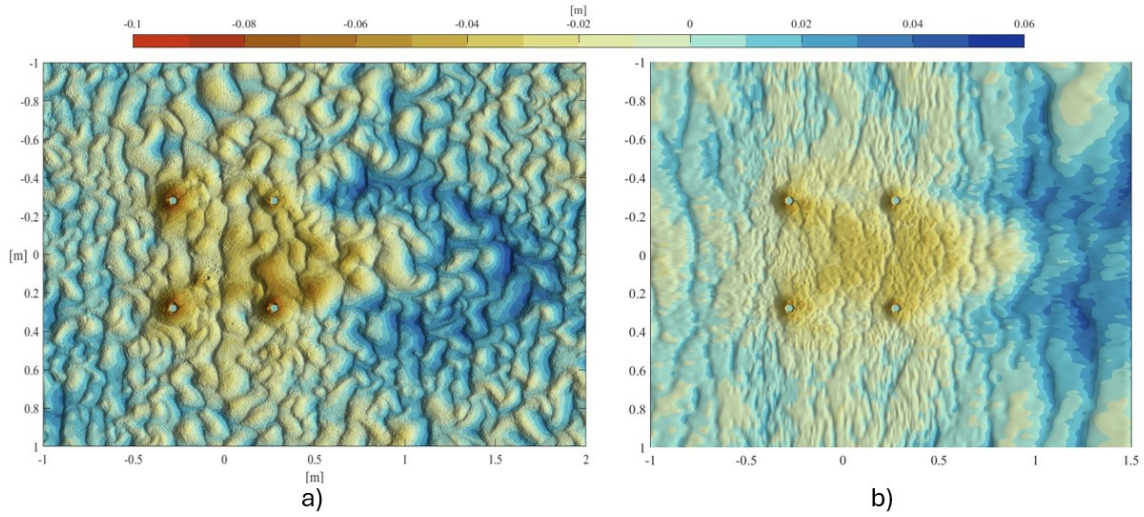

Figure 4.11: Comparison of bed levelat 420 minutes for live bed regime - a) Lab 3D scan - b) TUDflow3D Model results

As done for the clear-water regime, a more quantitative analysis of the bed level response in the live-bed regime is performed by comparing average scour depths across defined monitoring areas, as shown in Table 4.6. After 90 minutes, both the numerical model and laboratory data indicate a clear scour response, particularly in Areas 1 to 3, with normalized scour depths around S/D=0.5. At this early stage, the numerical model shows good agreement in the central areas but tends to overestimate scour in lateral Areas 5 and 6 compared to the lab results, where little to no scour is observed.

After 420 minutes (7 hours), scour deepens further, especially in downstream Areas 2 to 4. Both the model and lab results indicate scour depths between S/D=0.7 and S/D=0.9, confirming the progression of global scour in the live-bed regime. The agreement in magnitude between the model and laboratory measurements is strong across all areas, with a maximum difference of 0.05 S/D. This consistency demonstrates the model's ability to capture not only the spatial distribution but also the overall magnitude of scour development under live-bed conditions.

Table 4.6: Estimated normalized scour depth S/D for live-bed regime at 90 and 420 minutes

Time / Source	Area 1	Area 2	Area 3	Area 4	Area 5	Area 6
90 min (Model)	0.40	0.50	0.50	0.15	0.40	0.40
90 min (Lab)	0.25	0.45	0.35	0.15	0.00	0.20
420 min (Model)	0.50	0.75	0.95	0.70	0.45	0.50
420 min (Lab)	0.55	0.70	0.90	0.75	0.55	0.55

These results demonstrate a clear improvement in the representation of global scour with the adopted morphodynamic model setup. The combination of upstream domain extension and removal of the relaxation factor allows for a more realistic simulation of the large-scale sediment dynamics observed in the experiments.

The numerical model demonstrates a strong capability in capturing both local and global scour processes under clear-water and live-bed conditions. For local scour, model predictions align closely with laboratory echo-sounder data and spatially averaged scour depths, with RMSE values around 8 mm. Scour initiation and asymptotic evolution are well represented, showing the robustness of the model to predict this phenomenon.

Global scour is also realistically reproduced. In the clear-water regime, the model correctly predicts minimal scour development with moderate spatial variability, while in the live-bed regime, it captures the formation of scour within and downstream of the jacket structure. Spatial analyses using defined monitoring areas show that the model reliably predicts both the magnitude and distribution of scour, with deviations generally within 0.05 S/D from experimental values.

Overall, the model shows consistent performance across regimes, both in temporal evolution and spatial scour patterns. The adopted morphodynamic setup—including domain extension and removal of relaxation factor for global scour—proves effective in simulating complex sediment dynamics, reinforcing the model's applicability for engineering-scale scour prediction.

4.2. Observation of flow conditions

The objective of this section is to observe the behavior of the hydrodynamics around the jacket structure and with this try to understand their link to the scour response observed previously. This will be done through the observation of the amplification of horizontal velocities, when compared to the inflow velocity, the patterns of vertical velocities and amplification of bed shear stresses, when compared to the bed shear stress value without the structure placed.

It should be noted that the velocity fields presented in this section are derived from time-averaged flow data over a 10-second window (from 20s to 30s), taken after the model spin-up phase and prior to the initiation of any morphodynamic processes or bed evolution. While this interval may be relatively short

to capture fully developed flow conditions typically associated with steady currents, it is considered statistically meaningful based on Taylor's frozen turbulence hypothesis.

4.2.1. Flow Velocities

The amplification of horizontal velocities along the lateral sides of the jacket piles, as well as the formation of a lee-side wake vortex immediately downstream of each pile, are clearly visible in Figures 4.12 and 4.13, which present results for both flow regimes. In both cases, velocity amplification reaches up to 1.5 times the inflow velocity around the upstream piles, while slightly lower amplification is observed around the downstream piles.

For the live-bed regime, the horizontal velocity amplification is less pronounced compared to the clear-water regime, and the downstream velocity deficit is less distinctly defined. As with the clear-water case, the velocity amplification near the downstream piles is reduced to approximately 1.3 times the inflow velocity, indicating a decrease of about 15% due to the shadowing effect imposed by the upstream structures. The overall amplification pattern is more confined to the interior of the jacket foundation, reflecting the influence of the intensified flow interactions in the live-bed regime.

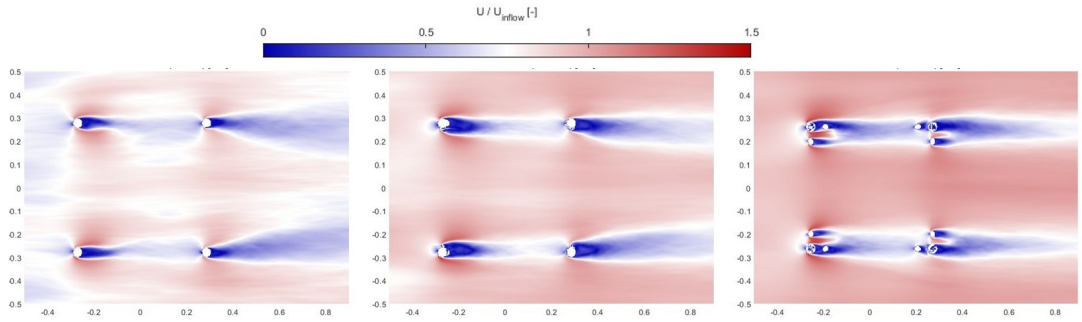

Figure 4.12: Normalized horizontal velocity magnitude on a horizontal plane above different distances: (2 cm, 5 cm, and 15 cm) for clear water regime

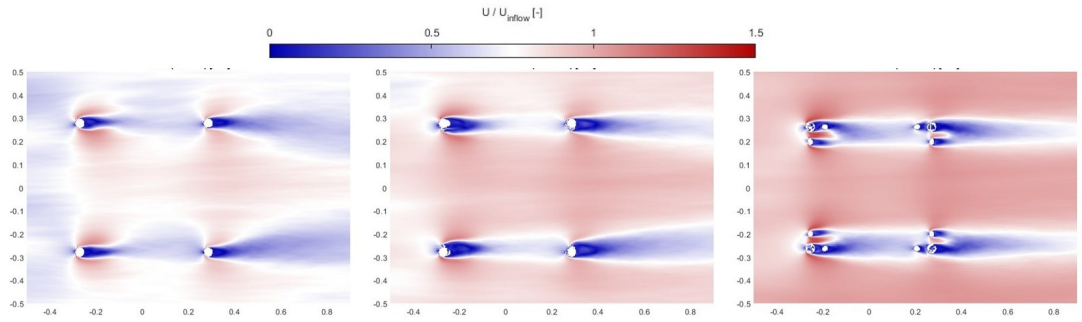

Figure 4.13: Normalized velocity magnitude on a horizontal plane above different distances: (2 cm, 5 cm, and 15 cm) for live bed regime

The vertical velocity components are presented in Figures 4.14 and 4.15 for both flow regimes. Negative vertical velocities observed in front of the piles indicate downward flow, commonly referred to as downflow, while positive vertical velocities downstream of the piles reflect flow separation and potential sediment pickup. At higher elevations above the bed, these upward velocities tend to shift toward the interior of the jacket structure. This behavior is likely due to the geometric transparency of the jacket, which allows for complex flow recirculation between the piles and braces.

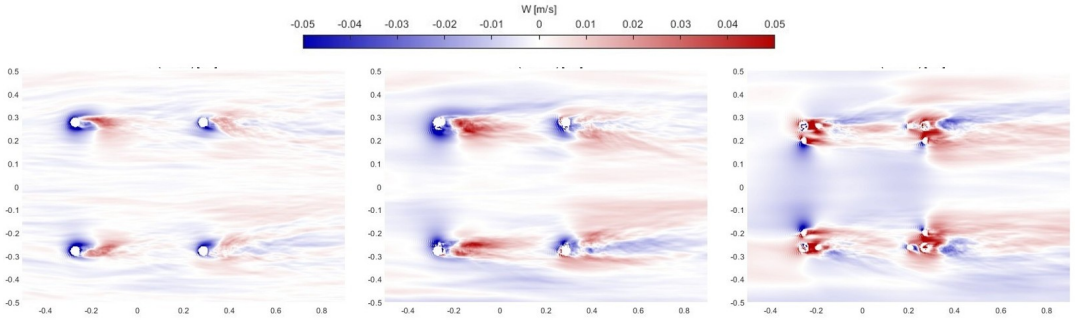

Figure 4.14: Vertical velocity magnitude on a horizontal plane above different distances: (2 cm, 5 cm, and 15 cm) for clear water regime

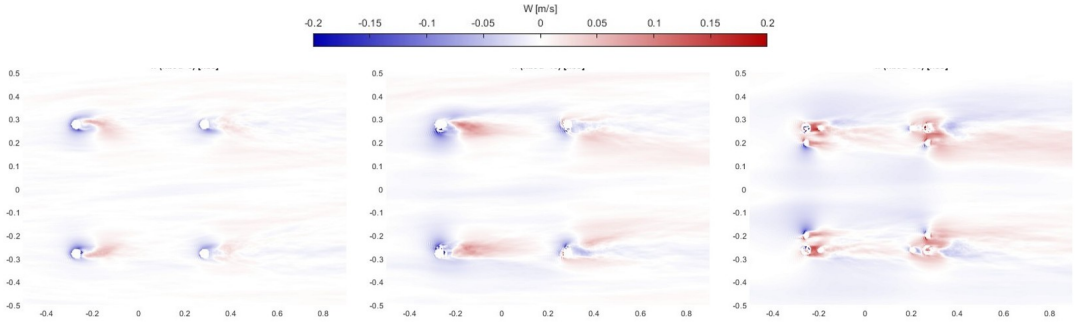

Figure 4.15: Vertical velocity magnitude on a horizontal plane above different distances: (2 cm, 5 cm, and 15 cm) for live bed regime

4.2.2. Bed Shear Stress Amplification

This section examines the amplification of bed shear stress caused by the presence of the jacket structure. Understanding the behavior provides valuable insight into the hydrodynamic effects induced by the structure at laboratory scale, which can be linked to velocity amplification, scour development, and ultimately scaled up to field conditions.

TUDflow3D computes various types of bed shear stress. For this analysis, we focus on the time-averaged flow-induced bed shear stress, which reflects the direct interaction between the flow and the bed surface. Although this specific value is not directly used in sediment transport computations (e.g., bed load or suspended load fluxes), due to relaxation factors and the instantaneous nature of it, the calculation methodology is the same and remains relevant for identifying hydrodynamic drivers of scour.

The results are presented as normalized bed shear stress fields, using the reference value of an unobstructed bed (i.e., without the structure). Figures 4.16 and 4.17 show the distribution of average bed shear stress for the clear-water and live-bed regimes, respectively. All four piles (upstream piles A and B, and downstream piles C and D) are identified within the domain.

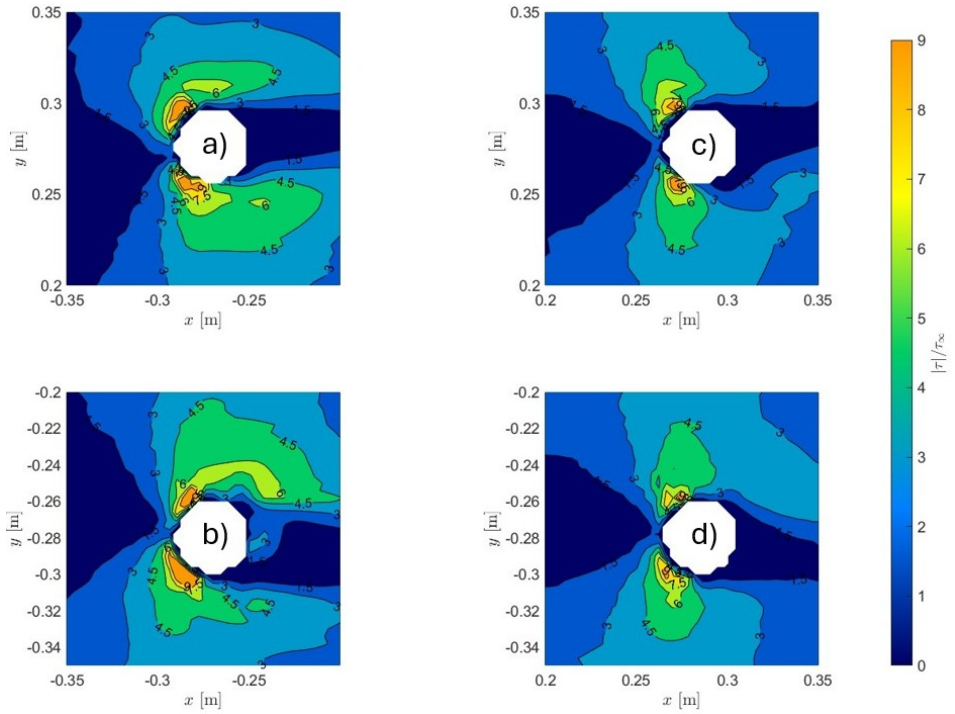

Figure 4.16: Normalized time-averaged bed shear stress for the clear-water regime

For both regimes, the amplification of bed shear stress reaches values of approximately 9 near the upstream piles, whereas slightly lower values between 7 and 8 are observed around the downstream piles. This trend confirms the shadowing effect created by the upstream piles, as also seen in the velocity fields. It helps explain the higher scour intensity observed at the upstream legs compared to the downstream ones.

In addition, the region of elevated bed shear stress exhibits an inward tilt toward the center of the structure, particularly on the upstream-facing side of the piles. This directional pattern mirrors the shape of the local scour footprints seen in the simulations, reinforcing the physical connection between hydrodynamic forcing and morphological response.

These spatial trends emphasize that local scour is likely to initiate and develop more aggressively around the upstream piles, while the downstream piles experience reduced forcing and thus milder scour. Also that bed shear stresses can serve as a predictor for the shape of the scour hole.

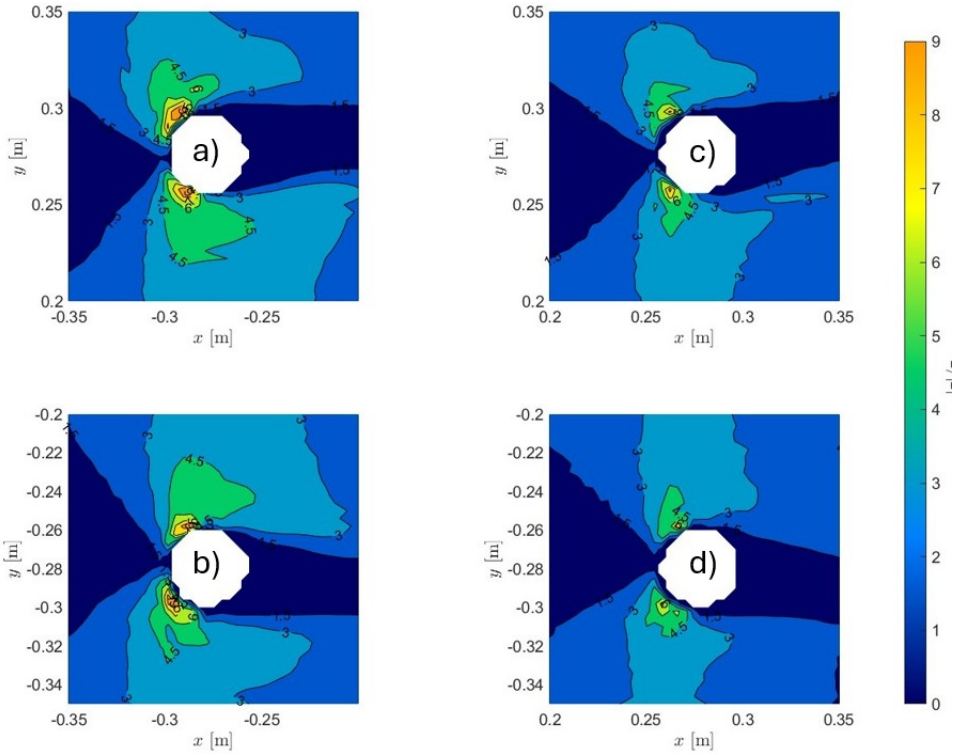

Figure 4.17: Normalized time-averaged bed shear stress for the live bed regime

The hydrodynamic comparison confirms that the model developed in this study accurately reproduces the expected flow characteristics and bed shear stress distribution around the piles of a J4L structure. Key flow parameters—such as increased streamwise velocities near the upstream piles, the presence of downflow zones and lee-wake vortices, and the formation of inward-tilted shear stress amplification zones—are clearly captured. These patterns are consistent with well-established hydrodynamic behavior around pile groups and reflect the realistic performance of the model under both clear-water and live-bed regimes.

A notable aspect is the relation between velocity and bed shear stress. Since bed shear stress scales with the square of velocity, even moderate variations in flow speed have a significant impact. For example, a velocity reduction of approximately 25% near the upstream piles leads to a drop in normalized bed shear stress from roughly 8.5 to 6.5. This highlights the strong sensitivity of shear stress to local velocity variations and the influence of structural interference on both parameters.

It is important to note that the bed shear stress values presented here are time-averaged over a hydrodynamically stable period prior to the onset of morphodynamic changes. As such, they represent the imposed flow forcing before any feedback with the evolving bed morphology occurs. While they do not capture the dynamic interaction during active scour, they provide a reliable baseline for identifying regions where scour is likely to initiate.

The full picture of the time averaged bed shear stresses on the jacket for both regimes can be observed on Appendix B.

Comparable magnitudes were reported by Satari et al. (2024), who evaluated the same J4L configuration using CFD RANS model that was compared to velocity measurements from a lab experience. Their results—showing horizontal velocity amplifications of approximately 1.5 and bed shear stress amplifications up to 8—exhibited similar spatial patterns and magnitudes, reinforcing the validity of the present model and confirming the characteristic hydrodynamic behavior of jacket structures.

For the purpose of this chapter, the presented results are sufficient to demonstrate that the model seems to replicate the dominant flow features expected for a J4L configuration at laboratory scale. The spatial

correspondence and amplification trends confirm the model's ability to resolve relevant hydrodynamic patterns that influence scour initiation.

4.3. Sensitivity analysis

This chapter presents a comprehensive sensitivity analysis focused on the main modeling assumptions and configurations that affect the scour evolution around a 4LJ.

The objective of this analysis is twofold: (1) to identify which numerical setups best replicate the laboratory-scale scour measurements, and (2) to evaluate the sensitivity of model outputs to variations in key parameters. Four aspects are systematically analyzed: the morphological acceleration factor (Morphac), the relaxation factors, the grid resolution, and the size of the computational domain. For each parameter, simulations were performed under both clear-water and live-bed regimes to evaluate consistency across conditions.in.

4.3.1. Morphological acceleration factor Sensitivity Analysis

To assess the impact of the morphological acceleration factor morphac on model predictions, simulations were conducted under both clear-water and live-bed conditions. Four different morphac values were tested: 10, 50, 100, and 200. Due to computational time constraints, the simulation with morphac = 10 was only run up to 90 minutes of equivalent physical time, as it would otherwise require several weeks to complete. This has been done before for a jacket, where it was obtained a result of not much sensitivity until 400. Either way, 100 was selected, to be on the safe side and then the sensitivity will be made for 200 as well, as an upper threshold.

The importance of this sensitivity analysis comes with the importance of applicability of this factor. As explained before, part of the feasibility of these models is the timeframe where the simulations can be done. With a Morphac of 10, the whole simulation could take weeks, which will limit how applicable these type of simulations are. Table 4.7 summarizes the tested cases.

Table 4.7: Morphac assigne value for each case evaluated

Case Name	Morphac
M10	10
M50	50
M100	100
M200	200

For local scour, the model results were evaluated against laboratory measurements at the echo-sounder locations, following the same approach used in the previous section. For the clear-water regime, the average RMSE was approximately 18% or 8 mm, with the lowest error observed for the simulation using Morphac = 100. In the live-bed regime, the average RMSE was slightly lower, at around 16% or 9 mm as an absolute value. A slight trend was observed in which higher Morphac values led to increased predicted scour depths when observed the time series of the echo sounder, particularly under live-bed conditions.

For global scour, further insights are obtained from a plan-view perspective. Figure 4.18 presents the bed level at the final timestep for each case on the clear water regime. The M50 simulation exhibits smaller, less defined bedforms both upstream and downstream of the jacket, indicating a more localized sediment response. In contrast, the M100 and M200 cases show more pronounced and developed dunes, suggesting a broader morphodynamic impact. Downstream of the jacket, all cases show sediment deposition; however, the extent and magnitude of this deposition increase progressively from M50 to M200.

For the live bed regime Figure 4.19 further confirm this trend. These figures compare the final timestep for the different morphac cases, and it becomes clear that while the scour footprint maintains a similar shape, its magnitude increases with higher morphac values. The use of a consistent color scale across all images facilitates this comparison: for instance, in the case of M50, the maximum scour

downstream of the jacket reaches approximately 0.05 m, whereas for M200, it rises to around 0.10 m. This represents a significant difference in the global scour behavior downstream of the structure.

When comparing these results with the laboratory measurements, the numerical model does not fully replicate the global behavior. In the physical experiments, bedforms were confined to the downstream region of the jacket, as expected under clear-water conditions where the bed is not yet mobilized upstream. In contrast, the TUDflow3D simulations with this setup produce bedforms both upstream and downstream of the structure, indicating a more active sediment transport response. This discrepancy suggests that in the numerical model, sediment mobilization is overestimated, potentially influencing global scour behavior.

Despite these differences, the general morphological behavior remains consistent across cases and aligns well with the experimental observations on local scale.

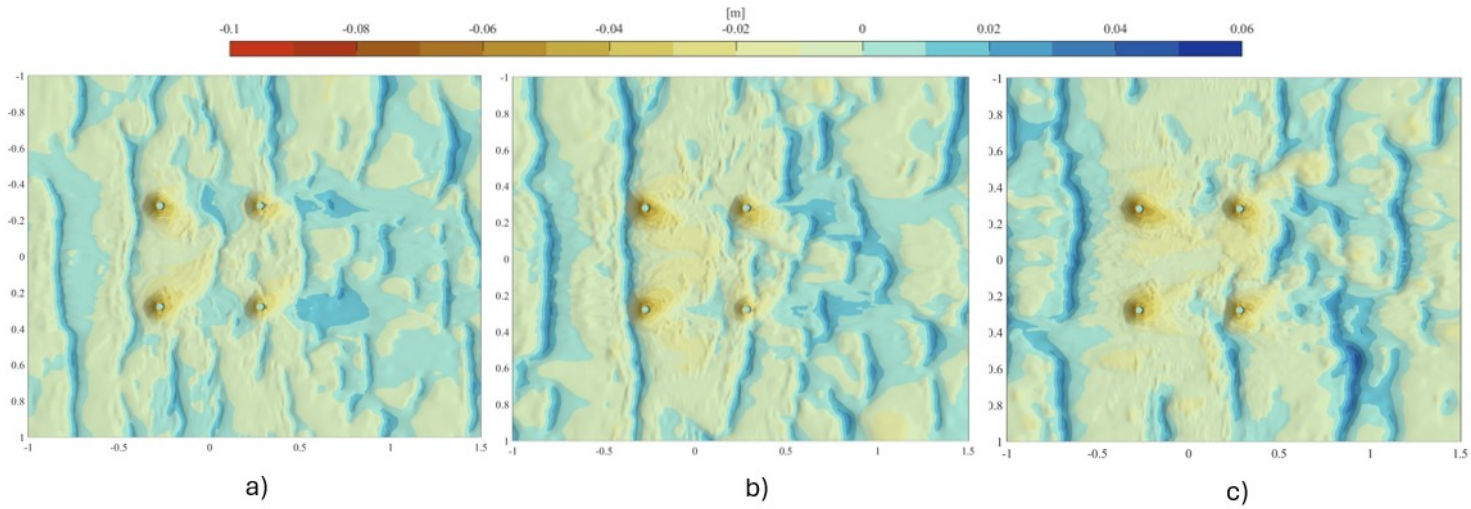

Figure 4.18: Plan view of bed scour development at 420 minutes for a morphac of (a) 50, (b) 100, and (c) 200 under the clear-water regime.

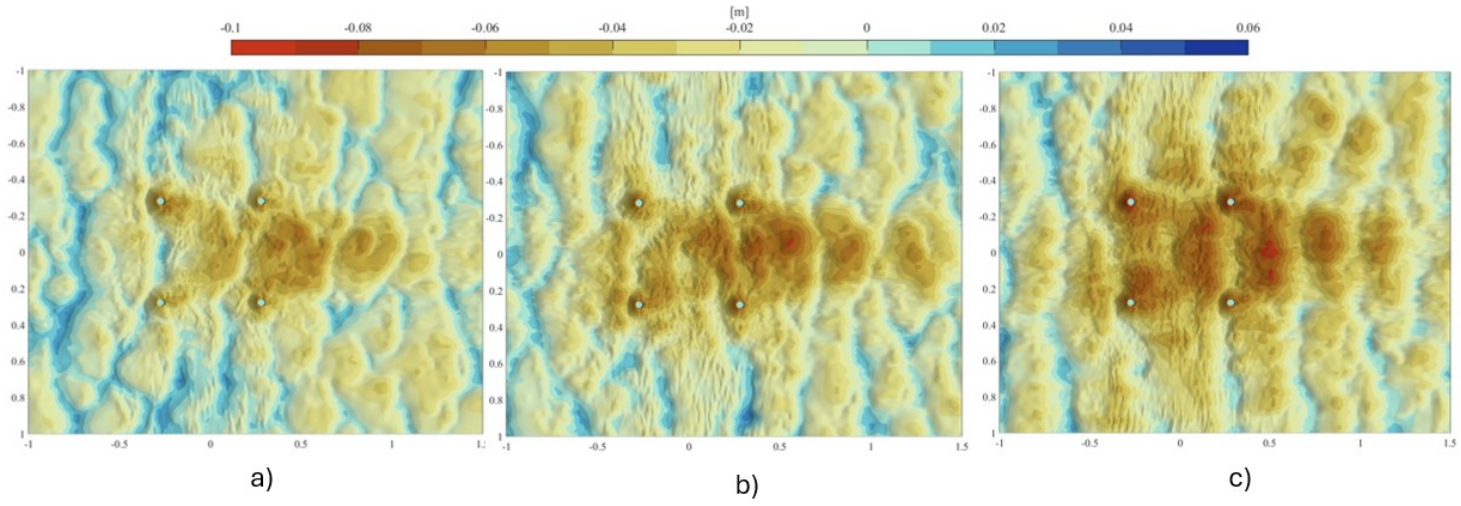

Figure 4.19: Plan view of bed scour development at 420 minutes for a morphac of (a) 50, (b) 100, and (c) 200 under the live bed regime.

This highlights the importance of a combined interpretation measures for complex structures like a 4LJ. Relying solely on one indicator focus on local scour, such as RMSE, may not show the sensitivity of

the model to varying parameters. Therefore, a comprehensive analysis incorporating both quantitative and qualitative comparisons is essential.

Overall, it can be concluded that local scour is not influenced by this order of magnitude of morphac. The differences locally are negligible and are a good representation of the lab experiments, as expected by the validation process of de Wit et al. (2023). On the other hand, for global scour the increase in morphac does have an effect on the overall level of the bed, over estimating the scour processes happening around the jacket.

In Appendix B, it can be observed the comparison of the echo sounders data of the lab for each simulation mentioned in this section as well as the bed state for 15, 90 and 420 minutes. These figures also show the amplified scour trend, showing as well the positive trend that with a higher morphac, there is an higher absolute value of scour for global behavior.

4.3.2. Relaxation Factor Sensitivity

As discussed on section 3.1, the relaxation factor plays a key role in smoothing near-bed velocities and pressure gradients across time.

The motivation for analyzing the relaxation factor lies in its expected impact on the global scour patterns. By damping sharp gradients in pressure and near-bed velocities, the relaxation factor promotes a more continuous and field-like behavior across the computational domain, as opposed to abrupt cell-by-cell variations. This more physically consistent behavior better reflects observed phenomena in real-world conditions.

Such damping also manifests as a smoothing effect on the bed shear stress fields, which are central to sediment mobilization and transport processes. Because of this, it becomes important to investigate and interpret how this smoothing affects the morphology outcomes, particularly the broader scour patterns rather than just isolated local effects.

Additionally, the initial model configuration applies a relaxation factor to suspended load-related variables. This provided further motivation to explore how varying the relaxation strategy—whether applied to suspended load, bedload, both, or neither—affects the model outputs.

To systematically evaluate the influence of relaxation factors on the computed bed shear stresses and sediment fluxes, multiple configurations were tested under both clear-water and live-bed regimes.

Three configurations are analyzed:

- **RFA**: A relaxation factor is applied to bed load.
- **RFB**: A relaxation factor is applied to both the suspended load and bedload transport.
- **RFC**: No relaxation factor is applied to either the suspended load or the bedload transport.

These configurations are tested under both clear water and live bed regimes.

For local scour, the model responses vary significantly between configurations. RFA shows the best overall performance in both regimes, with an average RMSE of approximately 15% and an absolute error around 8 mm. In contrast, RFB exhibits substantially higher errors—around 26% RMSE for the clear-water regime and up to 40% for the live-bed regime. RFC yields intermediate results, with RMSE values close to 20%.

These findings suggest that RFA provides the most accurate representation of local scour, which aligns with expectations, as it follows the configuration used by de Wit et al. (2023). However, these RMSE values alone do not capture the full behavior of the scour evolution. When analyzing the time series from each echo sounder (see Appendix), both RFB and RFC consistently show reduced scour depths, indicating a general underestimation of scour magnitude. This becomes more evident when examining the overall bed evolution in plan view, where spatial patterns reinforce the limitations of those two cases in capturing the correct scour development.

To assess scour behavior from a more global perspective, plan view plots are analyzed for each case, as shown in Figure 4.20.

For the clear water regime, a consistent feature across all simulations is the presence of sediment deposition behind the piles—though the morphology and extent differ between cases. In RFA and RFB, where a relaxation factor is applied to the bedload, dune forms can be observed again, which are not observed on the lab. In contrast, RFC, which does not include any relaxation factor, shows a bed morphology behind the piles that does not form these dunes.

A particularly notable feature in RFC is the migration of a dune from upstream to downstream, influencing the long-term scour pattern.. Early in the simulation, a slight reduction in horizontal velocity upstream was observed, initiating a feedback mechanism that originates the migration of the dune. In RFA and RFB, this migrating dune dissipates approximately 30 minutes into the simulation probably because of the applied bedload relaxation.

For the live bed regime, the impact of the relaxation factor is significantly more pronounced than in the clear water case. This result is intuitive: since the relaxation scheme targets the velocity fields used to compute sediment transport, higher velocity magnitudes amplify the effect of temporal smoothing introduced by relaxation, or in other words the damping of this relaxation factor and the absence of it is more noticeable.

The global deposition pattern is clearly visible in plan view, as shown in Figures 4.21 where it is presented the bed level for the last timestep of each simulation. RFB shows significantly more sediment accumulation across the domain, consistent with the dampened velocity field caused by relaxation. An important finding is what happens globally to RFC, which behaves similarly to RFA inside the jacket footprint but shows less intense scour downstream, with deposition downstream, which resembles what happens in the lab experience.

It should be noted that, similar to the clear-water regime, a disturbance in the velocity field was observed at the beginning of the simulations. In most cases, this initial instability is effectively mitigated by applying the bedload relaxation factor. However, in RFC—where no relaxation was used—the disturbance persists.

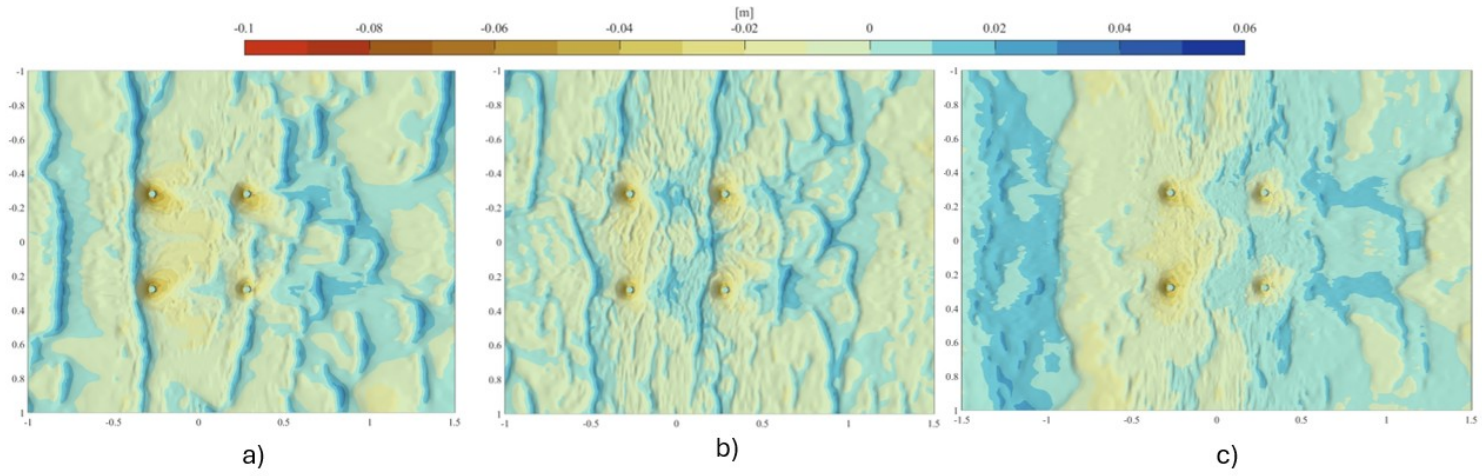

Figure 4.20: Plan view of bed scour development at 420 minutes for Case (a) RFA, (b) RFB, and (c) RFC under the clear water regime.

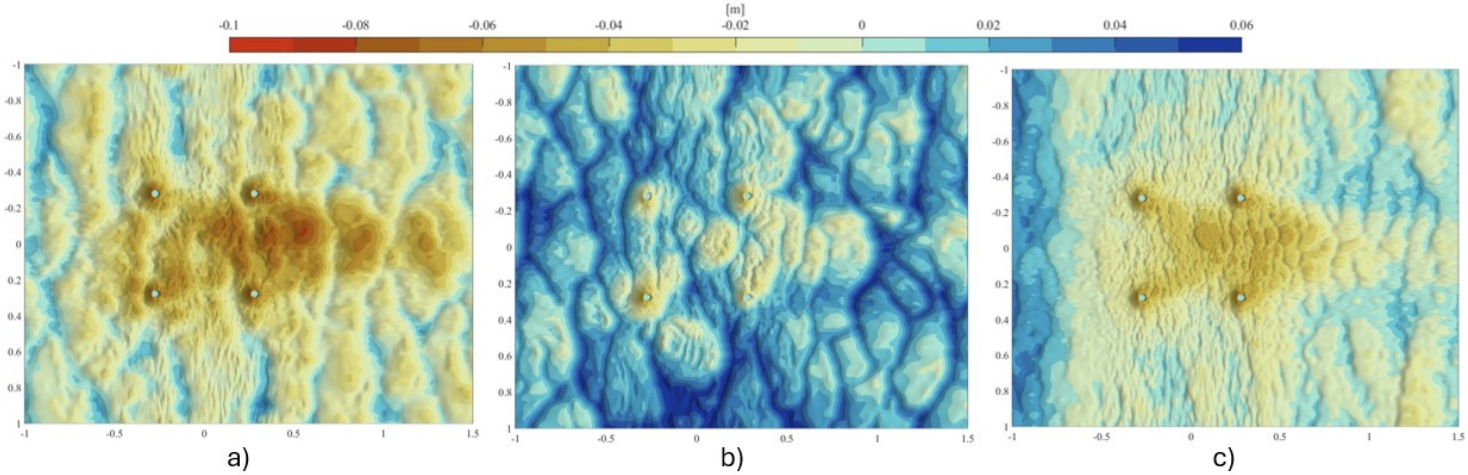

Figure 4.21: Plan view of bed scour development at 420 minutes for Case (a) RFA, (b) RFB, and (c) RFC under the live bed regime.

Finally, RFA emerges as the most suitable configuration for capturing local scour behavior in both flow regimes. In contrast, for global scour, RFC demonstrates the closest agreement with observed downstream deposition patterns. However, its performance is affected by the presence of upstream dune formations that disrupt the overall bed morphology.

These findings indicate that activating the relaxation factor for suspended load (as in RFB) tends to induce excessive deposition across the entire bed, while suppressing the relaxation factor for bed load (as in RFC) helps better represent global scour patterns. Nonetheless, this improvement comes at the cost of underestimating local scour depths. Therefore, a trade-off exists between accurately capturing global bed evolution and maintaining precision in local scour predictions.

The figures showing the scour evolution over time for all simulations, along with the corresponding model error comparison, are presented in Appendix B. These results highlight the influence of the relaxation factor on scour behavior and gives a better overview. This figures where also used to interpret the results given in this section.

4.3.3. Grid size Sensitivity Analysis

To assess the influence of mesh resolution, a finer mesh was tested by reducing the minimum grid size, which in turn controls the resolution in all spatial directions. While all simulations used the same physical domain (6x vs 4y), they differed in their grid resolution, directly impacting computational demand.

Although decreasing the grid size improves numerical accuracy, it significantly increases the computational cost. Since refinement occurs in all three directions (X, Y, and Z), the total number of cells—and consequently the simulation time—can rise exponentially. This becomes especially critical in morphodynamic simulations using a morphological acceleration factor (Morphac), where runtimes can extend from several days to multiple weeks depending on the mesh setup.

For the D/10 simulation, a simpler mesh was used, with uniform cell size across the entire jacket footprint and no additional local refinement. In contrast, the D/13 simulation employed an optimized mesh distribution with coarser cells on the center of the jacket, which reduced the total number of cells by approximately 30% compared to the uniform mesh, while maintaining adequate resolution near critical regions. Therefore not only the grid size was tested but also a different mesh configuration.

The refined configuration adopts a minimum grid size of 3 mm instead of 4 mm, offering a notable improvement in resolution without excessively compromising simulation time.

The mesh configurations and details are summarized in Table 4.8.

Table 4.8: Mesh configurations and simulation time details.

Configuration	X cells	Y cells	Z cells	Total Cells (M)	Sim. Time (days)
D/10	434	352	224	34.2	4–5
D/13	519	414	288	61.1	8–9

For the clear-water regime, the results indicate that reducing the minimum grid size from 1/10 to 1/13 of the structure's characteristic length does not significantly impact the scour response. This is evident in Figure B.23, where both configurations yield nearly identical scour depths, locally and globally, around the expected value of 0.04 m.

For local scour both relative (%RMSE) and absolute (mm) errors are comparable across grid sizes, with minor variations. Additionally, the time series comparisons for each echo sounder (provided in the Appendix A) confirm the strong agreement between simulations, reinforcing the conclusion that grid sensitivity has limited impact on model accuracy in this regime as observed by De Wit (2023).

The plan view evolution over time, shown in Figure 4.22 also shows no different response when different grid sizes are used. While finer grids slightly smooth out dune formations, the overall scour patterns remain consistent, suggesting no notable difference in global behavior. A grid refinement of 30% does not significantly influence the final outcomes.

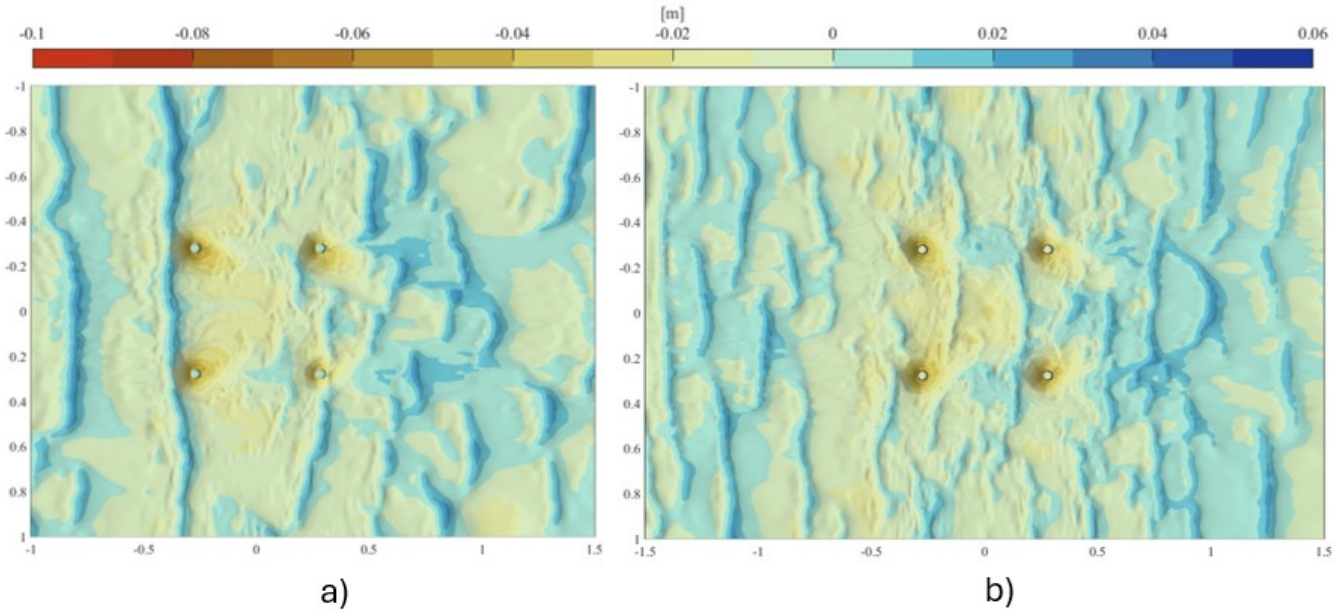

Figure 4.22: Plan view of bed scour development at 420 minutes for different grid resolution - Cases (a) D/10 and (b) D/13 under the clear water regime.

For the live-bed regime, simulations with the finer grid could not be completed due to computational limitations caused by the large number of cells. This sensitivity case remains to be verified, although based on the findings by De Wit (2023) and the similar behavior observed in the clear-water regime, no significant impact is expected. Further investigation is needed to confirm this assumption.

Grid resolution was found to have limited impact on the resulting scour patterns, both locally and globally, when refining the mesh beyond the baseline setup. Furthermore, the adoption of the optimized mesh configuration did not alter the simulation outcomes but provided a significant reduction in the total number of computational cells. This improvement in efficiency justified its use in all subsequent simula-

tions, as it offered a more favorable balance between computational cost and numerical performance. The details of this configuration are discussed in Section 3.2.1.

While coarsening the grid could reduce computational time, it would compromise the geometric fidelity of the structure. In the current configuration, the inclined members of the jacket are resolved by approximately five grid cells, and the main pile by ten. Halving the resolution would reduce the number of cells representing these components, significantly degrading the accuracy of the structural representation.

Conversely, using a finer grid would substantially increase simulation time—extending to several weeks—posing challenges for the practical feasibility of these models. This is especially critical given the relatively short simulation time window available to capture the key stages of scour development. Since the finer grid did not yield significant differences in local or global scour behavior, maintaining a resolution of approximately ten grid cells across the key structural dimensions appears to be a reasonable and efficient compromise between accuracy and computational cost.

4.3.4. Influence of the Domain

As observed in previous simulations, the formation of dunes upstream in the numerical domain can significantly impact model performance. If not properly controlled—particularly through the application of bedload relaxation factors—these bedforms may propagate downstream, eventually altering the morphology across a large portion of the computational domain, as illustrated in Figure 4.21.

As presented in section 3.2.1 a recommendation of extending the domain upstream by 5 water depths for the correct development of turbulence is important for the correct representation of the morphodynamic development, presented by de Wit (2015) . In this section it is tested the effect of this enlargement of the domain vs the domains used by De Wit (2023). This results in a larger domain of 12 times the jacket footprint, vs a domain of 6 times the jacket footprint on the current direction, respectively.

Table 4.9 summarizes the impact of this domain enlargement, including the increase in cell count and associated computational cost. For this case, the number of cells nearly doubled, resulting in a similar increase in simulation time. This modification was implemented for both flow regimes.

Table 4.9: Mesh configurations for different domains

Configuration	X cells	Y cells	Z cells	Total Cells (M)	Sim. Time (days)
6x vs 4y	434	352	224	34.2	4–5
12x vs 4y	679	352	224	53.5	8–9

On Figure 4.23, the bed at the second timestep of the smaller domain reveals a pronounced dune on the upstream side at the edge of the domain as mentioned, which would propagate downstream if no relaxation factor is applied to the bed load. In contrast, Figure 4.24 showing the same timestep but with an extended upstream domain and no morphological updates in the first four water depths exhibits no dune formation. This behavior persists throughout the simulation, confirming that the chosen relaxation approach successfully suppresses the dune.

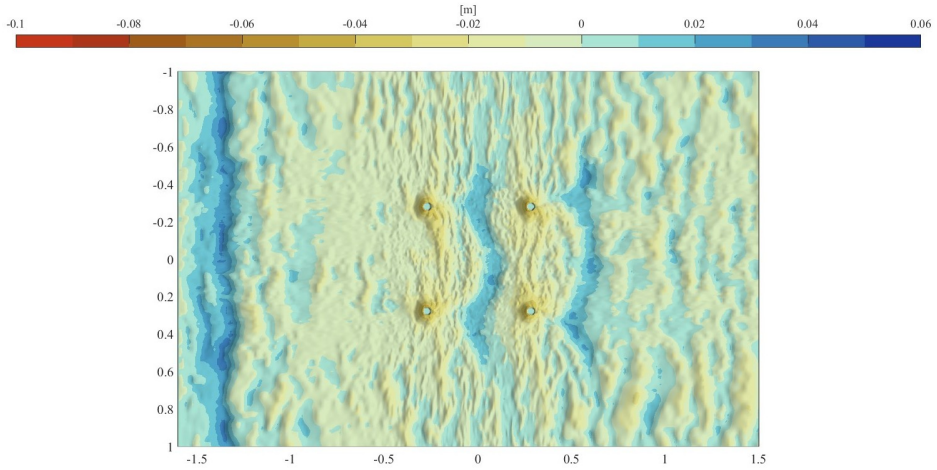

Figure 4.23: Plan view of bed scour development for the second timestep where the dune formation is observed - Smaller domain

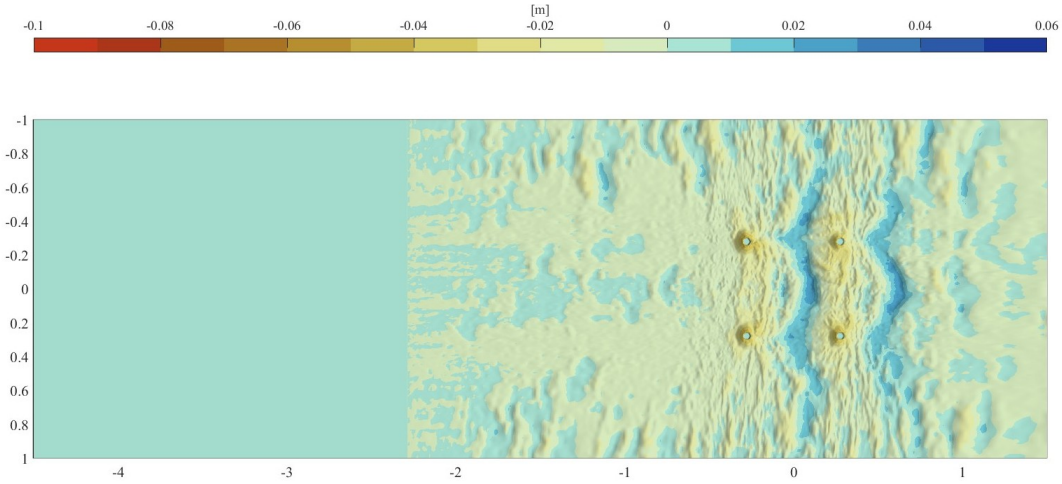

Figure 4.24: Plan view of bed scour development for the second timestep with the larger domain

These results highlight the importance of including an upstream domain extension to avoid disturbances in the global and also local scour patterns. Proper development of turbulence upstream has a notable influence on the morphodynamic response, particularly on the large-scale evolution of scour features. This suggests that hydrodynamic stability and flow conditioning play a critical role in accurately capturing global scour behavior.

For local scour, although the final magnitude of the scour hole was not altered by extending the upstream domain, omitting this extension may still lead to important consequences due to the influence of migrating bedforms. This is illustrated in Figure 4.25, which compares the scour depth evolution at Echo Sounder 2 under clear-water conditions for both the smaller domain (6x vs 4y domain) and the extended domain configuration (12x vs 4y).

While the overall spatial scour patterns and temporal trends around the piles appear similar between both setups, this comparison was specifically performed to evaluate whether the upstream domain extension also affects local scour.

The results reveal a difference in behavior towards the end: in the smaller domain without upstream extension, migrating dunes lead to a stagnation or even a slight reduction in scour depth toward the end of the simulation. This could falsely suggest that equilibrium has been reached. In contrast, the extended domain allows for more natural dune evolution, resulting in a continuous increase in scour depth over

time. This behavior matches experimental observations at the upstream piles, where equilibrium was not reached by the end of the test (Welzel et al., 2023). These findings underscore the importance of adopting an extended domain configuration to accurately replicate the ongoing development of both local and global scour processes.

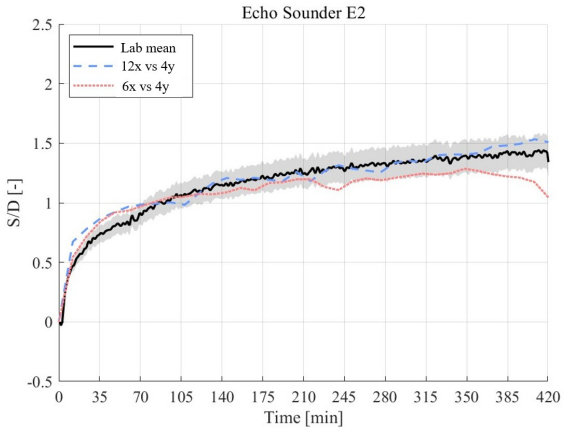

Figure 4.25: Scour depth time series under clear-water conditions for the final setup and the base case at Echo Sounder 2

Summary of Findings for the model assessment chapter

This section highlighted how each numerical setting affects both the local and global scour behavior:

Morphac values up to 200 had minimal impact on local scour predictions, but significantly affected global scour patterns, especially under live-bed conditions. A value of 100 was found to offer a good balance between accuracy and computational feasibility.

Applying a relaxation factor to the bed load (RFA) yielded the best local scour performance. However, for global scour, the case without any relaxation (RFC) better captured the downstream sediment deposition patterns observed in experiments, though in this case there was a disturbance on the overall bed patterns, coming from the migration of dunes upstream.

Reducing the grid size improved spatial resolution but did not result in significant changes in scour magnitude or shape. An optimized mesh configuration maintained model accuracy while reducing computational cost by approximately 30%, and was thus adopted for subsequent simulations.

Extending the domain upstream improved the development of turbulence and eliminated artificial dune formation at the domain boundary, allowing for improvement in both global and local scour behavior.

These results demonstrate that TUDflow3D provides a robust representation of local scour, when following the numerical setup proposed by de Wit et al. (2023), now successfully applied to a different jacket geometry such as a 4LJ foundation. For global scour, however, the model performance is more sensitive to specific numerical parameters. In particular, the morphac and the relaxation factors significantly influence the predicted large-scale bed evolution. The combination of omitting the relaxation factor while extending the computational domain upstream was found through the results observed in this sensitivity analysis. which offers the most realistic reproduction of global scour patterns, representing a favorable trade-off between numerical accuracy and computational feasibility.

5

Field scale numerical model

This chapter investigates the morphodynamic and hydrodynamic response of scour around a J4L foundation under field-scale conditions, for both clear-water and live-bed regimes. Although scour processes have been extensively studied at laboratory scale, significant uncertainty persists when extrapolating these results to field conditions—particularly for complex structures such as four-legged jackets. Currently, no widely accepted framework exists for reliably predicting either the equilibrium scour depth or the associated timescales at field scale for jacket foundations.

To address this gap, the use of numerical modeling proves particularly advantageous. A series of field-scale simulations are performed using the mobility criterion as the foundation for scaling. One of the key methodological challenges lies in defining a simulation duration that balances physical representativeness with computational feasibility. To evaluate scale effects, the field-scale results are directly compared to laboratory-scale simulations. In addition, the laboratory data are scaled up using the methodology proposed by Broekema and de Wit (2025), which combines geometric similarity with empirically derived correction factors to predict field-scale scour behavior.

The objective is to evaluate the extent to which field-scale simulations reproduce key features observed at laboratory scale—such as local and global scour evolution, velocity amplification, and bed shear stress—and to assess the applicability of the scaling methodology for predicting scour around jacket-type foundations on field dimensions.

5.1. Field scale results - Morphodynamics

To analyze the morphodynamics at field scale, the same methodology as in the laboratory-scale comparison is applied. Echosounder locations are scaled accordingly and positioned at equivalent locations within the field-scale domain. The resulting scour depth and timescales are evaluated using dimensionless axes, enabling a direct comparison with the laboratory measurements.

In addition, the overall bed evolution is assessed using plan-view plots of the bed level at selected time intervals. This allows for a qualitative evaluation of the global morphodynamic response across the domain.

5.1.1. Local scour

The evolution of local scour around the piles is analyzed for both clear-water and live-bed regimes using data from echo-sounders positioned and scaled to represent field-scale conditions. Each figure presents the comparison between laboratory- and field-scale results for multiple echo-sounder locations, distinguishing between upstream and downstream piles.

Figure 5.1 shows the scour development under clear-water conditions. Both lab and field-scale results are plotted using the same vertical axis (S/D) for consistent comparison. Although an attempt was made to use a dimensionless time scale based on the formulation by Sumer and Fredsøe (2002), this proved ineffective; the dimensionless time failed to align the scour evolution across scales. Therefore,

each scale is plotted with its original time axis: hours for the laboratory and days for the field, while maintaining the same dimensionless vertical scale.

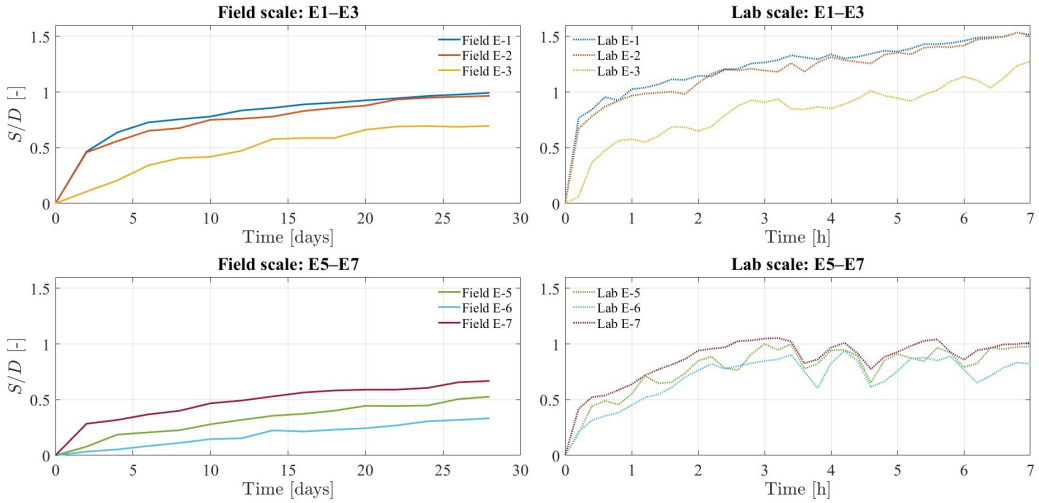

Figure 5.1: Local scour evolution at upstream and downstream piles under clear-water conditions: comparison between laboratory- and field-scale results.

For the clear-water regime, the results indicate that equilibrium conditions are not yet reached after 30 days of morphological time at field scale. However, the scour envelope appears well developed. Although the final scour depth cannot be precisely determined on this plot, the current results suggest slightly lower magnitudes compared to the laboratory case. The temporal evolution of scour at field scale appears less dynamic than in the laboratory-scale numerical model, exhibiting a smoother and more consistent hyperbolic trend.

Figure 5.2 presents the scour development under live-bed conditions. In this case, equilibrium is reached much faster—approximately within 2–3 days of morphological time in the field-scale model. The scour evolution follows a smoother exponential trend at field scale, whereas the laboratory data show more dynamic fluctuations. The final scour depths stabilize around $S/D \approx 1.1$ for upstream while for downstream locations is below 1. A slight reduction in downstream scour is observed after three days, which is not an expected behavior of scour. This happens because of the sediment deposition downstream which affects the local scour.

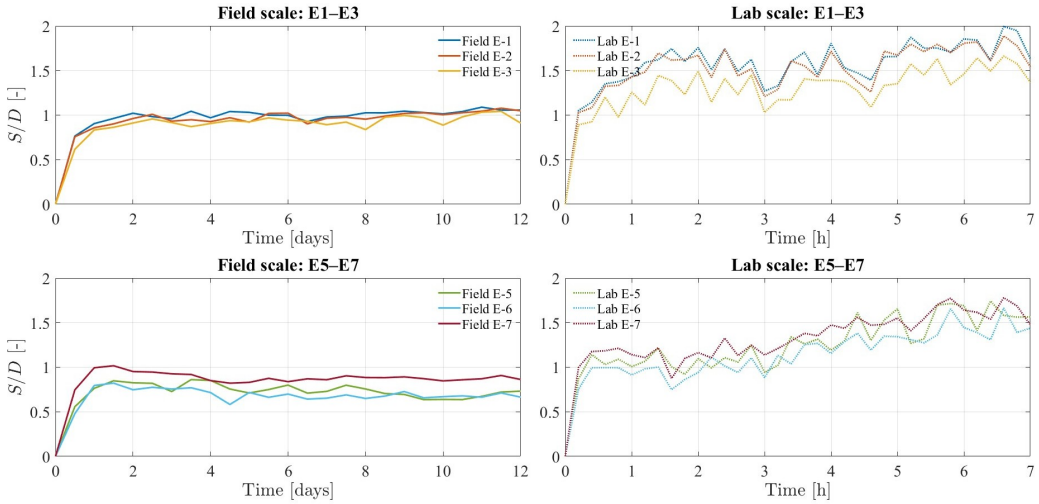

Figure 5.2: Local scour evolution at upstream and downstream piles under live-bed conditions: comparison between laboratory- and field-scale results.

In both regimes, the magnitude of scour is consistently greater at upstream piles than at downstream ones. This trend is consistent with both laboratory measurements and numerical model results. Additionally, field-scale simulations yield lower scour depths than lab-scale cases as expected. The timescale required to reach equilibrium in the live-bed regime is on the order of days, whereas in the clear-water regime it appears to extend to several weeks or even months, as equilibrium is clearly not achieved within the simulated period of 30 days.

5.1.2. Global scour

Regarding global scour for clear water regime, echo-sounders E4 and E8 display minimal scour, maintaining values below 0.1 S/D with limited temporal variability—much lower than what was observed in the lab and lab-scale numerical simulations.

To complement the time-series analysis, bedform patterns are shown in Figure 5.3. The results confirm that the scour development remains in its early stages, likely far from equilibrium. The observed state is comparable to that of the lab experiments later than 90 minutes of lab time.

Two key observations can be drawn from the plan view results. First, the dynamic scour behavior typically observed downstream is not yet present in the field-scale simulations. This absence has been apparent since the early stages of scour development and differs from the lab-scale results, where dynamic fluctuations were evident. No dunes are present in the field-scale case—unlike in the laboratory model—suggesting that the dynamic downstream behavior may not develop under these conditions. Also, lower magnitude of global scour or better said, no global scour is present, therefore raising the question if this is the case for the field.

Second, the overall scour footprint, especially the characteristic downstream pattern oriented at approximately 30 degrees from the flow direction, aligns well with the patterns documented in laboratory experiments, indicating that some spatial features of the scour geometry are preserved across scales.

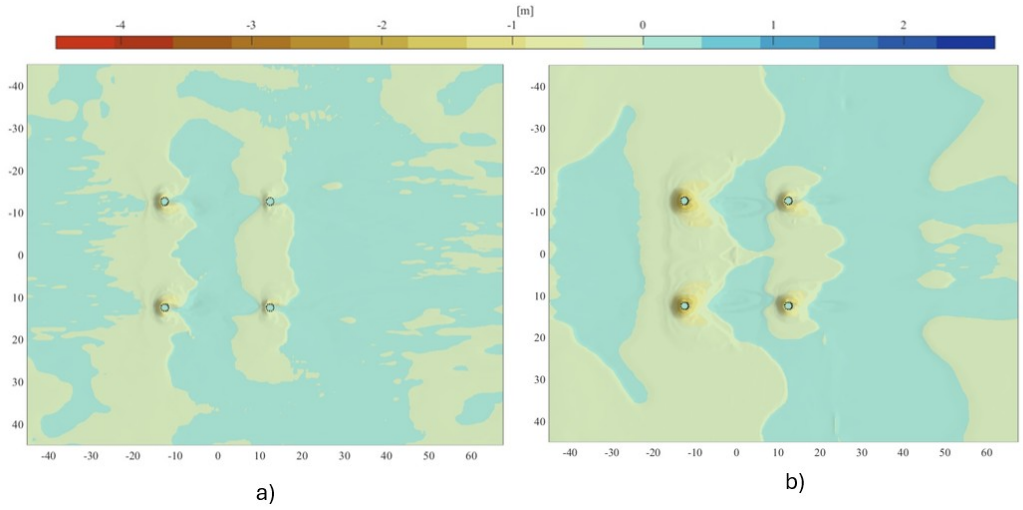

Figure 5.3: Bed level results at field scale for the clear-water regime — a) After 5 days; b) After 30 days.

Figure 5.4 shows the plan view of bed level evolution under live-bed conditions at two time instances: after 2 days and after 12 days of morphological time. The extended upstream domain effectively prevents the upstream migration of dunes. However, significant sediment deposition is observed downstream, which appears to influence the local scour behavior near the downstream piles filing back the scour holes, contradicting what it was observed on the lab scale models. The causes of this deposition and whether it represents a realistic morphodynamic response were not investigated in this study due to time constraints.

Given that equilibrium for local scour appears to be reached within the first 2–3 days, and that the influence of downstream sedimentation becomes significant afterward, the analysis of results will focus

primarily on this early time window. This ensures that the assessment reflects the undisturbed scour development more accurately.

Values on E4 and E8 reach approximately 0.4 S/D, which is lower than those observed in the lab-scale model. However, these values should be interpreted with caution, as they may still be influenced by downstream sediment accumulation, and are therefore not conclusive.

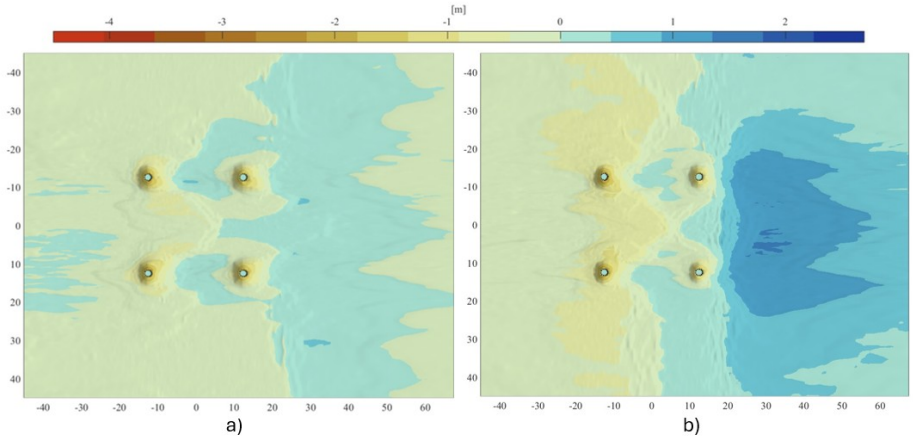

Figure 5.4: Bed level results at field scale for the live-bed regime — a) After 2 days; b) After 12 days.

The field-scale morphodynamic results provide a comprehensive view of both local and global scour development under clear-water and live-bed conditions. For local scour, the magnitude is consistently lower than in laboratory simulations, and equilibrium is achieved only under live-bed conditions. The timescale for reaching equilibrium in the live-bed regime is on the order of 2–3 days, whereas for the clear-water regime, equilibrium is not attained even after 30 days, suggesting that the characteristic timescale lies in the order of weeks to months.

In both regimes, scour is more pronounced at upstream piles than downstream ones. This spatial asymmetry aligns with patterns observed in laboratory experiments and numerical lab-scale models.

Regarding global scour, the clear-water regime shows minimal development, with echo-sounders E4 and E8 registering values below $0.1\,S/D$, and plan-view plots confirming the absence of dune formation or significant bed-level change. The global scour footprint is still in an early stage, and no dynamic downstream behavior—such as scour amplification or sediment wave migration—is observed within the 30-day window.

Under live-bed conditions, global scour behavior is more complex. Although equilibrium local scour is reached early, downstream sediment deposition becomes dominant in later stages, partially filling the scour holes and disturbing the long-term trends. This sediment infill process, which was not observed in the laboratory-scale model or physical tests, introduces uncertainty regarding the realism of the morphodynamic response at field scale. Due to time constraints, the origins and implications of this behavior were not investigated further.

Overall, the field-scale model successfully captures the primary features of local scour development, including equilibrium behavior under live-bed conditions and the spatial distribution of scour depths around the jacket foundation. However, global scour remains less developed in both regimes compared to the laboratory results, and sediment dynamics downstream— under live-bed conditions—require further investigation to assess their physical validity.

5.2. Hydrodynamics Comparison – Field Scale Results

To understand the effects of scaling, the hydrodynamic behavior and response is compared to the results obtained in the observation of flow conditions at lab scale. This allows for the assessment of how hydrodynamic processes scale and enables interpretation of the resulting morphodynamics for

both flow regimes. As discussed in Section 2.1.5, smaller-scale models typically exhibit more frequent eddies and higher vorticity due to reduced pile size. This section evaluates these effects using results from validated and in-house numerical models.

The comparison focuses on horizontal and vertical velocity magnitudes, as well as the amplification of bed shear stresses. These quantities were extracted at the end of the spin-up period—when the bed remained fixed and morphodynamic updates had not yet begun—ensuring a meaningful comparison of hydrodynamic patterns, consistent with the approach used in Chapter 4.

A key distinction in the field-scale model is the use of a longer spin-up period, which was necessary due to the larger domain when compared to lab scale. To ensure statistically reliable time-averaged flow fields, a recording duration of 300 seconds was selected. This timeframe guarantees the capture of at least 50 macroscale structures, based on the pile diameter and inflow velocity, providing a robust basis for hydrodynamic comparison following the same approach that in the lab scale.

5.2.1. Horizontal Velocities

Figures 5.5 and 5.6 show the normalized horizontal velocities for the clear-water and live-bed regimes, respectively.

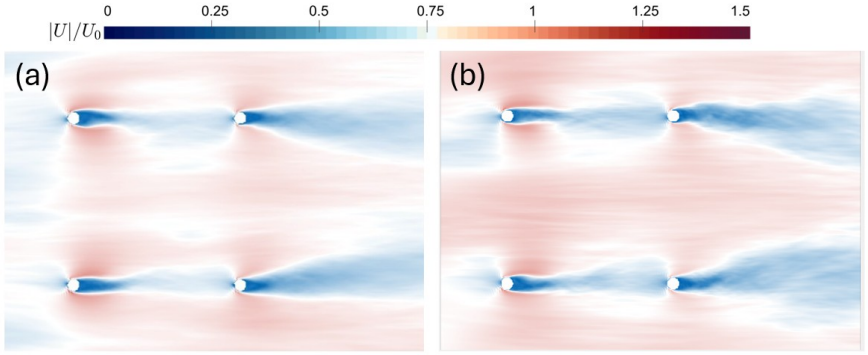

Figure 5.5: Time averaged normalized horizontal velocity at a plane 2 cm above the bed in lab scale (a) or 90 cm in field scale (b) (clear-water regime).

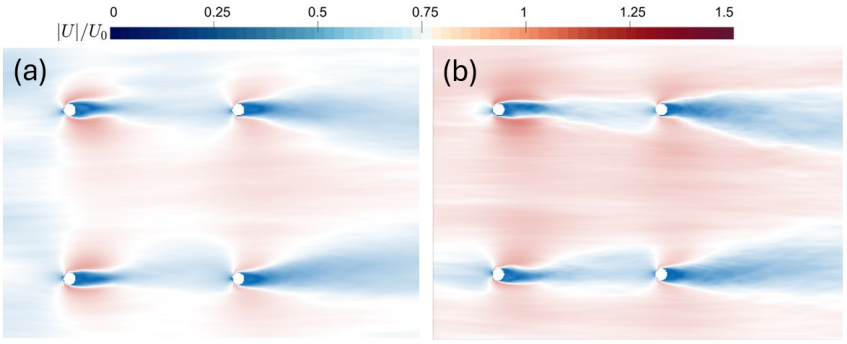

Figure 5.6: Time averaged Normalized horizontal velocity at a plane 2 cm above the bed in lab scale (a) or 90 cm in field scale (b) (live bed regime).

In the clear-water regime, both lab and field-scale results from TUDflow3D show similar horizontal velocity amplification, with a factor of approximately 1.5 compared to the inflow velocity. However, the field-scale simulation shows this amplification extending beyond the footprint of the jacket structure, unlike the lab-scale model where it remains confined.

For the live-bed regime, both models show similar amplification magnitudes (around 1.5) around the

piles. In both regimes, a consistent observation across all models is that upstream piles experience greater velocity amplification than downstream piles, which aligns with expected flow behavior.

5.2.2. Vertical Velocities

Figures 5.7 and 5.8 present the vertical velocity distributions for both flow regimes. I

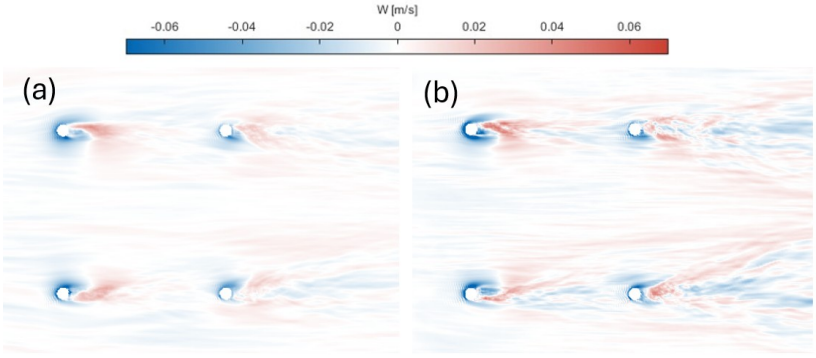

Figure 5.7: Time averaged vertical velocity at a plane 2 cm above the bed (lab scale) or 90 cm (field scale) for: (a) TUDflow3D model – lab scale, and (b) TUDflow3D model – field scale (clear-water regime).

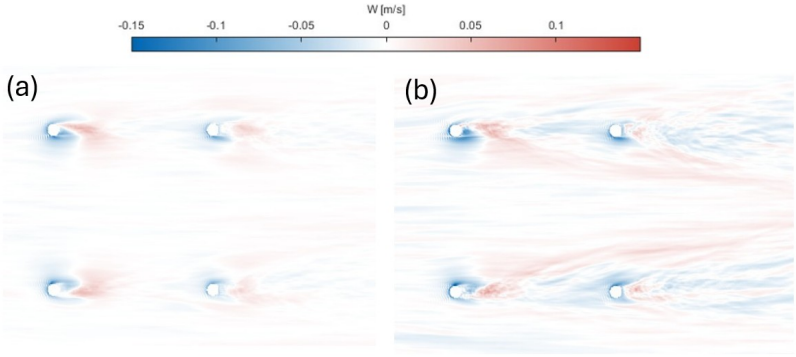

Figure 5.8: Time averaged vertical velocity at a plane 2 cm above the bed (lab scale) or 90 cm (field scale) for: (a) TUDflow3D model – lab scale, and (b) TUDflow3D model – field scale (live bed regime).

In the clear-water regime, the field-scale results replicate the patterns observed from the lab scale model result, such as downflow in front of the pile and upward motion along the sides due to vortex shedding. These vortices appear larger and more intense at field scale.

For the live-bed regime, both models show similar vertical flow patterns, with stronger magnitudes in the field-scale case. The consistent trend of higher velocities around upstream piles remains evident across all models.

5.2.3. Bed Shear Stresses

To interpret the scour response, bed shear stresses are analyzed next. Since bed shear stress is proportional to the square of velocity, a velocity amplification of 1.5 theoretically results in a shear stress amplification of approximately 2.25. However the lab-scale model show actual shear stress amplifications of around 8, due to vortex-induced turbulence and flow separation.

Figure 5.9 compares the bed shear stress distributions for the live-bed regime around an upstream pile. The behavior fo the clear water regime was comparable on terms of magnitude of the amplification and shape.

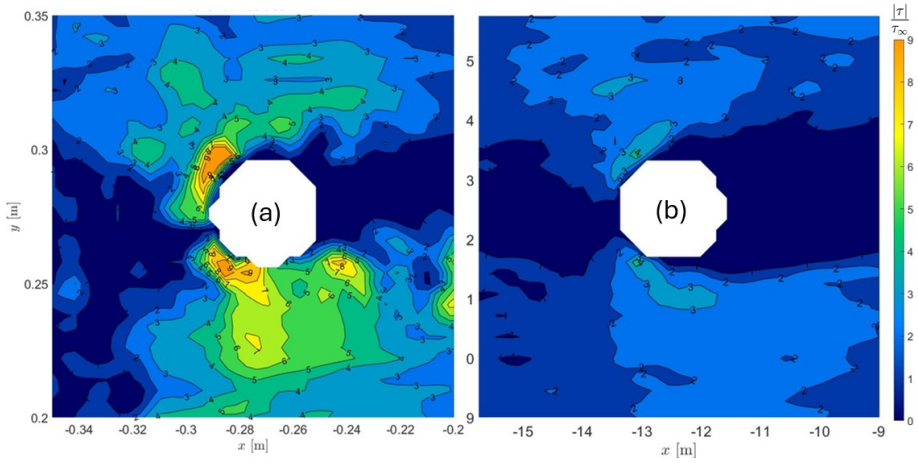

Figure 5.9: Normalized time-averaged bed shear stress for (a) lab scale and (b) field scale model results for the live bed regime

The lab-scale model show peak amplification near the pile of around 9 for the upstream piles, while the field-scale model shows a lower amplification of approximately 4 to 5. For the downstream piles the amplification of the lab scale results is around 7 to 8 while for the field scale si around 3 and 4. The spatial pattern is consistent across all models, with the highest stresses at the front of the pile, slightly tilted inward. The influence area in the field-scale case is smaller, likely due to reduced wake vorticity and turbulent intensity.

These results are consistent with the findings of Ettema et al. (2006), who showed that smaller structures generate stronger vortices and higher vorticity, leading to increased bed shear stress. Consequently, this suggests that scour magnitudes at field scale may be lower due to these reduced hydrodynamic intensities.

The comparison between lab- and field-scale hydrodynamic results shows that velocity amplification—both horizontal and vertical—scales consistently across regimes. For both clear-water and live-bed conditions, similar amplification factors of approximately 1.5 (relative to the inflow velocity) were observed, with upstream piles consistently exhibiting higher flow intensities.

In contrast, differences were found in bed shear stress amplification. While the lab-scale simulations showed peak amplifications up to nine times the reference stress, the field-scale model produced values closer to five. This 45% reduction in amplification occurred despite maintaining the same mobility ratio. The observed discrepancy is attributed to weaker vortex generation and reduced turbulent intensity at larger scales.

These findings align with the hypothesis of Ettema et al. (2006), who proposed that a decrease in relative roughness D/D_{50} at larger scales results in diminished vortex-induced turbulence. As a result, lower bed shear stress intensities may emerge, contributing to the reduced scour magnitudes observed at field scale for both flow regimes. This gives an insight on an over estimation of vorticty, bed shear stresses and consequently scour magnitude at lab experiments.

5.3. Scaling up lab results

Until now, the main scaling effects relevant to scour have been described as twofold. First, the dimensionless scour depth S/D is expected to decrease at field scale due to the increased pile diameter relative to a fixed sediment grain size. This has also been observed on the reduction of the amplification of be shear stresses around the structure.

Second, the characteristic timescale of scour development is influenced by the ratios of equilibrium scour depth and velocity according to Silva-Muñoz and Broekema (2025). These effects have been discussed for monopile foundations. In this section, however, we apply and analyze these principles for jacket-type foundations, which have more complex geometries and potentially different hydrodynamic responses.

To account for these scaling effects, Broekema and de Wit (2025) proposed the relations discussed in Section 2.1.5, which allow estimation of the field-scale equilibrium scour depth based on laboratory results, and a consistent approach for timescale transformation from lab to field conditions.

Table 5.1 summarizes the geometric and empirical parameters used, along with the resulting scaling factors for both clear-water (CW) and live-bed (LB) regimes. When working with dimensionless scour values (such as S/D), the geometric factor n cancels out. Therefore, the only correction needed is through n_s for the clear-water regime, and $n_s \cdot \omega_s$ for the live-bed regime, yielding factors of approximately 0.51 and 0.64, respectively, that will reduce the magnitude of scour fo the lab scale results. This matches the behavior already observed in both model results and previous literature.

It is also worth noting that the timescale scaling factor is significantly larger in the clear-water regime compared to the live-bed regime. This is consistent with physical expectations, as higher flow velocities in the live-bed regime lead to a more rapid scour response, which is reflected in the smaller scaling correction factor.

Table 5.1: Summary of geometric scaling parameters, correction factors, and resulting scaling factors for equilibrium scour depth and timescale.

Regime	n	n_s	n_d	n_{lp}	ω_s	ω_t	S_{eq} scaling	T_c scaling
CW	45	0.51	1.42	–	–	–	23	185
LB	45	0.51	1.40	0.16	1.26	0.27	29	80

These scaling factors are then applied to scale the laboratory results to field-scale predictions for averaged scour profiles for upstream and downstream piles. The results of this transformation, for both numerical models, are presented and compared in Figures 5.10 and 5.11.

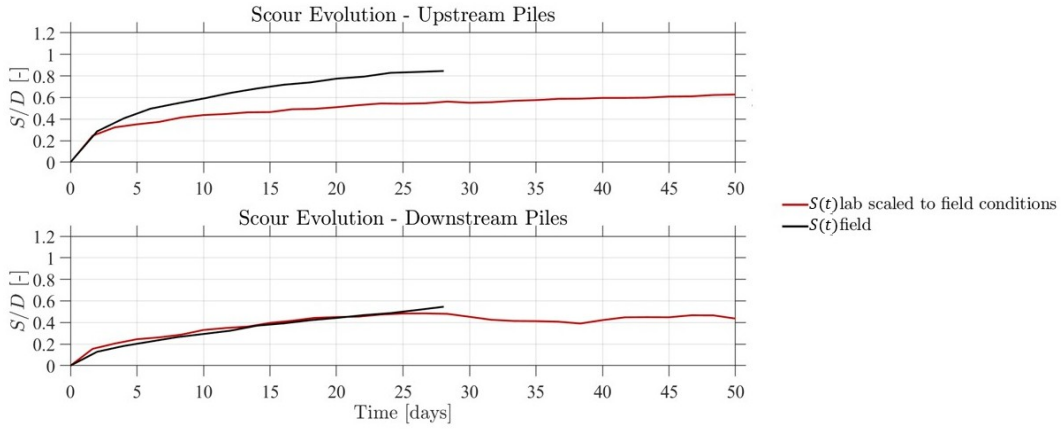

Figure 5.10: Comparison of scaled laboratory results and field-scale predictions for averaged scour depth (S/D) under clear-water regime. Results are shown for both upstream (up) and downstream piles (down).

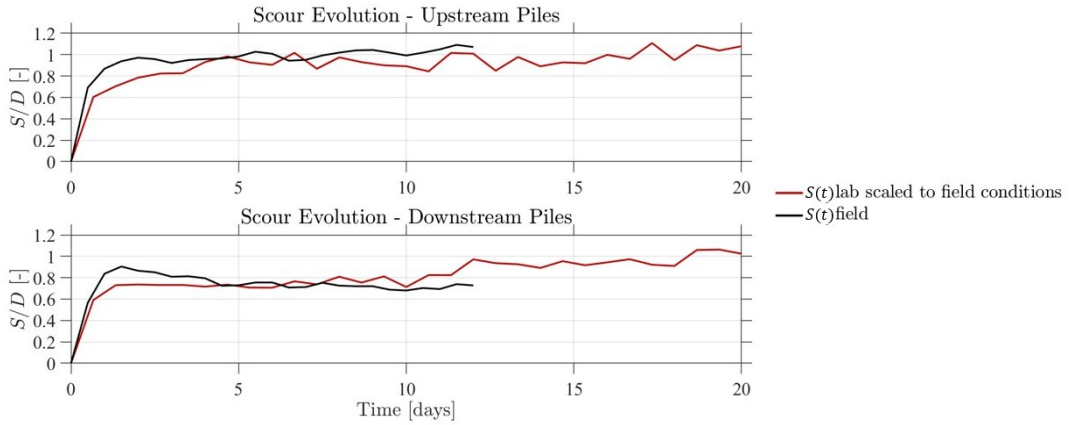

Figure 5.11: Comparison of scaled laboratory results and field-scale predictions for averaged scour depth (S/D) under live-bed regime. Results are shown for both upstream (up) and downstream (down) piles.

For the clear-water regime, the scaled laboratory results tend to underestimate the scour magnitude, particularly for the upstream piles. Downstream pile magnitudes initially match well between the lab and field data. After 30 days, the scaled up laboratry results start to show a dynamic beavior, influenced by the dunes downstream on the lab scale numerical model. This was no observed on the field scale model, but in order to be sure if they will appear or not a longer simulation needs to be done. These dynamics ultimately influence the scour envelope and its temporal evolution.

The time scaling appears appropriate for both clear and live bed regime, showing the evolution of the envelope with the same shape and scour rate.

The live-bed regime shows a better agreement between the scaled laboratory and field-scale results, both in terms of scour magnitude and temporal evolution. The scaled lab data successfully capture the steep initial growth observed in the field, which is characteristic and very important for live-bed conditions.

One discrepancy arises after approximately 3 days, where a reduction in scour is observed in the field-scale model. This is related to boundary effects specific to the numerical setup and is not present in the lab. Despite this, the final scour depth remains around 1 in both cases, confirming a strong match.

These results highlight the importance of incorporating the correction factors for velocity scale (w_s) and time scale (w_t), which are critical for accurately reproducing the live-bed scour behavior using scaled laboratory data.

To assess the accuracy of the predicted scour magnitudes, Table 5.2 presents a quantitative comparison between the results from the numerical model on laboratory scale, the results from the numerical model on field scale, and the analytically derived values from Broekema and de Wit (2025) for the equilibrium scour depth (S_{eq}/D). For the clear-water regime, the scaled values underestimate the field-scale scour, as also observed in the plotted results. Although the largest visual discrepancy appears upstream, the greatest relative difference in S_{eq} occurs for the downstream piles, reaching up to 40%. This deviation is attributed to the presence of dunes in the laboratory model, which reduce the scour depth over time by interrupting the exponential growth phase. These bedform-induced effects are not present in the field-scale clear-water regime, reinforcing the earlier observation that dune dynamics in laboratory conditions significantly influence scour development and may not accurately reflect field-scale behavior.

Table 5.2: Comparison of equilibrium scour depths (S_{eq}/D) between lab scale model results, field-scale model results and field scale scaling predictions.

Regime	S_{eq}/D Lab	S_{eq}/D Field	S_{eq}/D Scaled (Broekema, 2025)	Difference (%)
CW upstream	1.40	1.00	0.71	29
CW downstream	1.00	0.85	0.51	40
LB upstream	1.60	1.10	1.02	7
LB downstream	1.50	1.02	0.95	6

In contrast, the live-bed regime shows significantly better alignment. Both upstream and downstream locations display low discrepancies (7% and 6%, respectively) between laboratory and field-scale values. This consistency confirms the effectiveness of the applied scaling laws, particularly the inclusion of the velocity and time correction factors (ω_s and ω_t), in accurately reproducing live-bed scour behavior.

Overall, the analysis presented in this section demonstrates the utility and limitations of applying geometric and empirical scaling factors for laboratory models to scour predictions around jacket-type foundations. While the clear-water regime reveals some limitations due to physical processes not directly transferable between scales (e.g., dune migration), the live-bed regime validates the robustness of the applied framework.

This confirms that, when appropriate correction factors are applied, scaled laboratory experiments can yield meaningful and realistic predictions of scour development at field scale. Moreover, it demonstrates that the methodology proposed by Broekema and de Wit (2025) is effective not only for monopiles but also for more complex structures such as jacket foundations. The consistency observed in both upstream and downstream scour patterns further supports the robustness of the scaling approach for different regions around the structure.

5.4. Field scale results summary

The field-scale simulations presented in this chapter provide detailed insights into the development of scour around jacket foundations and offer a solid basis for evaluating the applicability of laboratory results at realistic scales. Local scour was found to exhibit consistent spatial patterns across scales, with scour magnitudes at upstream piles exceeding those at downstream ones in both regimes. However, field-scale scour magnitudes were systematically lower than their laboratory counterparts. While the live-bed regime reached equilibrium within 2–3 days of morphological time, the clear-water regime continue developing after 30 days, suggesting a much longer characteristic timescale.

Global scour development showed more variability. Under clear-water conditions, minimal global scour and no dunes downstream were observed at field scale, in contrast to dynamic behaviors seen in the laboratory simulations. In the live-bed regime, local scour reached equilibrium around 3 days, but downstream sediment deposition began to affect the scour footprint in later stages. This downstream infill was not observed in lab-scale results and remains an open question, potentially influenced by the extended field domain and unsteady sediment dynamics.

The comparison between field- and laboratory-scale results, reinforced by the scaling approach of Broekema and de Wit (2025), demonstrates that scaled laboratory data can provide realistic predictions of field-scale scour magnitudes and timescales. The strong agreement observed in the live-bed regime highlights the robustness of the applied methodology—not only for monopile foundations, for which it was originally developed, but also for more complex jacket structures. In contrast, the discrepancies identified under clear-water conditions—particularly those associated with dune migration and delayed scour development—underscore the limitations of direct scaling when regime-specific physical processes are not adequately accounted for.

6

Analysis of model results: Enhancing scour understanding

This chapter directly addresses one of the core research objectives: enhancing the understanding of scour behaviour—both local and global—around 4LJ foundations. The chapter is structured into separate sections for local and global scour, each assessing magnitude, spatial distribution, and temporal development under clear-water and live-bed regimes at both laboratory and field scales. As well in this chapter are evaluated empirical scour relations developed for monopiles to determine their applicability and limitations when applied to jackets. By doing so, the study investigates how well monopile-based formulations capture regime-dependent behavior, upstream–downstream differences, and scale effects.

A further research objective is to demonstrate the advantages and flexibility of numerical modeling for scour assessment. The use of a CFD morphodynamic model enables high-resolution analysis of both hydrodynamic and morphological processes, providing outputs that are difficult to obtain experimentally. Collectively, the results in this chapter provide both process insight and practical guidance for the design and maintenance of jacket foundations in diverse marine environments.

6.1. Local scour

To characterize scour around jacket foundations, it is essential to assess different aspects of the scour depth. The spatial extent of its influence and its evolution over time are of interest. While these aspects have been extensively studied for monopile structures, research on 4LJ remains relatively limited. In this section, the validated numerical model is leveraged to go beyond existing efforts by providing a detailed, time-resolved analysis of local scour patterns around jacket-type foundations under lab and field-scale conditions.

6.1.1. Local Scour Footprint

This section explores different methods to define a representative scour footprint. In this context, the local scour footprint refers to the area of the bed that is directly influenced by the presence of the pile.

According to Bolle et al. (2010), which based their findings on monopile foundations, the region within approximately 0.5 D of the pile generally forms a plateau corresponding to the maximum local scour depth. Beyond this plateau, the bed profile transitions into a sloping region where the bed level gradually recovers to its undisturbed state. A similar range for the horizontal influence of local scour—around 1.5 D–1.9 D—is reported by Welzel et al. (2023).

To estimate the horizontal extent of local scour influence, Bolle et al. (2010) proposed approach is used with an additional term. While this method was originally formulated for monopiles—where global scour is negligible—jacket foundations also experience global scour, which must be accounted for. In this study, a modified formulation is tested in which the global scour depth is subtracted from the local

scour depth before multiplying by the slope, thereby isolating the extent attributable to local scour. This adapted approach is applied to both flow regimes and to piles located upstream and downstream.

The resulting formulation is given by:

$$\text{Local scour footprint} = 0.5D + \text{sediment slope} \times (\text{Local scour depth} - \text{Global scour depth})$$

The results for the extent of local scour influence, expressed as multiples of D, are summarized in Table 6.1. The resulting distances represent the expected reach of local scour from the pile perimeter on both the inner (facing the other pile) and outer sides.

Table 6.1: Extent of local scour influence (from pile perimeter) for upstream and downstream piles under clear-water and live-bed regimes. Distances are expressed in multiples of D.

Location	**Clear-water**				**Live-bed**			
	Upstream		Downstream		Upstream		Downstream	
	Inner	Outer	Inner	Outer	Inner	Outer	Inner	Outer
Distance	$2.5D$	$3D$	$2D$	$2.5D$	$2.5D$	$2.5D$	$1.5D$	$2D$

From this it can be observed that the scour footprint is smaller towards the inner side of the jacket, this mainly because global scour is much higher inside than outside. Also, for the live bed regime the scour footprint is smaller, even if the scour depth magnitude is higher. This is mainly due to the significant magnitude of global scour.

To evaluate these results, the calculated distances were compared using plots such as Figure 6.2, which illustrates their application for the live-bed regime on the upstream piles at 420 minutes. In the cross-section view, the horizontal extent of local scour is shown on either side of the pile, while the plan view depicts the corresponding extent for each pile footprint.

The results show that the proposed distances delimit the region influenced by each pile, thus defining a clear boundary between local and global scour. Furthermore, it has shown the role of global scour in the temporal evolution and spatial extent of local scour. This analysis was carried out for both flow regimes and for piles located upstream and downstream, showing the same results as on the figure in this section; the complete set of figures is presented in the Appendix C.

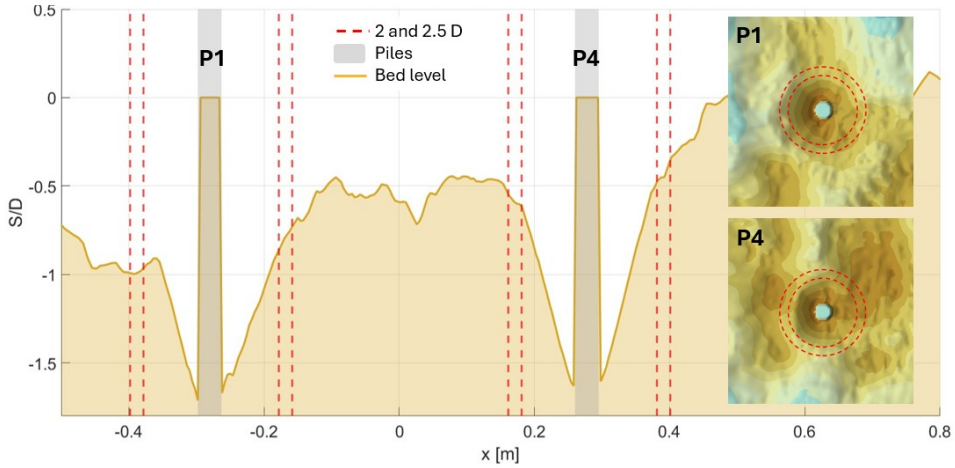

Figure 6.1: Example application of the local scour footprint results for the live-bed regime on upstream piles. The cross-section view shows the extent of local scour from the pile perimeter, while the plan view indicates the corresponding extents for each pile footprint.

To assess this behavior over the entire morphodynamic evolution, a ring-based method is applied to track the temporal and spatial evolution of the scour footprint on all the timesteps of the model. In this approach, the scour depth is averaged within concentric rings centered on the pile, starting at the pile perimeter. The first ring is a zero-thickness boundary at the pile edge, followed by successive rings of uniform thickness D/2 (0.02 m), extending outward to a radial distance of 3D, resulting in seven discrete rings. This setup captures the radial variation in scour intensity over time. An example of the ring layout is shown in Figure 6.2.

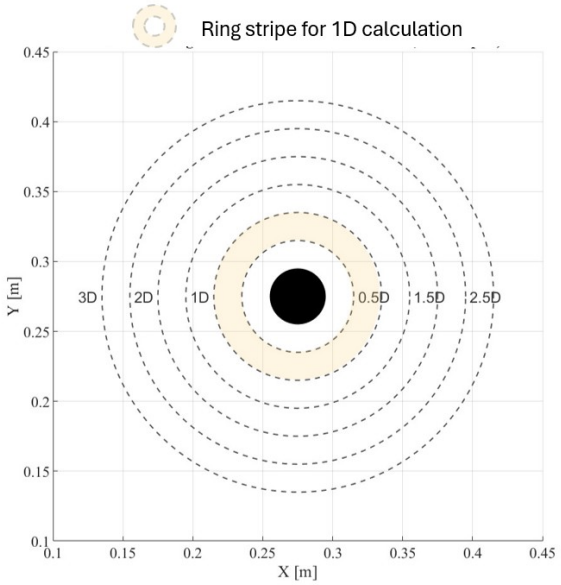

Figure 6.2: Layout of concentric rings used for average scour depth analysis around a specific pile.

The analysis is performed averaging the upstream and downstream piles, given the different nature of each and for both clear-water and live-bed regimes. Figure C.5 illustrates the results for the clear-water regime on the upstream piles. The live bed regime results are presented on Appendix C.

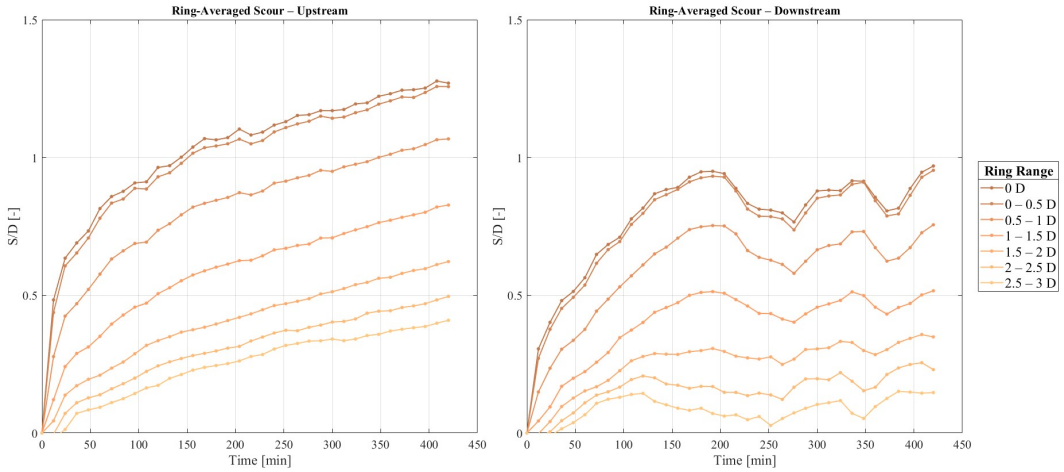

Figure 6.3: Scour evolution for upstream (Left) and downstream (Right) piles for the clear water regime.

The results show that the average scour depths for the first two rings — up to 0.5D — are nearly identical thought the whole morphological time, confirming the idea of the plateau described by Bolle et al. (2010). Beyond this region, a geometrical decrease in scour depth is observed up to a distance of three times the diameter replicating the effect of contour lines for the clear water regime. This supports

the idea of a maximum value around 0.5D and also suggests that local scour effects can extend to 3D through the almost the whole scour time evolution, as calculated on the last timestep.

When analyzing the results by regime, some differences emerge between the clear-water and live-bed conditions. In the clear-water regime, the scour response in the outer rings develops gradually. Even after 30 minutes, the first signs of scour appear on the outer rings, indicating that the footprint of local scour evolves over time.

In contrast, the live-bed regime exhibits an immediate and fully developed scour footprint from the start of the simulation. Another observation is on the downstream piles for live bed regime, after the 200 minutes there is a sudden rise on scour not following the exponential behavior, and it coincides when global scour almost reaches this magnitudes of scour, so this is a clear presence of interaction of global scour affecting the time development and magnitude of local scour.

Another important observation is that, for the live-bed regime, the area of influence is smaller than in the clear-water regime. At a radial distance of 2.5 D, the scour depths are nearly identical. This finding is consistent with the previously computed areas of influence.

The same analysis is conducted for the field scale model results, as illustrated in Figure C.7. Similar to the laboratory-scale observations, the results show that the maximum scour depth occurs within the first two rings, indicating that the scour depth remains at the same magnitude around approximately 0.5D. Additionally, for both the clear-water and live-bed regimes, the scour footprint extends up to around 2.5D.

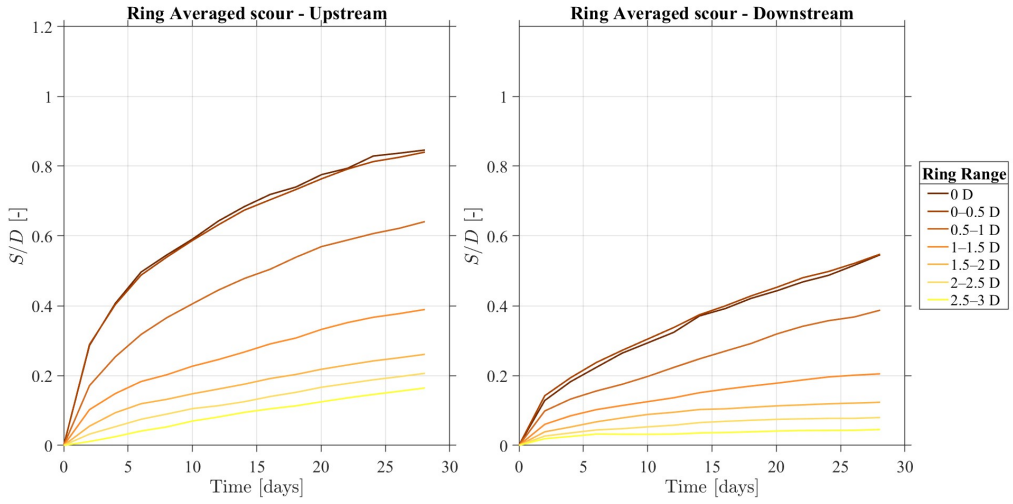

Figure 6.4: Scour evolution for upstream (Left) and downstream (Right) piles for the clear-water regime.

For the clear-water regime, no delay is observed in the development of the scour footprint, contrary to what was noted in the lab-scale model. The scour evolution follows a clear exponential trend without the oscillatory behavior seen in the laboratory results.

In the live-bed regime, the field-scale model also exhibits a smoother trend, likely due to a less dynamic sediment bed. It can also be noted that on the downstream piles the values after 3 days are disturbed by the boundary condition observed in section 5.1. The presence of sand waves is notably reduced in the field-scale results for both regimes, highlighting a possible scale effect.

The average scour trends align well with the data collected by echo-sounders on laboratory and field scale, showing their usefulness in capturing local scour development. In both regimes, upstream piles consistently experience higher scour magnitudes. Overall, the field-scale simulations demonstrate similar patterns to those in the lab-scale model—both in terms of scour footprint extent and the plateau of maximum scour depth at approximately 0.5D.

The adapted method to determine the area of influence of local scour, modified to account for global scour in jacket foundations, proved effective in delineating the boundary between local and global scour.

Temporal analysis using the ring shows that this behavior is achieved through the whole morphodynamic evolution in time.

6.1.2. Equilibrium scour depth − Local Scour

In order to proceed to calculate the time response of scour for different models, first it needs to be assess the reliability of the fitting procedure. It was chosen the hyperbolic relation used by Welzel et al. (2019) as it has already been used before for 4LJ foundations equilibrium time determination.

To assess this fitting, the timescale of local scour for the numerical model was compared to the laboratory experiment. This approach was individually applied to each echo sounder. The resulting fits are provided in Appendix C.

The analytical formula captures the early scour development, with the fitted curves showing good agreement with the initial slopes of the laboratory measurements. Results suggest that downstream piles have likely reached equilibrium, while upstream piles have not, with estimated equilibrium times approaching 500 minutes for the clear water regime. Some upstream echo sounders even show values exceeding 600 minutes. This asymmetry in timescales is consistent with the observations from Welzel et al. (2023).

A summary of averaged equilibrium times across the echo sounders upstream and downstream is presented in Table 6.2.

Table 6.2: Mean equilibrium times (t_{90}) [min] for upstream and downstream echo sounders for both the laboratory experiment and numerical model

Condition	Lab Fit	Model Fit
Clear Water		
Upstream	486	451
Downstream	193	263
Live Bed		
Upstream	93	106
Downstream	106	187

In the live-bed regime, the averaged scour evolution from the upstream echo-sounders closely matches the timescale to equilibrium observed in the laboratory model. However, for downstream locations, the lab-scale numerical model overestimates the time required to reach equilibrium, suggesting a slower response caused by the interaction of global scour with local scour. Under clear-water conditions, the overall trend is consistent, with the average equilibrium times for upstream piles exceeding the 420-minute morphological simulation time. While the averaged timescales suggest reasonable agreement, this can be misleading, individual sensor responses vary considerably. For instance, echo-sounders E1 and E2 show equilibrium around 250 minutes, whereas E3 continues evolving past 800 minutes, for the lab scale numerical model.

To better assess the equilibrium time of the upstream piles under clear-water conditions, additional plots were generated using a logarithmic scale, with a focus on the tail of the scour evolution curve to identify the growth pattern at the end.

Figure 6.5 presents both the full scour evolution and a zoomed-in view of the tail for upstream sensor E1. The results indicate that the exponential trend in scour growth persists, suggesting that true equilibrium has not yet been reached. In contrast, the fitted hyperbolic curve prematurely converges toward an equilibrium value, with a t_{90} value of 287 minutes, failing to capture the ongoing scour development. This discrepancy implies that the estimatedt_{90} may be unreliable, particularly when the scour curve has not fully stabilized.

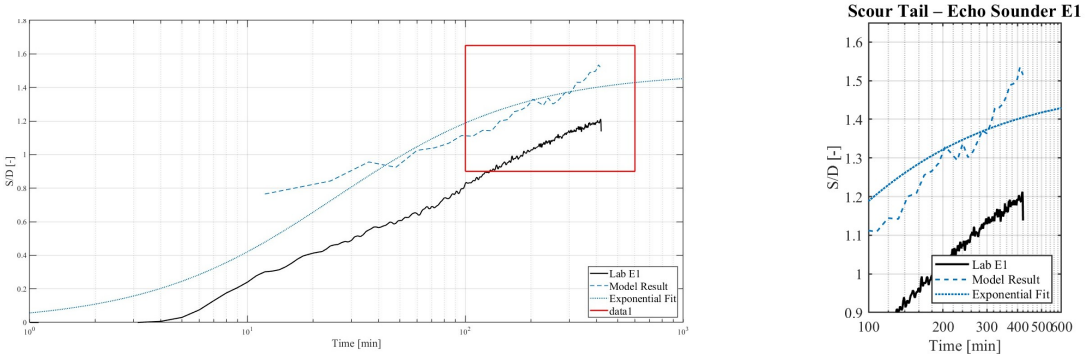

(a) E1 – Full evolution (Model)

(b) E1 – Tail (Model)

Figure 6.5: Model scour evolution for upstream sensor E1 under clear-water conditions.

Figure 6.6 illustrates the model results at upstream sensor E3. The tail of the time series displays a clear exponential growth, indicating that equilibrium has not yet been reached, as well as the fiiting hyperbolic relation to estimate the time to reach equilibrium. The hyperbolic fit estimates a time to equilibrium of approximately 800 minutes, which may serve as a representative value for the upstream piles, but not conclusive. This highlights the limitations of the current formulation, already highlighted by Silva-Muñoz and Broekema (2025) when defining that scour behavior around the pile behavior is characterized by a double hyperbolic or exponential formulation.

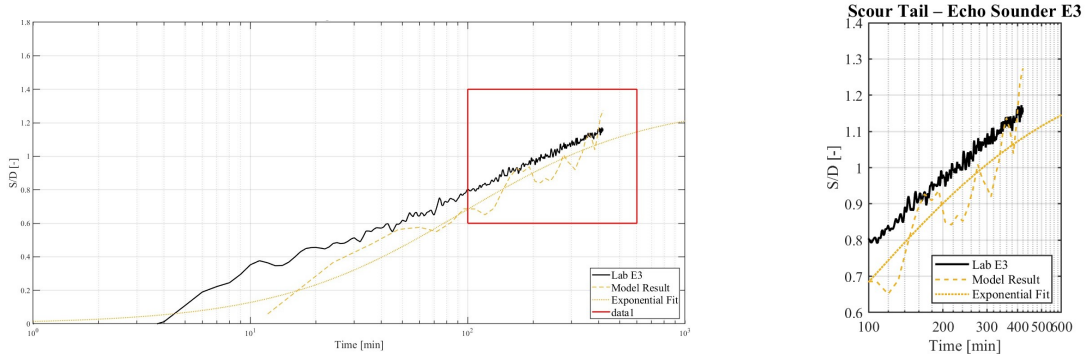

(a) E3 – Full evolution (Model)

(b) E3 – Tail (Model)

Figure 6.6: Model scour evolution at upstream sensor E3 under clear-water conditions.

Although the limitations of the exponential fitting approach are acknowledged, it remains a valuable tool for comparative analysis of scour development across different areas examined with the same method, but it does not mean that the timescales calculated will be the true equilibrium depth.

Once this limitation was determined, the post processing of only the numerical model results were done for characterizing better the scour behavior around the pile. It was of interest to explore the spatial variation of the timescale to reach equilibrium, average scour values within concentric rings (as previously defined) were fitted using this method. The results for both the clear-water and live-bed regimes are provided in the Appendix C.

Comparing the equilibrium times derived from the averaged scour depth within the 0.5 D0.5D ring to those obtained from the echosounder measurements shows good agreement. For the clear-water regime, the downstream piles reached equilibrium in approximately 300 minutes. In the live-bed regime, equilibrium times were about 93 minutes for the upstream piles and 150 minutes for the downstream piles, thereby supporting the validity of the results.

The result shows that regions closer to the pile reach equilibrium more rapidly for both regimes, increasing the equilibrium time as there is more distance from the pile. For instance, in the clear-water regime,

the outermost downstream ring requires more than twice the time to stabilize compared to the innermost ring. A similar pattern is observed under live-bed conditions (Table C.2), although the absolute timescales are shorter.

While the exact magnitudes derived from the fitting should be interpreted with caution, the observed spatial trends provide useful insights. In particular, they offer a trend of how scour behavior evolves radially from the pile. This can inform expectations of scour development in regions farther away, even if precise values remain uncertain due to the limitations of the fitting method.

To extend the analysis to field scale model results, exponential fits were also applied to the first ring ($0\,D$) of the field-scale model results for both regimes. These results are summarized in Table 6.3.

Table 6.3: Exponential fit results for the 0 D ring under both regimes (field scale).

Clear-Water Regime				
Ring	$t_{90,\text{Up}}$ (days)	$t_{90,\text{Down}}$ (days)	$S_{\text{eq,Up}}$ [-]	$S_{\text{eq,Down}}$ [-]
0 D	60	160	1.00	0.85
Live-Bed Regime				
Ring	$t_{90,\text{Up}}$ (days)	$t_{90,\text{Down}}$ (days)	$S_{\text{eq,Up}}$ [-]	$S_{\text{eq,Down}}$ [-]
0 D	2.2	3.0	1.05	1.02

Several key observations can be made. For both regimes, the downstream pile requires longer to reach equilibrium, which contrasts with the lab-scale results. In the clear-water regime, equilibrium at the upstream pile is reached in approximately 60 days, compared to 160 days downstream. Scour depth magnitudes are lower than in the lab scale, ranging from 0.85 to 1.0 S/D. In the live-bed regime, equilibrium times are significantly shorter—around 2 to 3 days—and align with was is observed in the scour evolution of time. This reinforces the idea that the fitting procedure is useful when the scour evolution already reached equilibrium, or the scour has stabilized. When this has not happened (clear water regime) the results can be taken as an order of magnitude, but not with certainty that after that period of time the equilibrium has been reached.

Important to mention, for the live-bed regime was applied only to the first 3 days of simulation, to ensure undisturbed conditions. A more detailed discussion of scale effects is provided in the section of scaling from this chapter.

This section has shown that a single term hyperbolic equation can have limitations at the time of determining equilibrium for scour depth. This might be to the lack of a second term that can account for the later development of scour, as observed on piles. The model matches laboratory and field scale model results well for the live bed regime, where scour already reached equilibrium. Furthermore, spatial trends indicate that areas closer to the pile reach equilibrium faster, a pattern observed consistently in both lab and field simulations. Finally, field-scale results show longer times to equilibrium in the clear-water regime, with the downstream pile reaching stability later than upstream, in contrast to the lab-scale behavior, and the order of magnitude for clear water regime for equilibrium is in the order of magnitude of months, while for live bed regime is in days.

6.2. Global scour

In this study, global scour is investigated under both clear-water and live-bed regimes at laboratory and field scales, looking as well at the extension of the footprint of the scour, the scour magnitude around the jacket and the timescale of it.

These objectives are addressed through the definition of a measurement methodology and detailed spatial–temporal analysis of scour development.

6.2.1. Global scour footprint

This section analyses the magnitude of scour and the spatial extent of the jacket foundation's influence on the surrounding sediment.

To quantify the magnitude of global scour, both a reference area and a consistent analysis framework are required. Global scour refers to the general lowering of the seabed across a wider region, beyond the immediate vicinity of the piles. In this study, a structured approach is applied to define both the spatial footprint and the temporal evolution of global scour.

As shown in Figure 6.7, a series of concentric square regions are defined around the centre of the jacket structure. Each square represents a fraction of the total jacket footprint (0.55 m), allowing the results to be expressed in dimensionless form and relative to the structure's overall extent. The average scour depth within each square is computed by subtracting the value of the previous inner square, yielding the mean scour depth for the strip between the two boundaries. This method is analogous to the ring-based approach previously applied to local scour, but employs square regions to better capture the development of scour patterns over time. In addition, the effect of local scour is removed from the global scour analysis by excluding a circular area with a diameter equal to three times the pile diameter, in line with the previously determined local scour footprint.

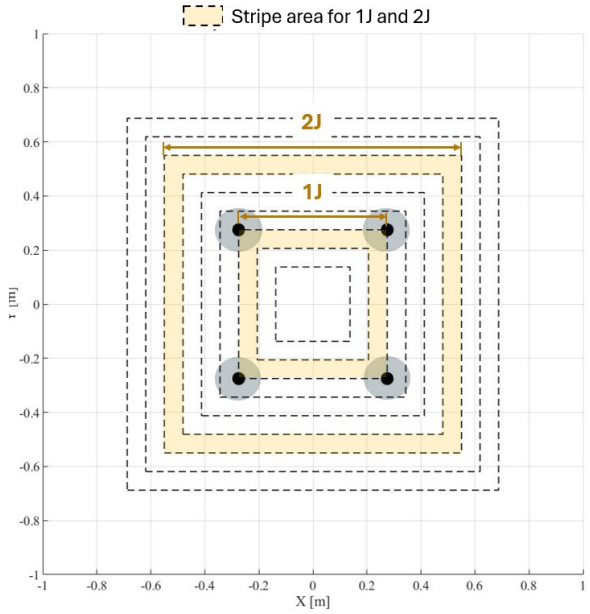

Figure 6.7: Square regions used for computing the global scour footprint.

Based on literature, it was hypothesized that the timescale of global scour development is slower than that of local scour, and that the associated scour depths are of lower magnitude. To test this, three timesteps are examined for both regimes using the square regions described above, with the jacket footprint taken as the unit length. The results are presented in Tables 6.4 and 6.5.

Table 6.4: Normalized scour depth (S/D) for the clear-water regime at different times, across concentric square regions (multiples of the jacket footprint J).

Time	**Dimensionless scour depth S/D for each area analyzed in terms of J**								
	0.5	0.5–0.75	0.75–1.0	1.00–1.25	1.25–1.5	1.5–1.75	1.75–2.0	2.0–2.25	2.25–2.5
90 min	-0.02	-0.01	0.02	0.03	0.08	0.03	-0.04	-0.03	-0.02
210 min	0.13	0.09	0.01	0.03	0.09	0.08	0.04	0.01	0.00
420 min	0.35	0.32	0.31	0.24	0.20	0.11	0.01	0.02	0.04

For the clear-water regime, even after 210 minutes, seabed changes remain relatively small, with maximum values around 0.10 D. After 420 minutes, global scour reaches magnitudes of approximately 0.30 D, but the affected area is limited to between 0.75 J and 1.0 J. Outside the jacket footprint, scour depths range from 0.10 to 0.20 D, and beyond 1.75 J the values are negligible, cloase to 0.

Table 6.5: Normalized scour depth (S/D) for the live-bed regime at different times, across concentric square regions (multiples of the jacket footprint J).

Time	Dimensionless scour depth S/D for each area analyzed in terms of J								
	0.5	0.5–0.75	0.75–1.0	1.00–1.25	1.25–1.5	1.5–1.75	1.75–2.0	2.0–2.25	2.25–2.5
90 min	0.77	0.72	0.58	0.42	0.32	0.18	0.04	-0.03	-0.07
210 min	0.72	0.70	0.60	0.52	0.47	0.31	0.18	0.11	0.04
420 min	0.85	0.80	0.69	0.52	0.47	0.36	0.28	0.17	0.12

In contrast, the live-bed regime shows an almost immediate seabed response. After only 90 minutes, scour depths within the jacket already reach values of 0.70–0.80 D. By 420 minutes, scour inside the jacket is in the range of 0.70–0.90 D, and at a distance of 2 J it still reaches approximately 0.30 D, indicating that the global scour footprint extends well beyond the jacket footprint.

To compare the magnitude and spatial distribution between regimes, both cases are plotted on the same scale in Figure 6.8. These results show that scour magnitude decreases with distance from the jacket center. For the clear-water regime, significant scour is largely confined within the jacket footprint, while for the live-bed regime, the influence extends to approximately 2 J, well beyond the jacket boundary.

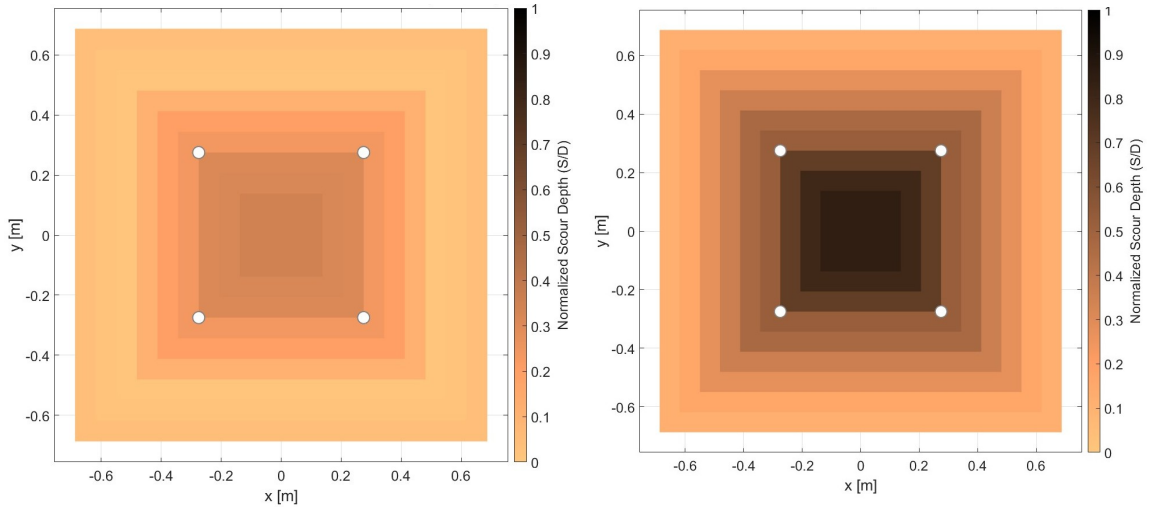

(a) Clear-water regime

(b) Live-bed regime

Figure 6.8: Average dimensionless scour depth around the jacket footprint under both regimes: a) Clear-water; b) Live-bed.

For the field-scale results, the clear-water regime did not exhibit any measurable global scour depth. This absence is likely linked to the limited simulated duration. Using the scaling approach proposed by Broekema and de Wit (2025), 200 minutes of simulation time corresponds to approximately 30 days in the field, suggesting that the lack of global scour may be due to a delayed morphological response. Nevertheless, differences in scour patterns are also evident. In the laboratory clear-water case, dunes on the downstream side appear as early as 90 minutes. These features are absent in the field-scale simulation, leaving the actual magnitude of global scour under clear-water conditions uncertain.

For the live-bed regime, the global scour results were also inconclusive. The measurements were influenced by an unexpected upstream migration of dunes, a phenomenon not observed in the laboratory experiments or on field campaigns and not anticipated in the physical behavior. Consequently, the

field-scale live-bed results do not provide a definitive estimate of global scour magnitude, though it is plausible that it is lower than the values observed at laboratory scale.

6.2.2. Timescale Analysis for Global Scour

The timescale of the scour response is also evaluated for global scour. As discussed in the previous sections, the temporal behavior differs significantly between the two flow regimes, requiring distinct approaches for each case.

For the clear-water regime, it was observed that in the innermost regions—particularly around the perimeter of the piles—the scour initiation began around 200 minutes into the simulation, displaying a near-linear increase before the end of the experiment. Although the simulation duration was insufficient to capture the full development, it can already be concluded that the global scour response is substantially slower than that of local scour, if there is a response. To better capture the full evolution, longer simulation times would be required.

In contrast, for the live-bed regime, the response is markedly different. The spatial analysis made on the section before indicate that the scour values from 210 minutes and 420 minutes were close, hinting to approaching equilibrium or at least having developed almost fully. This allows for a fitting procedure to be applied, using the same exponential model proposed by Welzel (2023) for local scour. The fit is applied to two regions: the strio of the jacekt footprint, 1J and another one outer around 1.75 J.

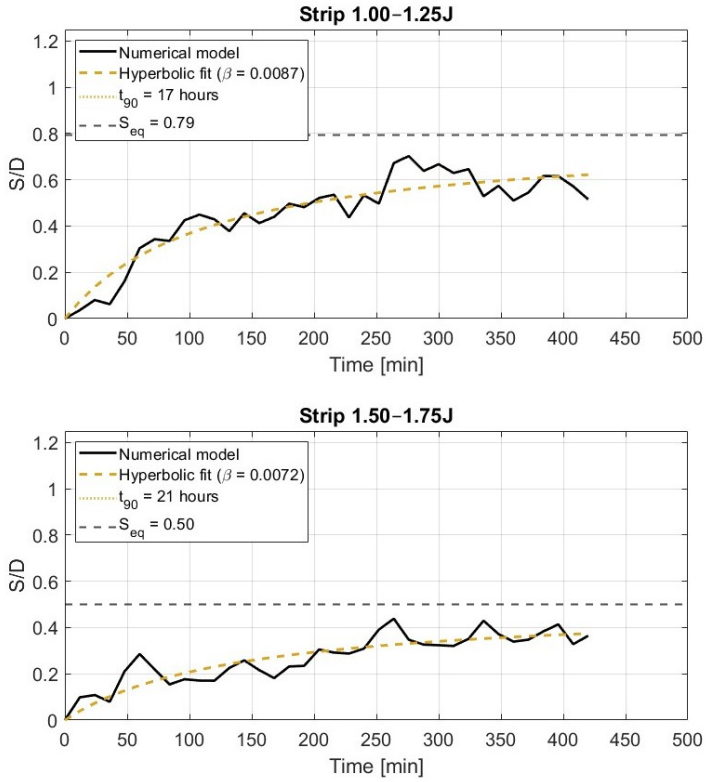

Figure 6.9: Scour evolution in time for the strips of 1.0-1.25 J and 1.5-1.75 J with the fitting of the hyperbolic equation.

Evolution seems to follow an exponential trend with oscillations in the evolution, as observed before in global scour. To identify whether equilibrium has been reached, the same fitting hyperbolic equation is fitted, as done for local scour. Figure 6.9 shows that the fitted curves match the numerical model results. The estimated times to reach equilibrium scour depth are approximately 17 hours for the 1J strip and around 20 hours for the outer strip. This implies that even at 420 minutes, equilibrium is not attained, and that outer regions require more time to develop, although their timescales are of similar magnitude to the inner regions.

Additionally, the global scour under live-bed conditions develops significantly faster and reaches a more

extensive footprint than in the clear-water regime. These findings also support the conclusion that global scour evolves on a considerably longer timescale—at least five times longer—than local scour equilibrium under live-bed conditions. However, this estimate remains uncertain due to limitations.

6.3. Comparison with Bibliography

This section compares numerical results for scour around a jacket foundation with the monopile-based formulation of Sheppard and Miller Jr. (2006) and other literature. The analysis covers both laboratory and field scales, distinguishing between upstream and downstream piles, and evaluates the formula's accuracy, its ability to capture scale effects, and the observed differences in scour magnitude and variability.

According to the literature, Sheppard and Miller Jr. (2006) proposed a formulation to estimate the equilibrium scour depth under different flow regimes for monopiles. By applying the expression introduced in Section 2.1, the resulting values are summarized in Tables 6.6 and 6.7. The numerocal model results where the averaged scour depths around the pile with the ring 0.5 D for both lab-scale and field-scale model results. To quantify the spatial variability of scour around the piles, the standard deviation of the scour depth was computed. The computation of this standard deviation was made for the both the last timestep and 10 time steps before the end of the simulation, where equilibrium was reached for most of the piles. The results showed almost the same magnitude of 0.16, showing consistency on the spread of the values of scour on time.

Table 6.6: Comparison of equilibrium scour depth (S_{eq}) and standard deviation for upstream and downstream piles between analytical relations and numerical models on lab scale results

Regime	Analytical calculation	Numerical model results			
	S_{eq} (S/D) Sheppard (2006)	Upstream piles		Downstream piles	
		S_{eq} (S/D)	Std dev	S_{eq} (S/D)	Std dev
Clear water	1.70	1.40	0.14	1.00	0.15
Live bed	2.10	1.60	0.14	1.50	0.14

For the lab-scale simulations, it was observed that the Sheppard and Miller Jr. (2006) formulation slightly overestimates the equilibrium scour depth in both flow regimes. The results align more closely with the upstream pile scour values. The spatial standard deviation remains on the order of 0.16 D, which differs with the standard deviation obtained by Sumer and Fredsøe (2002) for monopiles, which was around 0.7 S/D.

These results are also comparable to the observations by Chen et al. (2023), who reported upstream scour depths around 1.5 S/D. Notably, the setup in Chen et al. (2023) involved a lower pile spacing ratio (G/D = 6) compared to the configuration in this study (G/D = 12). This difference in spacing resulted in a more pronounced reduction in scour depth at downstream piles—approximately 30% in this study, versus 70% in Chen's case, which highlights the importance of the G/D ratio for the difference between upstream and downstream scour values.

Table 6.7: Comparison of equilibrium scour depth (S_{eq}) and standard deviation for upstream and downstream piles between analytical relations and numerical models on field scale results

Regime	Analytical calculation	Numerical model results			
	S_{eq} (S/D) Sheppard (2006)	Upstream piles		Downstream piles	
		S_{eq} (S/D)	Std dev	S_{eq} (S/D)	Std dev
Clear water	0.90	1.00	0.20	0.85	0.15
Live bed	1.05	1.10	0.20	1.00	0.16

At the field scale, the comparison with Sheppard's prediction shows good agreement. It is worth highlighting that the formulation implicitly includes scale effects by incorporating the pile-to-grain-size ratio (D_p/D_{50}), a parameter also emphasized in Broekema and de Wit (2025). This enhances the applicability of Sheppard's approach for field-scale predictions. The standard deviation values are again consistent with the lab results, remaining around 0.2 S/D.

Finally, field data from other studies confirm the validity of these results. For example, Bolle et al. (2012) reported live-bed scour depths in the range of 0.9–1.35 S/D, while Harris and Whitehouse (2021) observed values between 1.1–1.3 S/D. These ranges align well with the outcomes of the present numerical model and suggest that the computed variability falls within typical bounds observed in real-world conditions.

Analytical formulas developed for monopiles are not well suited to capture the complex interactions between piles in a jacket foundation, such as the differences in scour behaviour between upstream and downstream locations. These formulations can overestimate scour depths, but they may still provide a reasonable order-of-magnitude estimate for the expected scour at the front pile. Moreover, they are capable of reflecting scale effects, as observed in the present results, and can be used to approximate scour magnitudes at field scale.

The standard deviation of scour depth, calculated across different timesteps and for both laboratory and field scales, remains of the same order of magnitude. This consistency suggests that the standard deviation could serve as a robust indicator of the spread of local scour values. Furthermore, the similarity in spread between laboratory and field scales indicates potential scalability of the results. However, to properly assess the distribution characteristics and the shape of the frequency curve, a more comprehensive statistical analysis would be required.

Regarding global scour, there are limited studies mentioning the magnitudes of it, making this study a first for tackling the study of magnitudes and time evolution of it. When compared to groups of piles in a live bed regime, the magnitudes for global scour surpasses what was observed by Sumer and Fredsøe (2002) which was 0.5 S/D for a group of piles with 4 piles. Also in terms of footprint, field campaigns by Rudolph et al. (2004) observed a footprint of 2J, for a 4LJ, although the shape was different due to different orientation, the overall footprint is similar to what was observed here.

6.4. Summary of the chapter

This chapter advanced the understanding of scour processes around jacket foundations by examining both local and global scour under clear-water and live-bed regimes, at laboratory and field scales.

The modified approach by Bolle et al. (2010) proved effective in quantifying spatial footprints and distinguishing between local and global effects. Analysis of the full time series revealed that this scour footprint persists throughout scour evolution. Field-scale simulations reproduced the same patterns but with reduced magnitudes, highlighting scale effects. Timescale analysis showed that scour equilibrium occurs later at locations farther from the pile, with estimated equilibrium times on the order of months for the clear-water regime and days for the live-bed regime at field scale.

For global scour, live-bed conditions produced a footprint extending up to twice the jacket footprint radius, with rapid initial development. In contrast, clear-water conditions led to slower, more localized scour, while field-scale results were influenced by simulation duration and, in some cases, unexpected morphological behavior. The square-based method provided a consistent framework for quantifying global scour magnitude and extent.

Comparison with empirical formulas for monopiles showed that these relations tend to overestimate scour, particularly downstream, but can still provide reasonable order-of-magnitude estimates for upstream piles and capture scale effects. As well, campaign field results show consistency with the equilibrium values obtained in field scale model result-

Overall, the numerical model demonstrated strong flexibility in generating detailed, process-based outputs, enabling direct observation of scour development in field conditions and supporting the evaluation of empirical relationships as well as allowing comparison with real field data.

7

Discussion

The purpose of this chapter is to convey all the numerical modeling results presented in the preceding chapters, placing them in the context of the research objectives and existing literature. Rather than reiterating the outcomes, the focus here is on extracting their practical meaning, assessing their reliability, and identifying their implications for both engineering design and scientific understanding.

It considers both the performance of the numerical model and the applicability of its results to real-world conditions. By reflecting on the patterns, magnitudes, and timescales observed for local and global scour, this discussion aims to connect the individual analyses into a coherent interpretation that addresses the overarching questions of this research.

7.1. Performance of the CFD LES Model

This study has shown the performance of TUDflow3D at the time of recreating scour patterns for a 4LJ foundation on both local and global scour for lab and field scales.

On this section is discussed the performance of the model when compared to the lab experiment results from Welzel et al. (2023) and the field scale model, as well as the observation of the hydrodynamic and sensitivity analysis. This is based on the findings from Chapters 4 and 5.

7.1.1. Morphodynamics evolution

For the lab scale numerical model, the numerical model results was compared against laboratory data using echo-sounder measurements and spatial bed-level maps. The model reproduced local scour development accurately, with absolute errors of approximately 6 mm and 8 mm for the clear-water and live-bed regimes which represent around 10-12% of the maximum scour for both regimes , respectively. When averaged over areas around the piles, relative errors were below 15% for clear-water and 5% for live-bed conditions when compared to lab results, showing the robustness of the model to reproduce local scour.

In terms of timescale, the evolution of the echo sounders show same rates of evolution for both regimes, reaching equilibrium in the same order of magnitude.

For the field scale model results on local scour, the model showed also a scour time evolution comparable to the one on the lab, with a comparable area of influence and a hyperbolic evolution of local scour. The magnitudes were of smaller magnitude when compared to the lab scale model results, of around 30% when compared on dimensionless scour depth (S/D).

For global scour, the laboratory-scale numerical model successfully reproduced the main scour and deposition patterns. In the clear-water regime, no scour was observed upstream of the jacket—consistent with expectations—while scour developed inside the jacket footprint and deposition occurred downstream. The downstream scour behavior was dynamic, influencing the evolution of the echo sounder and producing oscillations similar to those recorded in the laboratory. The model also reproduced the

general time frame of global scour evolution, although it tended to overestimate average scour depths on the clear water regime.

In the live-bed regime, the numerical model reproduced the same patterns as the laboratory experiments: higher scour magnitudes in the central area of the jacket and between the downstream piles, with comparable magnitudes and similar timescale evolution, as well as deposition downstream the jacket.

For the field-scale numerical model, global scour behavior differed from the laboratory-scale results. In the clear-water regime, no measurable global scour was observed, raising the question of whether it occurs at all under these conditions. However, the short simulated morphological time frame may be the cause, as global scour typically develops later, and in this case even local scour remained in its early stages.

In the live-bed regime at field scale, the response deviated from expectations. Deposition features downstream began migrating upstream, disrupting the development of global scour. The reason for this behavior was not identified in this research.

It can be said that TUDflow3D shows strong performance in reproducing scour features both locally and globally on lab scale conditions and for local scour in field scale conditions for a 4LJ foundation. However for global scour at field scale conditions, the results were non conclusive.

7.1.2. Hydrodynamic observation

In terms of replicating hydrodynamics, the model's time averaged velocities and bed shear stresses fields were observed. It was observed a shadow effect for both quantities, even for a higher G/D ratio than 10, differing from what is expected in groups of piles.

For the laboratory-scale numerical model, bed shear stress was amplified by up to 8–9 times the ambient values in the regions surrounding the pile bases, particularly on the upstream side. The field-scale model reproduced similar spatial amplification patterns, but with lower magnitudes. Peak amplification reached approximately 4-5 times the undisturbed bed shear stress. This reduction aligns with the observations of Ettema et al. (2006), who reported that smaller structures tend to generate stronger vortices and higher vorticity levels, leading to greater bed shear stress amplification. The reduced amplification at field scale is directly related to the smaller scour magnitudes observed in the simulations, with reductions of about 40-45% in bed shear stress corresponding to a reduction in local scour.

7.1.3. Sensitivity Analysis

Based on the validation done by de Wit et al. (2023) assumptions were made on domain, grid size, morphac and relaxation factors for the model setup. Therefore, a series of sensitivity analyses were conducted to investigate the influence of numerical setup parameters on model results and to enhance the scour prediction accuracy.

- **Mesh resolution:** A grid size of $D/10$ was used and verified to be sufficient. Finer meshes did not significantly improve results, while incurring in high computational costs.
- **Morphological factor:** As shown in de Wit et al. (2023), the morphac parameter does not influence the magnitude of local scour considerably, but it does influence global scour magnitude. Increasing morphac from 50 to 200 doubled the depth of global erosion for the live bed regime.
- **Relaxation factors:** The suspended load relaxation factor had a strong effect on scour evolution. Its use resulted in excessive sedimentation. Conversely, turning off bedload relaxation improved results by allowing more realistic deposition dynamics on the live bed regime, but it also reduced the scour magnitude locally.
- **Domain size and morphology:** Domain extension was necessary to mitigate the formation of dunes that disrupted the evolution of the scour in the clear water regime and the amplification of scour on the live bed regime observed on the downstream area. This happened because of the formation of migrating dunes on the upstream boundary for a not correct development of turbulence caused by the SEM. Following recommendations from de Wit (2015), five water depths were added to the upstream boundary without morphological updates. This adjustment prevented turbulence instabilities and eliminated the propagation of artificial dunes.

Based on the findings of this section, it can be said that TUDflow3D is a robust and reliable tool for predicting local scour around four-legged jacket (4LJ) foundations. The model, previously validated for a different jacket geometry using the same numerical setup, produced similarly accurate results in this study, with the same order of magnitude for the error assessment. The extended upstream domain implemented here improved the replication of the global flow field, which at the end influences local scour development. The model performed well under both clear-water and live-bed regimes, further demonstrating its robustness across different hydraulic conditions.

Regarding global scour, TUDflow3D was able to reproduce the overall behavior in both magnitude and spatial extent for lab scale. The results showed sensitivity to numerical parameters such as computational domain size, relaxation factors, and the morphological acceleration factor (Morphac). For global scour simulations, disabling the relaxation factor yielded a more realistic large-scale response.

Furthermore, TUDflow3D successfully replicated local scour patterns at field scale, with scour magnitudes aligning well with empirical predictions and reported field measurements. These findings highlight the model's applicability for both laboratory- and field-scale scour assessment around jacket foundations.

7.1.4. Simulation time

To evaluate the computational demand of the simulations performed in this study and assess their feasibility for engineering applications, Table 7.1 summarizes the runtimes for local and global scour simulations at both laboratory and field scales. At laboratory scale, simulations required approximately eight days, with the clear-water regime completing slightly faster due to the larger timestep permitted by lower velocities under a fixed CFL condition. At field scale, runtimes were identical for both regimes; however, in the live-bed case, the total computational time could be reduced by up to 50%, as equilibrium was reached after roughly one-third of the simulated morphological time.

Table 7.1: Comparison of computational time at laboratory and field scales.

Scale	Clear-water regime	Live-bed regime
Laboratory scale	7 days	8 days
Field scale	12 days	12 days

These results highlight that, while the CFD LES approach is computationally expensive—requiring several days to over a week per simulation— for these mega structures, it is still feasible for new geometries given the robustness of the model. This also highlights the necessity of the morphac of 100 in all simulations, which significantly reduced computational time without compromising model performance.

7.2. Applicability

To place the results of this research in a practical, field-oriented context, this section discusses both local and global scour outcomes. The aim is to interpret the findings, identify their limitations, and highlight the aspects that can be reliably applied in practice. By linking the numerical results to real-world conditions, this discussion extracts actionable insights while acknowledging the constraints inherent to the modeling approach.

7.2.1. Local scour applications

Beyond the magnitudes and variability of local scour, it is essential to consider their practical implications for the design and protection of subsea infrastructure. Field-scale models consistently produced smaller scour depths than laboratory-scale results. This difference is supported by previous monopile scaling studies, the observed reduction in bed shear stresses, and field measurements for jacket foundations, which indicate local scour magnitudes of 0.9–1.3 D. These values align with the field-scale numerical model and are lower than the 1.4–1.7 D observed in laboratory-scale models and experiments, confirming that laboratory results may overestimate the in-situ scour response.

The adapted relation from Bolle et al. (2010) was effective in defining the spatial extent of local scour,

which ranged from approximately 1.5 to 3 D depending on the regime. This footprint provides a reference for the placement of subsea cables and armour layers, ensuring that protective measures are focused where they are most needed. The standard deviation of scour depth around piles remained consistent across regimes and scales, making it a robust measure for assessing spatial variability. While higher scour depths typically occurred at the front of piles and upstream piles were more affected than downstream ones, this distinction becomes less relevant in environments dominated by tidal currents. In locations such as the North Sea, where this mega structures will be placed, flow direction reverses every six hours, causing the “front” and “back” of piles to alternate, which redistributes scour and makes the entire pile perimeter part of the influence zone. Moreover, the transition zone between local and global scour—identified in this study—shows that the two processes interact and should be considered jointly in design.

The timescale of scour development showed marked differences between regimes. In clear-water conditions, even the laboratory-scale experiments did not conclusively reach equilibrium, and field-scale modeling suggests that equilibrium could take several months—or even years when tidal variability and wave action are considered. This has direct implications for construction planning, as offshore campaigns are often scheduled during summer for 1–2 months of optimal access, meaning cable installation may occur before the bed reaches equilibrium. In contrast, live-bed conditions at field scale reached local equilibrium in roughly three days, highlighting the strong regime dependence of scour timescales and its importance in scheduling infrastructure installation.

7.2.2. Global scour applications

For the clear-water regime, the primary scour footprint is located within the jacket structure, even between the piles, with magnitudes reaching approximately 0.3 D. The time evolution of scour in this regime was significantly delayed—such development was not yet observed in the field-scale results. A key question remains whether this delayed scour will occur at the field scale at all. In the field-scale model, the bed inside the jacket appeared less dynamic than in the laboratory, and no dune formation or downstream deposition was observed. Using the scaling parameter derived from the lab-scale clear-water model, global scour initiation is expected after 30 to 35 days. Therefore, the presence of this feature in field conditions remains to be confirmed.

The live-bed regime presents a significantly different behavior. While for the lab experiment and numerical model the orders of magnitude reach until 1 D, the field scale numerical model does not show the same patterns or evolution, while even accreting towards the end of the simulation. This is atypical for live-bed conditions, where global scour has been consistently observed in the lab scale numerical model, on the lab experiment and in field campaigns such as Bolle et al. (2012) and Rudolph et al. (2004). Consequently, the actual magnitude of global scour under field-scale live-bed conditions remains uncertain, but it can be said that what was observed on the field scale numerical model was not what is expected to happen in terms of global scour.

Additionally, scour patterns under live-bed conditions were found to be asymmetrical. Specific downstream regions within the jacket—particularly in the zones between the piles—exhibit maximum scour depths, while otherwise upstream it gets significantly reduced.

Laboratory-scale results indicate that the time required to reach equilibrium for global scour can be at least eight to ten times longer than that for local scour. While this relationship could not be directly confirmed under field-scale conditions, the observation remains relevant, particularly because the live-bed regime is characterized by significantly shorter timescales. Understanding when global scour stabilizes is of practical interest. What can be confirmed is that, under live-bed conditions, global scour evolves rapidly during the early stages of the simulation.

It is important to note that these global scour patterns are likely influenced by the current direction as well. As discussed earlier, alternating tidal currents can affect the observed scour orientation and distribution. While the spatial patterns may shift, the scour magnitudes and sheltering effects are expected to remain of similar magnitude.

8

Conclusions and recommendations

In this chapter, the main conclusions of the research are presented in direct response to the research objectives outlined in Chapter 1. To address these systematically, the chapter is structured into separate sections, each corresponding to one of the main research objectives.

Finally, recommendations for further research are provided, aimed at building upon the findings of this study and supporting the continued advancement of knowledge in this field.

8.1. Conclusions

Performance of the CFD LES Model TUDflow3D

This research presents the first application of the CFD LES model TUDflow3D to 4LJ foundation for offshore wind turbines. It was evaluated the model's capability to reproduce scour patterns observed in laboratory experiments and to validate the physical processes represented.

The results demonstrate that TUDflow3D can accurately simulate both local and global scour at laboratory scale. The robustness of TUDflow3D is in the simulation of local scour. The model shows accurate prediction of scour behavior near the piles and low sensitivity to numerical parameters.

In the case of global scour, the numerical model could replicate the large-scale bed deformation patterns; however, this requires specific adjustments to the numerical setup that differ from those used for local scour, needing calibration. Three parameters of the sensitivity analysis (morphac, relaxation factors, and domain size) were found to influence global scour outcomes.

For the hydrodynamics, the model was able to reproduce the characteristic downflow and horseshoe vortex, as well as the expected amplification of velocities and bed shear stresses around the piles.

It was also able to produce a numerical model at field scale, which presented realistic results for local scour development around a 4LJ foundation. The mobility similarity method accounted for the maintaining of bed shear stresses, showing as a strong scaling methodology for scour numerical models between field and lab scale. However for global scour, the results were not conclusive, as it differed to lab scale models and field campaign observations.

Although CFD LES models are computationally demanding, the simulations in this study were completed within a copmutation time of less than two weeks, while still producing reliable results across all cases. In the live-bed regime, both laboratory- and field-scale reached equilibrium within approximately a computation time of one week, demonstrating the practical feasibility of applying such models within reasonable computational limits.

The main advantages of TUDflow3D lie in the flexibility of post-processing, which enables a level of detail hard to achieve in laboratory experiments, and in its capability to scale results up to field conditions while maintaining validity. These strengths make it a powerful complement to laboratory studies, rather than a replacement, advancing both research and engineering practice in scour prediction.

Local scour characteristics

In this study, the local scour footprint for lab scale was found to range between $1.5-2.5\,D$ for the live-bed regime and $2.5-3\,D$ for the clear-water regime. This was found understanding that its extent depends on the local scour depth and the sand repose angle (as in a monopile) but also including the influence of global scour around the pile. Furthermore, ring-based analysis revealed that the footprint remains nearly constant throughout the entire simulation, showing a radial decay of scour after 0.5 D.

This radial decay in scour depth is accompanied by an increase in the time required to reach equilibrium. Although the magnitude of this increase varies depending on the flow regime, a consistent trend is observed: regions located further from the pile take longer to stabilize.

The evolution of scour around jacket structures was also found to be comparable to that observed for monopiles. In both cases, it was observed that a single-hyperbolic function is insufficient to fully capture the time evolution of scour. Instead, a two-phase exponential process might be closer to the scour evolution, as observed for monopiles.

Scour magnitudes in the field-scale model were smaller than those obtained in the laboratory-scale simulations, around 30% when compared in dimensionless scour (S/D). This difference is attributed to the reduced amplification of time-averaged bed shear stresses at larger scales. These findings are consistent with field measurements from campaigns. This supports the notion that local scour magnitudes in the field are generally smaller than those observed in laboratory-scale studies.

The time for equilibrium on field conditions seems to be of the order of magnitude of months for clear water regime, and for the live bed regime, in the order of magnitude of days.

The spatial distribution of peak bed shear stresses around the jacket piles corresponds closely with the location of the scour footprint. This relationship, previously observed for monopiles, is also evident for 4LJ foundations.

The shadowing effect by the upstream piles is strong for the clear water regime, showed in decreasing of velocities on the downstream piles, regardless of a high G/D ratio (12) when compared to data from bibliography, which limits it until 10. This was observed for both laboratory and field scale results.

Global scour characteristics

At laboratory scale, both the magnitude and timescale of global scour vary markedly between flow regimes.

In the clear-water regime, scour in the central bed area remains limited—around 0.3 D—and its onset is delayed. This confirms the slower morphodynamic response characteristic of clear-water conditions and indicates that global scour, if present, evolves over much longer timescales.

In contrast, live-bed conditions produce substantially larger scour magnitudes, reaching up to 1 D, with notable spatial variability across the measurement domain. The scour footprint extends beyond the footprint of the jacket, up to twice its width, behavior observed on field campaigns, with the most pronounced erosion observed within the central region and downstream of the structure. Although the response is slower than for local scour, global scour in the live-bed regime follows an exponential growth pattern, similar to local scour.

Empirical formulations for monopiles

The findings from the field scale model results were further validated using the scaling relationships proposed by Broekema and de Wit (2025) to scale up lab scale results to field scale, which showed good agreement for both the rate of scour development and the final equilibrium scour depth. Although the scaling factors slightly underestimated scour magnitudes—by approximately 5 to 30%—the predictions remained within a reasonable range. Is confirmed that this relation for scaling up lab results can also be applied on jacket foundations, when it was developed for monopiles.

When comparing the model results—both at laboratory and field scale—with the empirical relationship proposed by Sheppard and Miller Jr. (2006), remains a useful approximation for estimating equilibrium scour depth for the front piles of the 4LJ. While it is overestimated the scour at lab scale, it closely

matched the field-scale results. As such, this formula can serve as a reliable first estimate for scour magnitude in field-scale applications.

8.2. Recommendations

It is recommended to extend the simulation duration for the clear-water regime at field scale to better capture the full evolution of local and global scour. Additionally, for the live-bed regime at field scale it is important to study the global response of the bed as it does not align to what is observed on the field or on the lab scale models. While it can be expected a possible reduction in global scour magnitude at field scale, this would be likely driven by the reduced intensity of horseshoe vortices and lower bed shear stresses. However, since these mechanisms are not present all over the bed, the hypothetical reduction in magnitude can also be non existent and global scour depth might scale similarly as in the laboratory numerical model.

To address limitations of the current study, it is also recommended to incorporate tidally reversing currents in future numerical modeling. At field scale, equilibrium timescales were found to be at least 3 days for the live-bed regime, and potentially on the order of months for the clear-water regime. In contrast, tidal reversals occur over much shorter periods—typically hours. This mismatch in timescales can significantly influence both local and global scour behavior, altering the interpretation of upstream and downstream effects, as well as the distribution of scour around the structure. Although not included in the present study, this effect should be considered in future work to improve the reliability and applicability of scour predictions. Nevertheless, the current results provide a solid foundation and first step toward understanding scour magnitudes and timescales at larger scales.

Another suggestion to assess scale effects and validate what was observed here, it can be suggested to replicate the same laboratory experiment of the 4LJ foundation on a bigger scale than the one used by Welzel et al. (2023). In this way the scaling can be validated for global scour, using TUDflow3D for this validation as well, and also observe the scale effect of global scour which still remains a question.

Several physical parameters were not investigated in this section, such as the effect of varying sediment grain size on scour development, changes in current direction, and the influence of water depth relative to pile diameter. It is therefore recommended that, using the same setup and the validated model as a baseline, future studies assess the impact of these variables on scour processes around 4LJ foundations.

References

Ahmad, N., Kamath, A., & Bihs, H. (2020). 3d numerical modeling of scour around a jacket structure with dynamic free surface capturing. *Ocean Engineering Journal*, *213*, 107664.

Bayram, A., & Larson, M. (2000). Analysis of scour around a group of vertical piles in the field. *Journal of Waterway, Port, Coastal, and Ocean Engineering*, *126*(4), 215–220. https://doi.org/10.1061/(ASCE)0733-950X(2000)126:4(215)

Bolle, A., de Winter, J., Goossens, W., Haerens, P., & Dewaele, G. (2012). Scour monitoring around offshore jackets and gravity based foundations. *Proceedings of the Sixth International Conference on Scour and Erosion (ICSE 6)*.

Bolle, A., De Winter, J., Goossens, W., Haerens, P., & Dewaele, G. (2010). Scour monitoring around offshore jackets and gravity based foundations. *Proceedings of the International Conference on Coastal Structures*.

Broekema, Y. B., & de Wit, L. (2025). *Scaling laws for scour development at pile foundations* [Manuscript in review, Department of Hydrodynamics and Offshore Technology, Deltares, Delft, The Netherlands].

Cao, Y., Wu, N., Yang, J., Chen, C., Zhu, R., & Hua, X. (2024). Effect of scour on the fatigue life of offshore wind turbines and its prevention through passive structural control. *Wind Energy Science*, *9*(5), 1089–1104. https://doi.org/10.5194/wes-9-1089-2024

Chen, H., Zhang, J., Wang, F., Guo, Y., Guan, D., & Feng, L. (2023). Experimental investigation of the current-induced local scour around a jacket foundation. *Ocean Engineering Journal*, *256*, 111234.

Cimarelli, A., Leonforte, A., & Angeli, D. (2018). Direct numerical simulation of the flow around a rectangular cylinder at a moderately high reynolds number. *Journal of Wind Engineering & Industrial Aerodynamics*, *174*, 39–49. https://doi.org/10.1016/j.jweia.2017.12.020

Damiani, R., Robertson, A., & Song, H. (2016). *Jacketse: An offshore wind turbine jacket sizing tool* (tech. rep. No. NREL/TP-5000-65417). National Renewable Energy Laboratory (NREL). https://www.nrel.gov/docs/fy16osti/65417.pdf

de Wit, L. (2015, January). *3d cfd modelling of overflow dredging plumes* [Doctoral dissertation, Delft University of Technology]. https://resolver.tudelft.nl/uuid:ef743dff-6196-4c7b-8213-fd28684d3a58

de Wit, L., Plenker, D., & Broekema, Y. (2023, September). 3d cfd les process-based scour simulations with morphological acceleration. In T. U. Petersen & S. Sassa (Eds.), *Proceedings of the 11th international conference on scour and erosion*. International Society for Soil Mechanics; Geotechnical Engineering (ISSMGE). https://www.issmge.org/publications/online-library

de Wit, L., & van Rhee, C. (2013). Testing an improved artificial viscosity advection scheme to minimise wiggles in large eddy simulation of buoyant jet in crossflow. *Flow, Turbulence and Combustion*, *92*(3), 699–730. https://doi.org/10.1007/s10494-013-9517-1

Deltares. (2020). *Design and installation recommendations for offshore cable protection* (tech. rep.) (Internal advisory document on cable burial depth and scour risk management). Deltares.

Department for Business, Enterprise and Regulatory Reform. (2008). *Review of cabling techniques and environmental effects applicable to the offshore wind farm industry* (tech. rep.) (Technical Report No. 3.3–3.4 on Barrow OWF cable exposure and scour). Department for Business, Enterprise and Regulatory Reform (UK). https://www.bsee.gov/sites/bsee.gov/files/tap-technical-assessment-program/final-report-offshore-electrical-cable-burial-for-wind-farms.pdf

Deriaz, E., & Haldenwang, P. (2020). Non-linear cfl conditions issued from the von neumann stability analysis for the transport equation. *Journal of Scientific Computing*.

Díaz, H., & Soares, C. G. (2020). Review of the current status, technology and future trends of offshore wind farms. *Ocean Engineering*, *209*, 107381. https://doi.org/10.1016/j.oceaneng.2020.107381

Ettema, R., Kirkil, G., & Muste, M. (2006). Similitude of large-scale turbulence in experiments on local scour at cylinders. *Journal of Hydraulic Engineering*, *132*(1), 33–40. https://doi.org/10.1061/(ASCE)0733-9429(2006)132:1(33)

Harris, J. M., & Whitehouse, R. J. S. (2021). Scour development around monopile and jacket foundations in silty sands. *Proceedings of the 10th International Conference on Scour and Erosion (ICSE)*.

Jarrin, N., Benhamadouche, S., Laurence, D., & Prosser, R. (2008). A synthetic-eddy-method for generating inflow conditions for large-eddy simulations. *International Journal of Heat and Fluid Flow*, *29*(3), 628–640. https://doi.org/10.1016/j.ijheatfluidflow.2008.01.005

John Smith, J. D. (2021). Foundations in offshore wind farms: Evolution, characteristics and range of use. analysis of main dimensional parameters in monopile foundations. *Journal of Offshore Engineering*, *45*(2), 123–145. https://doi.org/10.1016/j.joffeng.2021.04.003

Khosronejad, A., Kang, S., Borazjani, I., & Sotiropoulos, F. (2011). Curvilinear immersed boundary method for simulating coupled flow and bed morphodynamic interactions due to sediment transport phenomena [Available online 21 March 2011.]. *Advances in Water Resources*, *34*(6), 829–843. https://doi.org/10.1016/j.advwatres.2011.02.017

Kim, H. S., Nabi, M., Kimura, I., & Shimizu, Y. (2014). Numerical investigation of local scour at two adjacent cylinders. *Journal of Hydro-environment Research*, *8*(3), 292–306. https://doi.org/10.1016/j.jher.2014.06.002

Lai, Y. G., Liu, X., Bombardelli, F. A., & Song, Y. (2022). Three-dimensional numerical modeling of local scour: A state-of-the-art review and perspective. *ASCE Journal*, *148*(5), 06022001.

Li, Q., Askarinejad, A., & Gavin, K. (2020). Impact of scour on lateral resistance of wind turbine monopiles: An experimental study. *Ocean Engineering*, *218*, 107993. https://doi.org/10.1016/j.oceaneng.2020.107993

Mansouri, Z., Selvam, R. P., & Chowdhury, A. G. (2022). Maximum grid spacing effect on peak pressure computation using inflow turbulence generators. *Results in Engineering*, *15*, 100491.

Melville, B. (2008). The physics of local scour at bridge piers. *Fourth International Conference on Scour and Erosion*, 28–38.

Nicoud, F., & Ducros, F. (1999). Subgrid-scale stress modelling based on the square of the velocity gradient tensor. *Flow, Turbulence and Combustion*, *62*(3), 183–200. https://doi.org/10.1023/A:1009995426001

Oh, K.-Y., Nam, W., Ryu, M., Kim, J.-Y., & Epureanu, B. (2018). A review of foundations of offshore wind energy converters: Current status and future perspectives. *Renewable and Sustainable Energy Reviews*, *88*, 16–36. https://doi.org/10.1016/j.rser.2018.02.005

Park, J., Wang, L., & Cho, S. (2023). Topology optimisation of offshore wind turbine jacket foundation for various soil conditions. *Ocean Engineering*, *284*, 116876. https://doi.org/10.1016/j.oceaneng.2023.116876

Pope, S. B. (2000). *Turbulent flows*. Cambridge University Press. https://doi.org/10.1017/CBO9780511840531

Qu, L., An, H., Draper, S., Watson, P., Zhao, M., Harris, J., Whitehouse, R., & Zhang, D. (2024). A review of scour impacting monopiles for offshore wind turbines. *Ocean Engineering*, *275*, 114245. https://doi.org/10.1016/j.oceaneng.2024.114245

Ranasinghe, R., Swinkels, C., Luijendijk, A., Bosboom, J., Roelvink, D., Stive, M., & Walstra, D. (2011). Morphodynamic upscaling with the morfac approach: Dependencies and sensitivities. *Proceedings of the 32nd International Conference on Coastal Engineering (ICCE 2010)*, *32*, 1085. https://doi.org/10.9753/ICCE.V32.SEDIMENT.59

Roulund, A., Sumer, B. M., Fredsøe, J., & Michelsen, J. (2005). Numerical and experimental investigation of flow and scour around a circular pile. *Journal of Fluid Mechanics*, *534*, 351–401.

Rudolph, D., Bos, K. J., Luijendijk, A. P., Rietema, K., & Out, J. M. M. (2004). Scour around offshore structures – analysis of field measurements. *Proceedings of the Second International Conference on Scour and Erosion (ICSE 2)*.

Satari, R., Sarma, B., Schendel, A., Welzel, M., Schlurmann, T., & Neuweiler, I. (2024). Hydrodynamics around a jacket-type foundation structure in steady current: A combined experimental and numerical study. *Ocean Engineering Journal*, *269*, 113278.

Sharples, J. (2011). *Offshore electrical cable burial for wind farms: State of the art, standards and guidance* (tech. rep.). Bureau of Safety and Environmental Enforcement (BSEE). https://www.

bsee.gov/sites/bsee.gov/files/tap-technical-assessment-program/final-report-offshore-electrical-cable-burial-for-wind-farms.pdf

Sheppard, D. M. (2003). *Large-scale and live-bed local pier scour experiments* (Coastal Engineering Technical Report No. 133). Civil and Coastal Engineering Dept., Univ. of Florida, Gainesville, Fla.

Sheppard, D., & Miller Jr., W. (2006). Live-bed local pier scour experiments. *Journal of Hydraulic Engineering*, *132*(7), 635–642. https://doi.org/10.1061/(ASCE)0733-9429(2006)132:7(635)

Shields, A. (1936). *Application of similarity principles and turbulence research to bed-load movement*. Preußische Versuchsanstalt für Wasserbau und Schiffbau.

Shih, T.-H., Liou, W. W., Shabbir, A., Yang, Z., & Zhu, J. (1995). A new k–ε eddy viscosity model for high reynolds number turbulent flows. *Computers & Fluids*, *24*(3), 227–238. https://doi.org/10.1016/0045-7930(94)00032-T

Silva-Muñoz, N. F., & Broekema, Y. B. (2025). A multi-scale approach for scour time development at monopiles due to currents. *Ocean Engineering*, *322*, 120504. https://doi.org/10.1016/j.oceaneng.2025.120504

Soulsby, R. (1997). *Dynamics of marine sands: A manual for practical applications*. Thomas Telford.

Sumer, B. M., & Fredsøe, J. (1998). Wave scour around group of vertical piles. *Journal of Waterway, Port, Coastal, and Ocean Engineering*, *124*(5), 248–256. https://doi.org/10.1061/(ASCE)0733-950X(1998)124:5(248)

Sumer & Fredsøe. (2002). *The mechanics of scour in the marine environment*. World Scientific.

Sumner, D. (2010). Two circular cylinders in cross-flow: A review. *Journal of Fluids and Structures*, *26*(6), 849–899. https://doi.org/10.1016/j.jfluidstructs.2010.07.001

Taylor, G. I. (1938). The spectrum of turbulence. *Proceedings of the Royal Society of London. Series A, Mathematical and Physical Sciences*, *164*(919), 476–490. https://doi.org/10.1098/rspa.1938.0032

The Carbon Trust. (2021). *Cable protection systems: Best practice guidelines* (tech. rep.). Offshore Wind Accelerator Programme. https://www.carbontrust.com/resources/cable-protection-systems-best-practice-guidelines

Tran, T.-T., Lee, K.-T., Kim, Y.-S., & Kim, N.-I. (2022). Development of a 3-legged jacket substructure for installation in the southwest offshore wind farm of korea. *Ocean Engineering*, *256*, 111469. https://doi.org/10.1016/j.oceaneng.2022.111469

van Rijn, L. C. (1984). Sediment pick-up functions. *Journal of Hydraulic Engineering*, *110*(10), 1494–1502. https://doi.org/10.1061/(ASCE)0733-9429(1984)110:10(1494)

van Rijn, L. C. (2007). Unified view of sediment transport by currents and waves. i: Initiation of motion, bed roughness, and bed-load transport. *Journal of Hydraulic Engineering*, *133*(6), 649–667. https://doi.org/10.1061/(ASCE)0733-9429(2007)133:6(649)

Veldhuizen, R., Broekema, Y., & Bruinsma, N. (2023). Scour development in layered soils around offshore monopile foundations. *Proceedings of the 11th International Conference on Scour and Erosion (ICSE-11)*, 17–21. https://www.issmge.org/publications/publication/scour-development-in-layered-soils-around-offshore-monopile-foundations

Welzel, M., Schendel, A., Hildebrandt, A., & Schlurmann, T. (2019). Scour development around a jacket structure in combined waves and current conditions compared to monopile foundations. *Coastal Engineering Journal*, *58*(5), 450–467.

Welzel, M., Schendel, A., Satari, R., & Sheppard, I. (2023). Spatio-temporal analysis of scour around complex offshore foundations under clear water and live bed conditions. *Coastal Engineering*.

Zhou, Z., Zhao, M., Cheng, L., & Teng, B. (2013). Numerical modeling of local scour around a monopile subjected to a steady current. *Coastal Engineering*, *76*, 1–13.

List of Figures

List of Tables

A

Appendix A: Formulas used for calculation

This appendix compiles the detailed formulations applied throughout this research project.

The equations presented here are those discussed in the literature review, Chapter 2 and subsequently implemented in the calculations described in the project chapters. They include threshold conditions for sediment motion, empirical scour depth relationships, and scaling laws for translating laboratory-scale results to field conditions.

For the calculation of the critical Shields number the following equations is used basd on Soulsby (1997):

$$\theta_{cr} = \frac{0.3}{1 + 1.2D_*} + 0.055\left[1 - \exp(-0.02D_*)\right] \tag{A.1}$$

where the dimensionless grain size D_* is given by:

$$D_* = D_{50}\left(\frac{g(\rho_s - \rho)}{\nu^2}\right)^{1/3} \tag{A.2}$$

with:

- D_{50} = sediment grain diameter [m],
- g = gravitational acceleration [m/s^2],
- ρ_s, ρ = sediment and fluid densities [kg/m^3],
- ν = kinematic viscosity of water [m^2/s].

For the estimation of the maximum scour depth of monopiles Sheppard (2003) proposed these formulations varying by regime:

In the *clear-water scour range* ($0.47 \leq U/U_c \leq 1$):

$$\frac{S_{\text{eq}}}{D^*} = 2.5\, f_1\left(\frac{H}{D^*}\right) f_2\left(\frac{D^*}{D_{50}}\right)\left\{1 - 1.75\left[\ln\left(\frac{U}{U_c}\right)\right]^2\right\} \tag{A.3}$$

In the *live-bed scour range up to the live-bed peak* ($1 < U/U_c \leq U_lp/U_c$):

$$\frac{S_{\text{eq}}}{D^*} = f_1\left(\frac{H}{D^*}\right)\left[2.2\frac{U/U_c - 1}{U_lp/U_c - 1} + 2.5\, f_2\left(\frac{D^*}{D_{50}}\right)\frac{U_lp/U_c - U/U_c}{U_lp/U_c - 1}\right] \tag{A.4}$$

In the *live-bed scour range above the live-bed peak* ($U/U_c > U_lp/U_c$):

$$\frac{S_{\text{eq}}}{D^*} = 2.2\, f_1 \left(\frac{H}{D^*}\right) \tag{A.5}$$

For scaling up lab experiment result of scour for monopiles, Broekema and de Wit (2025) proposed relations, as well different per regime.

For the determination of the equilibrium scour depth:

$$f_1 \left(\frac{H}{D^*}\right) = \tanh\left[\left(\frac{H}{D^*}\right)^{0.4}\right] \tag{A.6}$$

$$f_2 \left(\frac{D^*}{D_{50}}\right) = \frac{D^*/D_{50}}{0.4\,(D^*/D_{50})^{1.2} + 10.6\,(D^*/D_{50})^{-0.13}} \tag{A.7}$$

In these equations, S_{eq} is the equilibrium scour depth, V is the depth-averaged approach velocity of the flow, U_c represents the critical velocity for the initiation of sediment motion, and U_lp is the velocity at which maximum scour occurs in the live-bed regime. The variable H denotes the water depth.

$$S_{\text{eq,field}} = \left(1 + \left(\frac{\theta_c}{\theta}\right)^2 (1 - n_{lp})\right) n_s n\, S_{\text{eq,lab}} = \omega_s\, n_s n\, S_{\text{eq,lab}}. \tag{A.8}$$

Where the velocity scaling factor n_{lp} is defined as:

$$\left(\frac{U}{U_{lp}}\right)_{\text{field}} = n_{lp} \left(\frac{U}{U_{lp}}\right)_{\text{lab}}. \tag{A.9}$$

Once the field-scale equilibrium scour depth $S_{\text{eq,field}}$ is obtained, it can be used in the time scale formulation (Equation (2.5)) to yield the expression for the characteristic scour time at field scale:

$$T_{c,\text{field}} = \frac{n_s^2 n^2 S_{\text{eq,lab}}^2}{n_d^3 U_{\text{lab}}^3} = \frac{n_s^2 n^2}{n_d^3} T_{c,\text{lab}}. \tag{A.10}$$

For the live-bed regime, additional correction factors are necessary to account for the increased sediment mobility. The term ω_s has already been included in the equilibrium scour formulation to adjust for live-bed conditions. To balance this effect in the time scaling, a temporal correction factor ω_t is introduced, defined as:

$$\omega_t = \frac{1}{1 + (1 - n_{lp}) \left(\frac{\theta}{\theta_c}\right)^2}. \tag{A.11}$$

The complete scaling law for the characteristic scour time in live-bed conditions becomes:

$$T_{c,\text{field}}^{\text{LB}} = \omega_t \cdot \omega_s^2 \cdot \frac{n_s^2 n^2}{n_d^3} T_{c,\text{lab}}. \tag{A.12}$$

For clear-water conditions, the live-bed correction factor is not applied, implying $\omega_s = 1$. In such cases, the expression reduces to a straightforward scaling involving only flow velocity and structural dimensions.

B

Appendix B: Model assessment

This appendix presents the results of the hydrodynamics observation, the sensitivity analysis and the morphodynamics comparison, all part of Chapter: 4.

B.1. Morphodynamics comparison

This section presents cross-sections of the upstream and downstream piles for both flow regimes at the final timestep, allowing assessment of the horizontal extent of scour. The analysis illustrates how the model captures not only localized scour depths or maximum values, but also the overall scour pattern and spatial distribution.

B.1.1. Clear water regime

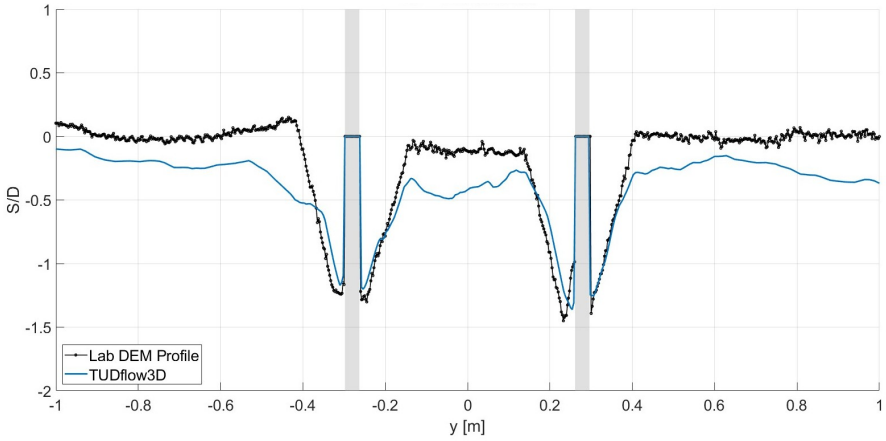

Figure B.1: Cross section of the upstream piles for the numerical model and the laboratory experiment at 420 minutes for the clear water regime

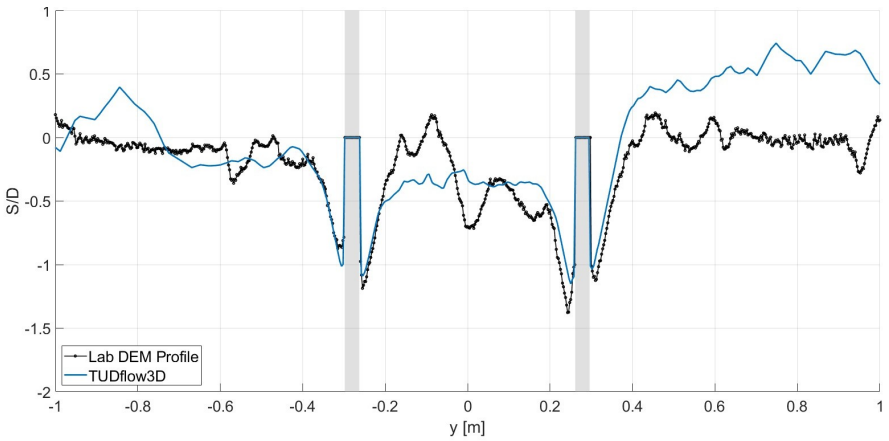

Figure B.2: Cross section of the downstream piles for the numerical model and the laboratory experiment at 420 minutes for the clear water regime

B.1.2. Live bed regime

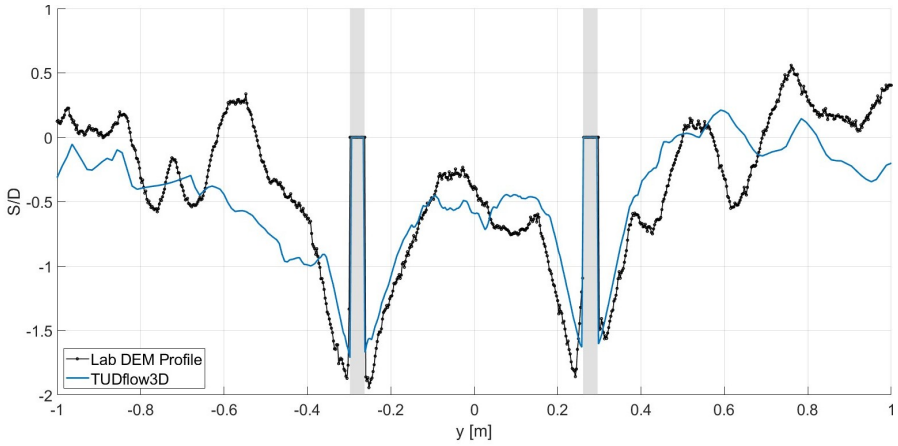

Figure B.3: Cross section of the upstream piles for the numerical model and the laboratory experiment at 420 minutes for the live bed regime

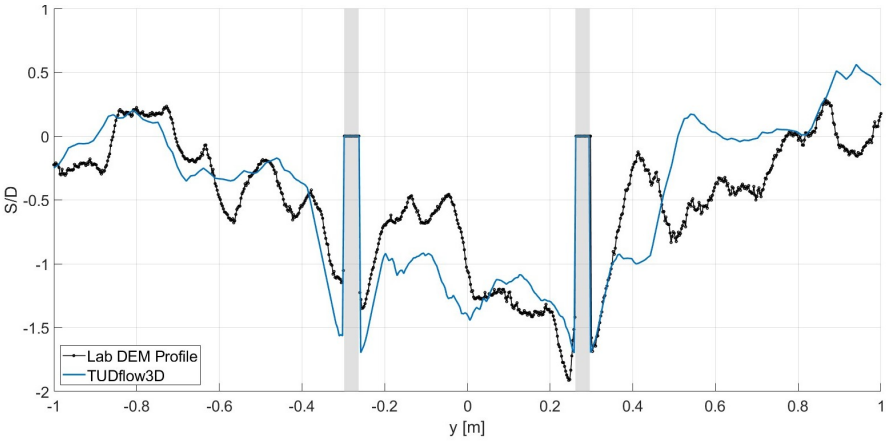

Figure B.4: Cross section of the downstream piles for the numerical model and the laboratory experiment at 420 minutes for the live bed regime

B.2. Hydrodynamics observation

In this section is shown the complete plan view of the amplification of the time averaged bed shear stresses for both regimes at laboratory scale.

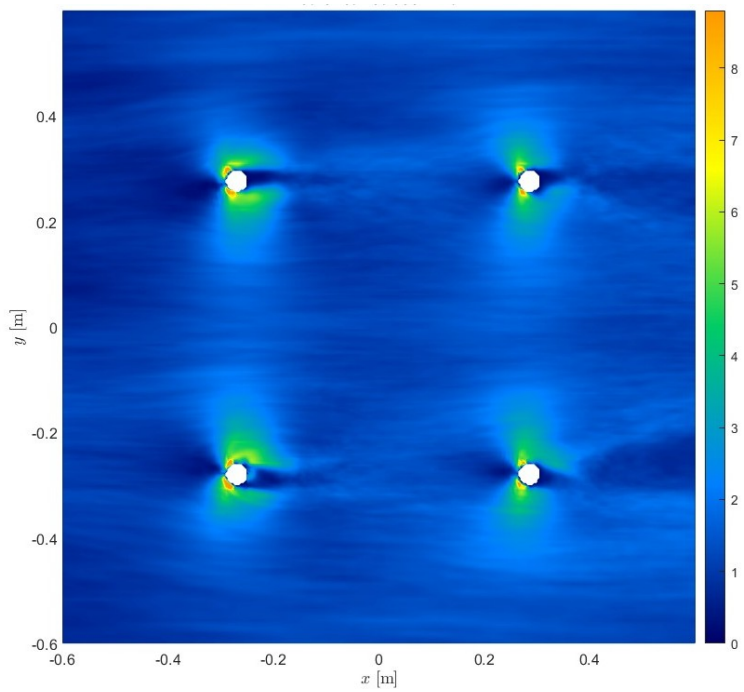

Figure B.5: Plan view of flow-induced time averaged bed shear stress — Clear-water regime.

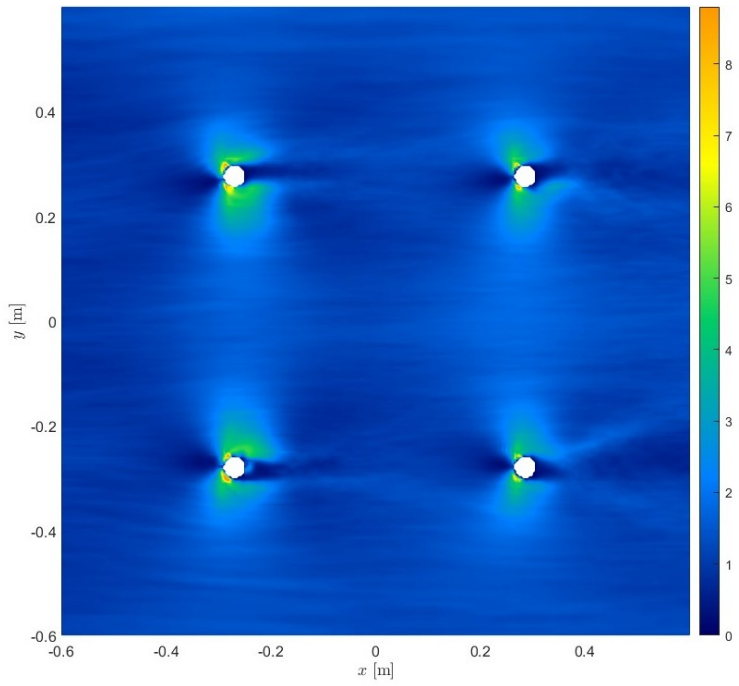

Figure B.6: Plan view of flow-induced time averaged bed shear stress - Live bed regime

B.3. Sensitivity analysis

In this section the plots of the sensitivity analysis are presented per numerical parameter varied. It is followed the same structure for all of them, including the error assessment per echo sounder (RMSE), cross section, plan view for all the variations as well as the timeseries for all the echosounders. The last one was only done for the morphac and

B.3.1. Relaxation Factor Sensitivity

It will be started by the clear water regime, followed by the live bed regime.

Clear water regime

Table B.1: %RMSE and RMSE (mm) between lab data and models for each Echo Sounder (E1–E7) on clear water regime

Echo Sounder	RFA		RFB		RFC	
	%RMSE	RMSE (mm)	%RMSE	RMSE (mm)	%RMSE	RMSE (mm)
E1	19%	10	9%	4	10%	5
E2	8%	4	22%	13	20%	11
E3	6%	3	25%	11	17%	8
E5	15%	6	32%	13	24%	10
E6	25%	10	43%	17	39%	15
E7	30%	9	17%	5	22%	7

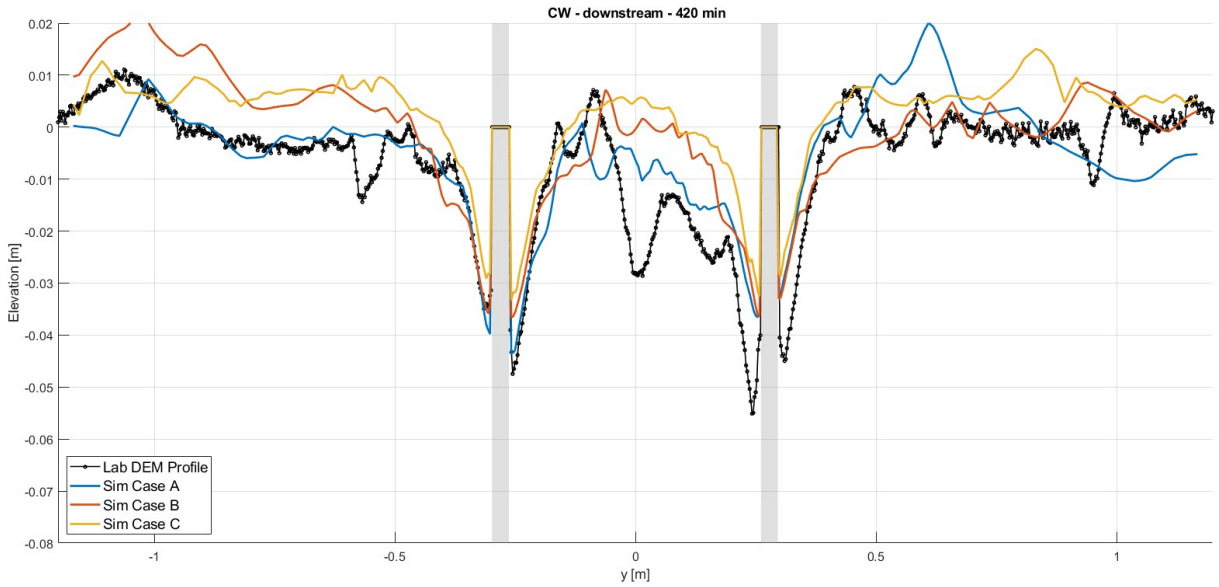

Figure B.7: Cross section downstream of the laboratory results and RFA, RFB and RFC at 402 minutes for the clear water regime

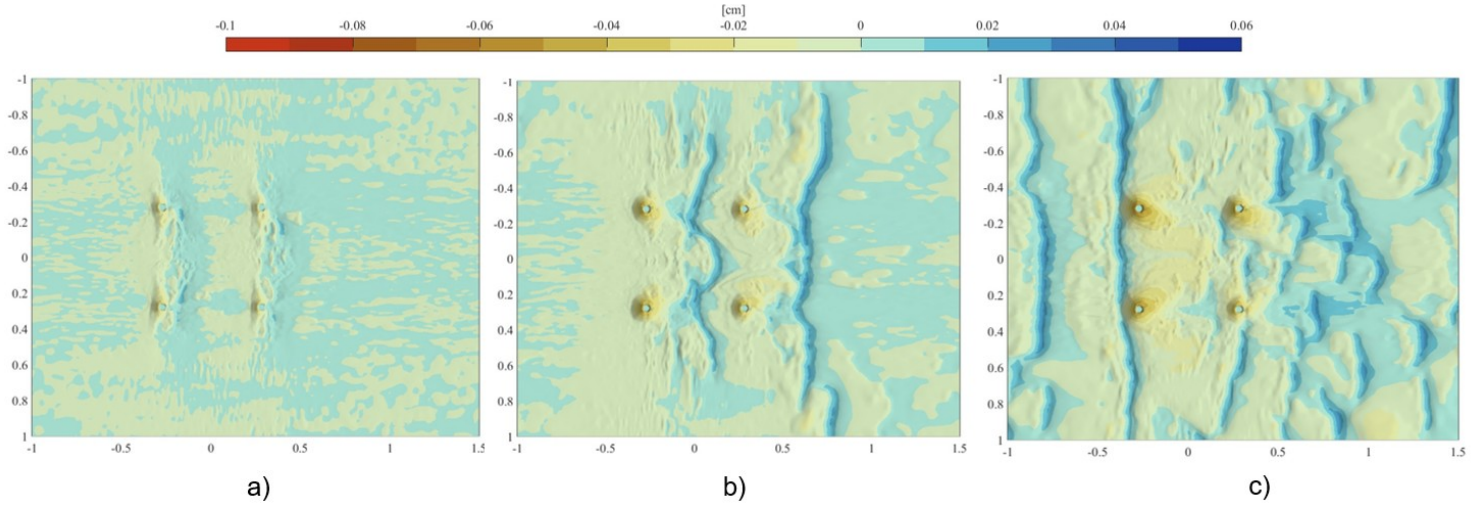

Figure B.8: RFA - Scour on the bed from a plan view after (a)15min, (b) 90 min and (c) 420 min for clear water regime

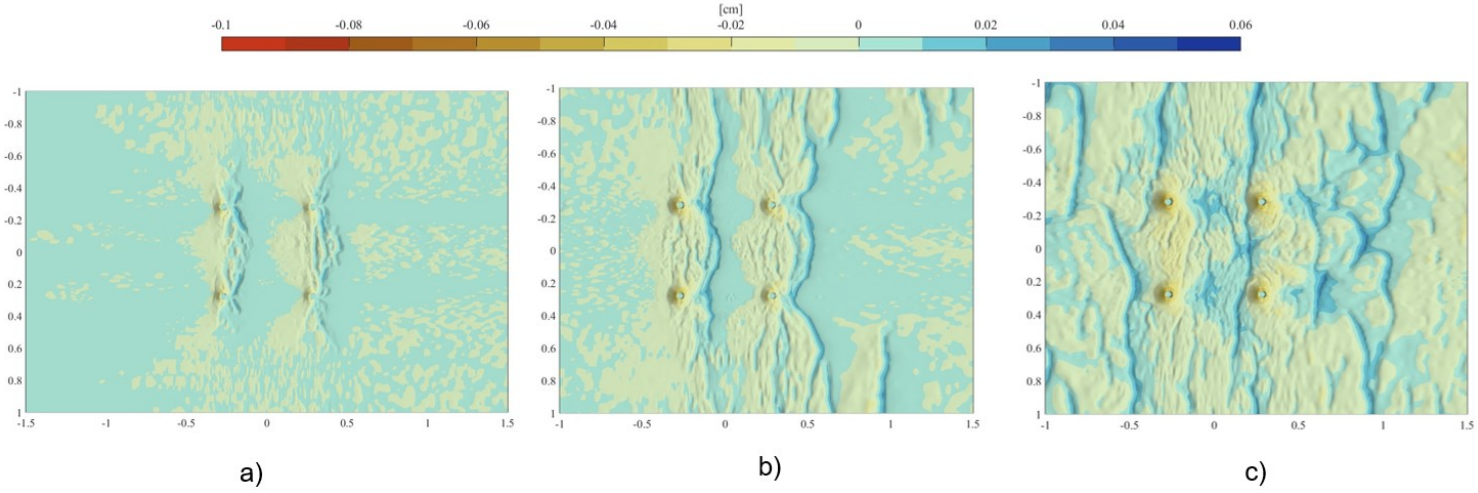

Figure B.9: RFB - Scour on the bed from a plan view after (a)15min, (b) 90 min and (c) 420 min for clear water regime

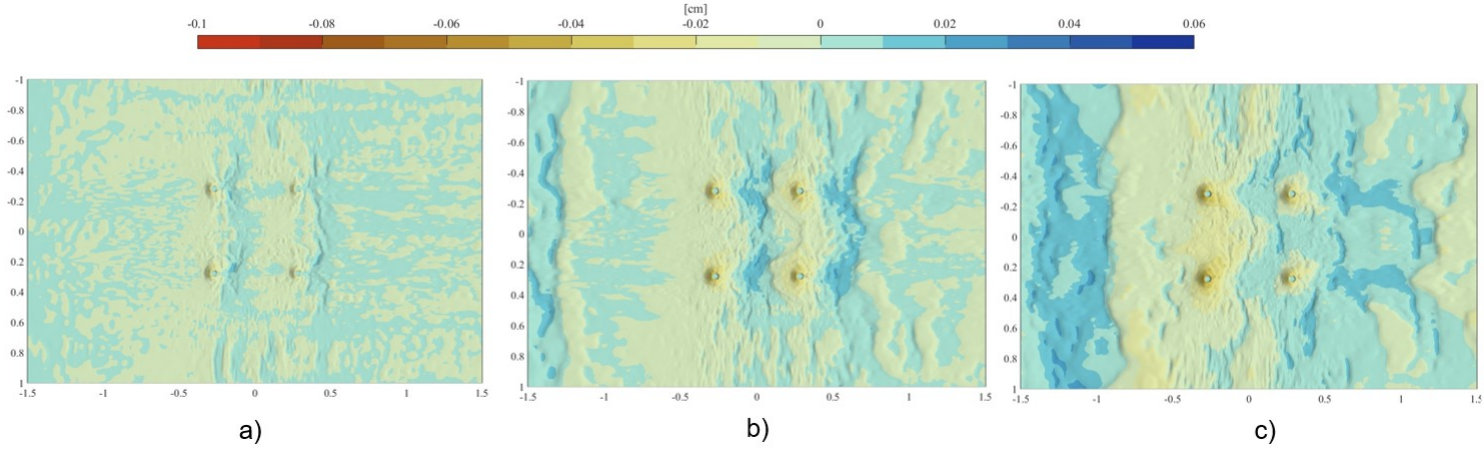

Figure B.10: RFC - Scour on the bed from a plan view after (a)15min, (b) 90 min and (c) 420 min for clear water regime

These Figures show the scour depth evolution for Experiments E1 to E7 under the clear-water regime. For each case, the influence of the relaxation factor on the computed scour depth is evaluated, highlighting model sensitivity during initial and long-term scour development.

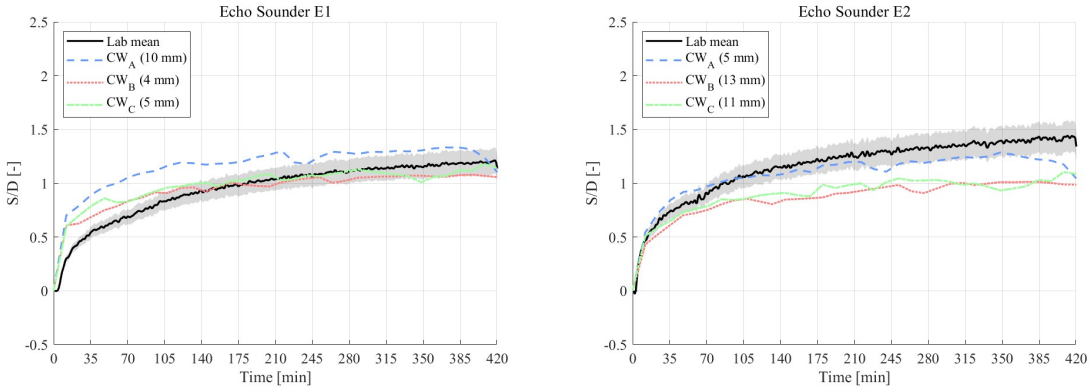

Figure B.11: Scour depth time series for E1 and E2 under clear-water regime.

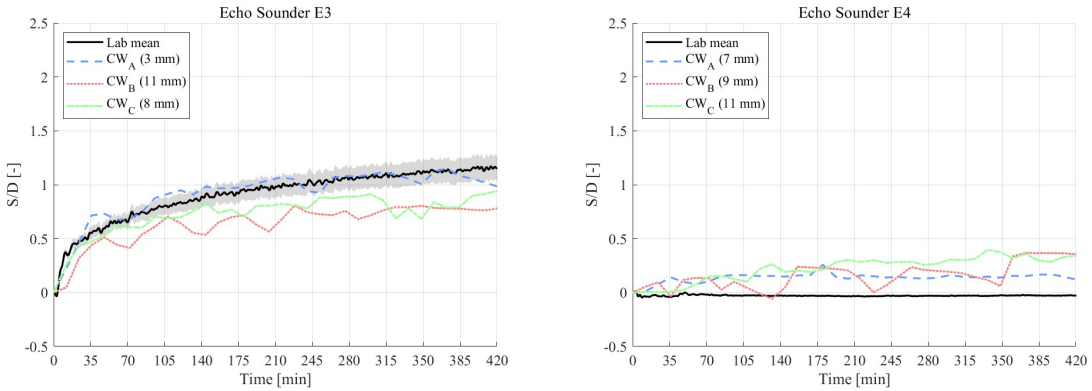

Figure B.12: Scour depth time series for E3 and E4 under clear-water regime.

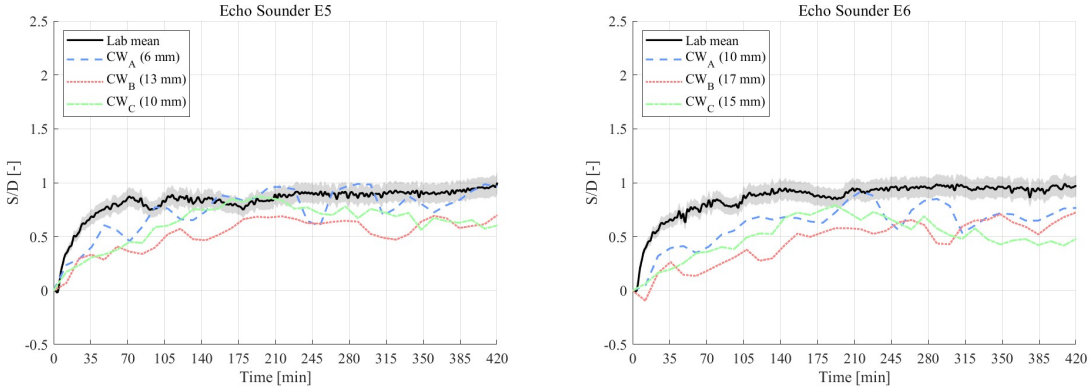

Figure B.13: Scour depth time series for E5 and E6 under clear-water regime.

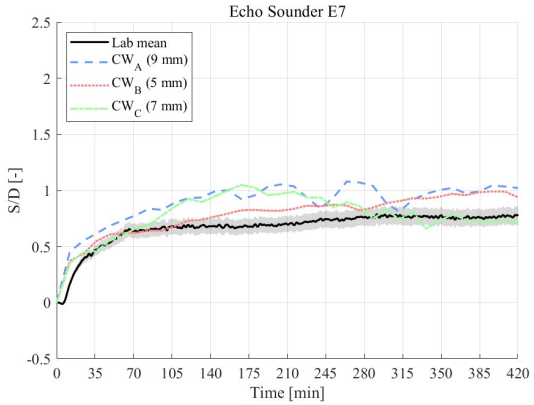

Figure B.14: Scour depth time series for E7 under clear-water regime.

Live bed regime

Table B.2: %RMSE and RMSE (mm) between lab data and models for each Echo Sounder (E1–E7) for the live bed regime

Echo Sounder	RFA		RFB		RFC	
	%RMSE	RMSE (mm)	%RMSE	RMSE (mm)	%RMSE	RMSE (mm)
E1	14%	9	34%	22	12%	8
E2	9%	7	44%	32	23%	17
E3	10%	8	51%	35	25%	17
E5	10%	7	44%	28	14%	9
E6	9%	6	51%	31	18%	11
E7	27%	14	31%	16	14%	8

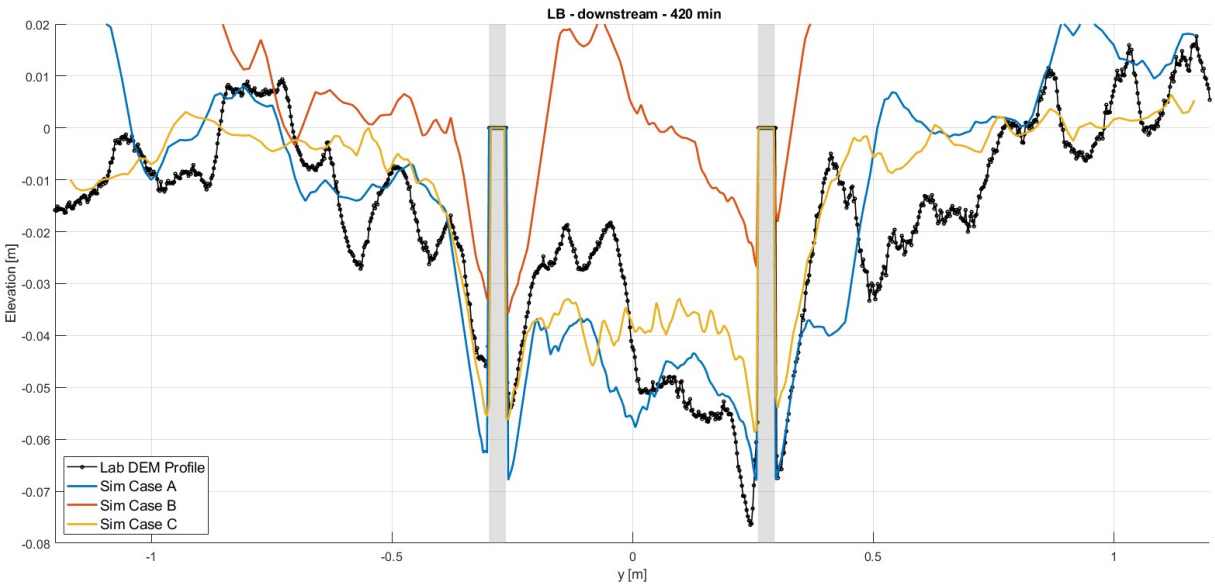

Figure B.15: Cross section downstream of the laboratory results and RFA, RFB and RFC at 402 minutes for the live bed regime

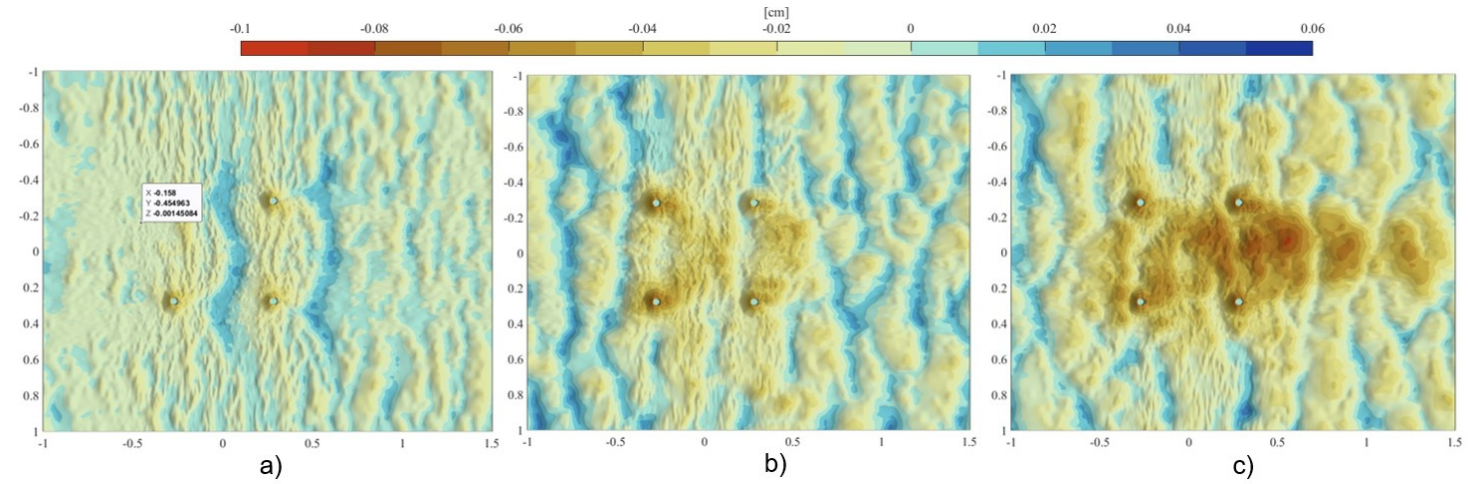

Figure B.16: RFA - Scour on the bed from a plan view after (a)15min, (b) 90 min and (c) 420 min for live bed regime

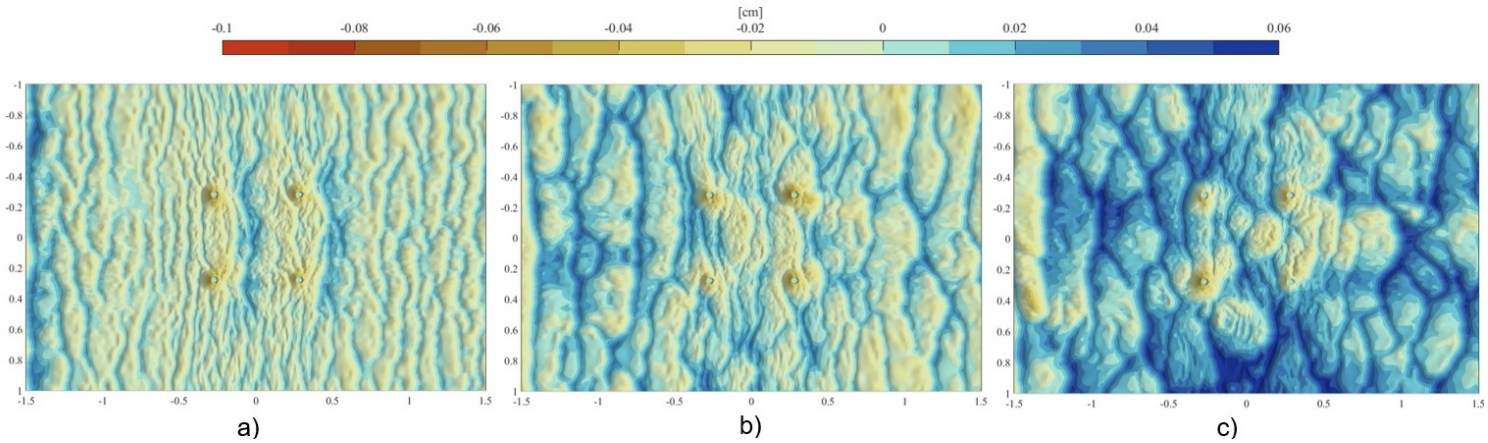

Figure B.17: RFB - Scour on the bed from a plan view after (a)15min, (b) 90 min and (c) 420 min for live bed regime

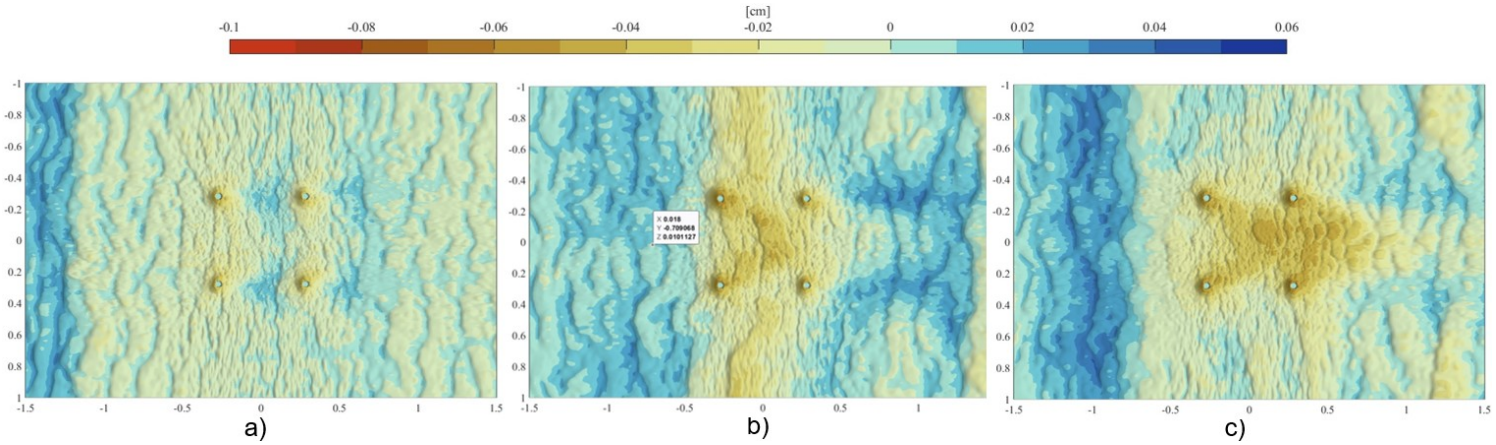

Figure B.18: RFC - Scour on the bed from a plan view after (a)15min, (b) 90 min and (c) 420 min for live bed regime

These Figures present the same analysis under the live-bed regime. The comparison enables the assessment of relaxation factor effects under mobile bed conditions, where sediment transport occurs throughout the simulation period.

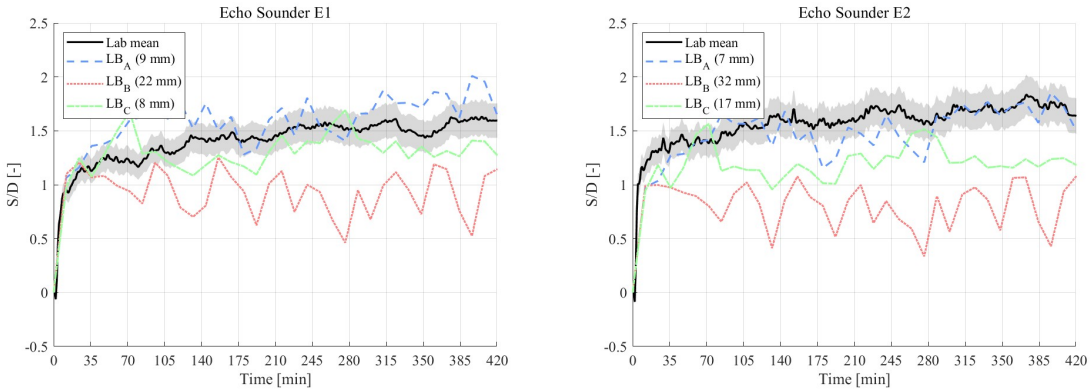

Figure B.19: Scour depth time series for E1 and E2 under live-bed regime.

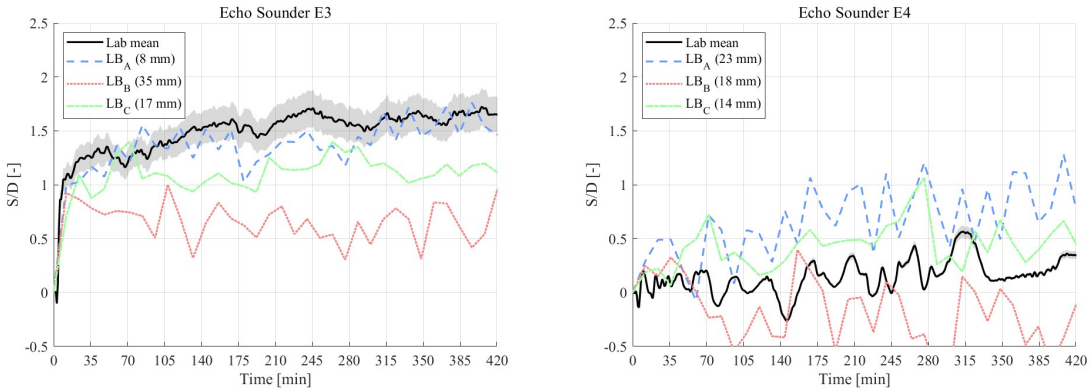

Figure B.20: Scour depth time series for E3 and E4 under live-bed regime.

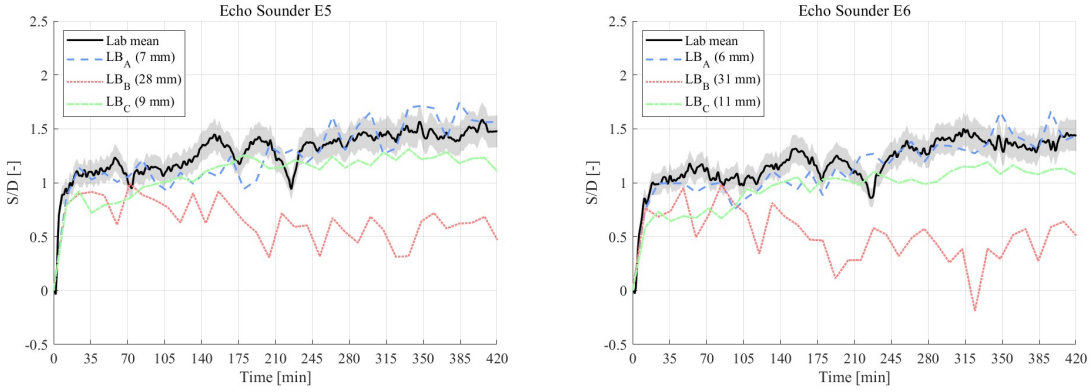

Figure B.21: Scour depth time series for E5 and E6 under live-bed regime.

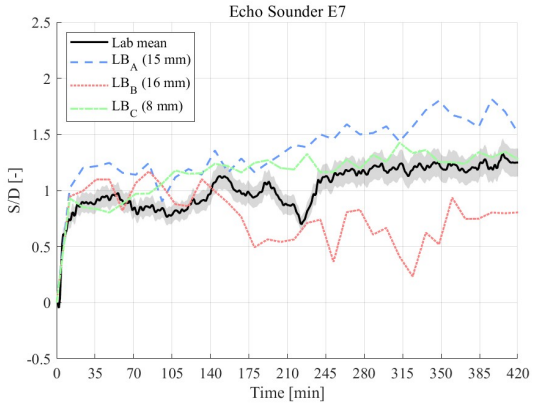

Figure B.22: Scour depth time series for E7 under live-bed regime.

B.3.2. Grid Resolution Sensitivity

Table B.3: Relative and absolute RMSE between lab data and model results for each echo sounder (E1–E7) under the clear-water regime.

Echo Sounder	**Case D/10**		**Case D/13**	
	%RMSE	RMSE (mm)	%RMSE	RMSE (mm)
E1	19%	10	25%	12
E2	9%	4	9%	5
E3	6%	3	10%	5
E5	15%	6	16%	7
E6	25%	10	28%	11
E7	30%	9	33%	10

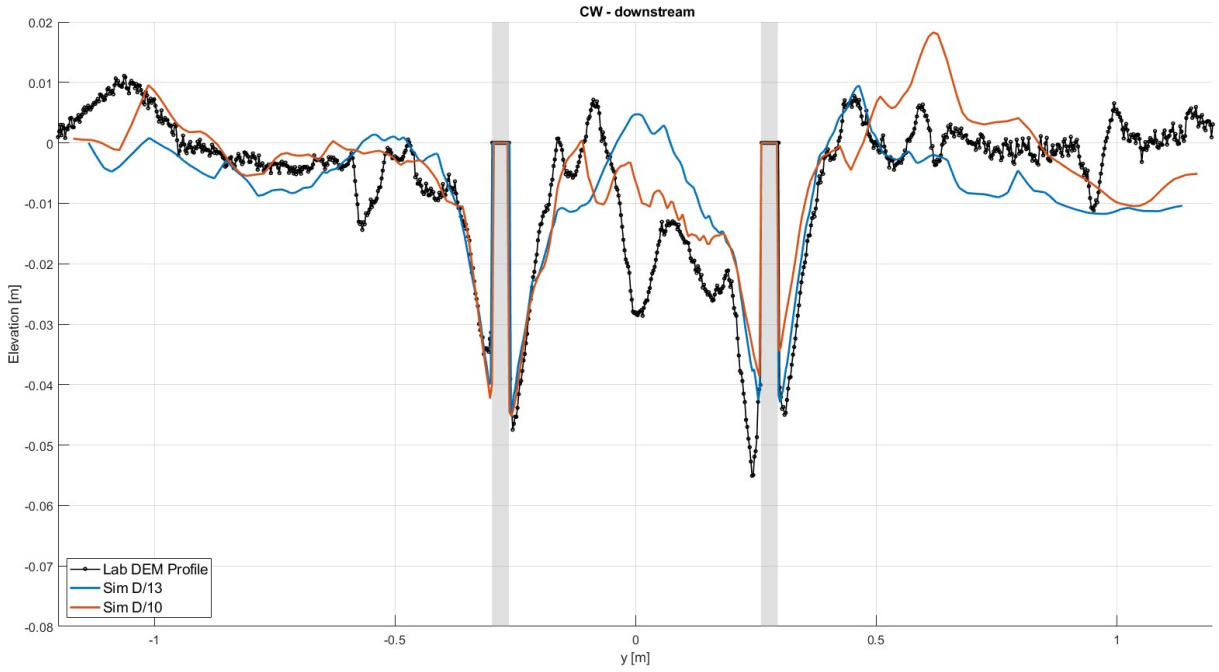

Figure B.23: Cross-section of downstream piles at 420 minutes, comparing numerical results (D/10 and D/13 grid sizes) with lab measurements.

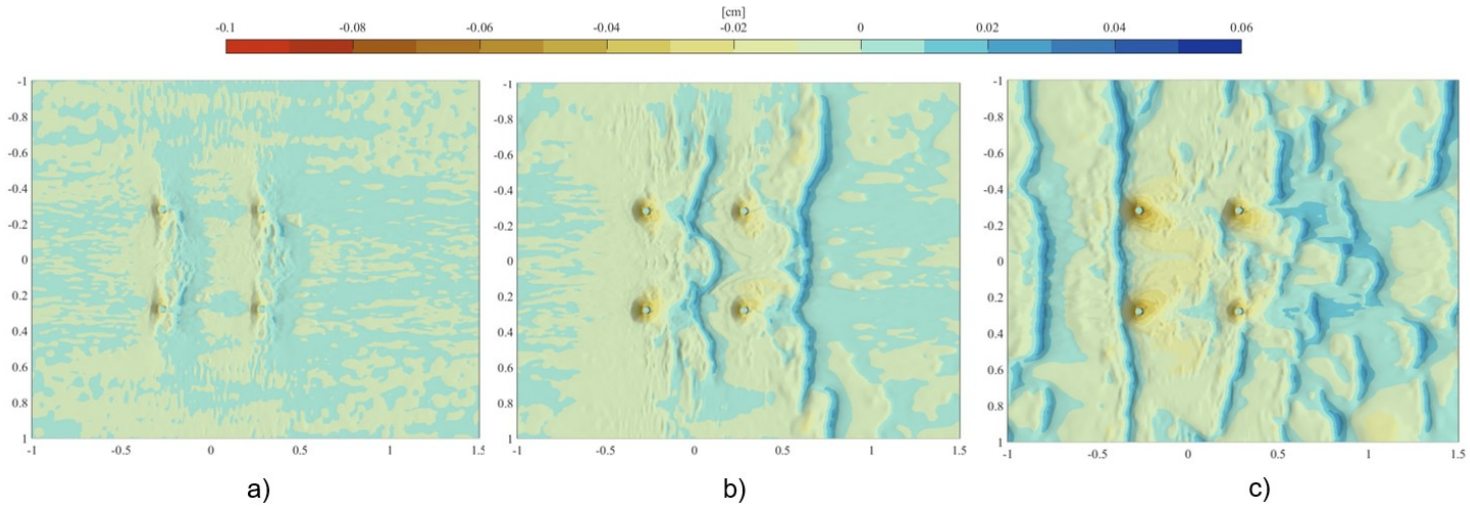

Figure B.24: Plan view of bed scour development (M100) at (a) 15 min, (b) 90 min, and (c) 420 min under the clear-water regime.

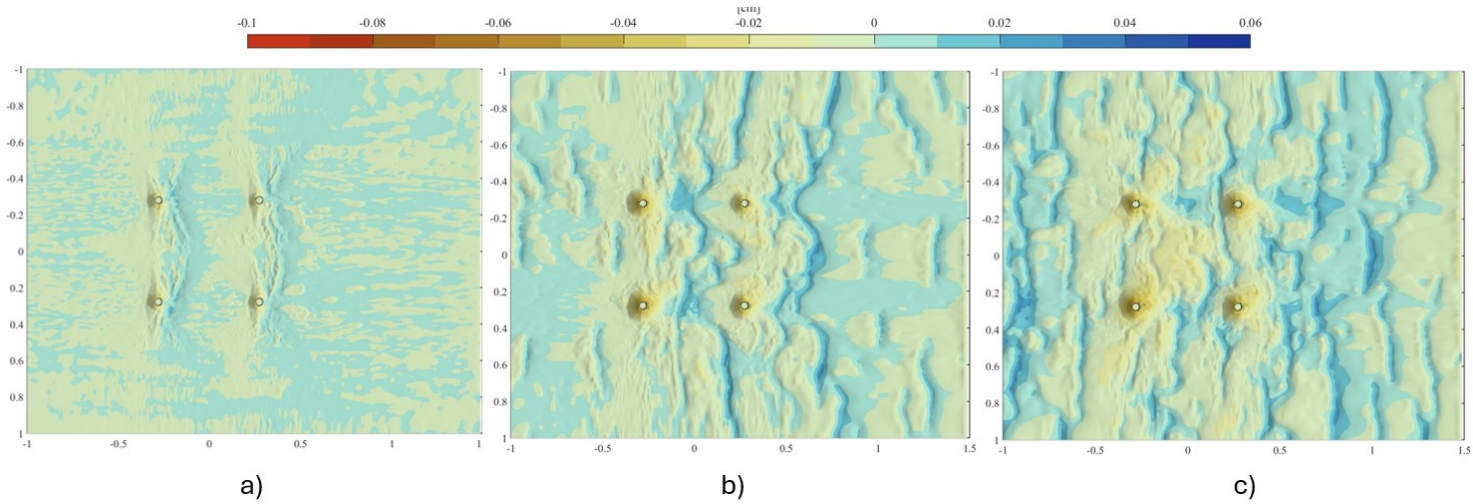

Figure B.25: Plan view of bed scour development (M200) at (a) 15 min, (b) 90 min, and (c) 420 min under the clear-water regime.

These Figures show the scour-depth evolution for Experiments E1–E8 under the clear-water regime, evaluating the effect of grid resolution.

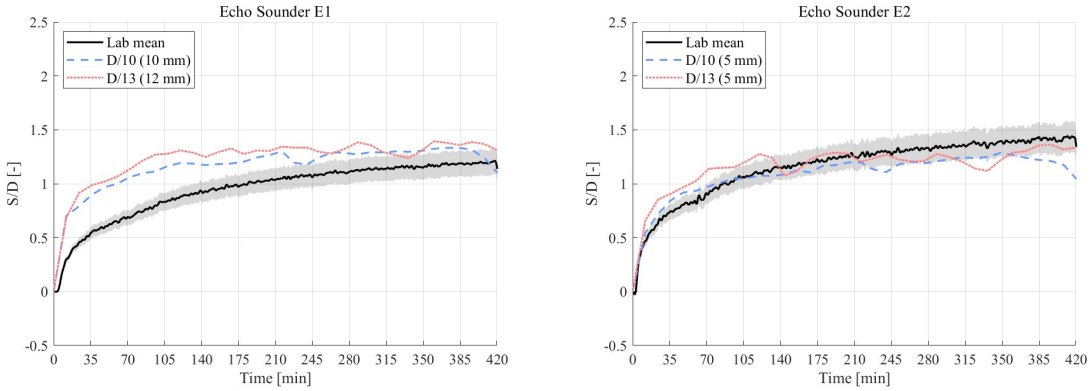

Figure B.26: Grid□sensitivity time series for E1 and E2 (clear□water).

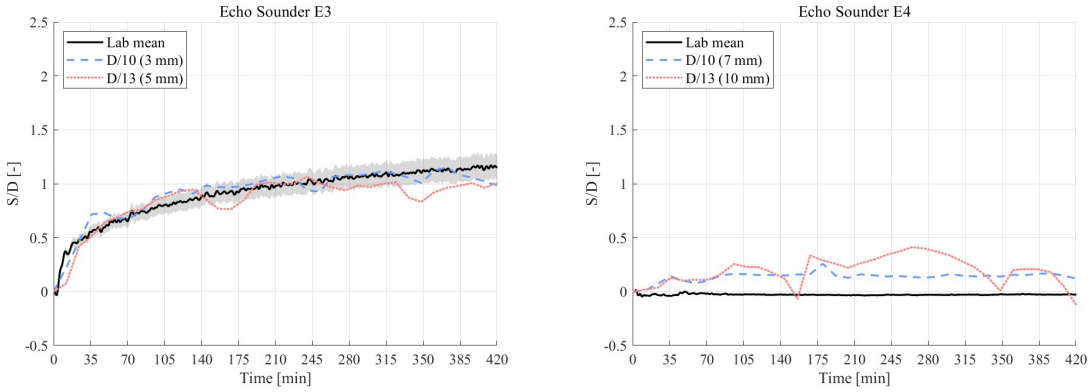

Figure B.27: Grid□sensitivity time series for E3 and E4 (clear□water).

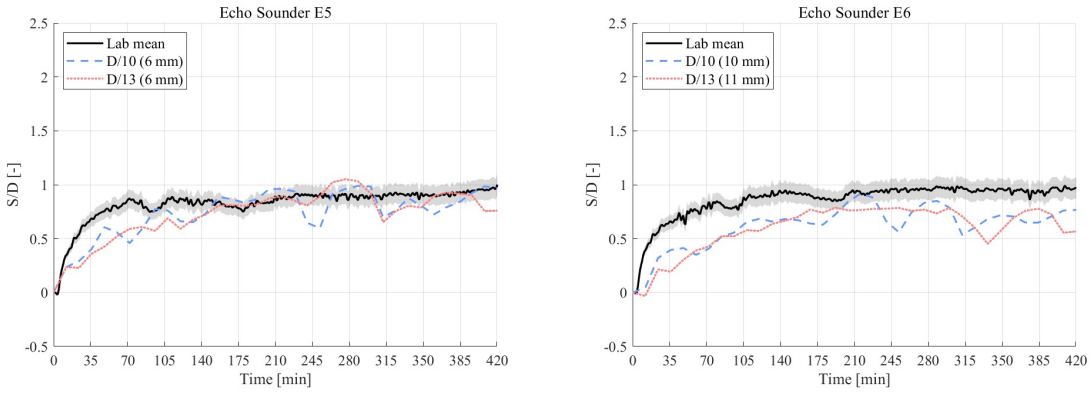

Figure B.28: Grid□sensitivity time series for E5 and E6 (clear□water).

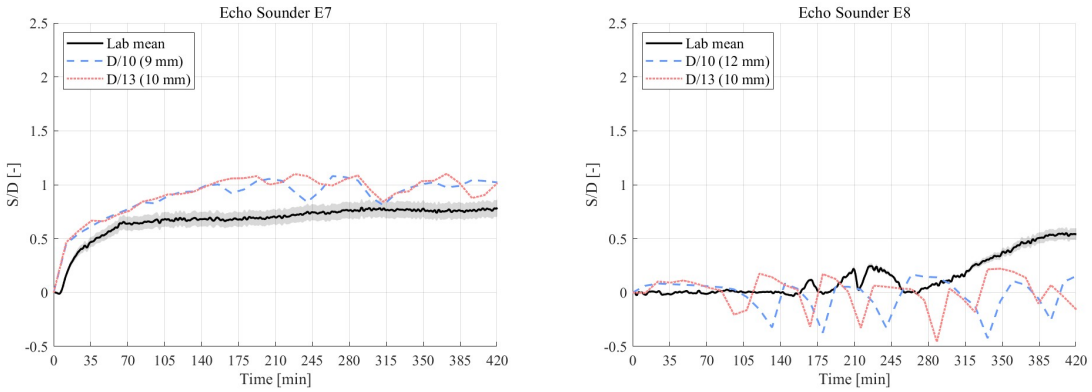

Figure B.29: Grid□sensitivity time series for E7 and E8 (clear□water).

B.3.3. Morphac Sensitivity Clear-Water Regime

Table B.4: %RMSE and RMSE (mm) between lab data and models for each Echo Sounder (E1–E7) for the clear water regime

Echo Sounder	Case M50		Case M100		Case M200	
	%RMSE	RMSE (mm)	%RMSE	RMSE (mm)	%RMSE	RMSE (mm)
E1	17%	8	20%	10	17%	8
E2	15%	9	9%	5	13%	7
E3	14%	7	6%	3	10%	5
E5	21%	8	15%	6	16%	6
E6	30%	12	26%	10	19%	8
E7	26%	8	30%	9	40%	13

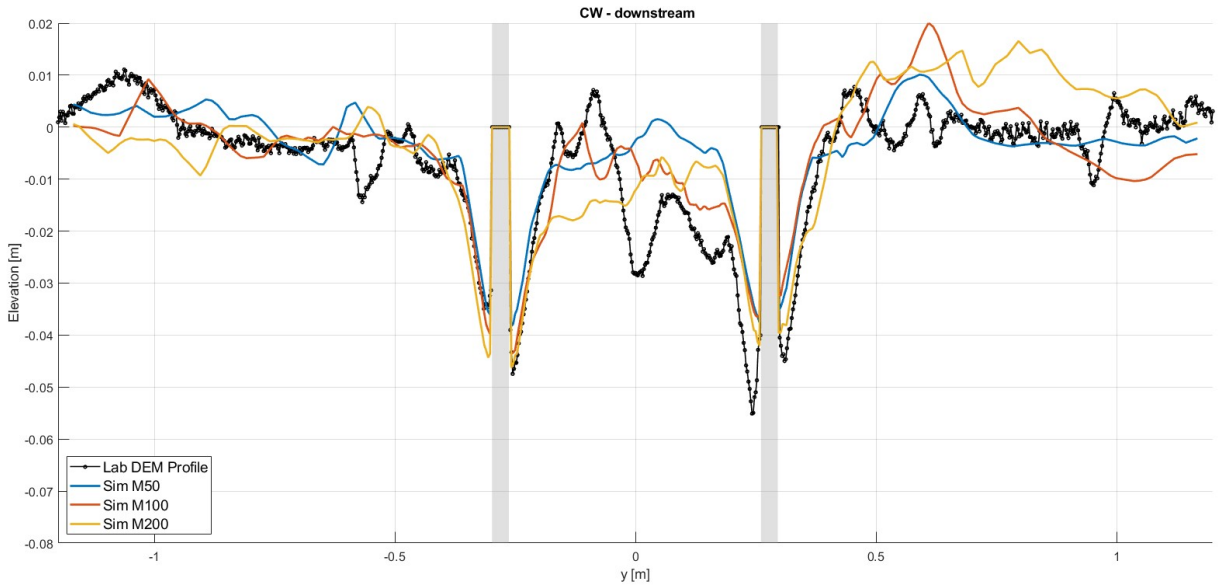

Figure B.30: Cross section downstream of the laboratory results and M50, M100 and M200 at 420 minutes for the clear water regime

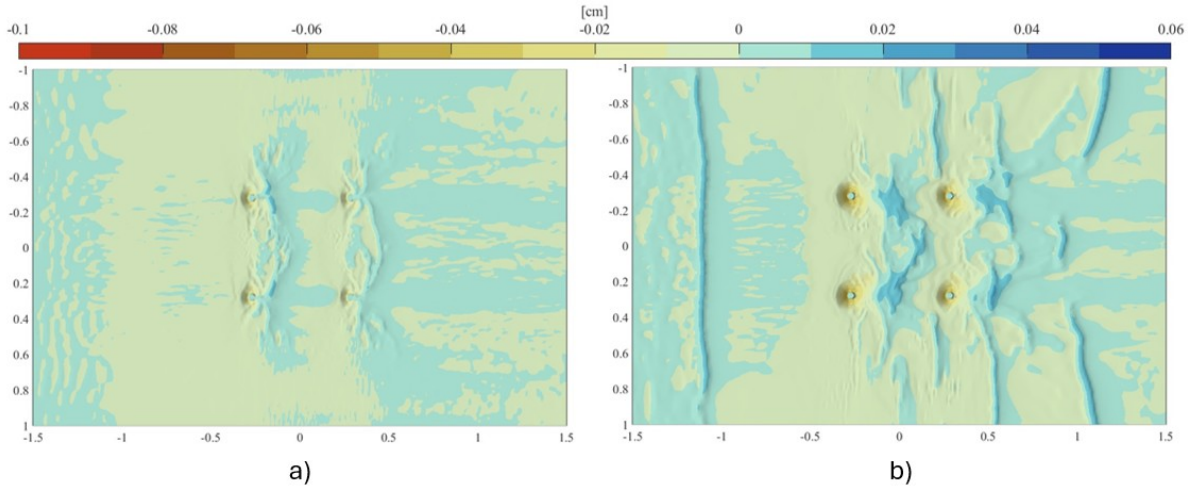

Figure B.31: M10 - Scour on the bed from a plan view after (a)15min and (b) 90 min for clear water regime

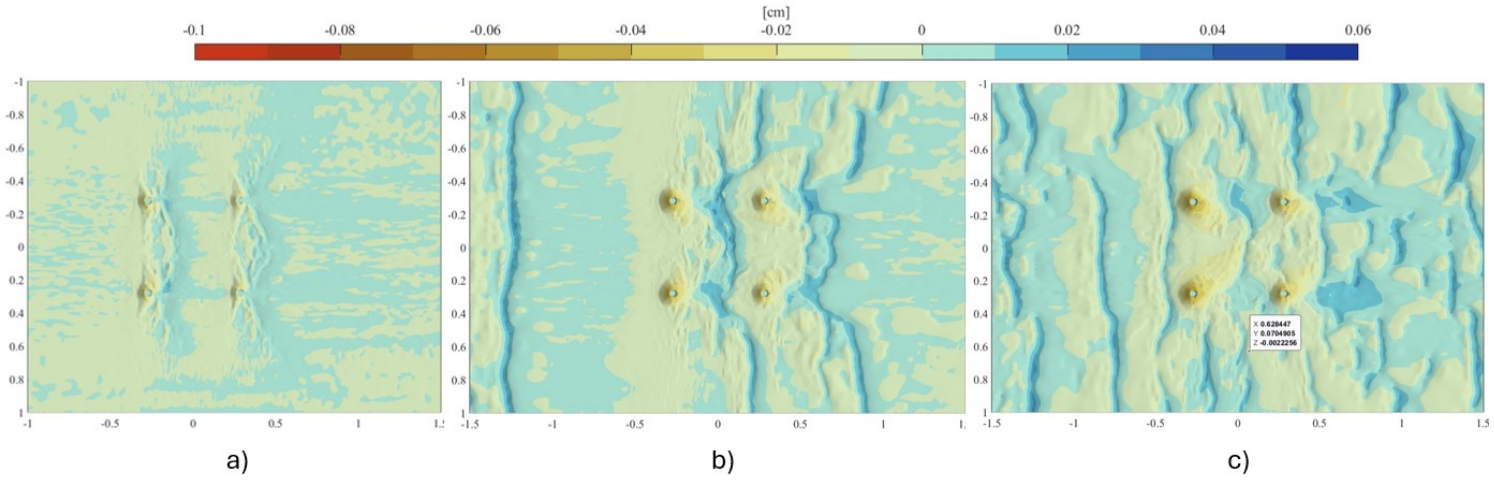

Figure B.32: M50 - Scour on the bed from a plan view after (a)15min, (b) 90 min and (c) 420 min for clear water regime

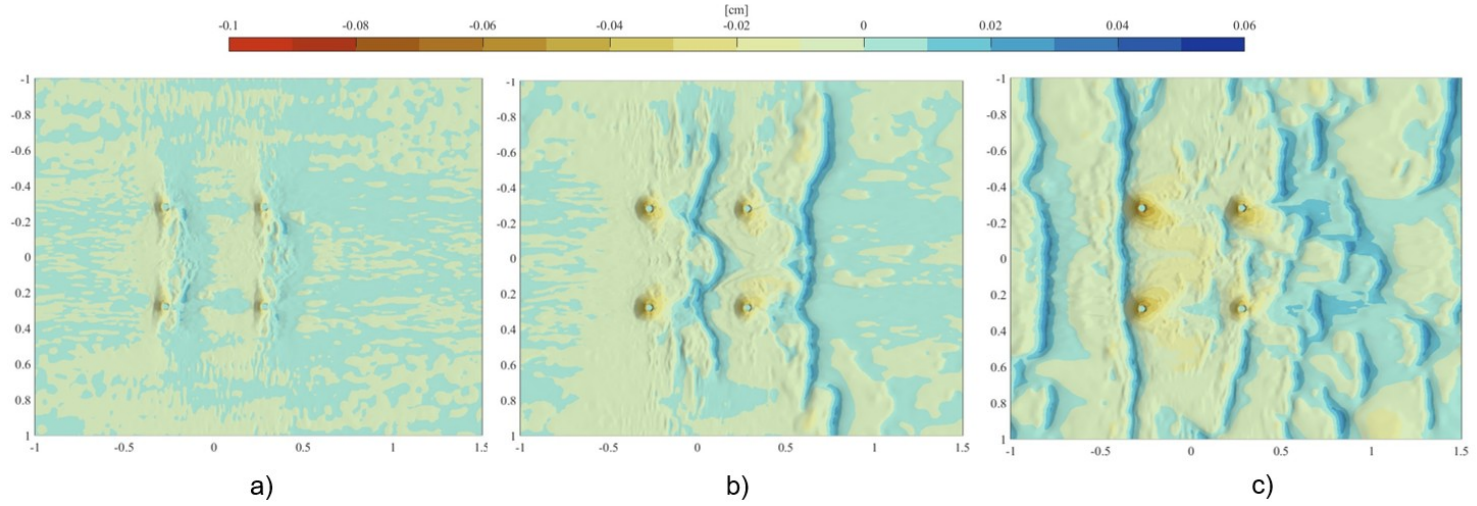

Figure B.33: M100 - Scour on the bed from a plan view after (a)15min, (b) 90 min and (c) 420 min for clear water regime

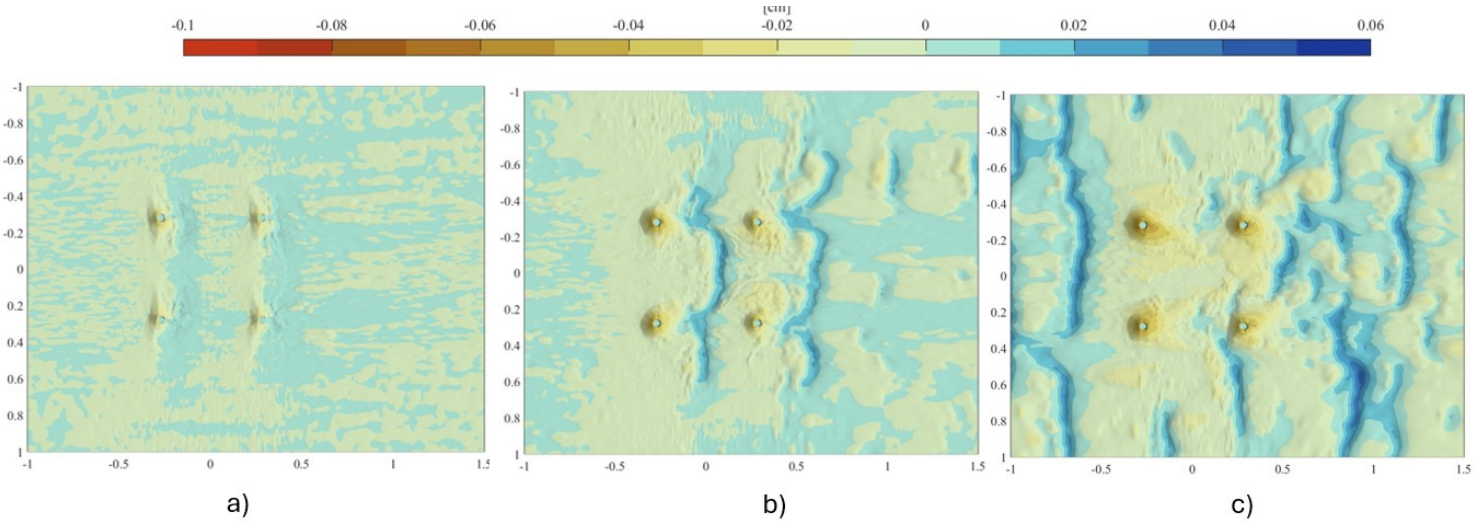

Figure B.34: M200 - Scour on the bed from a plan view after (a)15min, (b) 90 min and (c) 420 min for clear water regime

These Figures show the scour-depth evolution for echo sounders E1–E8 under the clear-water regime, evaluating the effect of morphac on the scour magnitude and evolution .

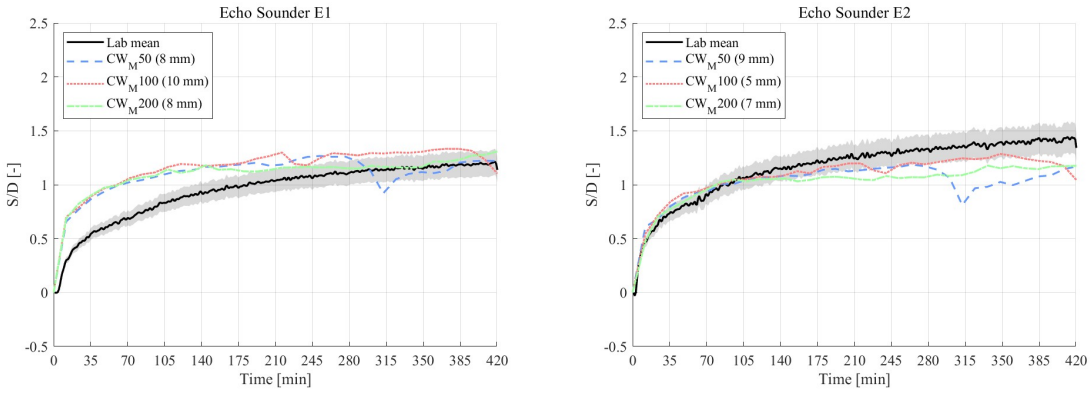

Figure B.35: Scour evolution for M50, M100 and M200 for E1 and E2 (clear-water).

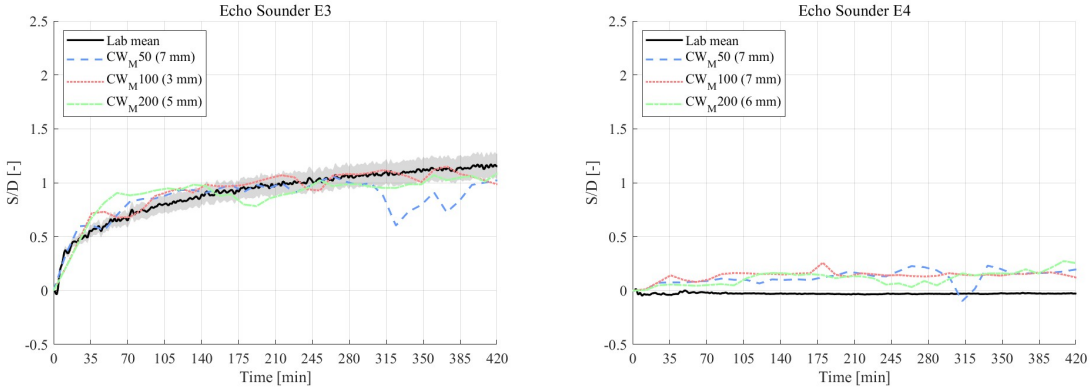

Figure B.36: Scour evolution for M50, M100 and M200 for E3 and E4 (clear-water).

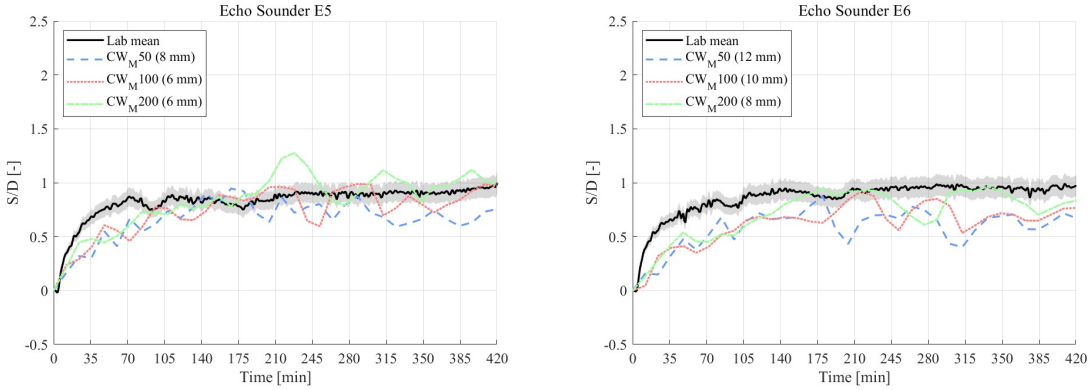

Figure B.37: Scour evolution for M50, M100 and M200 for E5 and E6 (clear-water).

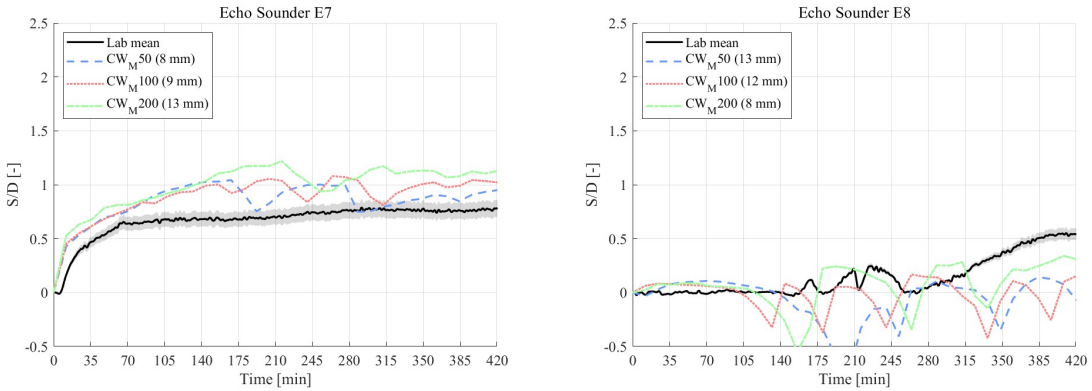

Figure B.38: Scour evolution for M50, M100 and M200 for E7 and E8 (clear-water).

B.3.4. Live bed regime

Table B.5: %RMSE and RMSE (mm) between lab data and models for each Echo Sounder (E1–E7) for the live bed regime

Echo Sounder	Case M50		Case M100		Case M200	
	%RMSE	RMSE (mm)	%RMSE	RMSE (mm)	%RMSE	RMSE (mm)
E1	10%	7	14%	9	20%	13
E2	17%	12	10%	7	13%	9
E3	19%	13	11%	8	14%	10
E5	13%	8	11%	7	15%	9
E6	14%	9	10%	6	15%	9
E7	20%	10	27%	14	40%	21

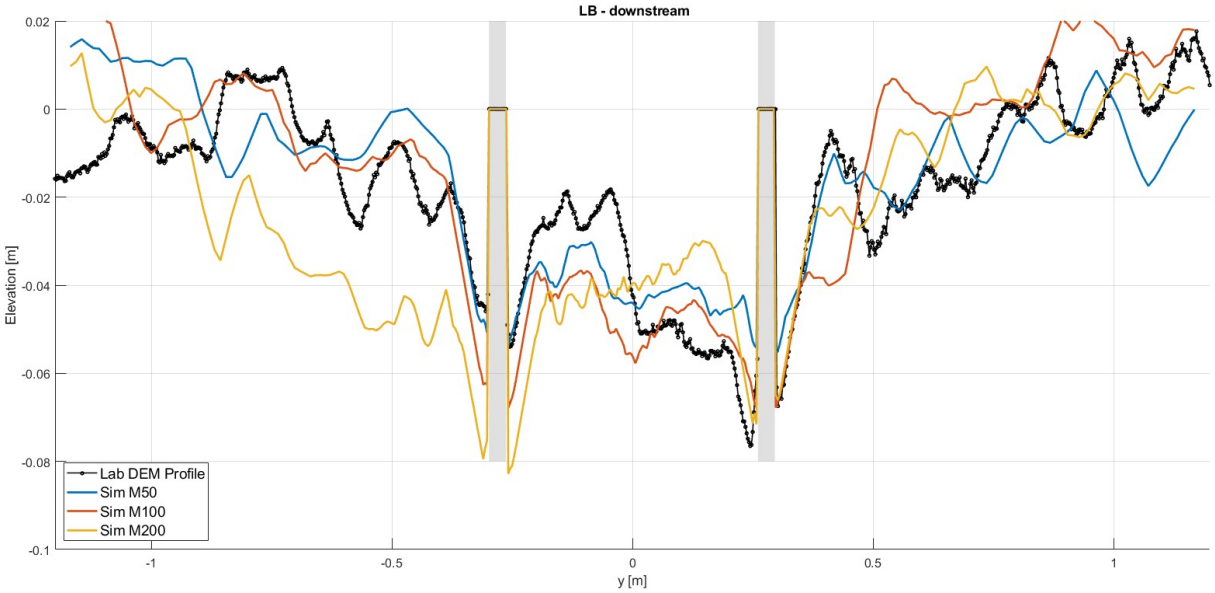

Figure B.39: Cross section downstream of the laboratory results and M50, M100 and M200 at 420 minutes for the clear water regime

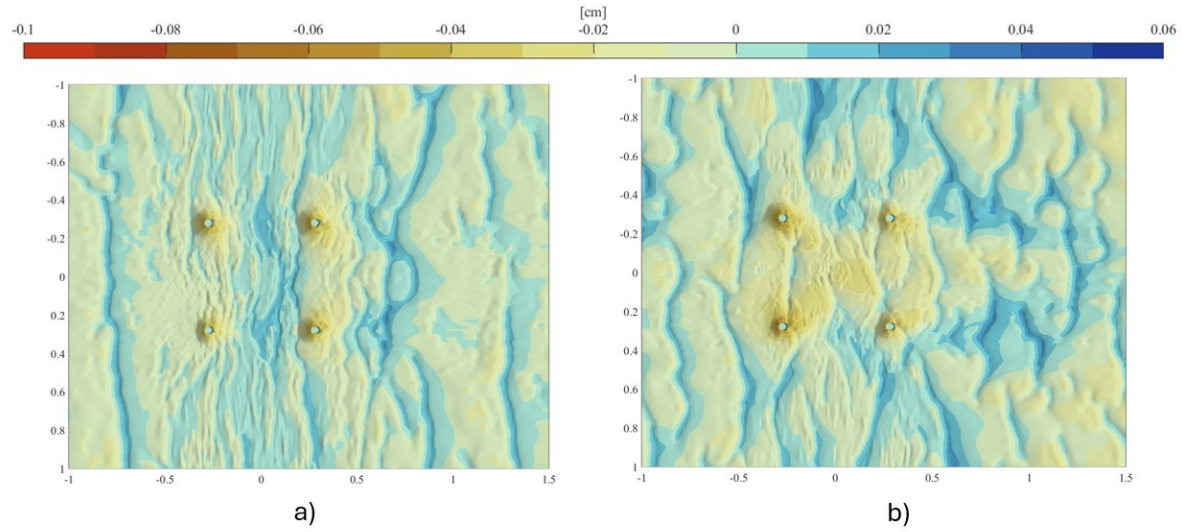

Figure B.40: M10 - Scour on the bed from a plan view after (a)15min and (b) 90 min for live bed regime

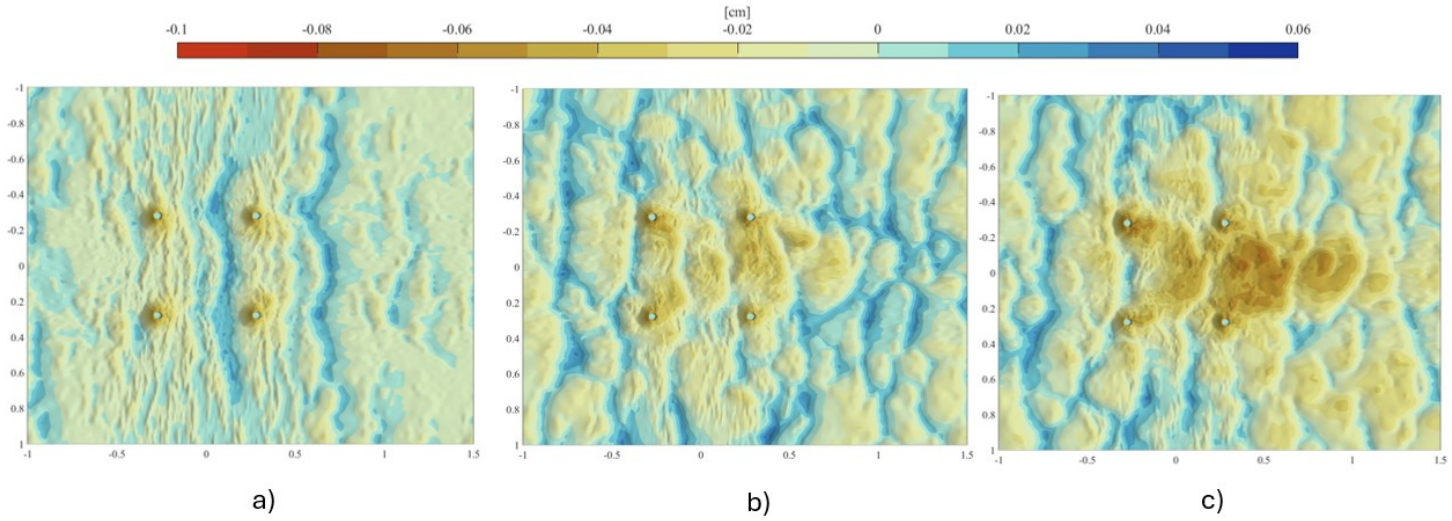

Figure B.41: M50 - Scour on the bed from a plan view after (a)15min, (b) 90 min and (c) 420 min for live bed regime

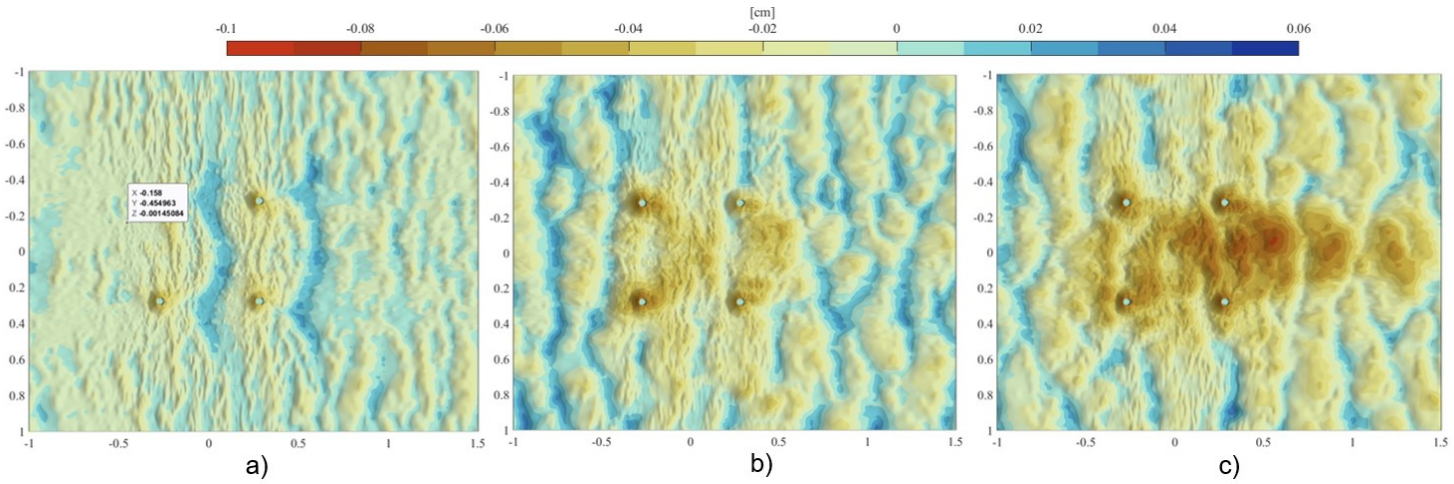

Figure B.42: M100 - Scour on the bed from a plan view after (a)15min, (b) 90 min and (c) 420 min for live bed regime

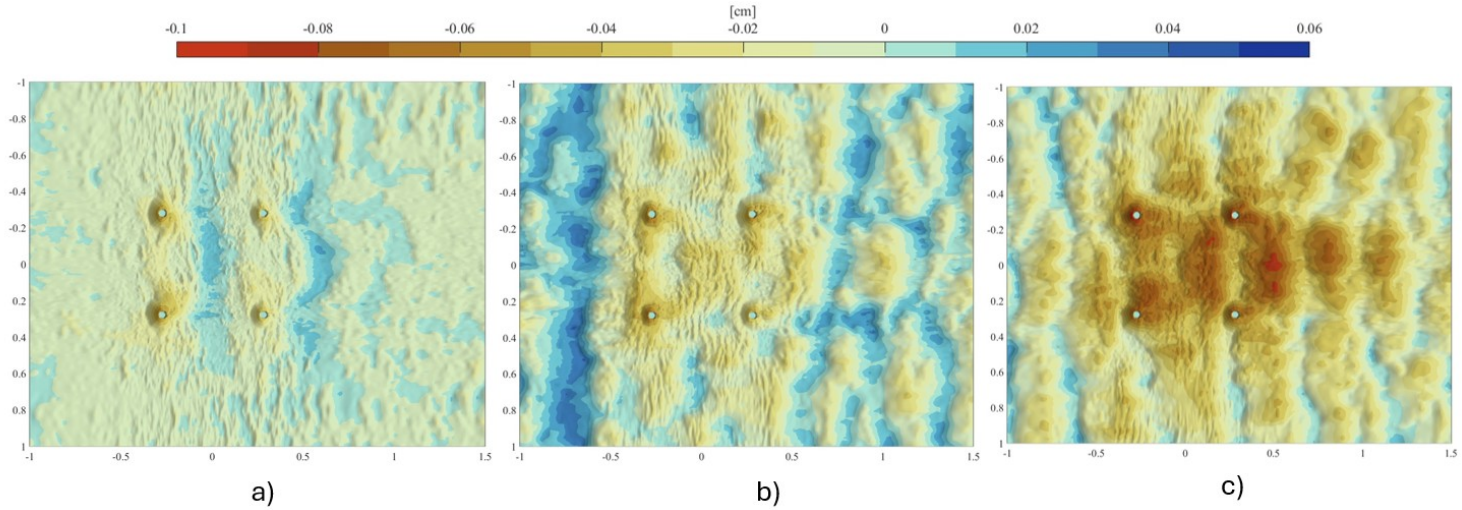

Figure B.43: M200 - Scour on the bed from a plan view after (a)15min, (b) 90 min and (c) 420 min for live bed regime

These Figures show the scour-depth evolution for echo sounders E1–E8 under the live bed regime, evaluating the effect of moprhac on scour magnitude and time evolution.

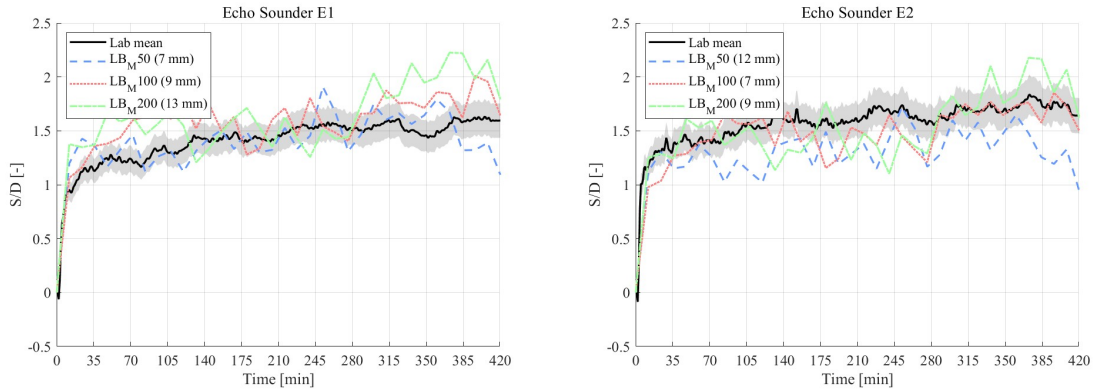

Figure B.44: Scour evolution for M50, M100 and M200 for E1 and E2 (live-bed).

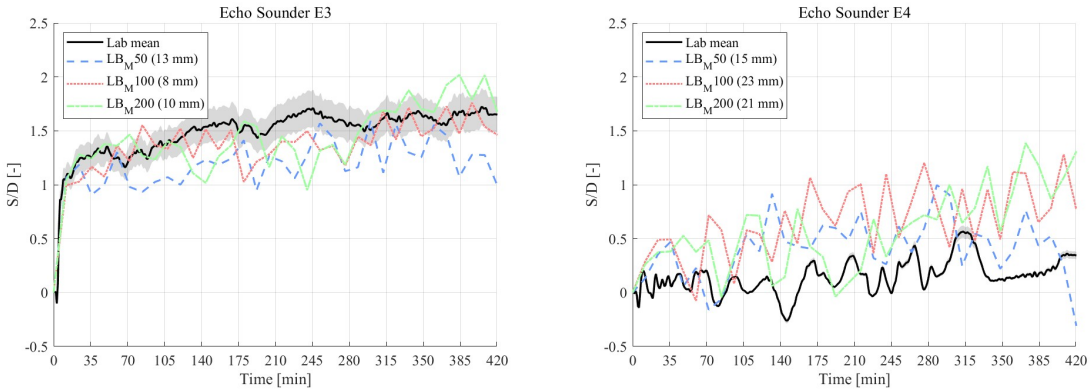

Figure B.45: Scour evolution for M50, M100 and M200 for E3 and E4 (live-bed).

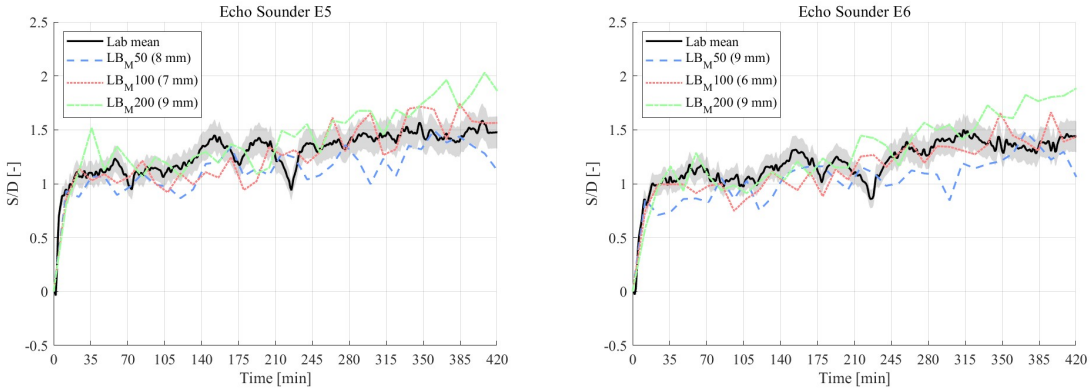

Figure B.46: Scour evolution for M50, M100 and M200 for E5 and E6 (live-bed).

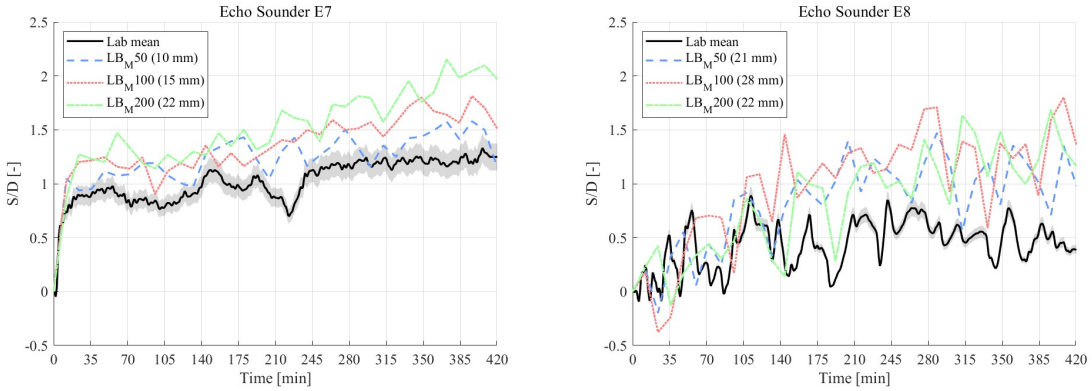

Figure B.47: Scour evolution for M50, M100 and M200 for E7 and E8 (live-bed).

B.4. Global scour time evolution

This methodology was applied to both hydrodynamic regimes. For the clear-water case, the highest scour magnitude occurred in Area 2, with values reaching approximately $0.25\ S/D$, consistent with the square-based analysis. Areas 1 and 3, still within the jacket footprint, also exhibited significant scour of about $0.2\ S/D$. Areas 4, 5, and 6 showed more stable behavior, although the numerical model tends to overestimate scour in the outermost zones.

In the live-bed regime, the insights are more pronounced due to the extension of global scour beyond the jacket footprint. Results for Areas 1 and 3, representing upstream and downstream regions between

piles, are shown in Figure B.48. The scour evolution in these areas aligns with the trends observed in the strip analysis, gradually approaching equilibrium. The downstream region (Area 3) reaches up to $1.0\ S/D$, while the upstream region (Area 1) remains lower at around $0.5\ S/D$, closely matching the laboratory data.

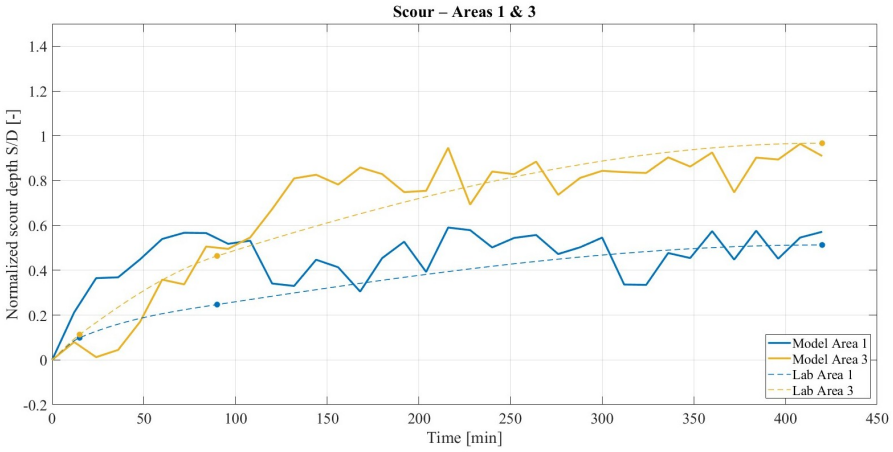

Figure B.48: Scour evolution in Areas 1 (upstream) and 3 (downstream) from both numerical and laboratory data under live-bed conditions.

Areas 2 and 4, located inside the jacket footprint and immediately downstream, are presented in Figure B.49. Both zones show increasing scour magnitudes, reaching approximately $0.7 - 0.8\ S/D$ by the end of the simulation. The trend suggests continued bed lowering, indicating that equilibrium may not yet be achieved.

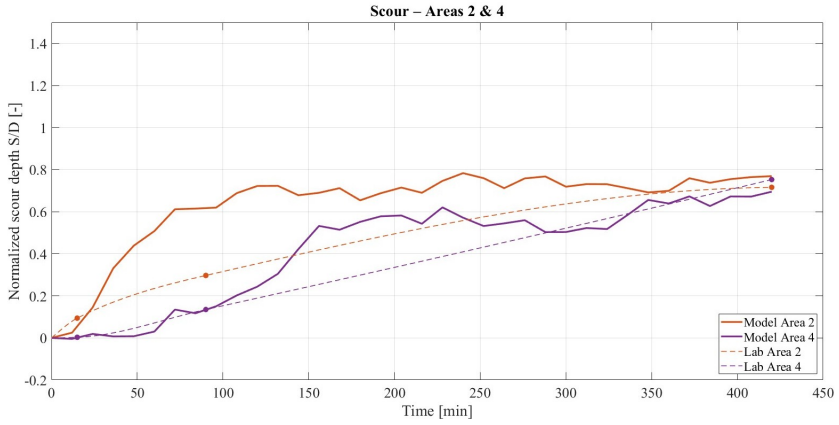

Figure B.49: Scour development in Areas 2 and 4 from model and lab results under live-bed flow.

Tthe results for Areas 5 and 6, which lie between piles along the current axis, are shown in Figure B.50. These areas display nearly uniform scour evolution, with limited differences between them and lower magnitudes of around $0.5\ S/D$. However, the numerical model does not fully capture the initial scour response in these zones, potentially suggesting premature equilibrium. In contrast, the lab data indicate that equilibrium has not yet been reached.

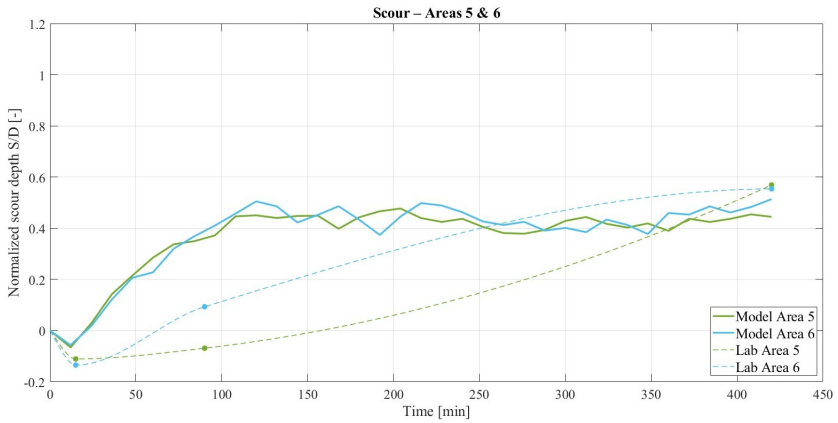

Figure B.50: Comparison of scour evolution in Areas 5 and 6 based on model and experimental results (live-bed regime).

Overall, under live-bed conditions, the highest scour occurs between the downstream piles (Area 3), reaching values close to $1.0\ S/D$. This is followed by the central region of the jacket (Area 2) and the downstream wake zone (Area 4), both exhibiting scour depths around $0.75\ S/D$. In contrast, the least affected regions are the upstream zone between piles (Area 1) and the lateral outer areas (Areas 5 and 6), where scour magnitudes remain comparatively lower.

Appendix C: Analysis of model results

This appendix provides the figures referenced on the chapter 6.

C.1. Scour footprint

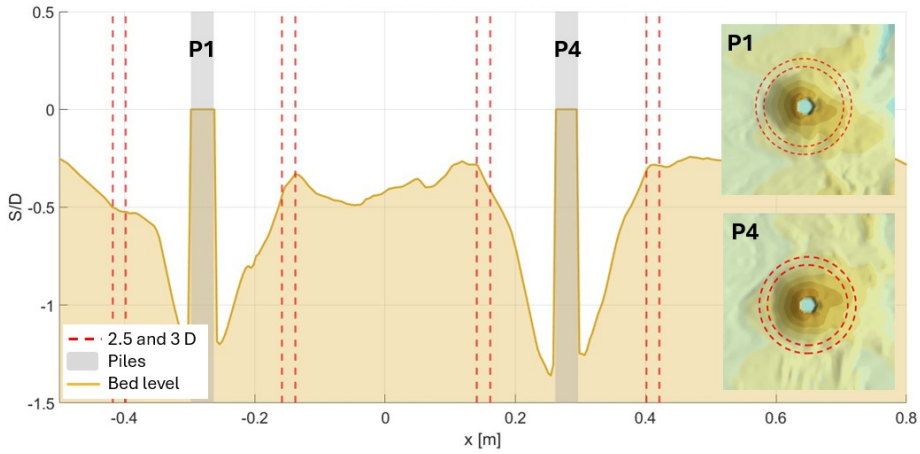

Figure C.1: Example application of the scour extent method for the clear water regime on upstream piles. The cross-section view shows the extent of local scour from the pile perimeter, while the plan view indicates the corresponding extents for each pile footprint.

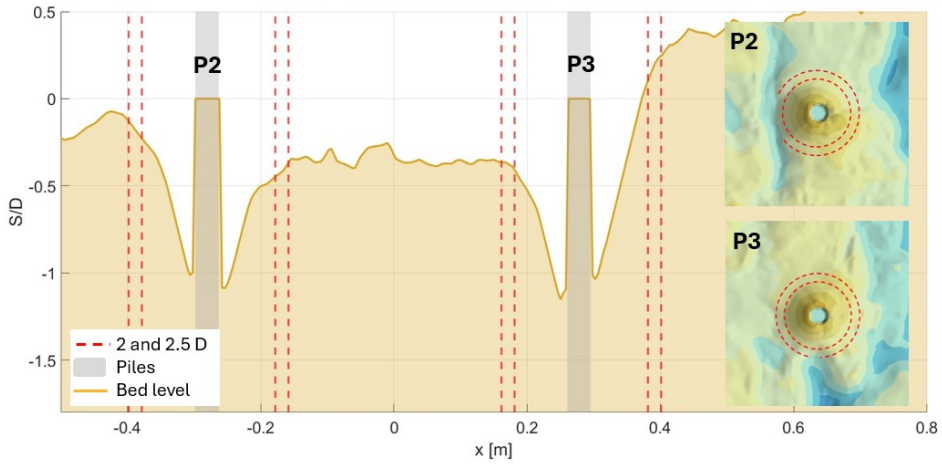

Figure C.2: Example application of the scour extent method for the clear water regime on downstream piles. The cross-section view shows the extent of local scour from the pile perimeter, while the plan view indicates the corresponding extents for each pile footprint.

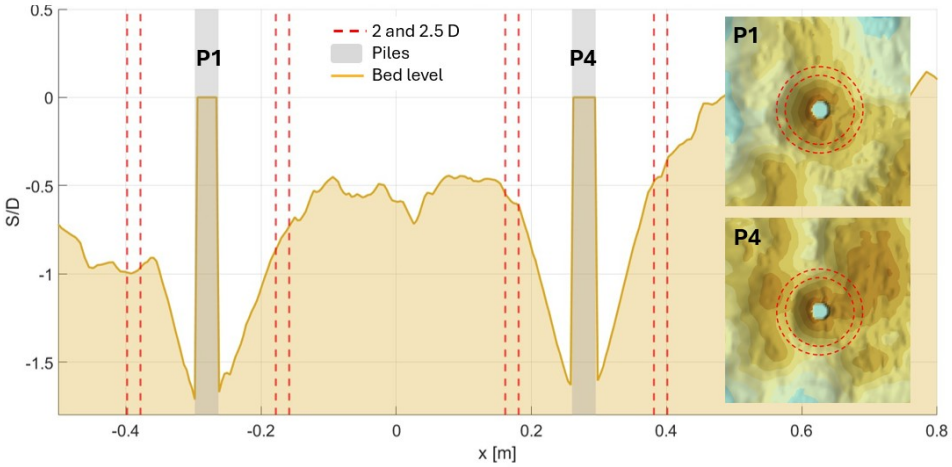

Figure C.3: Example application of the scour extent method for the live bed regime on upstream piles. The cross-section view shows the extent of local scour from the pile perimeter, while the plan view indicates the corresponding extents for each pile footprint.

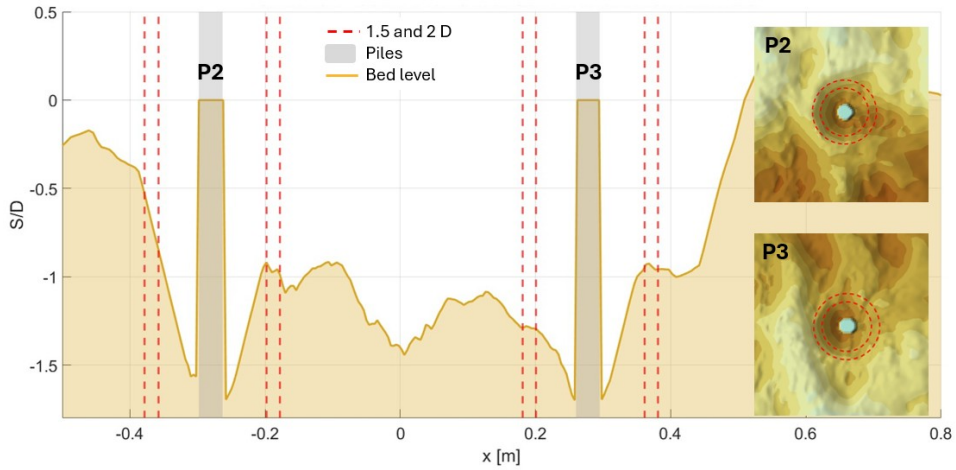

Figure C.4: Example application of the scour extent method for the live bed regime on downstream piles. The cross-section view shows the extent of local scour from the pile perimeter, while the plan view indicates the corresponding extents for each pile footprint

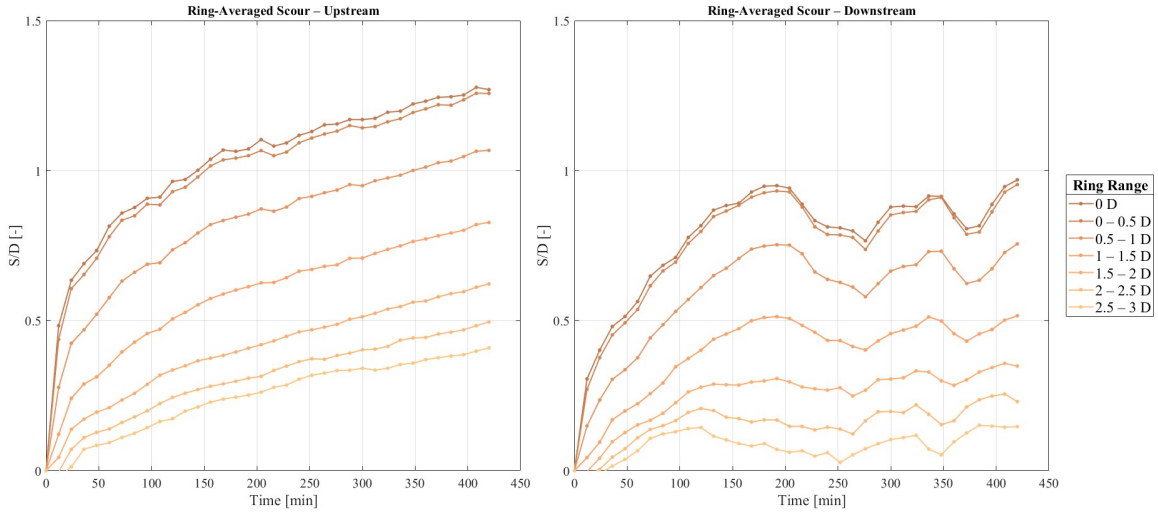

Figure C.5: Scour evolution for averaged scour values over rings for upstream (Left) and downstream (Right) piles for the clear water regime at laboratory scale

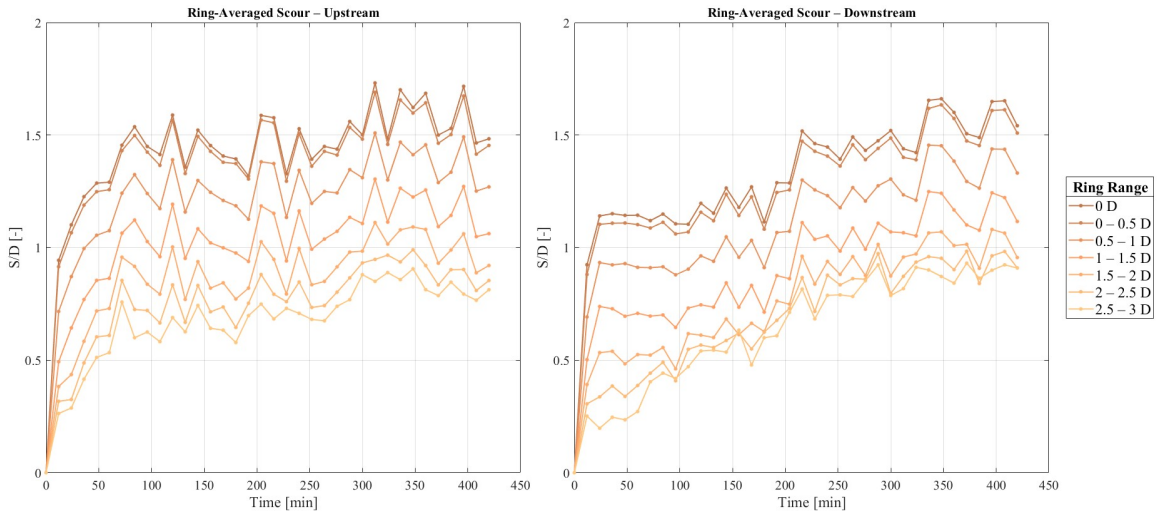

Figure C.6: Scour evolution for averaged scour values over rings for upstream (Left) and downstream (Right) piles for the live bed regime at laboratory scale

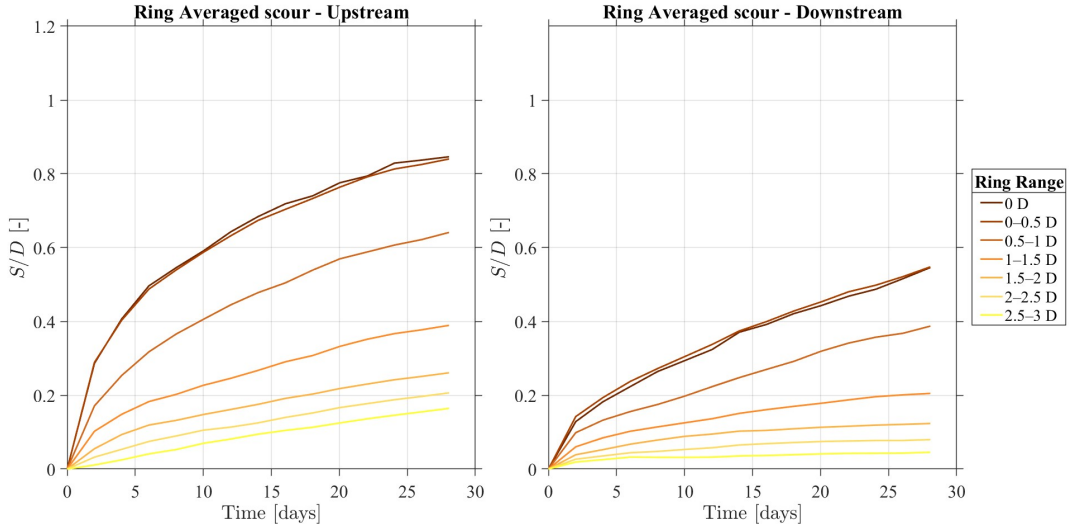

Figure C.7: Scour evolution for averaged scour values over rings for upstream (Left) and downstream (Right) piles for the clear water regime at field scale

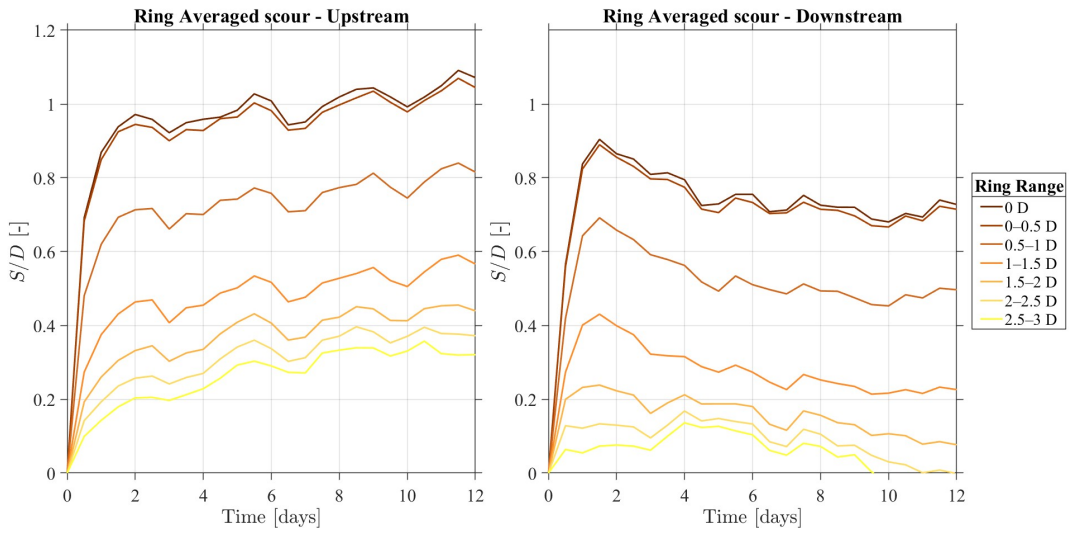

Figure C.8: Scour evolution for averaged scour values over rings for upstream (Left) and downstream (Right) piles for the live bed regime at field scal

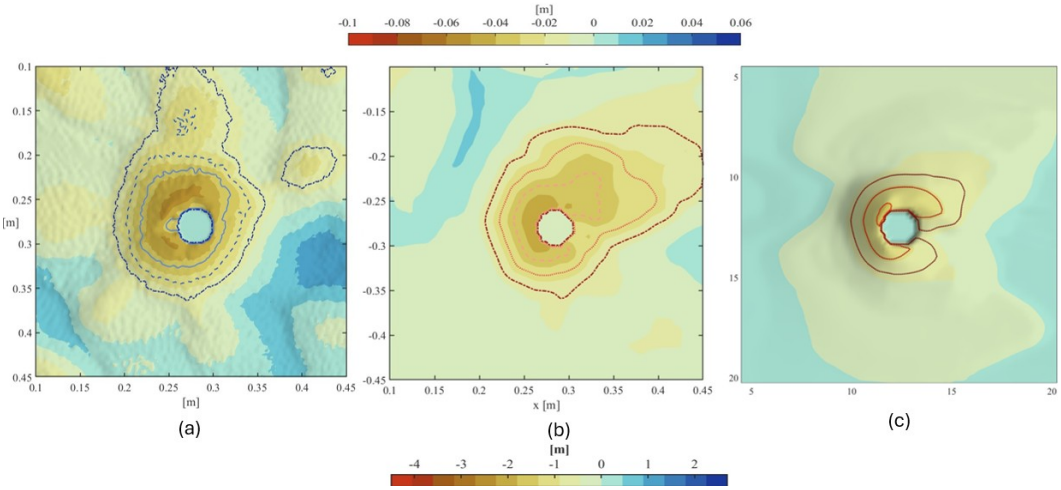

Figure C.9: Contour lines of erosion for a downstream pile at the end of simulation or model in the clear-water regime. (a) Lab results (b) TUDflow3D result at lab scale (c) TUDflow3D result at field scale

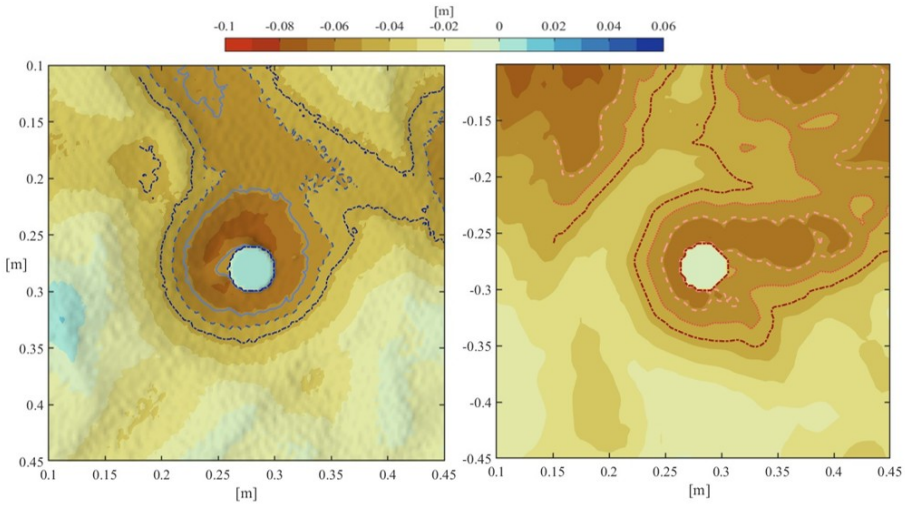

Figure C.10: Contour lines of erosion for a downstream pile after 420 minutes of simulation in the live-bed regime. Left: Lab results. Right: TUDflow3D results.

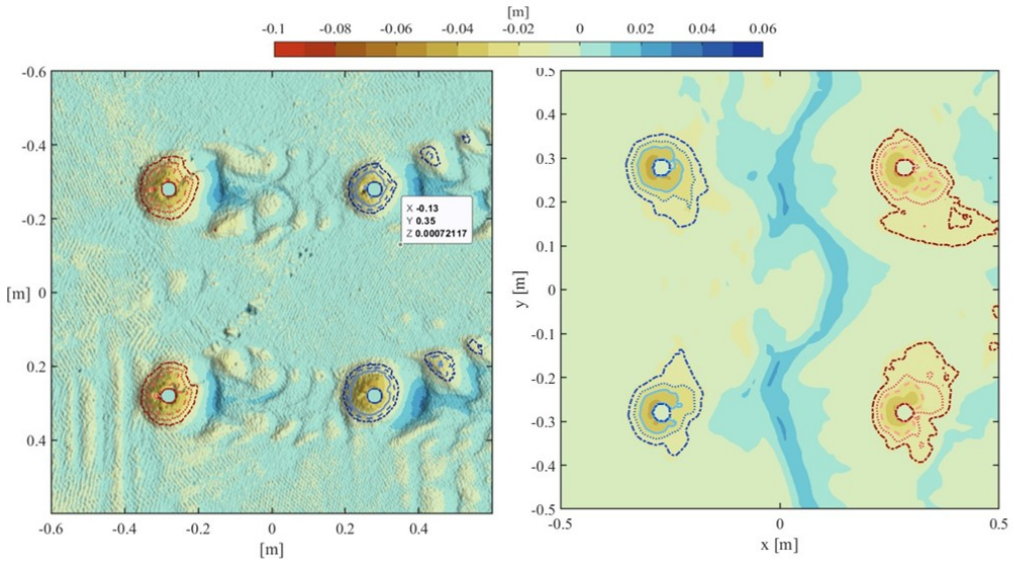

Figure C.11: Contour lines showing pattern of scour after 90 minutes of simulation for clear water regime - Left:lab results - Right: TUDflow3D results

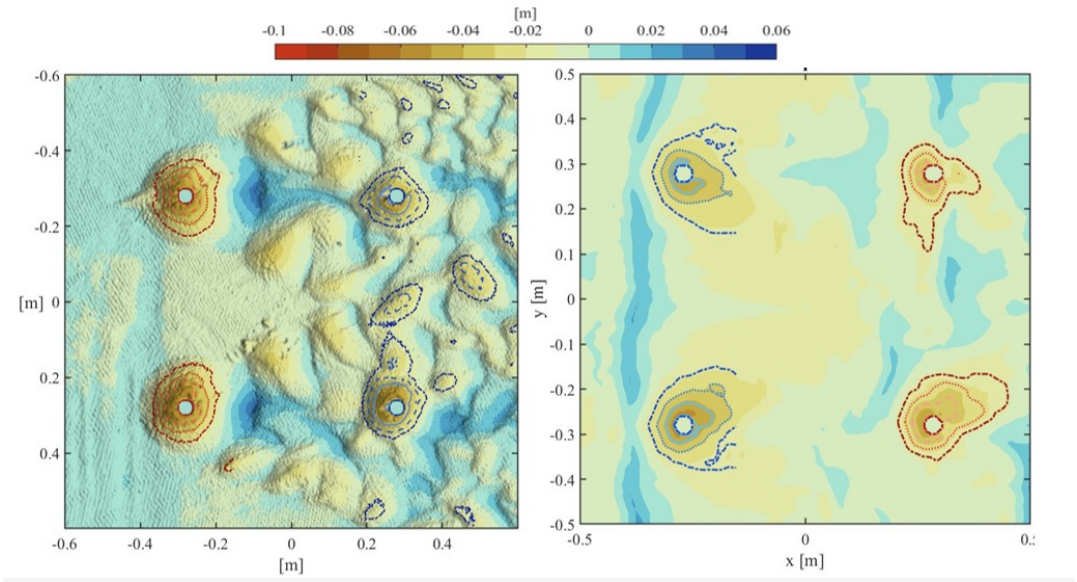

Figure C.12: Contour lines showing pattern of scour after 420 minutes of simulation for clear water regime - Left:lab results - Right: TUDflow3D results

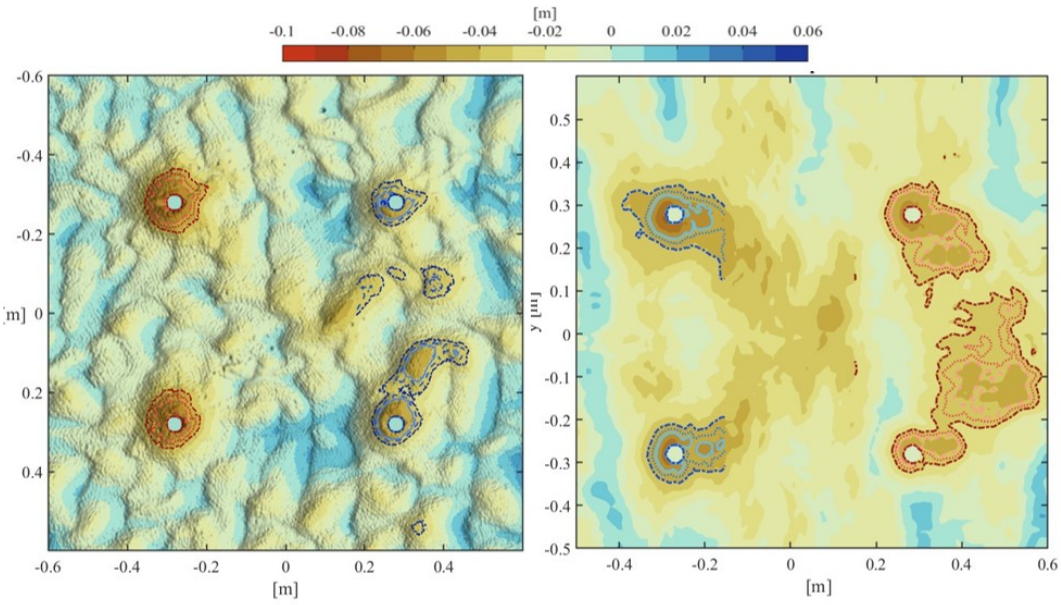

Figure C.13: Contour lines showing pattern of scour after 90 minutes of simulation for live bed regime - Left:lab results - Right: TUDflow3D results

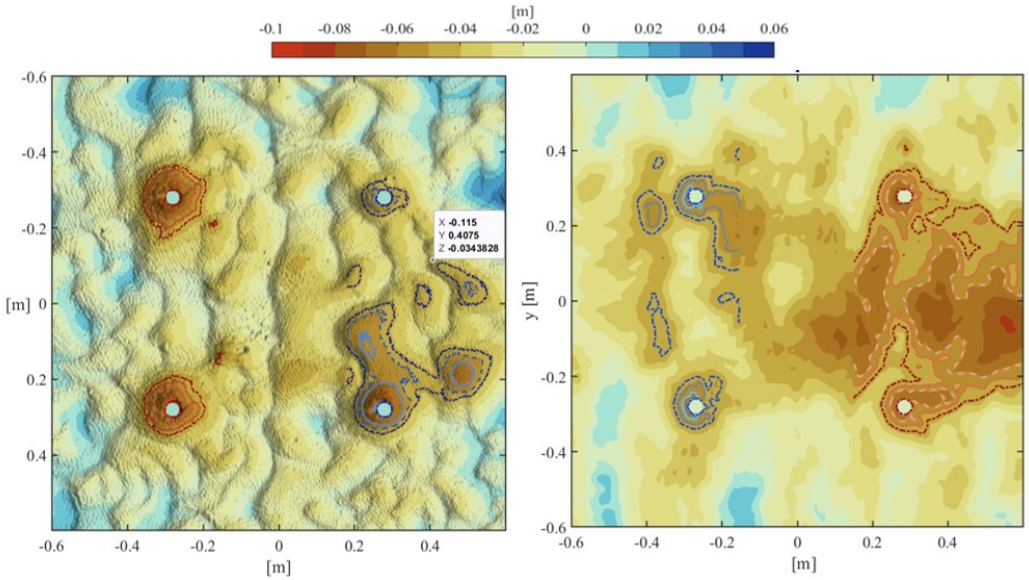

Figure C.14: Contour lines showing pattern of scour after 420 minutes of simulation for live bed regime -Left:lab results - Right: TUDflow3D results

C.2. Time to reach the equilibrium depth fitted to the lab results

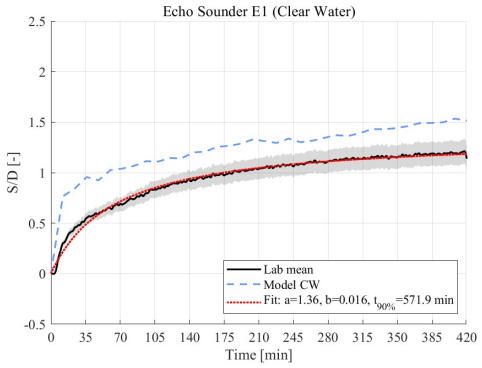

(a) E1 - Clear Water

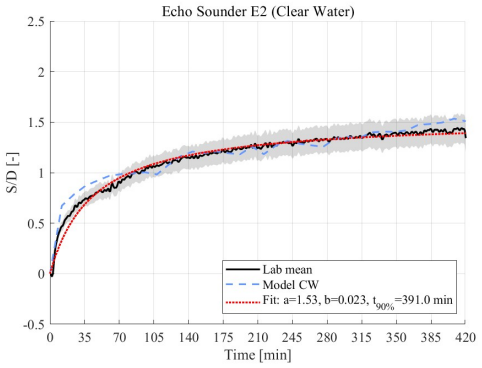

(b) E2 - Clear Water

Figure C.15: Time evolution of scour depth (S/D) under clear water conditions at E1 and E2 locations.

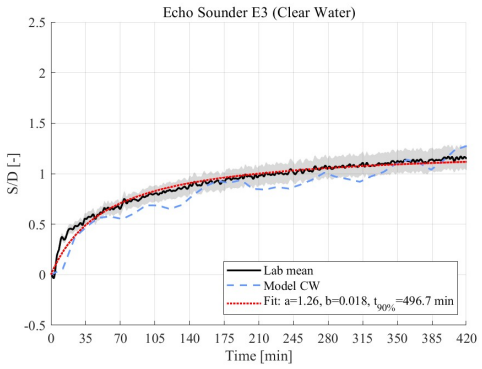

(a) E3 - Clear Water

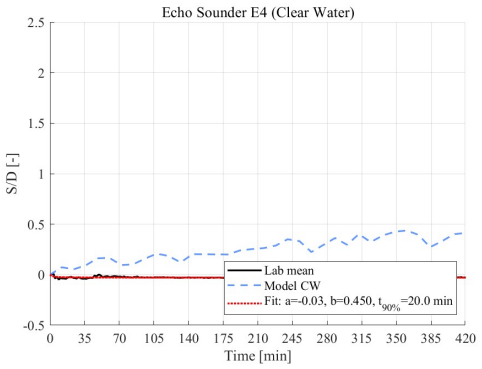

(b) E4 - Clear Water

Figure C.16: Time evolution of scour depth (S/D) under clear water conditions at E3 and E4 locations.

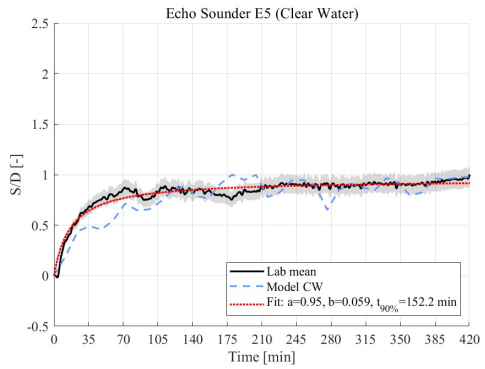

(a) E5 - Clear Water

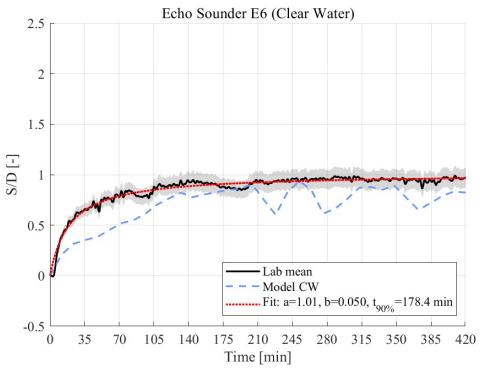

(b) E6 - Clear Water

Figure C.17: Time evolution of scour depth (S/D) under clear water conditions at E5 and E6 locations.

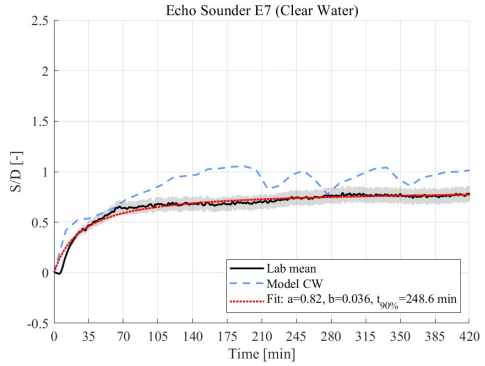

(a) E7 - Clear Water

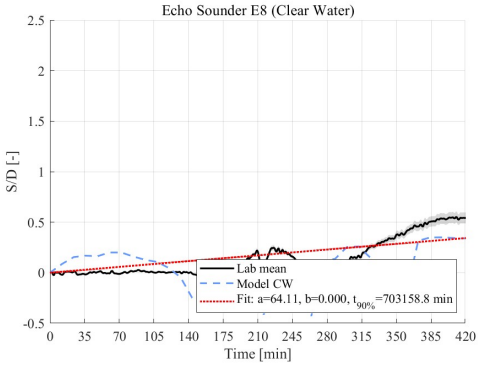

(b) E8 - Clear Water

Figure C.18: Time evolution of scour depth (S/D) under clear water conditions at E7 and E8 locations.

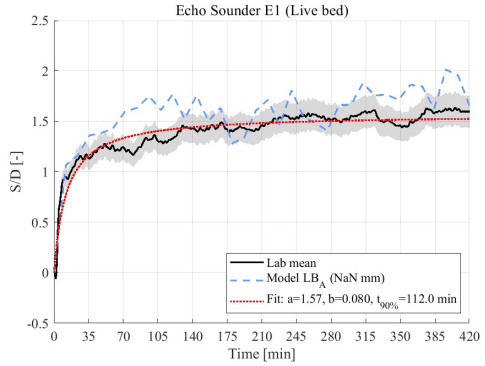

(a) E1 - Live Bed

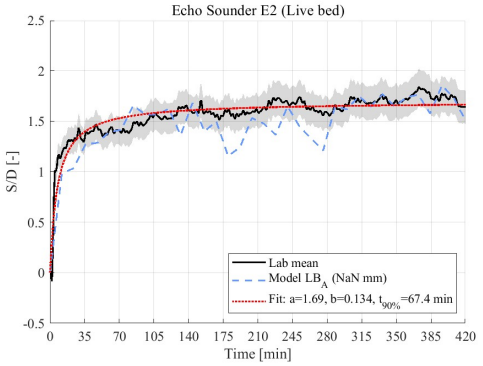

(b) E2 - Live Bed

Figure C.19: Time evolution of scour depth (S/D) under live bed conditions at E1 and E2 locations.

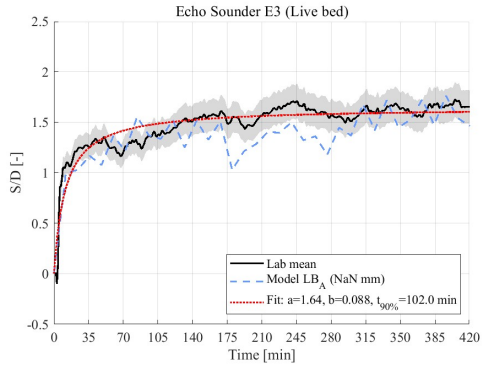

(a) E3 - Live Bed

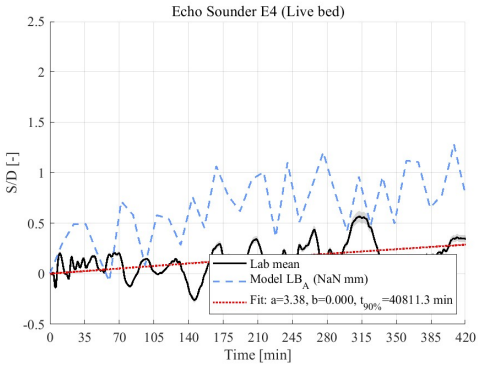

(b) E4 - Live Bed

Figure C.20: Time evolution of scour depth (S/D) under live bed conditions at E3 and E4 locations.

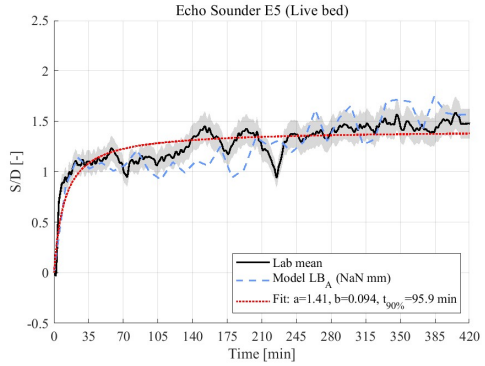

(a) E5 - Live Bed

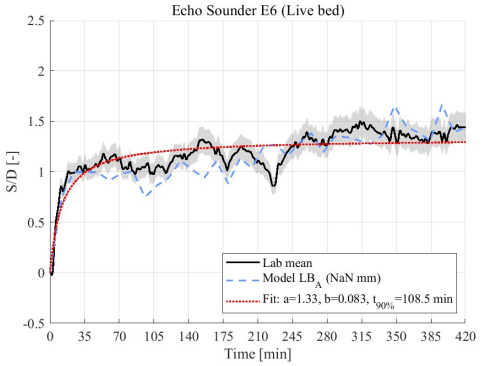

(b) E6 - Live Bed

Figure C.21: Time evolution of scour depth (S/D) under live bed conditions at E5 and E6 locations.

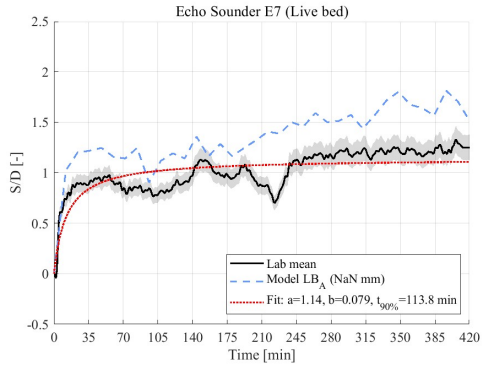

(a) E7 - Live Bed

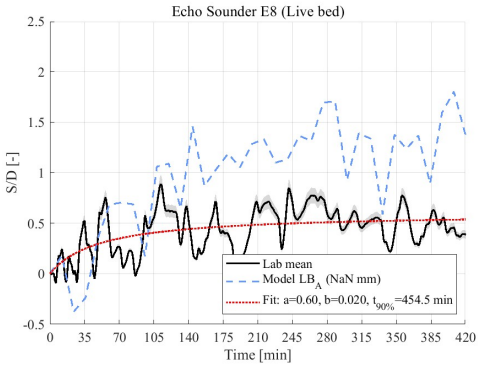

(b) E8 - Live Bed

Figure C.22: Time evolution of scour depth (S/D) under live bed conditions at E7 and E8 locations.

C.3. Time to reach the equilibrium depth fitted to the numerical model results

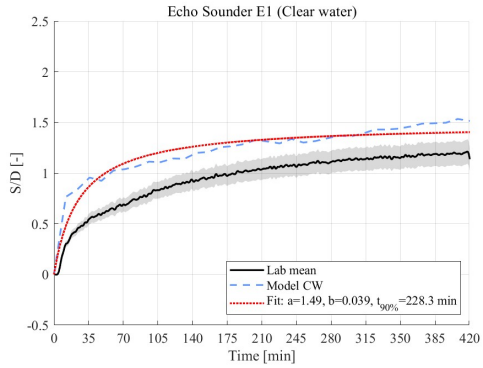

(a) E1 - Clear Water

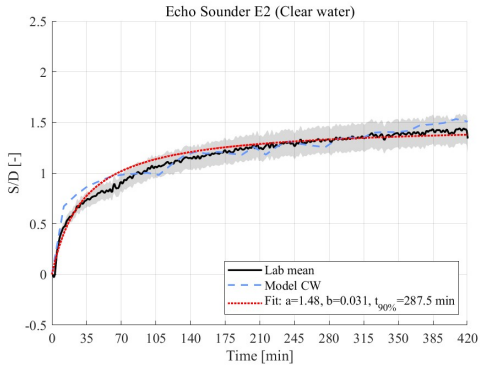

(b) E2 - Clear Water

Figure C.23: Time evolution of scour depth (S/D) under clear water conditions at E1 and E2, fitted to the numerical model results.

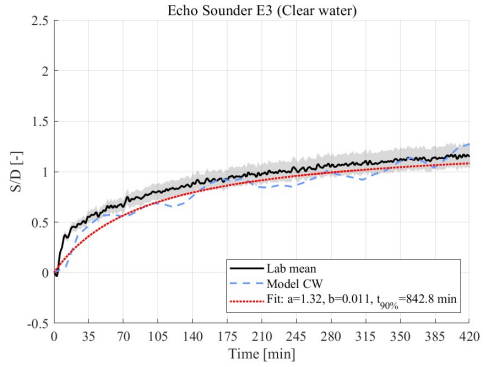

(a) E3 - Clear Water

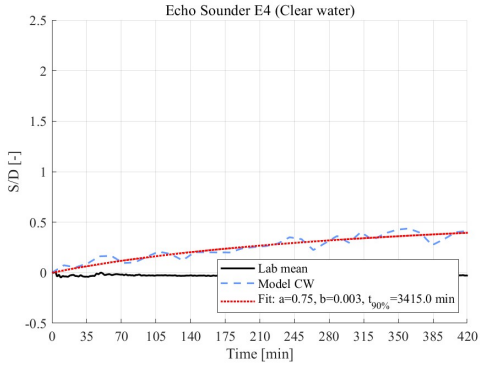

(b) E4 - Clear Water

Figure C.24: Time evolution of scour depth (S/D) under clear water conditions at E3 and E4, fitted to the numerical model results.

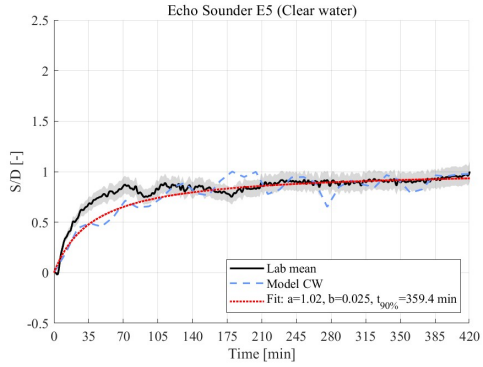

(a) E5 - Clear Water

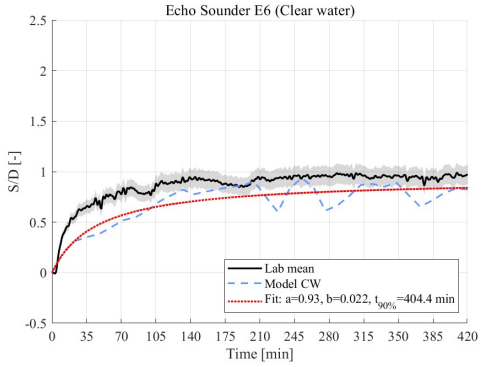

(b) E6 - Clear Water

Figure C.25: Time evolution of scour depth (S/D) under clear water conditions at E5 and E6, fitted to the numerical model results.

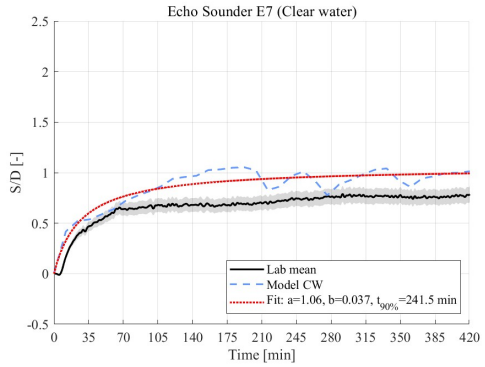

(a) E7 - Clear Water

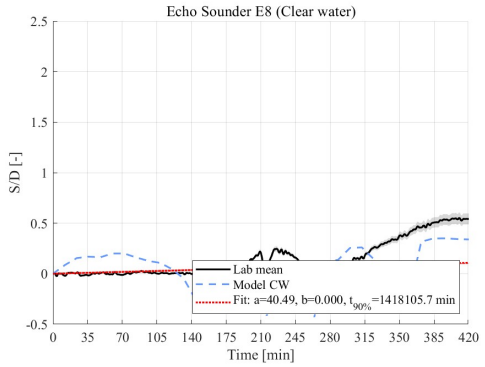

(b) E8 - Clear Water

Figure C.26: Time evolution of scour depth (S/D) under clear water conditions at E7 and E8, fitted to the numerical model results.

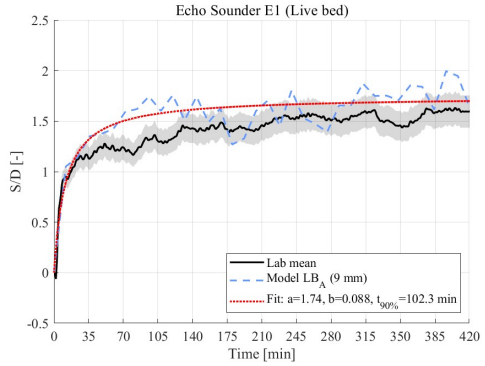

(a) E1 - Live Bed

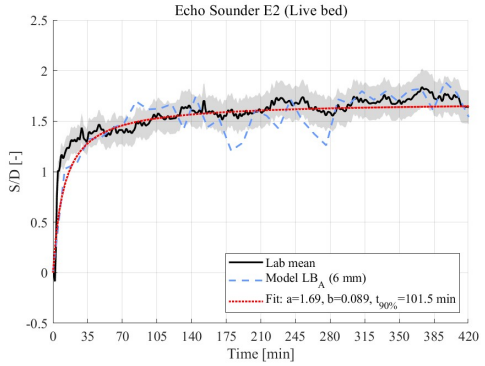

(b) E2 - Live Bed

Figure C.27: Time evolution of scour depth (S/D) under live bed conditions at E1 and E2 locations fitted to the numerical model results.

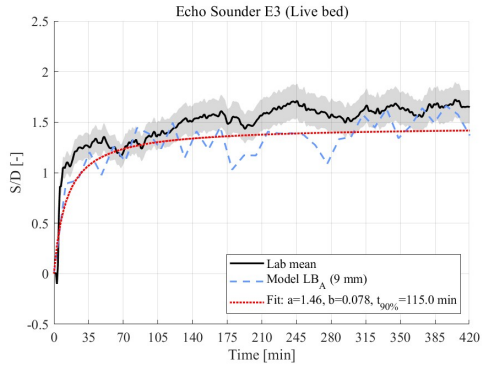

(a) E3 - Live Bed

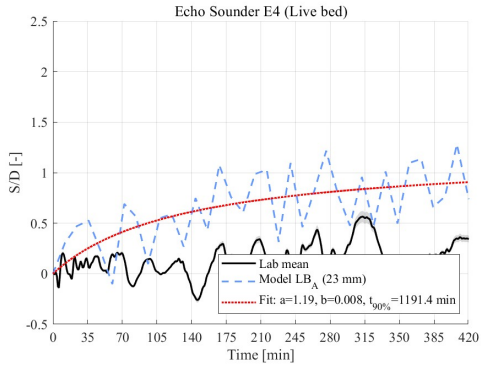

(b) E4 - Live Bed

Figure C.28: Time evolution of scour depth (S/D) under live bed conditions at E3 and E4 locations fitted to the numerical model results.

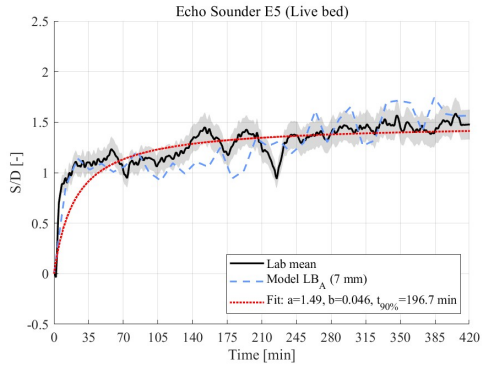

(a) E5 - Live Bed

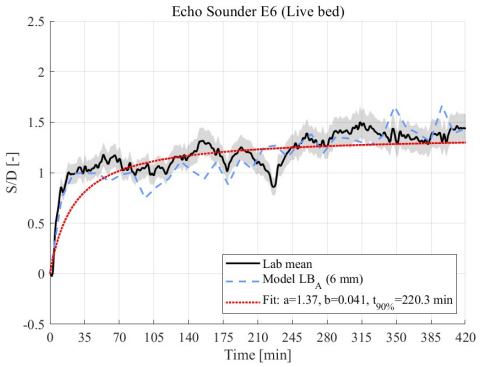

(b) E6 - Live Bed

Figure C.29: Time evolution of scour depth (S/D) under live bed conditions at E5 and E6 locations fitted to the numerical model results.

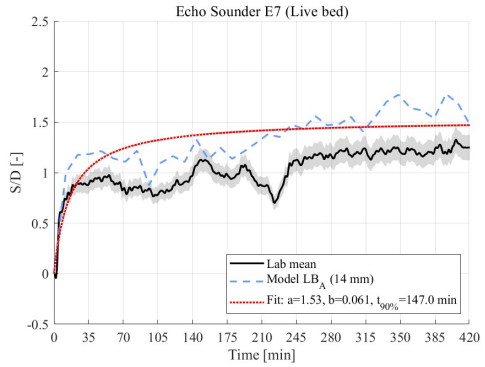

(a) E7 - Live Bed

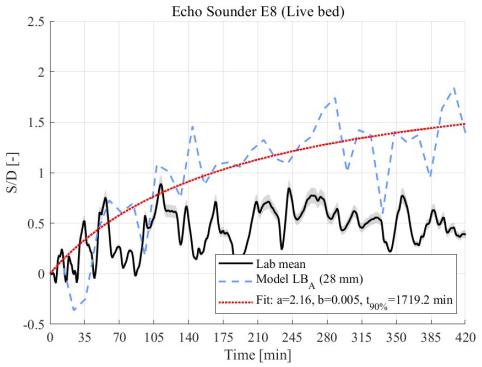

(b) E8 - Live Bed

Figure C.30: Time evolution of scour depth (S/D) under live bed conditions at E7 and E8 locations fitted to the numerical model results.

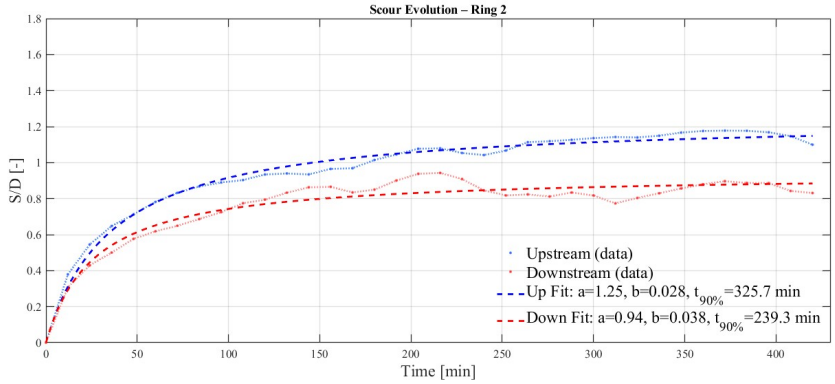

(a) Ring of 0.02 m

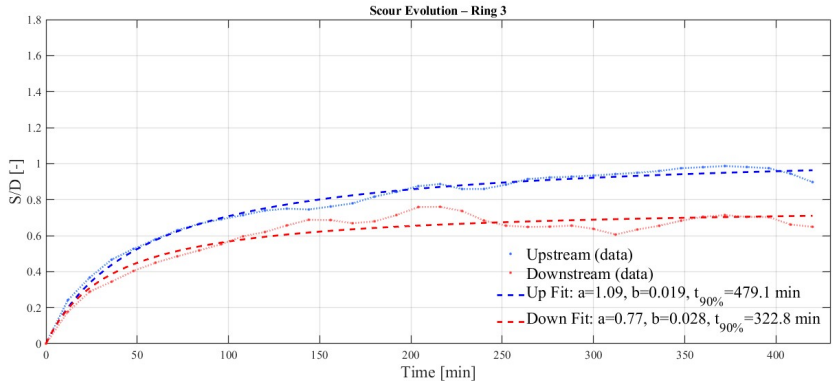

(b) Ring of 0.04 m

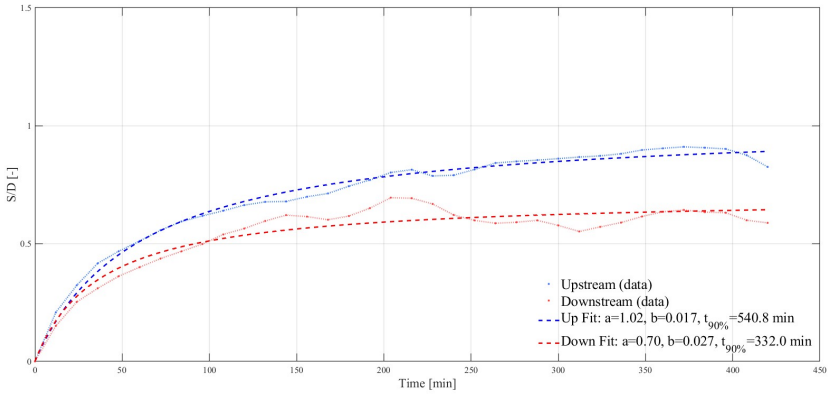

(c) Ring of 0.06 m

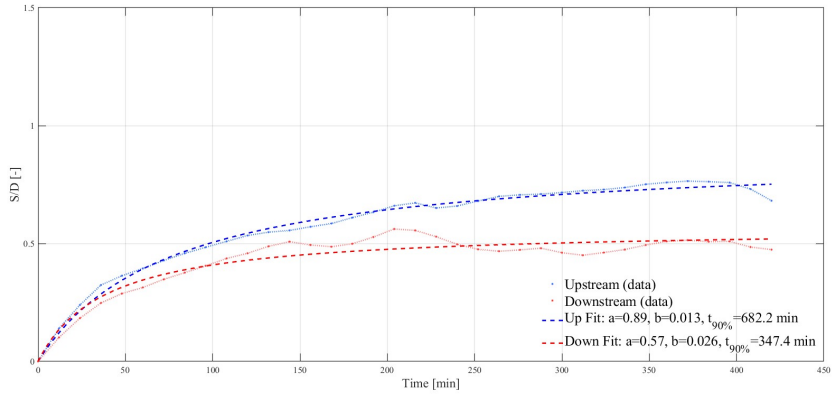

(d) Ring of 0.08 m

Figure C.31: Time fitting of average scour evolution around the piles for ring sizes of 0.02 m, 0.04 m, 0.06 m, and 0.08 m under clear water regime. (a)–(d) show upstream and downstream values.

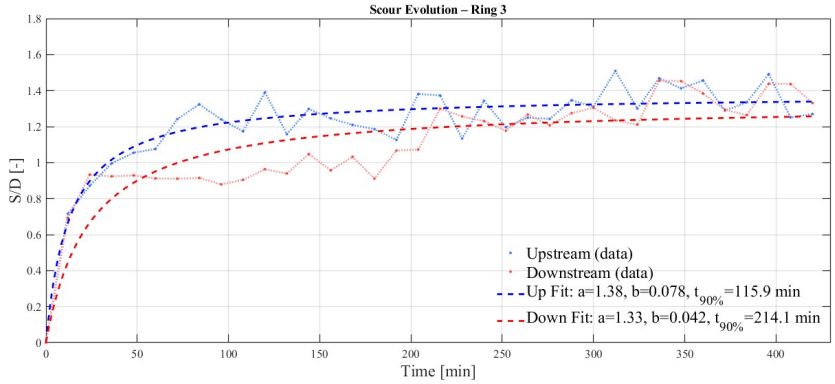

(a) Ring of 0.02 m

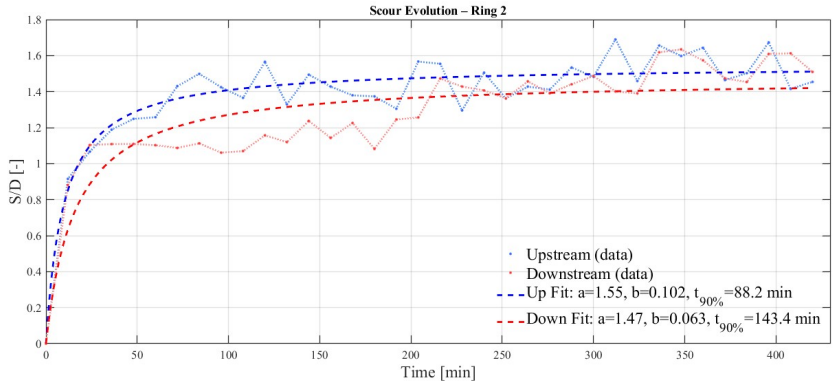

(b) Ring of 0.04 m

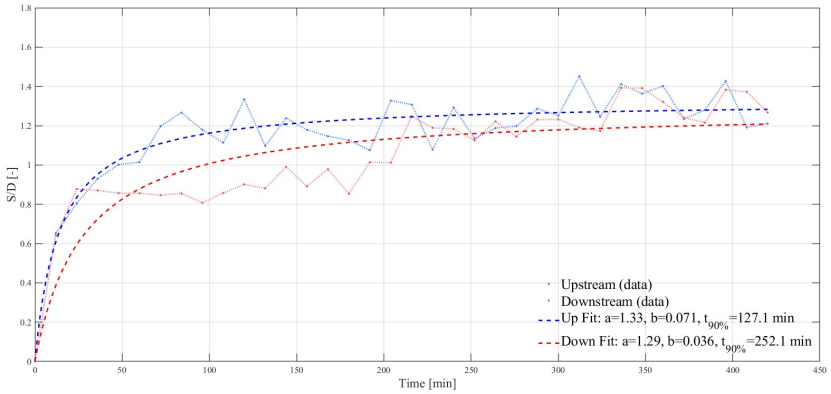

(c) Ring of 0.06 m

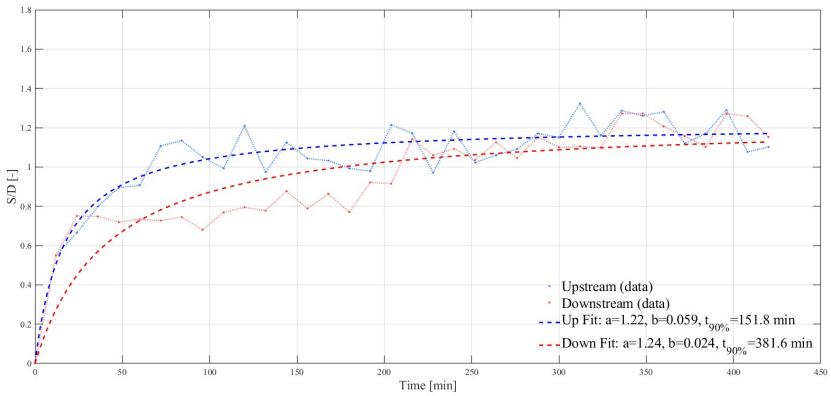

(d) Ring of 0.08 m

Figure C.32: Time fitting of average scour evolution around the piles for ring sizes of 0.02 m, 0.04 m, 0.06 m, and 0.08 m under live bed regime. (a)–(d) show upstream and downstream values.

Table C.1: Equilibrium times (t_{90}) and scour depths (S_{eq}) for upstream and downstream regions by ring (clear-water regime).

Ring	$t_{90,\text{Down}}$ (min)	$S_{\text{eq,Up}}$ [-]	$S_{\text{eq,Down}}$ [-]
0 D	305	1.4	1.0
0–0.5 D	330	1.3	1.0
0.5–1 D	454	1.2	0.8
1–1.5 D	652	1.0	0.6
1.5–2 D	784	0.9	0.4
2–2.5 D	731	0.8	0.2

Table C.2: Equilibrium times (t_{90}) and scour depths (S_{eq}) per ring (live-bed regime).

Ring	$t_{90,\text{Up}}$ (min)	$t_{90,\text{Down}}$ (min)	$S_{\text{eq,Up}}$ [-]	$S_{\text{eq,Down}}$ [-]
0 D	89	138	1.6	1.5
0–0.5 D	93	151	1.5	1.5
0.5–1 D	122	226	1.4	1.3
1–1.5 D	174	435	1.2	1.2
1.5–2 D	228	908	1.0	1.2
2–2.5 D	294	1392	0.9	1.3